Advances in Urban Traffic Network Equilibrium Models and Algorithms

Advances in Urban Traffic Network Equilibrium Models and Algorithms

PROEFSCHRIFT

ter verkrijging van de graad van doctor aan de Technische Universiteit Eindhoven, op gezag van de rector magnificus prof.dr.ir. F.P.T. Baaijens, voor een commissie aangewezen door het College voor Promoties, in het openbaar te verdedigen op dinsdag 18 mei om 11:00 uur

door

Dong Wang

geboren te Shandong, China

Dit proefschrift is goedgekeurd door de promotoren en de samenstelling van de promotiecommissie is als volgt:

voorzitter:	prof. dr. ir. T.A.M. Salet
1e promotor:	prof. dr. H.J.P. Timmermans
2e promotor:	prof. dr. Z. Gao (Beijing Jiaotong University)
copromotor:	dr. F. Liao
leden:	prof. dr. O. Nielsen (Technical University of Denmark)
	prof. dr. T.A. Arentze
	prof. dr. T. van Woensel

Het onderzoek of ontwerp dat in dit thesis wordt beschreven is uitgevoerd in overeenstemming met de TU/e Gedragscode Wetenschapsbeoefening.

Advances in Urban Traffic Network Equilibrium Models and Algorithms

A catalogue record is available from the Eindhoven University of Technology Library

ISBN: 978-90-386-5259-7
NUR: 955

Cover design: Dong Wang
Photograph: Siqi Liu

Printed by the Eindhoven University Press, Eindhoven, the Netherlands
Published as issue 313 in de Bouwstenen series of the Department of the Built Environment of the Eindhoven University of Technology

回报源于坚守

Acknowledgements

After four years in this wonderful country, it is time for me to complete my doctoral studies in the Netherlands. Not only did I gain a rich and colorful life, but I also achieved fruitful academic achievements in the Netherlands.

Here, I would like to thank my promotors, colleagues, and friends for their support and company.

First and foremost, I'd like to express my heartfelt gratitude to Prof. Dr. Ziyou Gao of Beijing Jiaotong University, who assisted me in developing the research proposal. I've been less involved in the transportation field after earning a master's degree in computing mathematics. As my promotor, he suggested several technical courses to assist me in expanding my knowledge base. Besides, he offered an excellent opportunity for me to study abroad and pursue my second doctorate.

I'd also like to thank Prof. Dr. Harry Timmermans for his assistance. He supported me in regaining confidence in English speaking as a promoter at Eindhoven University of Technology. When I first came to the Netherlands, I struggled to communicate with my Dutch colleagues in English. When I met with Harry, he was very patient in encouraging me to speak English. Furthermore, he helped me in revising my journal papers and applying for a job.

Dr. Feixiong Liao is another person I'd like to thank. He has been a great help to me both academically and in my everyday life in the Netherlands as a co-promotor and friend. On the academic front, he was involved in almost every phase of my doctoral research, from the application for studying abroad to the revision of the graduation thesis. I recall him telling me "start with the end" and "just sit on the bench", which have inspired me to concentrate on my research. On the other side, he took me to see the sea of tulip flowers and explore the Dutch border. He also let me experience the speed of 180 km/h in Germany. These encounters helped me appreciate life in the Netherlands more.

In addition, I would like to thank my committee members, Prof. Dr. O. Nielsen (Technical University of Denmark), T.A. Arentze, and T. van Woensel, for their valuable comments and suggestions to my thesis.

My thanks also go to my colleagues in our group. Mandy van de Sande encouraged us to have fit breaks, helping me keep healthy and integrate into the group faster. Chatting with her always made me feel friendly. Peter van der Waerden Peter likes to joke. He can make a boring environment more energetic. Any reasonable request in the office can be satisfied by Marielle Kruizinga. Coffee time with Mercè let me know more about the foreign customs and life. The journey of Airbeat One Festival is the most unforgettable

memory in the Netherlands. Thanks to Chenyu, Mengru, Xiaochen, and Yajie, who made the trip more beautiful. Shangqi, Xueting, Wentao, and Zhengying made me no longer alone on my way home at noon. Jing, Xiaoyue, and I had endless complaints about the stupid agent. Talking with Bojing, Gaofeng, Jia, Pengyou, and Qiyao benefitted me in graduation and job application. Having parties with Hexin, Jiajia, Qianqian, Wensi, and Zhihui brought a lot of happiness. I also appreciate the company with Bilin, Chaoyu, Guangde, Juan, Jianfei, Marianna, Sunghoon, Seheon, Tao, Wen, and Xiaofeng. The members in up-study group, Feixiong, Jing (Lyu), Jing (Qin), Kang, Songpo, Xiaochen, and Yajie, let me feel at home during Chinese festivals and gave me lots of support.

Last but not least, I would like to thank my parents and elder sister. With their support, I can cope with the pressure of scientific research more efficiently. No distance can weaken my love for you.

Summary

Urban traffic network equilibrium models and algorithms have drawn much attention in transportation research. Their applications in network planning, transport policy evaluations, and traffic management face challenges to address rich behavior realisms responding to various supplies. This thesis aims to extend the existing urban traffic network equilibrium models and develop efficient solution algorithms based on column generation (CG) schemes.

First, a generalized mean-variance (GMV) metric is proposed for modeling route choice. Travel time uncertainty is unavoidable due to several factors (e.g., weather and congestion) and affects travelers' route choice behavior significantly. The proposed GMV metric has a more generalized form than those widely used metrics in the literature. It can capture the influence of travelers' on-time arrival probability and schedule delays on travelers' route choice simultaneously. With the GMV metric, a user equilibrium (GMVUE) is formulated as a finite-dimensional variational inequality (VI) problem. A CG-based solution algorithm is then developed for GMVUE problem. The results illustrate that different weight coefficients of the GMV metric result in different flow distribution at GMVUE state. With the classic CG technique, more than half OD pairs generate less than three paths at equilibrium.

Second, four tolerance-based strategies are proposed for extending the classic CG algorithm to the bounded rational dynamic user equilibrium model (BR-DUE). Due to the cognitive limitations, travelers may choose non-optimal paths and/or departure times. A tolerance-based minimum disutility path search strategy allows travelers seeking non-optimal paths and accelerates the CG algorithm by decreasing the size of the path sets. Convergence curves of equilibrium models usually become flat when the solutions approach the equilibrium state. Self-adjusted convergence threshold strategy adjusts the relative convergence threshold dynamically and can decrease the number of dynamic network loading during the intermediate iterations. From the temporal dimension, a varied temporal resolution strategy tries to assign flows to narrow time regions via exploration and exploitation processes. Path search skipping strategy performs path search only at potential time intervals and accelerates the CG algorithm by decreasing the number of the path searches. With these four strategies, the TBCG algorithm leads to significant computation time reductions without the expense of solution quality.

Third, the supply-demand dynamics under different first-come-first-served (FCFS) mechanisms are suggested and embedded into a BR-DUE problem. Car-sharing services (CSS) have received increasing attention in the passenger mobility sector. Understanding the complex relations between supply and demand of shared cars (SCs)

is a critical step in the evaluation of CSS deployment. However, most studies focused on the evaluation of the dynamic supplies. To capture the interactions between them, the supply-demand dynamics under four FCFS mechanisms are formulated, namely, No waiting FCFS (NW-FCFS), aggregate-FCFS (A-FCFS), disaggregate FCFS (D-FCFS) and the VIP membership D-FCFS (VD-FCFS). Theoretically, four mechanisms have the same supply-demand dynamics under some conditions. D-FCFS and VD-FCFS mechanisms lead to more efficient SC utilization rates compared with other two mechanisms. Based on the TBCG algorithm, an adaptive CG algorithm is proposed for the BR-DUE problem by incorporating a path expansion strategy. Numerical examples demonstrate that different FCFS mechanisms tend to have different supply-demand dynamics and that the disaggregate mechanisms are more efficient in satisfying the demand of shared cars.

Lastly, refined spatial-temporal exploration and exploitation strategies are suggested to the boundedly rational dynamic activity-travel assignment (BR-DATA) problems. BR-DATA endogenously integrates activity-travel scheduling and dynamic traffic assignment to determine the interaction between land use transport supplies and activity-travel demands of boundedly rational travelers. The combinatorial explosion of ATPs involving multi-dimensional choice facets poses severe challenges to the model applicability in large networks. The existing DATA problems were confined to small networks. Based on the TBCG algorithm, the spatial-temporal exploration and exploitation strategies are refined to solve the BR-DATA problem. The spatial exploration strategy modifies the tolerance-based minimum disutility path search strategy of TBCG algorithm and can search for the non-FIFO ATPs. Temporal exploration strategy uses a more flexible criterion to extend the current time regions. Regarding the spatial exploitation strategy, it adjusts the original lower bound of the relative convergence threshold. Combined with the temporal exploitation strategy, these strategies are proved that the solutions derived from the refined TBCG algorithm satisfy the BR-DATA user equilibrium condition. The numerical results demonstrate that the algorithm has solid scalability and has large gains in computation time without losing solution quality.

In sum, the proposed urban traffic network equilibrium models address various aspects of UE models covering STA, DTA, and DATA with the consideration of supply uncertainty, bounded rationality, emerging mobility services, and network scalability in the respective models. The spatial-temporal exploration and exploitation strategies are expected to have broad applications in dynamic traffic assignment problems.

Contents

List of Figures

List of Tables

1 Introduction

1.1 Travel demand analysis

The development of social economies and the expansion of urban scales have increased the intensity and scope of passenger mobility. The imbalance between the lagging urban mobility supply and increasing travel demand has resulted in severe urban traffic problems, such as traffic congestion, imbalance of parking supply and demand, traffic safety, emission, and energy consumption. Transportation planning, aiming to achieve sustainable transportation conditions, is becoming more and more important. Transportation forecasting and management, the keys to a successful transportation planning process, usually rely on the development of rigorous travel demand models. Over the past decades, the development of travel demand models has been gradually shifting from aggregate trip-based models (or so-called four-step models) to disaggregate activity-based models (ABMs) (Bhat and Koppelman, 1999; Liao, 2013; Rasouli and Timmermans, 2014; Chow and Nurumbetova, 2015; Yang, 2018).

The four-step models are best seen within the overall framework of transportation system analysis that positions travel demand and network performance procedures as determining flow patterns toward equilibrium with input from and feedback to network supplies (de Dios Ortúzar and Willumsen, 2011). As the name suggests, four-step models consist of trip generation, trip distribution, mode choice, and traffic assignment. Specifically, trip generation determines the number of trips generated and attracted by each traffic analysis zone. Trip distribution matches the number of exchange trips between traffic analysis zones. Mode choice concerns the proportion of trips between origins and destinations that use particular transportation modes. As the last step of these models, traffic assignment allocates the travel demand to different paths (routes) to

achieve a user equilibrium (UE) or system optimal state. If the time dimension is considered, the dynamic traffic assignment (DTA) is in place to replicate time-related traffic phenomena, such as queue formation, propagation, and dissipation (Lo and Szeto, 2002; Han et al., 2019). Four-step models are popularly applied for travel demand analyses due to the well-defined process. Moreover, the enrichment of survey techniques and computing software further promotes the wide use of the four-step models (Boyce et al., 1994; McNally, 2007; Yang, 2018). However, trip-based models focus on the long-term aggregate behavior of travelers and have some limitations, such as ignoring the spatial and temporal interrelationship of travelers' trip chains, misspecification of spatial and temporal decisions, and misspecification of travel behavior at the individual level (Mcnally et al., 2000). These deficiencies appear most prominent in the inability of conventional models to perform adequately in complex policy applications. Driven by emerging transportation policies and growing complexity in activity patterns, the focuses of travel demand analysis are shifting to microsimulation, disaggregate, ABMs.

ABM places primary emphasis on activity participation and aims to adopt a holistic framework to recognize the complex interactions in activity and travel behavior (Bhat and Koppelman, 1999; Mcnally et al., 2000; Rasouli and Timmermans, 2014). Consequently, it can represent how policies, developments, and travel demand growth impact people's travel behavior (Bhat and Lawton, 2000). Moreover, the improved modeling methodologies, computation capacity, and data collection methods have facilitated the explosion of the research about the ABMs. The theoretical concepts of ABMs have emerged since the 1970s (Chapin, 1974). Jones (1977) proposed a theory that travel is derived from the needs to participate in activities at different space-time destinations. In addition, the random utility maximization choice theory (McFadden, 1978) built the foundation of the approach to activity-travel behavior analysis. According to Rasouli and Timmermans (2014), ABMs can be categorized as constraints-based (e.g., Jones et al., 1983), econometrics-based (e.g., Bhat et al., 2004), or rule-based approach (e.g., Arentze and Timmermans, 2004). Over the past two decades, a great number of ABMs have been proposed to capture individuals' behaviors and improve realism (e.g., Zhang, 2006; Prato, 2009). Particularly, at the core of ABM, activity-travel scheduling problems have been proposed to address different choice facets (e.g., choice of mode, path, location, timing, duration, and activity sequence) of travel behavior involved in conducting an activity program (Bowman and Ben-Akiva, 2001; Arentze and Timmermans, 2004; Liao et al., 2017). Parallelly, additional considerations, such as activity-travel time uncertainty (Sun et al., 2005; Liao et al., 2014), intra-household interactions (Bhat and Pendyala, 2005; Ho and Mulley, 2015; Fu and Lam, 2018), and space-time constraint (Liao et al., 2013; Chow and Nurumbetova, 2015), have been considered to improve the realism.

1.2 Traffic network equilibrium models

User equilibrium (UE) traffic assignment has been an active area of transportation research for many years with most model developments motivated by Wardrop's first principle (Wardrop, 1952; Yang and Bell, 1998; Çolak et al., 2016). At the UE state, no user can decrease his/her costs by unilaterally shifting from one path to another. All-or-Nothing and Incremental Assignment (Fisk, 1980; Sheffi, 1985) are two classical methods to distribute the traffic flows in the network. These methods are deterministic in nature and assume that the drivers are perfectly rational and have complete knowledge of the network. Although the UE models fall short in giving a proper estimate for any arbitrary networks, these methods contribute to framing models that approximate the decision-making process of the drivers for path choice.

One class of methods that attempts to do multiple path assignments is stochastic user equilibrium (SUE). Daganzo and Sheffi (1977) generalized the UE principle and defined the SUE problem to account for uncertainty in travel costs. Since the late 1990s, SUE has attracted much research interest and been studied by incorporating different discrete choice models, such as multinomial logit models (Zhou et al., 2012; Rasmussen et al., 2015), the generalized extreme value type models, and logit kernel models (Wen and Koppelman, 2001; Bekhor et al., 2002). SUE models aim to model the variations in driver perceptions and are flexible enough to allow drivers to choose paths based on their different perceptions (Gupta, 2010). Unlike UE, these models do not assume the drivers to have complete knowledge of the network conditions.

To deal with travel time uncertainty, reliability-based user equilibrium (RUE) models quantify uncertainty by different metrics. All these metrics are derived from two different approaches, namely, the mean-variance approach and the scheduling approach. Jackson and Jucker (1982) proposed the mean-variance metric as the weighted sum of the mean and variance of travel time. Aligned with this effort, Lo et al. (2006) factored travelers' different risk attitudes according to their on-time arrival probabilities using the concept of travel time budget (TTB) for degradable transport networks. As another extension, Chen and Zhou (2010) took the conditional expectation of travel time beyond TTB into consideration and suggested a form of mean-excess travel time (METT) that combines a buffer time with the tardy time. Regarding the scheduling approach, Small (1982) first proposed the classic schedule delay concept based on Vickrey (1969), which has been extended to several cases. For instance, Noland and Small (1995) analyzed the effects of uncertain travel time and derived the optimized expected utility function for both a uniform and an exponential distribution of travel time. To allow for time-dependent travel time distributions, Bates et al. (2001) proposed another form for the expected utility function and argued that the mean-variance approach and scheduling approach are approximated for a wide range of distributions. The resultant RUE models can capture the influences of path risk attitudes on path choice behavior.

Evolved from UE, dynamic user equilibrium (DUE) models (Tong and Wong, 2000; Huang and Lam, 2002; Long et al., 2016) considered the time dimension to

enhance the realism of traffic flow propagation. The developments of DUE models came along with the simulation-based approaches and analytical approaches. Simulation-based approaches (Mahut and Florian, 2010; Ben-Akiva et al., 2010) focus on traffic dynamics and microscopic flow characteristics, while analytical approaches can be used to demonstrate different properties of models and their solutions. Furthermore, the analytical formulations include fixed-point problems (Szeto et al., 2011; Han et al., 2019), mathematical programming models (Daskin, 1985; Carey and Watling, 2012), nonlinear complementarity problems (Ban et al., 2008; Han et al., 2011), and variational inequality (VI) problems (Lo and Szeto, 2002; Friesz and Han, 2019).

DUE models assume that travelers have perfect knowledge of traffic conditions throughout the whole network and choose paths with the minimum disutilities. Nevertheless, this assumption is hard to be realized due to the cognitive limitations of travelers. Even if travelers have fully mastered the network information, they would still choose non-optimal paths and/or departure times due to factors such as habit and inertia. It is argued by Simon (1955, 1957) that people demonstrate bounded rationality (BR) behavior and seek satisfactory rather optimal solutions because of limited information and limited capability of processing information. In response, the BR of travelers or consumers has been incorporated in a number of traffic assignment models (Di and Liu, 2016). Incorporating departure time choice, Szeto and Lo (2006) introduced the tolerance-based DUE problem and discussed its solution characteristics. Based on this work, Han et al. (2015) developed a boundedly rational dynamic user equilibrium (BR-DUE) model with variable tolerances, of which the DUE and tolerance-based DUE are special cases. Solution existence and three computational algorithms were proposed based on the corresponding VI and differential VI formulations. BR has also been incorporated into process models to capture the day-to-day learning behavior and traffic flow dynamics (Guo and Liu, 2011; Wu et al., 2013). Di and Liu (2016) provided a comprehensive review of theoretical models and empirical evidence of path choice with BR and confirmed that travelers do not usually choose the paths with the shortest travel times or the lowest disutilities.

Dynamic activity-travel assignment (DATA) is an extension of the classical DTA in the ABM paradigm. The DATA is advantageous in that it simultaneously captures the spatial-temporal interdependencies in activity-travel chains of a long-time frame and determines the demand-supply interactions at a high level of detail. Whereas, many travel demand forecasting systems have integrated ABM and DTA exogenously (e.g., Lin et al., 2008; Auld et al., 2016; Yasmin et al., 2017; Xiong et al., 2018; Yang, 2018; Najmi et al., 2019) that tend to deliver inconsistent temporal activity-travel patterns (ATPs). The formalism of DATA overcomes this shortcoming by representing full ATPs in augmented networks. Along this line of work, Lam and Yin (2001) and Lam and Huang (2002) were among the earliest attempts to take into account departure time choice and time-dependent activity participation in DUE models. Subsequently, several models

explicitly incorporated full-day ATPs in the DUE formulations using time-expanded car-only networks (Ramadurai and Ukkusuri, 2010; Ouyang et al., 2011), PT-only networks (Li et al., 2010; Fu and Lam, 2014, 2018), and multimodal networks (Chow and Djavadian, 2015). Particularly, Liu et al. (2015) formulated DATA in multi-state supernetworks (SNKs) (Liao et al., 2010, 2011, 2012, 2013), which represent the state-of-the-art for representing multimodal multi-activity trip chains. To characterize the BR behavior of travelers, Li et al. (2018) proposed a tolerance-based DATA model. These DATA models are sensitive to a broad spectrum of land use transport policies.

Despite the appealing theoretical developments, most existing traffic network equilibrium models were analyzed on predefined path or ATP sets. For example, Szeto and Lo (2006) considered 6 paths in a 10-node network and pointed out the necessity of path generation as a future research direction. Han et al. (2015) selected 119 paths of the Sioux Falls (24-node) network to assess the suggested algorithms to the BR-DUE model. Li et al. (2018) enumerated 578 ATPs for two-class travelers from only two residential zones in the Nguyen-Dupuis network (13-node). Path or ATP enumeration may be possible for some transport networks of special topologies. However, the number of possible time-dependent paths may be too large even for small general networks in dynamic contexts, and path or ATP enumeration is almost impossible for larger networks. Therefore, a method of path generation rather than enumeration is needed.

1.3 Column generation algorithm

Column generation (CG), as a technique to circumvent path enumeration, has been widely applied to traffic network equilibrium problems. It should be noted that CG, as a decomposition scheme, has also been applied to solve large-scale optimization problems (e.g., Smilowitz et al., 2003; Qureshi et al., 2009), which is however beyond the scope of this thesis. Path search and network loading are the two most time-intensive components in the CG algorithm for traffic network equilibrium models.

Path search is an important problem in transportation research and applications. Dijkstra algorithm (Dijkstra, 1959) and its extensions are the most applied for shortest path searches in the literature. In static real road networks, Zhan and Noon (1998) provided an evaluation of 15 shortest path algorithms and concluded that one of the Dijkstra's implementations (e.g., Dijkstra, 1959; Fredman and Tarjan, 1987; Cormen et al., 2009) might be a worthwhile choice to find a one-to-one or one-to-some shortest path. Incorporating travel time reliability, Frank (1969) introduced the concept of reliable shortest path problem. The application of advanced traveler information systems accelerates the development of the reliable shortest path finding problem in the past 20 years (Miller-Hooks and Mahmassani, 2003; Nie and Wu, 2009; Chen et al., 2013; Srinivasan et al., 2014). The dynamic characteristics of traffic networks require more sophisticated approaches. Dean (2004a) presented the label-setting and label-correcting

algorithm and analyzed their theoretical properties in first-in-first-out (FIFO) networks. Considering waiting behavior, Dean (2004b) discussed several techniques for speeding up dynamic programming in time-varying networks. It should be noted that path search algorithms are also adapted to solving scheduling problems in ABMs (Ramadurai and Ukkusuri, 2011; Liao et al., 2013).

Dynamic network loading (DNL) models are designed to represent the propagation of traffic over time in traffic networks (Himpe et al., 2016). They can produce network performances such as queue length, saturation, time-varying travel speed, the location of bottlenecks, and queue formation/dissipation. DNL models can be broadly categorized as delay function models (Nie and Zhang, 2005), point-queue models (Huang and Lam, 2002), the cell transmission model (CTM) (Daganzo, 1997), the link transmission model (LTM) (Yperman, 2007), and continuum traffic flow models (Lighthill and Whitham, 1955), etc. Since performing DNL is a time- and memory-consuming task, a number of traffic assignment algorithms were proposed to reduce the number of DNL. For example, Lu et al. (2009) proposed a descent direction method and proved this method outperforms the method of successive average (MSA). Carey and Ge (2012) compared four algorithms and concluded that the route-swapping method (Smith and Wisten, 1995) and the simple projection method (Rubio-Ardanaz et al., 2003) converge faster than the MSA and the alternating direction method (Lo and Szeto, 2002). Long et al. (2013b) applied the extra-gradient method to the DUE problem.

The CG algorithm can generate paths in an iterative process by combining path searches and traffic assignments. As shown in Figure 1.1, the CG algorithm has been applied and developed for solving different traffic network equilibrium problems. For solving static traffic assignment (STA) problems, Leventhal et al. (1973) developed the seminal CG algorithm of path generation and analyzed the solution properties in general transport networks. Afterwards, as depicted by orange circles, many applications of this algorithmic scheme were focused on UE (Friesz, 1985; Larsson and Patriksson, 1992; Lo and Chen, 2000; Chen et al., 2001; Larsson et al., 2004; Florian et al., 2009; Ryu et al., 2014; Patriksson, 2015; Chen et al., 2020), RUE and SUE (Bell, 1995; Bell et al., 1997; Bekhor and Toledo, 2005; Chen et al., 2009, 2010; Nikolova and Stier-Moses, 2014; Paul et al., 2018; Gentile, 2018). Since 2000, researchers started to apply the CG algorithm to solve DUE problems (Han, 2000; Jang et al., 2005; Lu et al., 2009, 2013; Long et al., 2013b; Levin et al., 2015; Javani and Babazadeh, 2020) and their extensions (Zhou et al., 2008; Zhang, 2009; Zhang et al., 2013) (e.g., dynamic SUE (DSUE) and BR-DUE), which are marked with blue circles. The CG algorithm has also been applied in three studies of DATA problems (Ramadurai and Ukkusuri, 2011; Ouyang et al., 2011; Fu and Lam, 2018) (shown in purple circles), but the network sizes are relatively small. These applications do not modify the CG scheme in dynamic contexts.

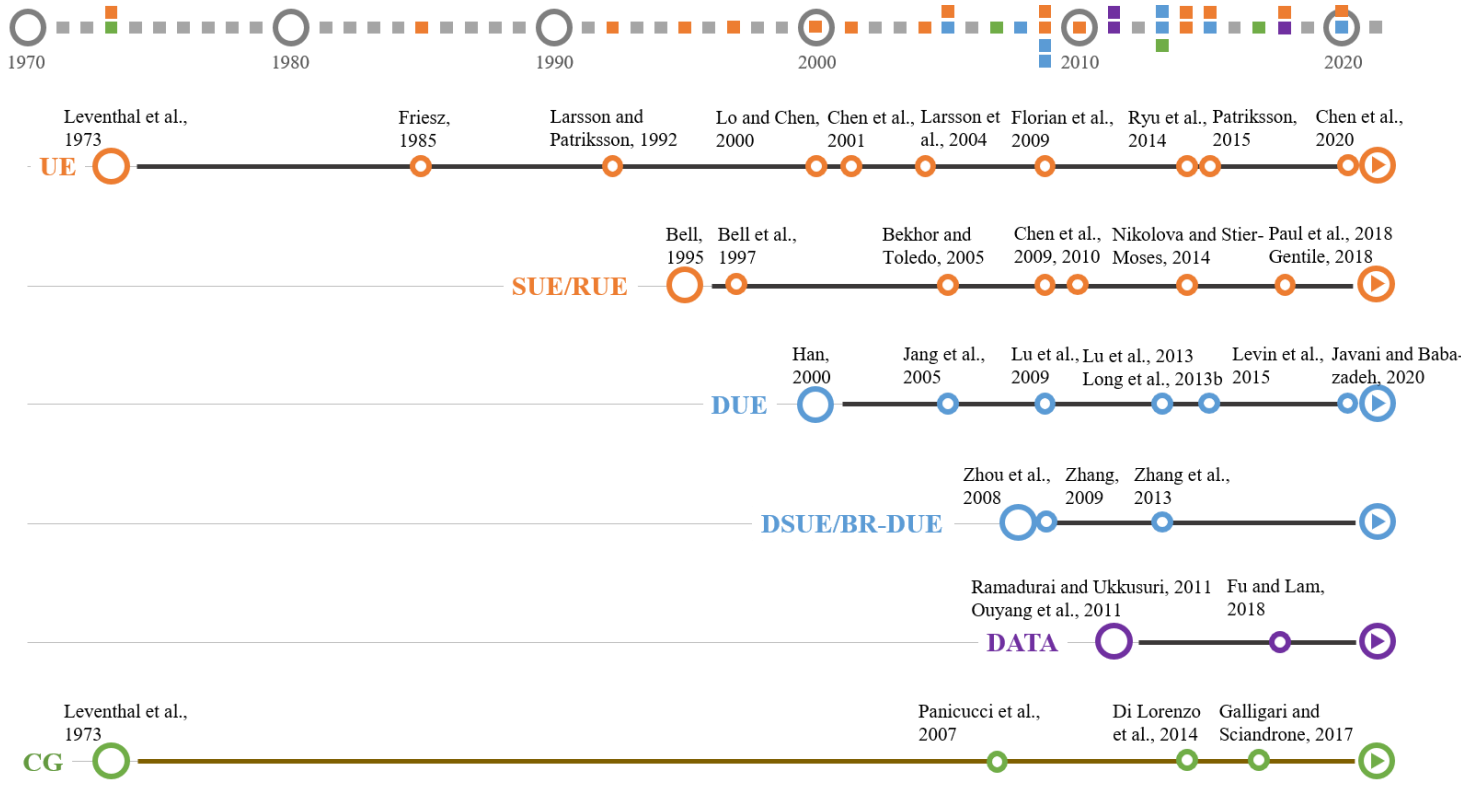

Figure 1.1 Representative studies with applications and developments of the CG.

Several strategies for balancing path search and network loading have been proposed in UE models to address large-scale transport networks (shown in green circles). Panicucci et al. (2007) suggested performing a CG procedure (path search) after a certain number of iterations rather than at every iteration. It is found that the best value of the iteration gap varies between 8 and 12. Aligned with this effort, Di Lorenzo et al. (2014) proved that the CG procedure must be applied within a prefixed number of iterations to guarantee convergence. The results of computational experiments illustrated that their proposed algorithm outperformed other algorithms. Based on this work, Galligari and Sciandrone (2017) designed a strategy adjusting the prefixed number for each origin and destination (OD) pair. This strategy yielded substantial computational time-savings, whilst retaining the global convergence property. However, these strategies are only limited to spatial paths.

1.4 Contributions and outline

This thesis embeds several travel behavior mechanisms and mobility services into network equilibrium models and develops advanced CG algorithms. First, to investigate the impact of travel time uncertainty on path choice behavior, the thesis proposes a generalized mean-variance (GMV) metric in the static context and applies an effective CG algorithm to solve the corresponding user equilibrium problem. Second, across the spatial and temporal dimensions, four tolerance-based strategies for extending the CG algorithm to the BR-DUE model are proposed by incorporating BR and dynamics. With these strategies, an efficient tolerance-based CG (TBCG) algorithm for BR-DUE is developed. Third, as emerging mobility services, one-way car-sharing services (CSS) are embedded in the BR-DUE problem with different first-come-first-served (FCFS) mechanisms. Algorithmically, a path expansion strategy congruently bridges the aggregate-disaggregate analyses and is incorporated in an adaptive CG algorithm. Lastly, several strategies of the TBCG algorithm are refined as spatial-temporal exploration and exploitation for solving boundedly rational dynamic activity-travel assignment (BR-DATA) problems in SNKs. The remainder of this thesis is organized as follows.

Chapter 2 provides the preliminary knowledge of path disutility, network equilibrium conditions, and the CG algorithm. The link and path travel times are first formulated in traffic networks. In the dynamic context, the path disutility is expressed as the weighted sum of path travel time, early or late arrival penalties. Then, UE, DUE, BR-DUE, and DATA user equilibrium conditions are expressed and the corresponding problems are formulated as VI problems. Besides, the properties of the existence and uniqueness of their solutions are analyzed. Lastly, the descriptions and run-time complexity of the CG algorithm are presented.

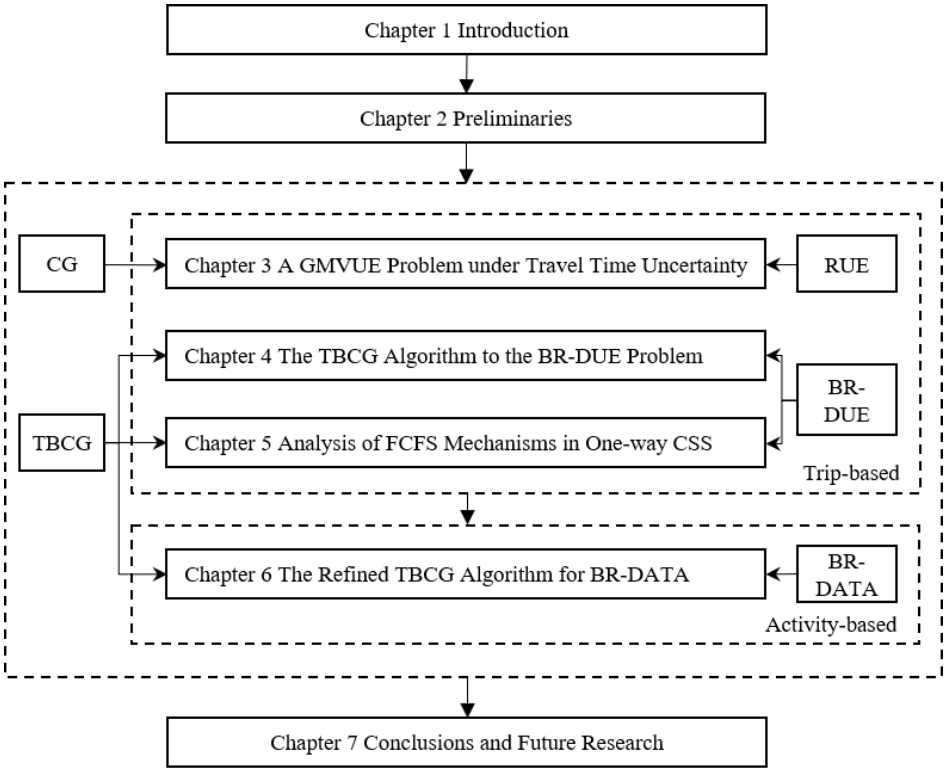

Figure 1.2 The structure of the thesis.

Chapter 3 investigates the impact of travel time uncertainty on path choice behavior in user equilibrium models based on a GMV metric. This model can capture the influence of risk attitudes and schedule unpunctuality on path choice using a generalization of expected travel time, variance, and expected early or late arrival penalties, of which travelers are assumed to minimize the GMV of trips considering a certain on-time arrival probability. This chapter establishes the properties of GMV and formulates the GMV-based user equilibrium (GMVUE) model as a VI problem, for which the existence and uniqueness of the solutions are also analyzed.

Chapter 4 proposes four tolerance-based strategies for extending the CG algorithm to the BR-DUE model. Specifically, (i) a tolerance-based minimum disutility path search strategy is developed to allow travelers seeking satisfactory paths; (ii) a self-adjusted convergence threshold strategy is applied for fast convergence at the intermediate iterations; (iii) a varied temporal resolution scheme, combining exploration and exploitation, is suggested to assign flows to narrow time regions rather than to the whole time horizon; and (iv) a path search skipping strategy is introduced by comparing the

lower bound of travel disutility and the minimum disutility between the OD pairs. With these strategies, an efficient TBCG algorithm for BR-DUE is developed.

Chapter 5 formulates the supply-demand dynamics of one-way CSS under different FCFS mechanisms and embeds them in a BR-DUE problem. Two disaggregate FCFS mechanisms are suggested to improve the utilization of shared cars given the same CSS supplies in the discrete-time domain. To accurately capture the choice of CSS in space and time, a path expansion strategy is proposed to cope with different waiting times under the disaggregate FCFS mechanisms. The path expansion strategy congruently bridges the aggregate-disaggregate analyses and is incorporated in an adaptive CG algorithm to solve the BR-DUE problem in a bi-modal supernetwork.

Chapter 6 refines the TBCG algorithm for solving BR-DATA problems in SNKs without ATP enumeration. The combinatorial explosion of ATPs involving multi-dimensional choice facets poses severe challenges to the model applicability in large networks. The proposed refined TBCG algorithm employs spatial-temporal exploration to allocate activity-travel flows only to potential ATPs in the intermediate assignment process. The spatial-temporal exploitation intensifies ATP generation and network loading, which results in fewer iterations and substantial speedups compared with the original CG algorithm. It is proved that the TBCG algorithm is capable of finding solutions that satisfy the BR-DATA user equilibrium conditions.

Finally, Chapter 7 concludes the thesis by discussing the main conclusions and the possible directions for future research.

2

Preliminaries

2.1 Introduction

Path travel time has been widely used as the subject of analysis in various traffic network equilibrium models (Lo and Szeto, 2002; Chen et al., 2011; Lu et al., 2013; Long et al., 2016) due to its appealing properties such as Lipschitz continuity, monotonicity, and differentiability with respect to traffic flow. Besides travel time, monetary cost, travel convenience, travel comfort, and travel safety are also important factors affecting travel behavior. Path disutility (or generalized travel cost) usually combines several factors in travel scheduling models.

User equilibrium (UE) or dynamic UE (DUE) state can be reached after long-term adaptations by assuming that path disutilities are continuous with respect to path flows and travelers choose paths with the minimum disutilities. As two extensions of the DUE state, dynamic activity-travel assignment (DATA) UE considers activity participation, and boundedly rational DUE (BR-DUE) takes bounded rationality (BR) behavior into consideration. For theoretical analysis, these equilibrium states are always formulated as different mathematical expressions. Algorithmically, the column generation (CG) algorithm provides an efficient framework for solving the network equilibrium models.

This chapter provides some preliminary knowledge about path disutility, UE and its extensions, and the CG algorithm. The remainder of this chapter is organized as follows. Section 2.2 provides the formulations of link travel time, path travel time, and path disutility. Section 2.3 introduces four different traffic network equilibrium conditions and the corresponding variational inequality (VI) problems. The properties of the solutions to these problems are also analyzed. Section 2.4 presents the flowchart of the traditional CG algorithm.

2.2 Path disutility

As a primary factor of trips, path travel time can be expressed as the sum of link travel times in the static context.

$$t_p^{rs}(\boldsymbol{f}) = t_{l_1}(\boldsymbol{f}) + t_{l_2}(\boldsymbol{f}) + \cdots + t_{l_m}(\boldsymbol{f}) \tag{2.1}$$

where $\boldsymbol{f}$ is the vector of f_p^{rs}, which denotes the path flow on path p of origin and destination (OD) pair rs; $l_1, l_2, \ldots, l_m$ are consecutive links of path $p = l_1$ - l_2 - ... - l_m; $t_p^{rs}(\boldsymbol{f})$ is the path travel time of p; $t_l(\boldsymbol{f})$ is the travel time on link l and can be calculated by the Bureau of Public Road (BPR) (U.S. Traffic assignment manual, 1964) link performance function

$$t_l(\boldsymbol{f}) = t_l^0 \left[1 + \beta_1 \left(\frac{u_l}{e_l}\right)^{\beta_2}\right], \ \ l \in A \tag{2.2}$$

where u_l, e_l and t_l^0 are the corresponding traffic flow, link capacity, and free-flow travel time respectively; β_1 and β_2 are deterministic parameters.

The link travel time changes over the time of the day. Combined with the time dimension, the path travel time can be calculated using the following nested function

$$t_p^{rs}(k, \boldsymbol{f}) = t_{l_1}(k, \boldsymbol{f}) + t_{l_2}\left(k + t_{l_1}, \boldsymbol{f}\right) + \cdots + t_{l_m}\left(k + t_{l_1} + \cdots + t_{l_{m-1}}, \boldsymbol{f}\right) \tag{2.3}$$

where k denotes a time interval. The notations is simplified as: $t_{l_1} = t_{l_1}(k, \boldsymbol{f})$, $t_{l_2} = t_{l_2}\left(k + t_{l_1}, \boldsymbol{f}\right)$, …, for short. To keep consistency, the notations attached with k refer to the same entities incurred by travelers departing during k. The link travel times associated with integer arrival time k are calculated by the following iterative function

$$t_l(k, \boldsymbol{f}) = \max\left\{t_l(k-1, \boldsymbol{f}) - 1 + \beta_3 \left(\frac{u_l(k)}{e_l}\right)^{\beta_4}, \ t_l^0\right\} \tag{2.4}$$

Eq. (2.4) is a generalized form of the point-queue travel time function (Liu et al., 2015). When β_3 and β_4 are equal to 1, the travel time function is a special case and equivalent to the one proposed by Huang and Lam (2002). The link travel time can also be obtained by a link travel time function (Nie and Zhang, 2005) or determined through different dynamic network loading methods, such as the cell transmission model (Daganzo, 1997) and the link transmission model (Yperman, 2007; Long et al., 2013b).

Besides travel time, monetary cost, and penalties of unpunctual trips are important considerations for trip scheduling. Travel cost is defined directly from the outcomes such as travel time and being early or late (Fosgerau et al., 2010). Travelers hold preferred arrival times (PATs) and incur early or late arrival penalties when the actual arrival times are less than or exceeding their PATs. Combined with the unpunctual penalties, the path disutility is calculated by a piecewise weighted sum as

$$c_p^{rs}(k,\boldsymbol{f})=\eta_1 t_p^{rs}(k,\boldsymbol{f})+\begin{cases}\eta_2\left[k^{rs*}-\kappa^{rs}-k-t_p^{rs}(k,\boldsymbol{f})\right] & \text{if } k+t_p^{rs}(k,\boldsymbol{f})<k^{rs*}-\kappa^{rs}\\ \eta_3\left[k+t_p^{rs}(k,\boldsymbol{f})-k^{rs*}-\kappa^{rs}\right] & \text{if } k+t_p^{rs}(k,\boldsymbol{f})>k^{rs*}+\kappa^{rs}\\ 0 & \text{otherwise}\end{cases} \tag{2.5}$$

where $c_p^{rs}(k,\boldsymbol{f})$ denotes the path disutility of p incurred by travelers departing during k for rs; η_1, η_2 and η_3 are the unit costs of travel time, early and late arrival time respectively. k^{rs*} is the PAT of travelers for rs; $[k^{rs*}-\kappa^{rs},\ k^{rs*}+\kappa^{rs}]$ is the indifferent band of arrival times without unpunctual penalties. Although this piecewise linear disutility function is not fully realistic but widely adopted in DUE models (Huang and Lam, 2002; Szeto and Lo, 2004; Han et al., 2011).

2.3 UE and its extensions

This subsection provides some preliminary knowledge about the UE, DUE, BR-DUE, and DATA problems.

2.3.1 UE conditions

According to Wardrop's first principle, the flow pattern at a UE state is stated as: for any OD pair, all used paths have equal path disutility, while the unused paths have equal or higher disutilities. Formally, the conditions can be expressed by a set of complementarity conditions:

$$\begin{aligned}&f_p^{rs*}\left[c_p^{rs}(\boldsymbol{f}^*)-c_{\min}^{rs}(\boldsymbol{f}^*)\right]=0,\\ &c_p^{rs}(\boldsymbol{f}^*)\geq c_{\min}^{rs}(\boldsymbol{f}^*),\end{aligned}\qquad \forall p\in P^{rs}, rs\in RS \tag{2.6}$$

where $\boldsymbol{f}$ attached with superscript "$*$" refers to a solution that fulfills the UE conditions; $c_{\min}^{rs}$ is the minimal disutility of OD pair rs; RS and P^{rs} are the sets of OD pairs and paths of rs respectively.

The demand of OD pair rs, Q^{rs}, is assumed fixed in this thesis. The UE problem is to find $\boldsymbol{f}$ such that Eq. (2.6) and the following demand conservation and non-negativity constraints are satisfied.

$$\sum_{p} f_p^{rs} = Q^{rs}, \forall p \in P^{rs}, rs \in RS \tag{2.7}$$

$$\boldsymbol{f} \geq 0 \tag{2.8}$$

The flow conservation Eq. (2.7) ensures that the demand of any OD pair is equal to the sum of the flows on all paths of the same OD pair. The UE problem Eqs. (2.6)-(2.8) can be formulated as a finite-dimensional VI problem VI($\boldsymbol{f}, \Omega_0$) to find a vector $\boldsymbol{f}^*$ such that

$$(\boldsymbol{f} - \boldsymbol{f}^*)^T \boldsymbol{c}(\boldsymbol{f}^*) \geq 0, \qquad \forall \boldsymbol{f} \in \Omega \tag{2.9}$$

$$\Omega_0 = \left\{ \boldsymbol{f} \mid \boldsymbol{f} \geq 0, \sum_{p \in P^{rs}} f_p^{rs} = Q^{rs}, \quad \forall\, rs \in RS \right\} \tag{2.10}$$

2.3.2 DUE conditions

DUE is an extension of the UE problem that aims to capture dynamic traffic flows and serves traffic operational management in the short-term. The DUE condition is stated as follows: for each OD pair at each time interval, the path disutilities experienced by travelers departing at the same time are equal and minimal. This condition is a dynamic version of Wardrop's first principle and implies that, at DUE, only those time-dependent paths between any OD pairs that have the minimal disutilities are used, and those paths that are not used must have disutilities higher than or equal to the minimal disutilities; in addition, no individual can reduce his/her path disutility by unilaterally adapting the departure time and path. Formally, it can be expressed as

$$c_p^{rs}(k, \boldsymbol{f}^*) \begin{cases} = c_{\min}^{rs}(\boldsymbol{f}^*) & \text{if } f_p^{rs*}(k) > 0 \\ \geq c_{\min}^{rs}(\boldsymbol{f}^*) & \text{if } f_p^{rs*}(k) = 0 \end{cases} \qquad \forall\, p \in P^{rs},\ rs \in RS,\ k \in K \tag{2.11}$$

where K is the set of all time intervals.

The DUE problem is to find $\boldsymbol{f}^*$ such that Eq. (2.11) and the following demand and non-negativity constraints are satisfied.

$$\sum_{p \in P^{rs}} \sum_{k \in K} f_p^{rs}(k) = Q^{rs} \quad \forall\, rs \in RS \tag{2.12}$$

$$f_p^{rs}(k) \geq 0 \quad \forall\, p \in P^{rs},\ rs \in RS,\ k \in K \tag{2.13}$$

The DUE problem Eqs. (2.11)-(2.13) can be formulated as a finite-dimensional VI problem VI$(\boldsymbol{f}, \Omega)$ to find a vector $\boldsymbol{f}^*$ such that

$$\sum_{rs \in RS} \sum_{p \in P^{rs}} \sum_{k \in K} c_p^{rs}(k, \boldsymbol{f}^*)\left[f_p^{rs}(k) - f_p^{rs*}(k)\right] \geq 0 \ \ \forall \boldsymbol{f} \in \Omega \tag{2.14}$$

$$\Omega = \left\{ \boldsymbol{f} \mid \boldsymbol{f} \geq 0, \sum_{p \in P^{rs}} \sum_{k \in K} f_p^{rs}(k) = Q^{rs}, \quad \forall\, rs \in RS \right\} \tag{2.15}$$

The existence and uniqueness of the solution for DUE depend on the relationship between the path disutility functions and the path flows. When the path disutility functions are continuous with path flows, the DUE problem has at least one solution, and this solution is unique when the Jacobian matrix of the path disutility functions is positive definite.

2.3.3 BR-DUE conditions

As aforementioned, BR-DUE models (Han et al., 2015) have attempted incorporating BR to reflect that travelers do not necessarily choose paths of the minimum disutilities. The condition of BR-DUE is stated as: for each OD pair at each time interval, the disutilities experienced by travelers departing at the same time are no larger than the minimum value plus a threshold. Formally, it can be expressed as $\forall p \in P^{rs}, rs \in RS,\ k \in K$

$$c_p^{rs}(k, \boldsymbol{f}^*) \begin{cases} \in [c_{\min}^{rs}(\boldsymbol{f}^*),\ c_{\min}^{rs}(\boldsymbol{f}^*) \cdot (1 + \varepsilon^{rs})], & \text{if } f_p^{rs*}(k) > 0 \\ \geq c_{\min}^{rs}(\boldsymbol{f}^*) \cdot (1 + \varepsilon^{rs}), & \text{if } f_p^{rs*}(k) = 0 \end{cases} \tag{2.16}$$

where ε^{rs} is the threshold of acceptable relative differences in the travel disutilities experienced by travelers of OD pair rs. It is obvious that Eq. (2.16) is equivalent to Eq. (2.11) when ε^{rs} equals zero, which means that the BR-DUE is a more general form. The BR-DUE problem can be formulated as a finite-dimensional VI problem VI$(\boldsymbol{f}, \Omega)$ (Han et al., 2015) to find a vector $\boldsymbol{f}^*$ such that

$$\sum_{rs \in RS} \sum_{p \in P^{rs}} \sum_{k \in K} \tilde{c}_p^{rs}(k, \boldsymbol{f}^*)\left[f_p^{rs}(k) - f_p^{rs*}(k)\right] \geq 0 \ \ \forall \boldsymbol{f} \in \Omega \tag{2.17}$$

$$\Omega = \left\{ \boldsymbol{f} \mid \boldsymbol{f} \geq 0, \sum_{p \in P^{rs}} \sum_{k \in K} f_p^{rs}(k) = Q^{rs}, \quad \forall\, rs \in RS \right\} \tag{2.18}$$

where $\tilde{c}_p^{rs}(k, \boldsymbol{f}^*)$ is formulated as follows

$$\tilde{c}_p^{rs}(k, \boldsymbol{f}^*) = \max\left\{c_p^{rs}(k, \boldsymbol{f}^*),\ c_{\min}^{rs}(\boldsymbol{f}^*) \cdot (1 + \varepsilon^{rs})\right\} \tag{2.19}$$

Han et al. (2015) pointed out that the existence of BR-DUE requires a mapping operator, which is a more general form of path disutility functions, to be continuous. This condition is weaker than the counterpart of DUE and the solutions are not unique. For the discrete time VI$(\boldsymbol{f}, \Omega)$ problem Eqs. (2.17)-(2.19), the analyses of the existence and non-uniqueness of the solutions are presented in Appendix 2.A.

2.3.4 DATA user equilibrium conditions

DATA couples daily activity-travel scheduling and dynamic traffic assignment (DTA) in a strong manner by directly assigning flows to activity-travel patterns (ATPs) in multi-state supernetworks (SNKs) (Liu et al., 2015). In a DATA model, travelers from the same home zone (a neighborhood in reality) are segmented by daily activity programs on an average day and classes in terms of preference differences. For the sake of convenience, travelers having the same activity programs and belonging to the same class are categorized as one class. An SNK is created for an OD pair in the DATA model for travelers who live in the same home zone and belong to the same class. Under the assumption that travelers have the full information and make activity-travel decisions to minimize ATP disutility, it is well-founded to claim that an activity-based DUE will be reached after long-term adaptations. The ATP flow patterns at equilibrium should satisfy the condition that the ATP disutilities experienced by travelers are equal and minimal for every combination of home zone and class. This condition implies that, at equilibrium, for a class of travelers at a home zone, the used ATPs have the minimum disutility and those unused ATPs should have disutilities higher than or equal to the minimum disutility. No traveler can reduce his/her ATP disutility by unilaterally adapting the ATP and departure time. Formally, the condition is expressed as

$$c_p^{ih}(k, \boldsymbol{f}^*) \begin{cases} = c_{\min}^{ih}(\boldsymbol{f}^*), & \text{if } f_p^{ih*}(k) > 0 \\ \geq c_{\min}^{ih}(\boldsymbol{f}^*), & \text{if } f_p^{ih*}(k) = 0 \end{cases} \qquad \forall\, p \in P^{ih}, i \in I, h \in H, k \in K \tag{2.20}$$

where $c_p^{ih}(k, \boldsymbol{f})$ is the disutility of ATP p incurred by travelers of class i at home zone h departing during time interval k, and $c_{\min}^{ih}(\boldsymbol{f})$ is the minimum disutility; $f_p^{ih}(k)$ denotes the flow on p by i at h that enters the network during k and $\boldsymbol{f}$ is the vector of $f_p^{ih}(k)$; P^{ih} and I re respectively the ATP set of i at h and the set of classes; H is the set of home zones.

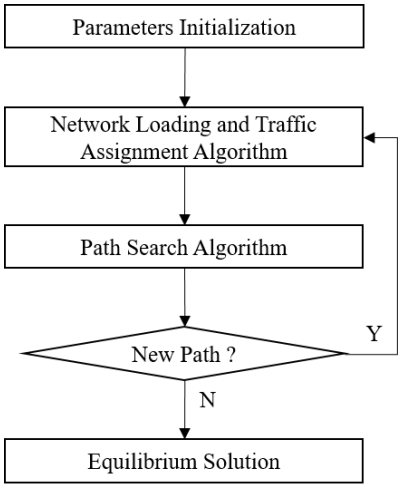

Figure 2.1 Flowchart of the traditional CG algorithm.

The DATA problem can be formulated as a finite-dimensional VI problem VI$(\boldsymbol{f}, \Omega)$ for finding a vector $\boldsymbol{f}^*$ such that

$$\sum_{i\in I}\sum_{h\in H}\sum_{p\in P^{ih}}\sum_{k\in K} c_p^{ih}(k,\boldsymbol{f}^*)\left[f_p^{ih}(k) - f_p^{ih*}(k)\right] \geq 0, \quad \forall \boldsymbol{f} \in \Omega \tag{2.21}$$

$$\Omega = \left\{ \boldsymbol{f} \mid \boldsymbol{f} \geq 0, \sum_{p\in P^{ih}}\sum_{k\in K} f_p^{ih}(k) = Q^{ih}, \quad \forall\, h \in H, i \in I \right\} \tag{2.22}$$

where Q^{ih} is the travel demand of class i at h.

The DATA problem has a similar VI formulation with the DUE problem. The conditions of existence and uniqueness of solutions depend on the relationship between the ATP disutilities and flows.

2.4 Column generation

To circumvent path enumeration, the CG algorithm has been embedded in the solution algorithms for the static traffic assignment (STA) and DTA problems. Specifically, at the initialization stage, a non-empty path set for each OD pair is created by the minimum disutility path search algorithms. Traffic assignment is performed on the path sets to create a snapshot of traffic flow realization, upon which new minimum disutility paths will be found and evaluated if being added to the path sets. This process is repeated until

no more new path can be found (Chen et al., 2001; Lu et al., 2009, 2016). The existing CG algorithms for STA and DTA have a similar skeleton, as shown in Figure 2.1. The CG algorithms for the DTA problem requires a higher magnitude of run-time complexities, which are $O(|N| \cdot |A| \cdot |K|)$ to conduct path searches and $O(\sum_{rs}|P^{rs}| \cdot |A'| \cdot |K| \cdot m_1)$ to load path flows at one iteration, where $|A'|$ is the maximum number of links in a path, m_1 is the number of dynamic network loadings, $|N|$, $|A|$, $|K|$ and $|P^{rs}|$ denote the numbers of elements in the corresponding sets. Despite effective, the majority CG algorithms for STA and DTA have followed a rigid structure and thus can be further improved by introducing self-adjustment in the process.

3

A GMVUE Problem under Travel Time Uncertainty*

3.1 Introduction

Travel time uncertainty can be accounted for from two different perspectives: supply degradations and travel demand fluctuations. Supply degradations fall within the category of exogenous sources and usually cause non-recurrent congestion, while demand fluctuations are regarded as endogenous factors and always lead to recurrent congestion (Lo et al., 2006; Li et al., 2008a; Chen and Zhou 2010; Li et al., 2011). Being the sources of travel time uncertainty, demand and supply aspects interact and affect travelers' path choice behavior significantly (Bates et al. 2001; Lam et al., 2008; Wang et al., 2014).

To capture the effects of travel time uncertainty on travelers' path choice behavior, travel time reliability (TTR) has been extensively studied. For example, Tilahun and Levinson (2010) used a computer-administered stated preference survey to estimate the value of TTR and explored the tradeoffs that travelers make for path choice. Woodard et al. (2017) stated that TTR strongly affects the desirability of paths in the road network. Moreover, various empirical studies (Li et al., 2010; Sweet and Chen 2011) have made a convincing proposition that TTR plays a key role in travelers' path choice behavior.

* This chapter is based on Wang, D., Liao, F., Gao, Z., Timmermans, H., 2020. A generalized mean-variance metric of route choice model under travel time uncertainty. Transportmetrica A: Transport Science, 1-30

To quantify TTR, various mean-variance approaches and scheduling approaches have been proposed with different metrics. For the mean-variance approach, based on travel time budget (TTB) and mean-excess travel time (METT), and several other models, Tan et al. (2014) examined the Pareto efficiency of traffic equilibria. Mean-standard deviation indifference curves were introduced to geometrically analyze the risk-taking behavior of travelers. Assuming that travelers want to minimize the mean and standard deviation of travel time, Wang et al. (2014) proposed a general TTR bi-objective user equilibrium (UE) model and proved that the model encompasses the single-objective of the TTB-UE model (Lo et al., 2006) and the late arrival penalized UE model (Watling, 2006). Regarding the scheduling approach, based on the "schedule delay" paradigm, Watling (2006) defined a new disutility function by adding a schedule delay term to the expected travel cost and developed a late arrival penalized UE model. Fosgerau and Karlström (2010) proved the equivalence of both approaches and derived that the preference parameters in the mean-variance approach depend on the parameters in the scheduling approach. Li and Hensher (2013) introduced a rank-dependent utility theory model and proposed an attribute-specific extension, where maximizing expected utility is a special case. In addition, several approaches based on alternative choice-making mechanisms, such as prospect theory and regret theory (Chorus 2012; Li and Huang 2017), were developed based on TTR.

To accommodate a variety of path risk attitudes, a generalized mean-variance (GMV) metric is proposed for path choice under travel time uncertainty in this chapter. GMV uses a form of 'generalized cost' structure with individual preferences for the associated terms. It can ensure a preferable on-time arrival probability and capture the influence of two mutually exclusive schedule delays on travelers' path choice. Three special forms of GMV are presented and the continuity and monotonicity are proved, which were only assumed in the previous studies. Due to the non-additivity of GMV, two dominance conditions are developed for finding the reliable shortest path. Moreover, a GMVUE problem is formulated as a variational inequality (VI) problem and solved by an effective traffic assignment algorithm with the column generation (CG) technique.

The remainder of this chapter is organized as follows. Section 3.2 provides the preliminary knowledge of path choice under travel time uncertainty. Section 3.3 introduces the GMV metric and analyses the corresponding UE model. The properties of GMV are also presented and analyzed. Section 3.4 develops a GMV-based traffic assignment algorithm for solving the GMVUE problem. Numerical examples are given in Section 3.5. Finally, conclusions are provided.

3.2 Preliminaries

This section provides some preliminary knowledge of path choice under travel time uncertainty in a transport network $G(N, A)$ composed of node set N and link set A.

3.2.1 Link and path travel time distribution

Based on the Bureau of Public Road (BPR) link function (Eq. (2.2)), the relationship between traffic flow and travel time due to supply degradations (Lo et al., 2006) can be established by

$$T_l(u_l,\, W_l) = t_l^0\left[1 + \beta_1\left(\frac{u_l}{W_l}\right)^{\beta_2}\right],\ \ l \in A \tag{3.1}$$

where T_l is the random travel time of link l; W_l is the corresponding random link capacity after degradation.

By assuming that W_l is independent of u_l and follows a uniform distribution, (Lo et al., 2006) analytically derived the mean μ_l and standard deviation (SD) σ_l of T_l as follows

$$\mu_l = E(T_l) = t_l^0 + \beta_1 t_l^0 u_l^{\beta_2}\frac{1-\theta_l^{1-\beta_2}}{\bar{c}_l^{\beta_2}(1-\theta_l)(1-\beta_2)}, \qquad \forall l \in A \tag{3.2}$$

$$\sigma_l = \sqrt{Var(T_l)} = \sqrt{\beta_1^2 (t_l^0)^2 u_l^{2\beta_2}\left\{\frac{1-\theta_l^{1-2\beta_2}}{\bar{c}_l^{2\beta_2}(1-\theta_l)(1-2\beta_2)} - \left[\frac{1-\theta_l^{1-\beta_2}}{\bar{c}_l^{\beta_2}(1-\theta_l)(1-\beta_2)}\right]^2\right\}}, \forall l \in A \tag{3.3}$$

where $\bar{c}_l^{\beta_2}$ and $\theta_l \bar{c}_l^{\beta_2}$ are the upper and lower bounds of the uniform distribution, respectively.

By assuming that link travel times are statistically independent, the travel time T_p of path p is the sum of related link travel times along p, and the mean and SD of T_p can be represented respectively as

$$\mu_p = E(T_p) = \sum_{l \in A} \mu_l x_{lp},\ \ \forall p \in P^{rs} \tag{3.4}$$

$$\sigma_p = \sqrt{Var(T_p)} = \sqrt{\sum_{l \in A} \sigma_l^2 x_{lp}},\ \ \forall p \in P^{rs} \tag{3.5}$$

where x_{lp} is a 0-1 variable regarding the link-path incidence relationship. $x_{lp} = 1$ denotes that link l is on path p, and $x_{lp} = 0$ otherwise.

Under the above assumptions, when those independent link travel times are added, the path travel time tends to be normally distributed according to the Central Limit Theorem even if the link travel times are not. Thus,

$$T_p \sim N\left(\mu_p, \sigma_p^2\right), \ \ \forall p \in P^{rs} \tag{3.6}$$

The Central Limit Theorem is applicable when a path contains many links. The assumptions of mutually independent and normally distributed link travel times or disutilities offer an alternative (Yin et al., 2004; Fu and Lam 2014), which leads to the normal distribution of path travel times or disutilities. To relax the assumptions, for example, Seshadri and Srinivasan (2017) relaxed the independence assumption in a robust traffic assignment model. Still, these assumptions are widely adopted due to the simplicity and analytic properties for path choice, network design, and land use modeling (Li et al. 2008a; Chen et al. 2013; Tan et al., 2014; Liao et al., 2014; de Jong and Bliemer 2015; Sun et al., 2018; Chen et al., 2018).

3.2.2 Travel time budget and mean-excess travel time

Lo et al. (2006) introduced the concept of TTB to relate travel time variability due to stochastic link capacity variations to travelers' risk-averse path choice behavior as

$$\xi_p(\alpha) = E\left(T_p\right) + \gamma(\alpha)\sqrt{Var\left(T_p\right)} = \mu_p + \gamma(\alpha)\sigma_p, \ \ \forall p \in P^{rs} \tag{3.7}$$

where $\xi_p(\alpha)$ is the TTB of path p required to ensure on-time arrival at confidence level α, and $\gamma(\alpha)$ is a parameter for describing the requirement of punctual arrival. A larger value of α corresponds to a larger $\gamma(\alpha)$. The value of $\xi_p(\alpha)$ can be expressed in relation to on-time arrival probability α:

$$P\left(T_p \leq \xi_p(\alpha)\right) = Y\left(\xi_p(\alpha)\right) = \alpha, \ \ \forall p \in P^{rs} \tag{3.8}$$

where $Y(\cdot)$ denotes the cumulative distribution function (CDF) of T_p. Let $X(\cdot)$ be the CDF of the standard normal distribution. Substituting Eq. (3.7) into Eq. (3.8) gives

$$\gamma(\alpha) = X^{-1}(\alpha) \tag{3.9}$$

Alternatively, Shao et al. (2006) assumed that the travel time variations are deduced from the daily demand variations, which follow a normal distribution. Based on the Central Limit Theorem, they concluded that the path travel time followed a normal

distribution and derived the formulation of TTB. Both formulations were developed by applying the Central Limit Theorem with the assumption of independent link travel times.

To capture the unreliability aspects of travel time variability, Chen and Zhou (2010) considered the tardy time and formulated METT as the following equation.

$$ð_p(\alpha) = \xi_p(\alpha) + E(T_p - \xi_p(\alpha)|T_p \geq \xi_p(\alpha)), \ \ \forall p \in P^{rs} \tag{3.10}$$

3.3 Formulation

This section first formulates a GMV metric and analyses its properties. Next, the corresponding UE model (GMVUE) and VI formulation are proposed.

3.3.1 Generalized mean-variance metric

Under travel time uncertainty, mean travel time (MTT), and travel time variance are two important components affecting travelers' choices. Travelers with different preferable on-time arrival probabilities have different attitudes toward travel time variability. For example, risk-averse travelers with a large on-time arrival probability perceive that travel time uncertainty will lead to a high penalty, and they may pre-assign a larger travel time for their trips. However, the early and late trips are undesirable but unavoidable in reality. To quantify travel time variability, a GMV metric is expressed as

$$c_p^{rs}=\omega_1\cdot\mu_p+\left[\omega_2(\alpha)\cdot E\left(T_p-\xi_p(\alpha)\right)^- \perp \omega_3(\alpha)\cdot E\left(T_p-\xi_p(\alpha)\right)^+\right]+\omega_4(\alpha)\cdot\sigma_p \tag{3.11}$$

where $\left(T_p-\xi_p(\alpha)\right)^-$ is the early arrival time defined as $\max\left(0,\xi_p(\alpha)-T_p\right)$; $\left(T_p-\xi_p(\alpha)\right)^+$ is the late arrival time defined as $\max\left(0,T_p-\xi_p(\alpha)\right)$; $\perp$ is an operator to denote that one and only one component of the two sides is effective; ω_1, $\omega_2(\alpha)$, $\omega_3(\alpha)$ and $\omega_4(\alpha)$ are collective weight coefficients, and $\omega_i(\alpha)$ $(i=2,3,4)$ denotes a preference parameter related to α.

Imposing a constraint $\omega_2(\alpha)\cdot\omega_3(\alpha)=0$, Eq. (3.11) is reduced to

$$c_p^{rs}=\omega_1\cdot\mu_p+\omega_2(\alpha)\cdot E\left(T_p-\xi_p(\alpha)\right)^- +\omega_3(\alpha)\cdot E\left(T_p-\xi_p(\alpha)\right)^+ +\omega_4(\alpha)\cdot\sigma_p \tag{3.12}$$

Setting aside the weight coefficients, the first term in Eq. (3.12) is the expectation of path travel time. It reflects the value of the average travel time within a long-time frame. The second term is the expected travel cost related to early arrival, which can be

seen as the opportunity cost of interrupting the prior trip. The third term is the expected travel cost of being late, seen as the opportunity cost of interrupting the current trip. The last term is the safety margin, which captures the sensitivity to path travel time dispersion.

Regarding the weight coefficients, ω_1 and $\omega_4(\alpha)$ are used to capture the degree of importance of MTT and variance to GMV. $\omega_4(\alpha)$ is set equal $\omega_1\gamma(\alpha)$ in this chapter to illustrate travelers' different risk attitudes toward travel time uncertainty unless otherwise specified. $\omega_2(\alpha)$ (≤ 0) and $\omega_3(\alpha)$ (≥ 0) are parameters to indicate the degrees of attitude toward the early and late arrivals.

Taken together, Lo et al. (2006) used the sum of the first and fourth terms represents the TTB to captures the "reliability aspect" (i.e., travelers arrive at the destination with a travel time less than or equal to the TTB). However, travelers may still arrive late with a probability $(1-\alpha)$, as shown by the red area in Figure 3.1. Therefore, Chen and Zhou (2010) introduced an additional term "$\omega_3(\alpha)\cdot E\left(T_p-\xi_p(\alpha)\right)^+$" to represent an additional safety margin, which is the mean late arrival time beyond the TTB. The proposed METT is the conditional expectation of the late trips (red area) and used to capture the estimation of travel time for risk-averse travelers. Alternatively, the second term "$\omega_2(\alpha)\cdot E\left(T_p-\xi_p(\alpha)\right)^-$" can be seen as the opportunity cost and used to hedge against early arrival. Mean-less travel time (MLTT) is the conditional expectation of the early trips (green area) for risk-prone travelers. Note that early and late arrivals are mutually exclusive, the operator $\perp$ in Eq. (3.11) and the condition $\omega_2(\alpha)\cdot\omega_3(\alpha)=0$ of Eq. (3.12) are used to represent either early or late arrival. The statements and extensions are expressed by the following remark.

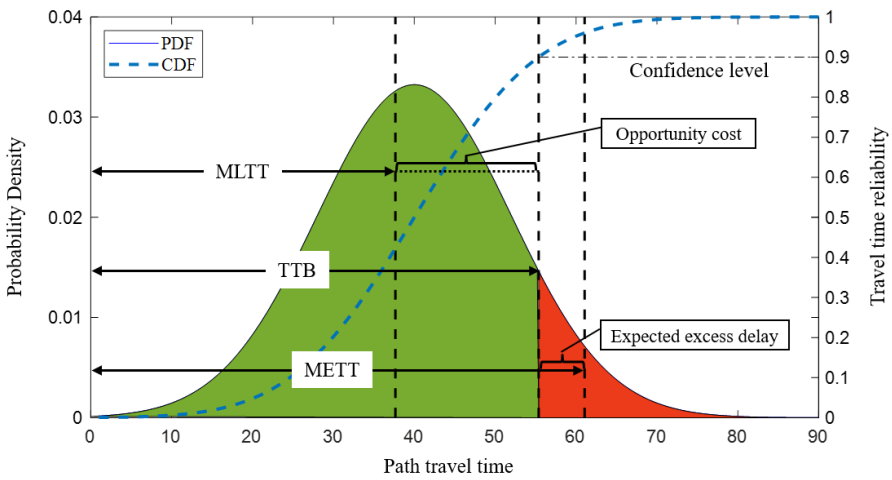

Figure 3.1 Illustration of relationships among MLTT, TTB, and METT.

Remark 3.1 GMV is a generalized mean-variance metric for path choice under travel time uncertainty:

(i) GMV is equivalent to the MTT (Hall, 1986) when travelers only concentrate on expected travel time, i.e., $\omega_1 = 1$ and $\omega_2(\alpha) = \omega_3(\alpha) = \omega_4(\alpha) = 0$.

(ii) GMV is equivalent to TTB (Lo et al., 2006) when travelers factor expected travel time and variance into their path choice decision, i.e., $\omega_1 = 1$, $\omega_2(\alpha) = \omega_3(\alpha) = 0$ and $\omega_4(\alpha) = \gamma(\alpha)$.

(iii) GMV is equivalent to METT (Chen and Zhou 2010) when travelers factor the reliable aspect of travel time variability (defined by TTB) and the unreliable aspect with the proportion of $\frac{1}{1-\alpha}$ into path choice decision, i.e., $\omega_1 = 1$, $\omega_2(\alpha) = 0$, $\omega_3(\alpha) = \frac{1}{1-\alpha}$ and $\omega_4(\alpha) = \gamma(\alpha)$.

(iv) GMV is equivalent to MLTT when travelers factor TTB and the early arrival with the proportion of $-\frac{1}{\alpha}$ into path choice decision, i.e., $\omega_1 = 1$, $\omega_2(\alpha) = -\frac{1}{\alpha}$, $\omega_3(\alpha) = 0$ and $\omega_4(\alpha) = \gamma(\alpha)$.

Proof. See Appendix 3.A.

As illustrated above, MTT, TTB, MLTT, and METT are four special cases of GMV. Since TTB and METT were developed by applying the Central Limit Theorem, this chapter uses the same theorem.

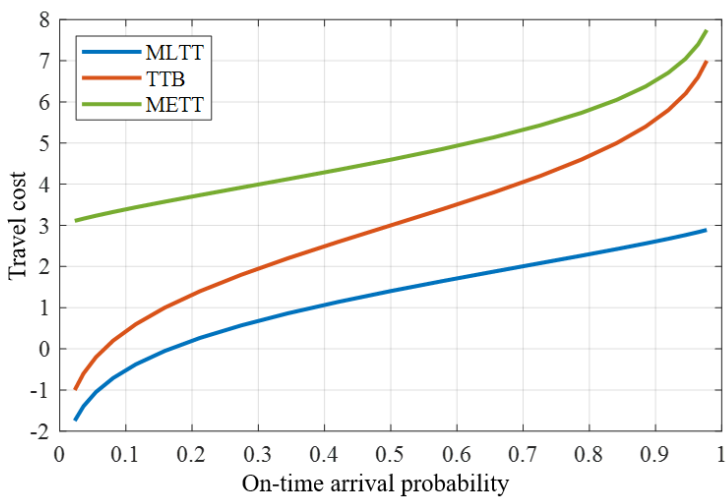

Figure 3.2 Monotonicity of MLTT, TTB, and METT.

3.3.2 Properties of GMV

Understanding the relationship between GMV and the value components, such as on-time arrival probability, expected travel time, and SD, is important for evaluating the path alternatives. Following the widely assumed condition that path travel times are normally distributed, continuity and monotonicity of GMV are obtained below.

Proposition 3.1 (Continuity and monotonicity)

(a) GMV (Eq. (3.12)) is continuous with α.

(b) TTB, METT, and MLTT, three different forms of GMV, are monotonically increasing with α.

Proof. See Appendix 3.B.

Although Proposition 3.1 is proved by assuming normally distributed path travel times, it can be easily obtained that the property of continuity is guaranteed with any other continuous distributions. For the monotonicity, as depicted by Figure 3.2, MLTT, TTB, and METT are increasing with the increase of on-time arrival probability. The late arrival coefficient $\omega_3(\alpha)$ of METT has a steep increase, which leads to that the value of METT (green curve) increases rapidly when α approaches 1. Whereas, the value of MLTT (blue curve) increases rapidly when α is very small.

Corollary 3.1 GMV is non-additive, i.e., the path GMV is not necessarily the sum of the associated link GMVs.

Proof. Based on Remark 3.1 (ii, iii), TTB and METT are two special cases of GMV. GMV is non-additive because of the non-additivity of TTB and METT. □

The non-additivity of GMV leads to the violation of Bellman's Principle of Optimality (Bellman, 1958) and disallows the application of classical shortest pathfinding algorithms to search for the minimal GMV path. Dominance-based methods (Chen et al. 2013) provide a straightforward way to overcome the non-additive property for solving the reliable shortest path problem. Inspired by their work, the following GMV-based dominance definitions and conditions are proposed.

Definition 3.1 Let $p_1^{rj} = p_1^{ri} \oplus p^{ij}$ and $p_2^{rj} = p_2^{ri} \oplus p^{ij}$ be two paths from node r to j with the same sub-path p^{ij}; p_1^{ri} GMV-based dominates p_2^{ri} (denoted by $p_1^{ri} \succ p_2^{ri}$) if and only if $u_1^{rj} < u_2^{rj}$ for any path $p^{ij} \in P^{ij}$ and any node $j \in N$, where $\oplus$ is a path concatenation operator.

Definition 3.2 A path $p_1^{ri} \in P^{ri}$ is a GMV-based non-dominated path, if and only if p_1^{ri} is not dominated by any other path $p_2^{ri} \in P^{ri}$.

Based on Definition 3.1 and 3.2, the GMV-based principle of optimality is presented as follows.

Corollary 3.2 A sub-path of any GMV-based non-dominated path must be a GMV-based non-dominated path itself.

Proof. "Reduction to absurdity" is applied to prove this corollary. Suppose p_2^{ri} is a sub-path of a GMV-based non-dominated path $p_2^{rj} = p_2^{ri} \oplus p^{ij}$ and $p_1^{ri} \succ p_2^{ri}$. Let $p_1^{ra} = p_1^{ri} \oplus p^{ia}$ and $p_2^{ra} = p_2^{ri} \oplus p^{ia}$, then $c_1^{ra} < c_2^{ra}$ for any path $p^{ia} \in P^{ia}$ and any node $a \in N$ according to Definition 3.1. It is reasonable to assume that $p^{ia} = p^{ij} \oplus p^{ja}$, where p^{ja} denotes any path from node j to a. Thus, $p_1^{ra} = (p_1^{ri} \oplus p^{ij}) \oplus p^{ja}$, $p_2^{ra} = (p_2^{ri} \oplus p^{ij}) \oplus p^{ja}$, and $c_1^{ra} < c_2^{ra}$ for any path $p^{jh} \in P^{jh}$ and any node $a \in N$. In other words, $(p_1^{ri} \oplus p^{ij}) \succ (p_2^{ri} \oplus p^{ij}) = p_2^{rj}$. This contradicts the precondition that p_2^{rj} is a GMV-based non-dominated path. □

Corollary 3.3 The path with the minimal GMV is a GMV-based non-dominated path.

This corollary, combined with Corollary 3.2, can be used to find the path with the minimal GMV. From an origin, the GMV-based non-dominated sub-paths are stored and extended until the destination is reached. To determine GMV-based non-dominated paths in a transport network under uncertainty, mean-variance (M-V) dominance and mean-GMV (M-GMV) dominance are proposed as follows.

Proposition 3.2 (M-V dominance) Given α and two different paths, p_1^{ri} and p_2^{ri}, of path set P^{ri}, $p_1^{ri} \succ p_2^{ri}$ if p_1^{ri} and p_2^{ri} satisfy either

(a) $\mu_1^{ri} \leq \mu_2^{ri}$ and $z\sigma_1^{ri} < z\sigma_2^{ri}$ or
(b) $\mu_1^{ri} < \mu_2^{ri}$ and $z\sigma_1^{ri} \leq z\sigma_2^{ri}$

where $z = \omega_1\gamma(\alpha) + \omega_2(\alpha)\alpha\gamma(\alpha) - \omega_3(\alpha)(1-\alpha)\gamma(\alpha) + \frac{\omega_2(\alpha)+\omega_3(\alpha)}{\sqrt{2\pi}} e^{-\left(\frac{\gamma(\alpha)}{\sqrt{2}}\right)^2}$.

Proof. See Appendix 3.C.

Proposition 3.3 (M-GMV dominance) Given α and two different path $p_1^{ri}, p_2^{ri} \in P^{ri}$, $p_1^{ri} \succ p_2^{ri}$ if p_1^{ri} and p_2^{ri} satisfy $\mu_1^{ri} \leq \mu_2^{ri}$ and $c_1^{ri} < c_2^{ri}$.

Proof. See Appendix 3.C.

Note that the M-V dominance identified in Proposition 3.3 is different from the counterpart in Chen et al. (2013), in which z is equal to $\gamma(\alpha)$. In addition, the M-GMV dominance is more effective for identifying the GMV-based non-dominated paths as stated by Proposition 3.4.

Proposition 3.4 Given p_1^{ri} and p_2^{ri}, if p_1^{ri} M-V dominates p_2^{ri}, then p_1^{ri} M-GMV dominates p_2^{ri}.

Proof. When $\mu_1^{ri} \leq \mu_2^{ri}$ and $z\sigma_1^{ri} < z\sigma_2^{ri}$, $c_1^{ri} - c_2^{ri} = \omega_1(\mu_1^{ri} - \mu_2^{ri}) + (z\sigma_1^{ri} - z\sigma_2^{ri}) < 0$. When $\mu_1^{ri} < \mu_2^{ri}$ and $z\sigma_1^{ri} \leq z\sigma_2^{ri}$, $c_1^{ri} - c_2^{ri} = \omega_1(\mu_1^{ri} - \mu_2^{ri}) + (z\sigma_1^{ri} - z\sigma_2^{ri}) < 0$. Therefore, p_1^{ri} M-GMV dominates p_2^{ri} according to Proposition 3.3. □

Based on this proposition, some GMV-based dominated paths that are not identified under the M-V dominance condition can be discarded when searching the minimal GMV path. This conclusion contributes to speeding up the path search process.

3.3.3 Illustrative example

Figure 3.3 depicts a network with one origin and destination (OD) (1, 6) to illustrate the different outcomes of TTB, METT, and MLTT. All link travel times are assumed to be normally distributed and independent with each other. The means and SDs are attached to the respective links. Suppose all travelers are risk-averse and use the same confidence level of on-time arrival probability $\alpha = 0.8$.

According to Remark 3.1 (ii-iv), TTB, METT, and MLTT are obtained by setting weight coefficients as $[1, 0, 0, \gamma(\alpha)]$, $[1, 0, 1/(1-\alpha), \gamma(\alpha)]$ and $[1, -1/\alpha, 0, \gamma(\alpha)]$ respectively. Figure 3.4 provides the comparison results, where the x-axis represents the three path choice metrics, and the y-axis represents the corresponding values. It is postulated that travelers search for paths with optimal values according to certain metrics. As shown, different path choice metrics lead to different optimal paths. For example, to avoid late arrival, travelers would add a safety margin to ensure their predetermined on-time arrival probability and choose path 3 with the minimal TTB (11.85). Besides the mean-variance of path travel time, travelers may budget their travel costs based on the expected travel delay cost, for which METT includes the expected excess delay beyond the TTB. Thus, travelers would switch to path 1 to decrease the expected excess delay. When travelers use MLTT as the metric, based on the last group of bars in Figure 3.4, path 1 is no longer the optimal choice, and travelers would switch to path 4. Similar to TTB and METT, MLTT is non-additive. For example, considering path 3 (consisting of links (1, 5) and (5, 6)), the MLTTs on links (1, 5) and (5, 6) are 2.53 and 2.97 respectively according to Eq. (3.12), but path 3 has a larger MLTT, i.e., 5.82 (greater than the sum of 2.53 and 2.97).

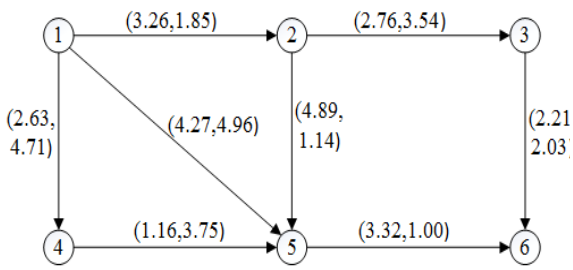

Path NO.	Node sequence
1	1 – 2 – 3 – 6
2	1 – 2 – 5 – 6
3	1 – 5 – 6
4	1 – 4 – 5 – 6

Figure 3.3 A simple network for illustrating different path choice metrics.

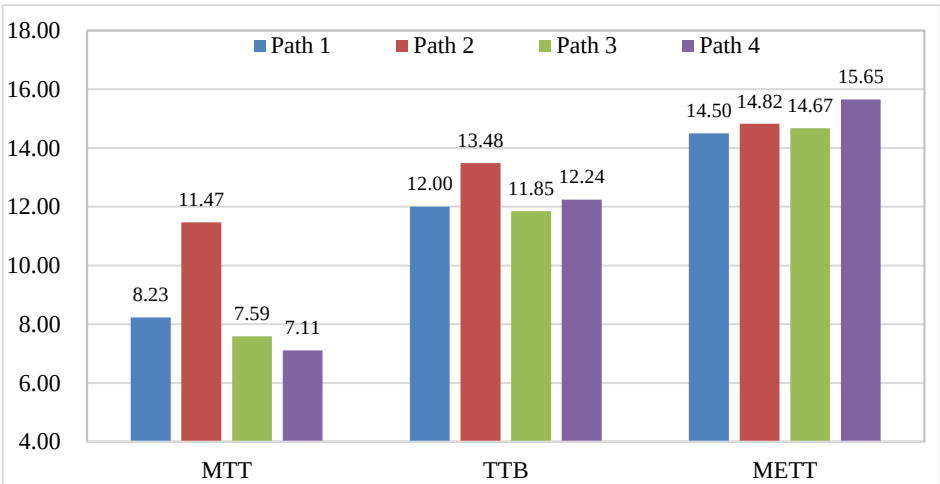

Figure 3.4 The results of different path choice metrics.

3.3.4 Path-based user equilibrium

The path-based approaches have become more common recently in networks with non-additive link travel costs. In combination, the CG technique (Leventhal et al., 1973) makes it possible to address large-scale networks. This chapter proposes a path-based user equilibrium model based on GMV. It is assumed that travelers aim to minimize GMV to accomplish their trips in traffic networks under uncertainty, and the GMV-based UE (GMVUE) is reached after long-term adaptations. The flow pattern at equilibrium is stated as: for any OD pair, all the used paths have equal GMV, while the unused paths have equal or higher GMVs. Formally, the conditions can be expressed by a set of complementarity conditions:

$$\begin{aligned} & f_p^{rs*}\left[c_p^{rs}(\boldsymbol{f}^*) - c_{\min}^{rs}(\boldsymbol{f}^*)\right] = 0, \\ & c_p^{rs}(\boldsymbol{f}^*) \geq c_{\min}^{rs}(\boldsymbol{f}^*), \end{aligned} \quad \forall p \in P^{rs}, rs \in RS \tag{3.13}$$

Under constraints Eqs. (2.7) and (2.8), the GMVUE problem Eq. (3.13) can be formulated as a finite-dimensional VI problem $\mathrm{VI}(\boldsymbol{f}, \Omega_0)$ to find a vector $\boldsymbol{f}^*$ such that

$$(\boldsymbol{f} - \boldsymbol{f}^*)^T \boldsymbol{c}(\boldsymbol{f}^*) \geq 0, \qquad \forall \boldsymbol{f} \in \Omega_0 \tag{3.14}$$

$$\Omega_0 = \left\{ \boldsymbol{f} \mid \boldsymbol{f} \geq 0, \sum_{p \in P^{rs}} f_p^{rs} = Q^{rs}, \quad \forall\, rs \in RS \right\} \tag{3.15}$$

Proposition 3.5 According to Chen and Zhou (2010), given that $\boldsymbol{c}(\boldsymbol{f})$ is non-negative, the solution of $\mathrm{VI}(\boldsymbol{f}, \Omega_0)$ is equivalent to the equilibrium solution of the GMVUE problem.

The existence of solutions to $\mathrm{VI}(\boldsymbol{f}, \Omega_0)$ requires that $\boldsymbol{c}(\boldsymbol{f})$ is a continuous function of $\boldsymbol{f}$, and Ω_0 is a compact closed convex set. For the GMVUE problem, the second requirement is satisfied for the linear demand constraints and non-negativity constraints depicted in Eq. (3.15). Note that the schedule delay $(T_p - \xi_p(\alpha))^-$ and $(T_p - \xi_p(\alpha))^+$ are random variables, which are discontinuous at several points. However, it is found below that the GMV formulation is continuous with the link traffic flows.

Proposition 3.6 The GMV established in Eq. (3.12) is continuous with link flows.
Proof. See Appendix 3.D.

Since link flow is the sum of all path flows using this link, the continuity of GMV to path flows is guaranteed with the incorporation of Proposition 3.6. Thus, there exists at least one solution to $\mathrm{VI}(\boldsymbol{f}, \Omega_0)$. The uniqueness requires that the Jacobian matrix of $\boldsymbol{c}(\boldsymbol{f})$ is positive definite, which, however, cannot be guaranteed.

3.4 Solution algorithm

In this section, a solution algorithm to the GMVUE problem is proposed. To address a real transportation network under travel time uncertainty, the algorithm integrates a GMV-based shortest path algorithm, a CG scheme, and MSA. Although the MSA with the predetermined sequence of step size may suffer slow convergence, it has been widely used in traffic assignment problems (Fu and Lam 2014; Levin et al. 2015) due to its simplicity and the forced convergence property.

Algorithm 3.1 (GMVSP) Search for a path with the minimal GMV

Step 1. Initialization

Create a path p_l^{rr} from r to itself, and set $\mu_l^{rr} = 0$, $(\sigma_l^{rr})^2 = 0$, and $c_l^{rr} = 0$. Add p_l^{rr} into label-vector P^{rr} and a list of candidate labels *SE*.

Step 2. Label selection

Take label $p_l^{ri} \in P^{ri}$ at node i from *SE* in a first-in-first-out order. If $SE = \emptyset$, then go to Step 4.

Step 3. Path extension

For every outgoing link ℓ of chosen node i (j denotes a successor node of i)

Step 3.1. Generate a new label $p_l^{rj} \in P^{rj}$. Set $\mu_l^{rj} = \mu_l^{ri} + \mu_\ell$, $(\sigma_l^{rj})^2 = (\sigma_l^{rj})^2 + \sigma_\ell^2$ and $c_l^{rj} = \omega_1 c_l^{rj} + z\sigma_l^{rj}$.

Step 3.2. If $p_l^{rj} \in P^{rj}$ is acyclic, then go to Step 3.3; otherwise, scan the next link.

Step 3.3. If p_l^{rj} is an M-GMV non-dominated path, insert p_l^{rj} into P^{rj} and *SE*, and remove all paths M-GMV dominated by p_l^{rj} from P^{rj} and *SE*.

End for.

Return to Step 2.

Step 4. Determine the GMV-based shortest path p_l^{rs} and stop.

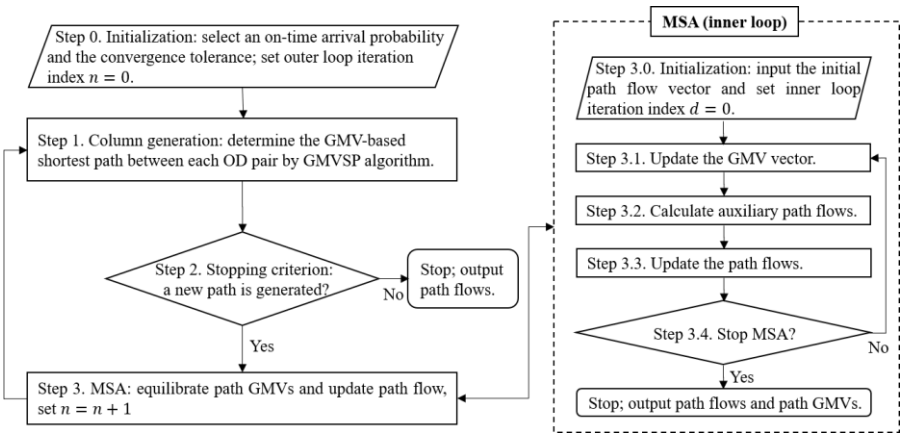

Figure 3.5 Flowchart of GMV-based traffic assignment algorithm.

As illustrated in Section 3.3, GMV is non-additive since the GMV of a path is not necessarily the sum of the GMVs of the associated links. To overcome this difficulty, a bi-criteria label-correcting method (Liao et al., 2014) is adopted to find a reliable path with the minimal GMV. The algorithm for solving the GMV-based shortest path problem is hereafter referred to as GMVSP, and the detailed steps are described above. Accordingly, the GMV-based traffic assignment algorithm has two loops (Figure 3.5). The outer loop is for updating the path sets (left-hand side of Figure 3.5). For each outer loop iteration n, the GMVSP algorithm is adopted to generate GMV-based shortest paths

for each OD pair and to update the path set using the CG technique. Next, the method of successive average (MSA) is used to assign traffic flows on the updated paths, which resides in the inner loop to solve the GMVUE model.

A gap function is defined to measure the convergence of MSA:

$$Gap(\boldsymbol{f}^d) = \frac{[\boldsymbol{c}(\boldsymbol{f}^d) - \boldsymbol{c}_{\min}(\boldsymbol{f}^d)]^T \boldsymbol{f}^d}{\boldsymbol{c}_{\min}(\boldsymbol{f}^d)^T \boldsymbol{f}^d} \tag{3.16}$$

where $\boldsymbol{c}_{\min}(\boldsymbol{f}^d) = (\dots, c_{\min}^{rs}(\boldsymbol{f}^d), \dots)$ is the minimal GMV of all OD pairs. Note that if the UE conditions are satisfied, the above gap function is less than a predefined convergence tolerance ε ($\varepsilon > 0$). The detailed steps are given by the GMVUE algorithm.

In the solution algorithm, path extensions and flow assignments are the most time-consuming components for large-scale networks. For the path searches, the run-time complexity of GMVSP with the Fibonacci heap is $O(|A||P| + |N|\mathrm{Log}(|N|))$, where $|A|$ and $|N|$ are the numbers of network links and nodes respectively, and $|P|$ is the maximum number of non-dominated paths associated with a node. The value of $|P|$ is smaller using M-GMV dominance condition than the M-V dominance condition according to Proposition 3.4. Regarding the flow updating, it should be noted that MSA is performed twice flow assignments (Step 3.2 and 3.3) at each iteration.

Algorithm 3.2 (GMVUE algorithm) Determine the flow patterns at equilibrium

Step 0. Initialization

Given α and ε, set $n = 0$ and $\boldsymbol{f_n} = 0$. For OD pair (r, s), let $P_0^{rs} = \emptyset$ be the initial set of used paths.

Step 1. (CG) Update path set for each OD pair

For each OD pair (r, s)

Call GMVSP to search the minimal GMV path p_l^{rs}. If $p_l^{rs} \notin P_n^{rs}$, then set $P_n^{rs} = P_n^{rs} \cup \{p_l^{rs}\}$, $f_l^{rs} = 0$ and $\boldsymbol{f_n} = [\boldsymbol{f_n};\ f_l^{rs}]$.

End for.

Step 2. (Stopping criterion) If $P_n^{rs} = P_{n-1}^{rs}$, then stop; otherwise, continue.

Step 3. (MSA) Update path flow

Step 3.0. Initialization. Set inner loop iteration index $d = 1$ and feasible path flow vector $\boldsymbol{f}^d = \boldsymbol{f}_n$.

Step 3.1. Update the GMV vector $c^{rs}(\boldsymbol{f}^d)$ for each OD pair (r, s).

Step 3.2. Perform all-or-nothing assignment on the basis of path GMV $c^{rs}(\boldsymbol{f}^d)$, yielding auxiliary path flows, $(\bar{\boldsymbol{f}}^d)^{rs}$, for each OD pair ($r$, s).

Step 3.3. For each OD pair (r, s), calculate new path flows $(\boldsymbol{f}^{d+1})^{rs} = (\boldsymbol{f}^d)^{rs} + \left[(\bar{\boldsymbol{f}}^d)^{rs} - (\boldsymbol{f}^d)^{rs}\right]/d$.

Step 3.4. Check the stopping criterion of MSA. If $Gap(\boldsymbol{f}^d) < \varepsilon$, set $\boldsymbol{f_n} = \boldsymbol{f}^d$ and $n = n + 1$, and go to Step 1; otherwise, set $d = d + 1$, and go to Step 3.1.

3.5 Numerical examples

This section presents two numerical examples to illustrate GMVUE. The first example is adopted for illustrating detailed results. The second example presents the convergence results in a relatively large traffic network. The solution algorithm is run on a personal computer with an Intel(R) Core(TM) i7-6700 3.40 GHz CPU and 8.00 GB RAM. The link performance uses the BPR function with $\beta_1 = 1$, $\beta_2 = 4$ on all the links. As a new special form of GMV, MLTT is focused on in this section and the corresponding weight coefficients equal $[1, -1/\alpha, 0, \gamma(\alpha)]$. Moreover, $\varepsilon = 10^{-5}$ and $\alpha = 0.9$ unless otherwise explained.

3.5.1 Example 1: six-node network

The small-scale test network (Figure 3.6) is adopted from Shao et al. (2006), which has two OD pairs, six nodes, seven links, and four paths. The link number, capacity, and degradable parameter are shown near the links. The demands for OD pairs (1, 3), (2, 4) are 15 and 40 units respectively. Although the uniqueness of the solutions to the VI problem cannot be guaranteed, it is found the flow patterns at the equilibrium states are stable with multiple random start points. The steady state is reached after 0.19 second of computation time on average. Based on the above setting, Figure 3.7 shows the convergence curves of the MSA. As seen, the path MLTTs and flows fluctuate greatly at the first 15 iterations and converge to a steady state gradually. The fluctuations during the convergence course is a common issue in MSA applications (Carey and Ge, 2012). At the steady state, travelers of OD pair (1, 3) are concentrated on path 1 and disfavor path 2 (flow curve is coincident with the x-axis) due to a higher MLTT of path 2. For OD pair (2, 4), paths 3 and 4 possess the same MLTT (25.07), and the traffic flows on both paths are 31.11 and 8.89 respectively. These results are consistent with the GMVUE conditions and constraints in Eqs. (3.13)-(3.15).

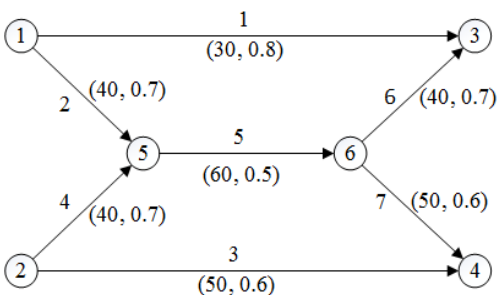

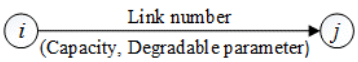

OD pair	Path	Link sequence	t_l^0
(1, 3)	1	1	22
	2	2 - 5 - 6	25
(2, 4)	3	4 - 5 - 7	17
	4	3	25

Figure 3.6 The test network.

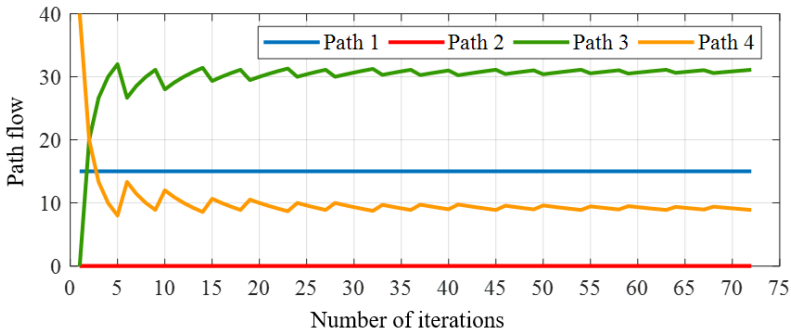

(a) Path flow

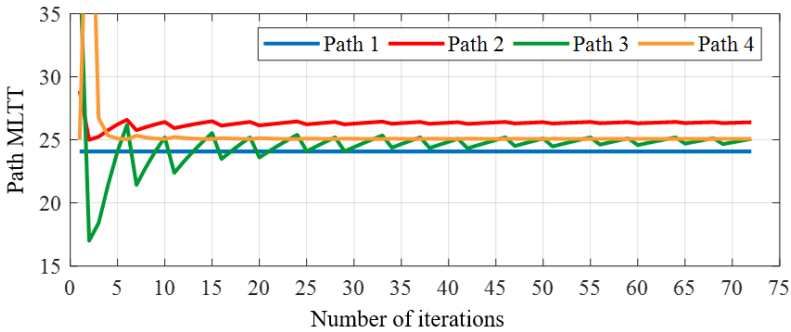

(b) Path MLTT

Figure 3.7 Convergence curves of the path flows and GMVs.

To illustrate the impact of on-time arrival probability on traffic flow, Figure 3.8 presents the equilibrium results of OD pair (1, 3) under different OD demands and different α, of which (a)-(b) and (c)-(d) correspond to 17 and 40 units of demand respectively (both are set arbitrarily for illustration purpose). As shown in Figure 3.8 (a), all travelers choose path 1 when $\alpha < 0.6$. If α is increased over 0.6, several flows on path 1 switch to path 2. When there are 40 units of demand, traffic flows are assigned to paths 1 and 2 under different α. When α is relatively small (less than 0.4), there are more travelers choosing path 1 to avoid the penalty caused by travel delays. When α is larger than 0.4, the traffic flow on path 2 is greater than that on path 1. These curves depicted in Figure 3.8 are consistent with the GMVUE conditions.

MLTT, TTB, and METT, as three special cases of GMV, take both expected travel time and travel time variance into consideration. Figure 3.9 shows the different equilibrium flows on path 1 under these metrics when the demand of OD pair (1, 3) is equal to 17 and 40 units respectively, where the left-hand side red dashed line denotes the total demand and the right-hand side denotes the half demand for reference purpose. Most travelers with high on-time arrival probability will choose paths with a small mean and variance of path travel time when the demand is small. Since the mean and variance

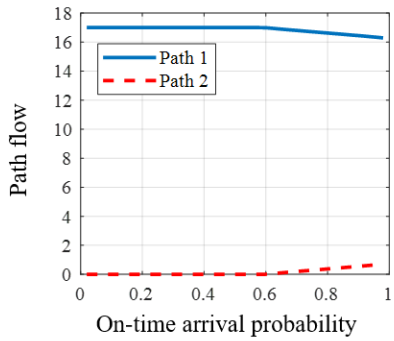

(a) path flow under 17 units of demand

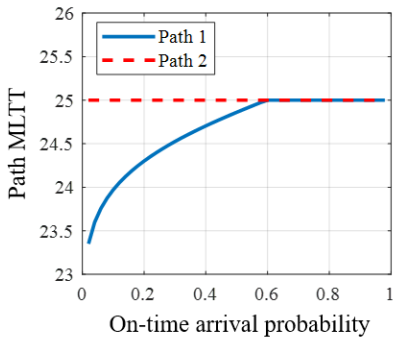

(b) path MLTT under 17 units of demand

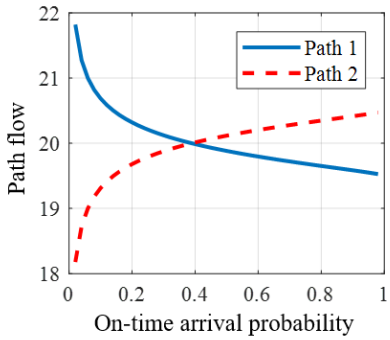

(c) path flow under 40 units of demand

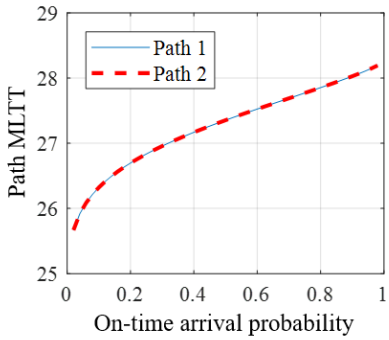

(d) path MLTT under 40 units of demand

Figure 3.8 Equilibrium results under different on-time arrival probabilities.

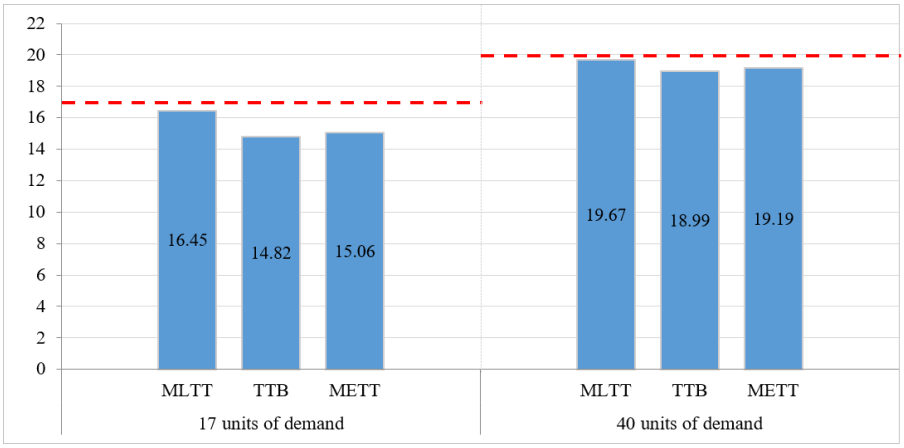

Figure 3.9 Travel flows on path 1 under different path choice metrics.

of travel time in path 1 are smaller than those of path 2, travel flows concentrate on path 1 under MLTT, TTB, and METT. When the demand increases to 40, traffic congestion occurs. Some travelers on path 1 shift to path 2 to avoid high penalties due to congestion. Fewer travelers choose path 1 under these criteria. The results are consistent with Eqs. (3.2) and (3.3), which indicates that traffic congestion results in a large mean and variance of path travel time.

3.5.2 Example 2: Anaheim network

This example uses a real network in the City of Anaheim (USA) to illustrate the effectiveness and present the sensitivity analysis of the proposed GMV-based traffic assignment algorithm. This network consists of 416 nodes, 914 links, and 1406 OD pairs. The network topology, link capacities, free-flow travel times, and original OD demands are obtained from http://www.bgu.ac.il/~bargera/tntp/. The demands are enlarged two times from the original demands to produce congestion effects. To analyze the uncertainty of this network, θ_l is obtained by linear projecting the length of link l to the interval [0.5, 0.9]. The algorithm is coded in PYTHON programming language and takes about 495.6 seconds to reach the GMVUE state (note that PYTHON is an interpreting programming language; the running time can be considerably reduced using a compiling programming language), where traffic assignments account for most of the running time due to its slow convergence process.

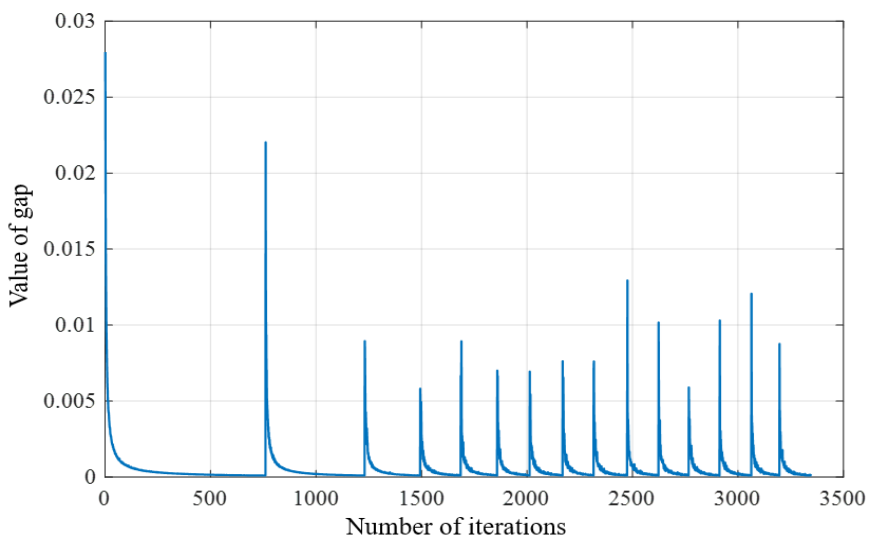

Figure 3.10 Convergence curve of the proposed algorithm.

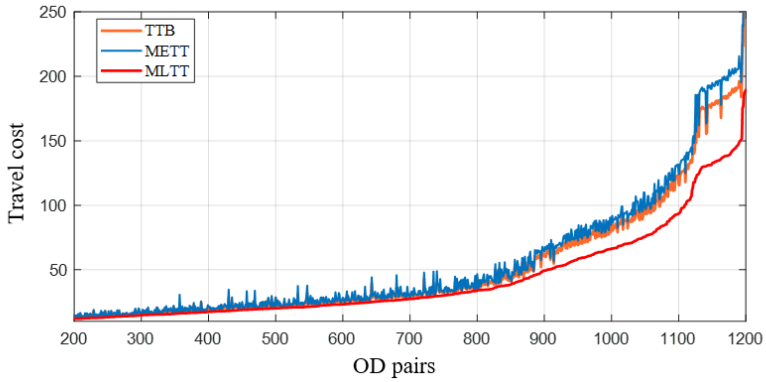

(a) Travel costs of various OD pairs.

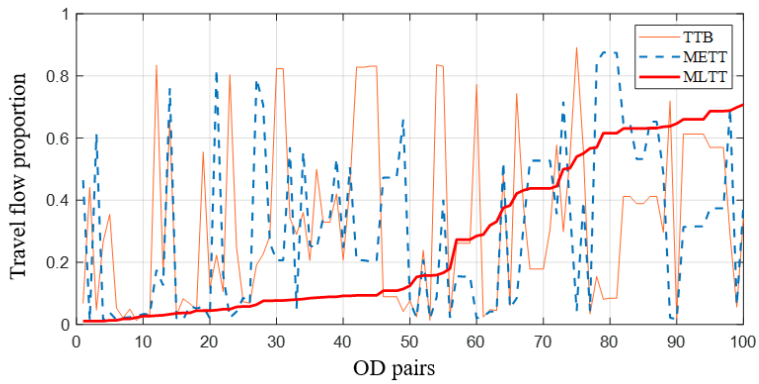

(b) Travel flow proportions of various OD pairs.

Figure 3.11 Comparisons of travel cost and flow under different metrics.

After new paths are generated, considerable flows shift from the existing paths to the new ones at the first few inner iterations due to small d. Hence, the first five inner iterations are excluded after new paths are generated, and the convergence curve is depicted in Figure 3.10. As shown, the curve consists of several fluctuations. When the result of the current outer iteration (see Figure 3.5) approaches the equilibrium solution, new paths have similar MLTTs as those used paths. As shown, fewer iterations are needed to achieve the equilibrium state. This conclusion is demonstrated by the decreasing distances between two adjacent peaks. Overall, the gap decreases to a small value within a few iterations and then move downwards slowly due to the nature of MSA.

To compare the path choice outcomes of MLTT, TTB, and METT, the values of MLTT are first sorted ascendingly and show the MLTT values of 1000 OD pairs in red (Figure 3.11 (a)). Correspondingly, the values of TTB and METT of the same OD pairs are shown in orange and blue respectively. Regarding the flow comparison, the common paths of each OD pair under different path choice metrics are found and the proportions

of the path flows to corresponding OD demands are calculated. For a clear presentation, the travel flow proportions of only 100 OD pairs are depicted in Figure 3.11 (b). It can be seen that at the equilibrium state, the travel costs and flows of the three metrics are different across OD pairs. Note that TTB is bounded by MLTT and METT despite the fluctuations of TTB and METT in Figure 3.11 (a). This result is consistent with the definitions of the metrics.

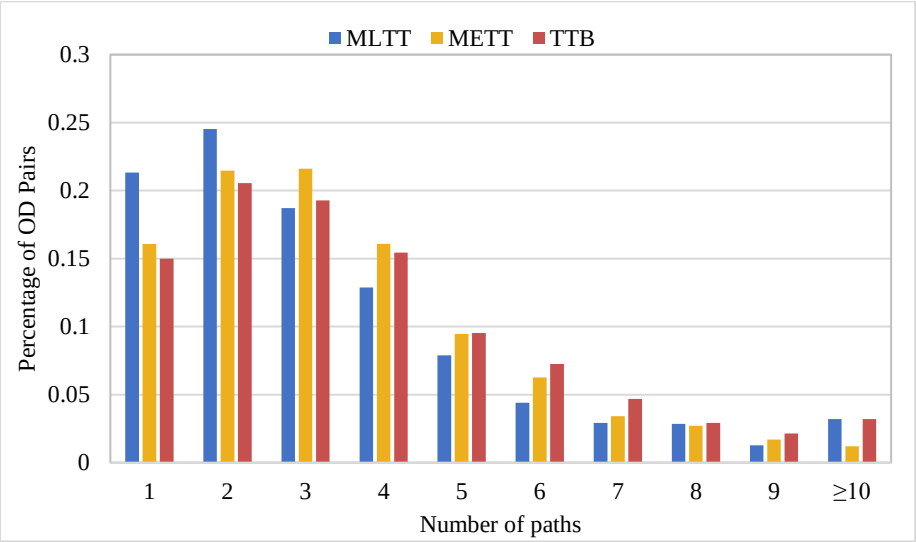

Figure 3.12 Distribution of the number of paths for the Anaheim network.

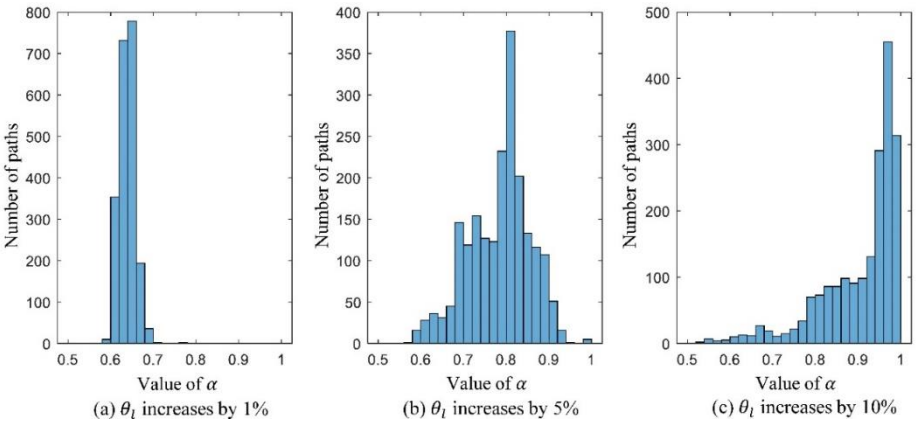

Figure 3.13 Numbers of paths with different on-time probabilities.

For further comparisons, the distributions of the numbers of paths per OD pair under different criteria are plotted in Figure 3.12. It shows that the number of paths of the OD pairs is primarily concentrated in the first four groups, with very few OD pairs having more than seven paths at equilibrium. In particular, with the MLTT criterion, about 65% of OD pairs use no more than three paths, while the percentage is around 55% for TTB. Although the numbers of the identified paths may also be affected by the congestion level, the results indicate that the CG scheme takes effects for identifying the relevant paths for traffic assignment. Also, the analyses further confirm that different criteria result in different path choice results.

The degree of supply uncertainty could be reduced by intelligent transportation system applications, for example, emerging traffic management measures and operations strategies. An example is that the lower bounds of the uniform distributions of capacities are increased due to the deployment of connected vehicles. To demonstrate the influence of these changes on TTR, α is adopted as the criterion to quantify TTR and set as 0.6 initially, and then $\theta_l(\forall l)$ is increased by 1%, 5% and 10% respectively. Figure 3.13 shows the on-time probability α of the paths after the capacity improvement. As shown, the values of α of most paths increase, indicating that the TTR of travelers is improved. Moreover, the rightward shift of the histograms illustrates that TTR gains more improvement with a higher θ_l. Taking Figure 3.13 (b) for example, although θ_l increases by only 5%, the improvement of TTR is significant: 81.8% of the paths have TTR within the range [0.7, 0.9]. It is also found that there are a few paths with TTR lower than 0.6. This outcome is caused by the fact that the generated paths for a minority of OD pairs are different and also have different means and variances. Based on the numerical results, it can be concluded that capacity improvements in the transport network improve TTR.

3.6 Conclusions

This chapter proposed a GMV metric for path choice under travel time uncertainty and developed a GMVUE in a transport network. Instead of focusing solely on expected travel time, the GMVUE model is capable of factoring travel time variance, early arrival, or late arrival into path choice considerations. As illustrated, GMV has a more generalized form than several currently widely used metrics, such as MTT, TTB, and METT. This chapter also analyzed some properties of GMV, including continuity and non-additivity. Continuity is satisfied without the assumption of normal and independent distributions. To overcome non-additivity, GMV-based dominance definitions and conditions were established and used to search for the reliable shortest paths. The GMVUE model was formulated as a VI problem. The existence and uniqueness of the solutions to the VI problem were also discussed. With the incorporation of a bi-criteria label-correcting algorithm, MSA, and CG technique, an effective traffic assignment algorithm without path enumeration was developed to solve the GMVUE model for real

networks. As illustrated in the numerical examples, different weight coefficients result in different GMV forms and traffic flow assignment schemes.

As observed above, the running time of the CG algorithm was too long even for small general static networks, not to mention in the dynamic context. The next chapter will incorporate the temporal dimension and the bounded rationality behavior and introduce several strategies to accelerate the CG algorithm. As the primary goal is to speed up the CG algorithm in the dynamic contexts, the uncertainty component is not considered in the following chapters.

4

The TBCG Algorithm to the BR-DUE Problem*

4.1 Introduction

As a relaxation of the assumption of perfect rationality, the concept of bounded rationality (BR) was proposed by Simon (1955, 1957) to capture the irrationality of people's decision-making. BR was first introduced to traffic modeling by Mahmassani and Chang (1987) and then widely applied in the transportation area. For example, Sivak (2002) founded that BR underlined the development of many of the early, common-sense countermeasures for traffic safety problems. As an extension of the classical Wardrop's user equilibrium (UE), boundedly rational UE (Han and Timmermans, 2006; Di et al., 2013; Di et al., 2013) embedded BR in the static traffic assignment (STA) problems. In the dynamic context, the tolerance-based dynamic UE (DUE) problem was introduced by Szeto and Lo (2006). The theoretical properties, including existence and continuity theory, were developed by Han et al. (2015). However, the numerical studies of the few existing boundedly rational DUE (BR-DUE) models were performed on predefined path sets in small networks (10-node network and Sioux Falls network). For the application of the BR-DUE models to larger networks, a method with path generation is needed.

* This chapter is based on Wang, D., Liao, F., Gao, Z., Timmermans, H., 2019. Tolerance-based strategies for extending the column generation algorithm to the bounded rational dynamic user equilibrium problem. Transportation Research Part B: Methodological 119, 102–121.

In a static transport network, Leventhal et al. (1973) proposed the column generation (CG) algorithm to find minimum disutility paths and add them to path sets along with the iterations. Since Leventhal et al. (1973), the CG algorithm has been applied for solving various traffic assignment problems (Friesz, 1985; Chen et al., 2009; Zhang et al., 2013; Levin et al., 2015). Parallelly, several strategies have been proposed to yield substantial computational time-savings. For example, Panicucci et al. (2007) and Di Lorenzo et al. (2014) suggested performing the path search process within a prefixed number of iterations, which can then be changed according to a dynamic adjustment mechanism proposed by Galligari and Sciandrone (2017). However, these strategies are limited to static contexts.

Considering both BR and the temporal dimension, this chapter develops a tolerance-based CG (TBCG) algorithm to solve the BR-DUE problem. Four tolerance-based strategies extending the CG algorithm are proposed across the spatial and temporal dimensions. First, a tolerance-based minimum disutility path search strategy is proposed to seek satisfactory paths. Second, a self-adjusted convergence threshold strategy is adopted to perform pseudo-equilibrium assignments at the intermediate iterations. Third, a varied temporal resolution scheme combing temporal exploration and exploitation is designed to assign flows to narrow time regions rather than to the whole-time horizon. Lastly, a path search skipping strategy is developed to perform path searches when necessary. With these spatial and temporal strategies, the TBCG algorithm efficiently finds the BR-DUE solutions.

The remainder of this chapter is organized as follows. Section 4.2 introduces the tolerance-based strategies for extending the CG algorithm to solve the BR-DUE problem. Numerical examples are given in Section 4.3 to assess the effectiveness of the proposed TBCG algorithm. Finally, conclusions are provided.

4.2 Tolerance-based column generation for BR-DUE model

This section presents four strategies covering both the spatial and temporal dimensions to extend the CG algorithm to solve BR-DUE (Eq. (2.16)). Thereafter, the TBCG algorithm is proposed and the algorithmic flowchart and pseudo-code are presented. In this chapter, the point queue method (Huang and Lam, 2002; Zhou and Taylor, 2014) is applied for modeling traffic flow propagation. To illustrate the mechanisms of the TBCG algorithm, a small case is used for detailing the key descriptions. To keep consistency, the notations used above attached with n refer to the same entities at iteration n. Furthermore, a potential time-dependent path set (PTPS) is created to store certain path and departure time pairs having the potentials to be the BR-DUE solutions. The PTPS at iteration n of rs is denoted by $\Phi_n^{rs} = \{(p, k)\}$.

4.2.1 Tolerance-based strategies

As path search and network loading constitute the most time-intensive components in a CG algorithm for traffic assignment, improving and balancing these two components are crucial for accelerating the algorithm. When considering the temporal dimension, time discretization is needed to solve the dynamic traffic assignment (DTA) problems in the discrete domain, since there is no known method for solving complex time-continuous models analytically. As indicated in Huang and Lam (2002), the length of one unit of time interval should be set small enough so that the discrete DTA model approximates its continuous counterpart. As travelers choose departure times and paths simultaneously, a smaller time interval leads to a large multiplier increase of the choices compared to the static UE, which aggravates the burden of computation. In addition, to solve BR-DUE, BR should be included in the path search and network loading components. To address these issues, the following strategies are suggested, particularly to be applied at the intermediate iterations

(i) a tolerance-based minimum disutility path search (TBMDPS) strategy is applied to allow for BR and reduce the number of path flow variables;

(ii) self-adjusted convergence thresholds are used to ensure fast convergences;

(iii) for temporal exploration, the temporal resolution is set stationary to explore the potential time region of BR-DUE; regarding temporal exploitation, the temporal resolution is dynamically set high to meet the required convergence precision;

(iv) a path search skipping strategy is adopted to decrease the number of path searches.

4.2.1.1 Tolerance-based minimum disutility path search

In the dynamic context, time-dependent paths with the minimum disutility can be found by dynamic programming (Dean, 2004; Liao, 2017). When the newly generated path $\bar{p}$ with disutility $c_{\bar{p}}^{rs}(k, \boldsymbol{f_n})$ satisfying Eq. (4.1) does not belong to the path set P_n^{rs} of rs at iteration n, $\bar{p}$ is added to P_n^{rs}. A similar criterion is widely used in the CG algorithm for the DUE problem (Lu et al., 2009, 2016).

$$c_{\min}^{rs}(\boldsymbol{f_n}) - c_{\bar{p}}^{rs}(k, \boldsymbol{f_n}) \geq 0 \tag{4.1}$$

In contrast to adding a new path with the minimum disutility to the path set, strategy (i) compares $c_{\bar{p}}^{rs}(k, \boldsymbol{f_n})$ and the minimum disutility of paths in P_n^{rs}. Only path $\bar{p}$ with extra disutility losses larger than a threshold is added to the path set, as shown in Eq. (4.2), where ϵ^{rs} is a relative indifference threshold of travelers of the origin and destination (OD) pair rs toward path switch. This condition is consistent with the travel behavior of BR. Specifically, in a long-term equilibrium process, travelers depart from

their origins at preferred time intervals and travel on preferred paths. Despite the existence of paths with similar or even smaller disutilities, they may prefer the familiar paths due to the inertial to adapt. The travelers switch paths only if the new ones lead to extra less disutility. Note that strategy (*i*) is OD related and will degenerate into Eq. (4.1) if ϵ^{rs} is equal to zero.

$$c_{\min}^{rs}(\boldsymbol{f_n}) - c_{\bar{p}}^{rs}(k, \boldsymbol{f_n}) \geq \epsilon^{rs} \cdot c_{\min}^{rs}(\boldsymbol{f_n}) \tag{4.2}$$

Let $\bar{C}_i(k)$ denotes the minimum disutility of arriving at node i and time interval k, $\bar{t}_{ij}^n(k)$ the arrival time at j and $\bar{c}_{ij}^n(k)$ the disutility of traversing link (i,j) when departing from i during k at iteration n, $F_j^i(\bar{t}_{ij}^n(k))$ is a two-tuple vector recording the preceding link and interval. The pseudo-code of the TBMDPS at iteration n is presented in Algorithm 4.1, which delivers the best worst-case run-time complexity.

Remark 4.1 Strategy (*i*) accelerates the CG algorithm by decreasing the size of the path sets. The size of the path sets in DTA models plays a major role in the computation time due to the large path expansion factor accounting for time-dependency. Specifically, the size of the time-dependent paths of DTA is $\sum_{rs}|P^{rs}| \cdot |K|$ (Huang and Lam, 2002; Long et al., 2016). This value is decreased to $\sum_{rs}(|P^{rs}| - m_2) \cdot |K|$ if m_2 paths are discarded due to the TBMDPS. The larger the value of $|K|$, the larger decrease it incurs. The path $\bar{p}$ satisfying Eq. (4.2), generated by the TBMDPS, is called an acceptable path. The input parameters of this algorithm are flexible to be linked with iteration-related variables, which make it possible to combine with the temporal strategies.

Algorithm 4.1 (TBMDPS) a tolerance-based minimum disutility path search

Input: $\bar{c}_{ij}^n(k)$ and $\bar{t}_{ij}^n(k)$, $\forall(i,j) \in A, k \in K$
Initially, set $\bar{C}_i(k) = \infty$ and $\bar{C}_r(k) = 0$, $\forall k \in K$, $\forall i \in N\backslash\{r\}$; $k = 1$.
while $k \leq |K|$
    for any $(i,j) \in A$
        if $\bar{C}_j(\bar{t}_{ij}^n(k)) < \bar{C}_i(k) + \bar{c}_{ij}^n(k)$ and $\bar{t}_{ij}^n(k) \leq |K|$
            $\bar{C}_j(\bar{t}_{ij}^n(k)) = \bar{C}_i(k) + \bar{c}_{ij}^n(k)$
            $F_j^i\left(\bar{t}_{ij}^n(k)\right) =< (i,j), k >$
        End
    End
    $k = k + 1$
End
for all s satisfying $rs \in RS$
    backtrack the optimal paths $\bar{p}$ through $F_j^i\left(\bar{t}_{ij}^n(k)\right)$
    if the disutility on $\bar{p}$ satisfies Eq. (4.2) and $\bar{p} \notin P_n^{rs}$, add $\bar{p}$ to P_n^{rs}
End

4.2.1.2 Self-adjusted convergence thresholds

Convergence curves depicted by the gap functions of DUE models usually become flat when the solutions approach the equilibrium (Lo and Szeto, 2002; Long et al., 2013b). Using a fixed small convergence threshold would lead to long computation times at the intermediate iterations. To allow for BR and drive the intermediate steps fast, strategy (*ii*) concerns the self-adjusted convergence thresholds, formulated in Eq. (4.3).

$$c_p^{rs}(k, \boldsymbol{f_n}) - c_{\min}^{rs}(\boldsymbol{f_n}) \leq \varepsilon_n^{rs} \cdot c_{\min}^{rs}(\boldsymbol{f_n}) \tag{4.3}$$

where ε_n^{rs} is the relative convergence threshold of travelers between OD pair rs at iteration n toward time change.

For each OD pair *rs*, Eq. (4.3) has a similar form to the BR-DUE condition, but the difference lies in the fluctuating convergence threshold ε_n^{rs} with reference to iteration n. Based on the relationship between the acceptable path $\bar{p}$ generated from strategy (*i*) and P_n^{rs}, ε_n^{rs} is changed differently in the following two cases.

Case (1): At least one acceptable path does not belong to the current path set, i.e. $\exists\, \bar{p} \notin P_n^{rs}$.

In this case, some traffic flows are more likely to shift to the new paths. To ensure fast convergence, the value of the convergence threshold increases by the following formula

$$\varepsilon_{n+1}^{rs} = \min\left(\frac{1}{\vartheta_1} \cdot \varepsilon_n^{rs},\ \varepsilon_{\max}^{rs}\right) \tag{4.4}$$

where $\vartheta_1 \in (0, 1)$ is a parameter for scaling and $\varepsilon_{\max}^{rs}$ is the maximum convergence tolerance for rs. Eq. (4.4) uses $\varepsilon_{\max}^{rs}$ as the upper bound to prevent the unrestricted increase of ε_{n+1}^{rs}.

Case (2): All acceptable paths fall within the current path set, i.e. $\forall\, \bar{p} \in P_n^{rs}$.

In this case, the traffic flows have converged to a state, in which all used paths belong to P_n^{rs} with ε_n^{rs}. To obtain a more precise assignment, ε_{n+1}^{rs} is decreased as below

$$\varepsilon_{n+1}^{rs} = \max(\vartheta_1 \cdot \varepsilon_n^{rs},\ \varepsilon^{rs}) \tag{4.5}$$

where ε^{rs} is used as a lower bound to ensure a required tolerance.

Remark 4.2 Strategy (*ii*) accelerates the CG algorithm by decreasing the number of network loadings. A larger ε_n^{rs} ensures faster convergence at iteration n. When no new

path is generated, ε_n^{rs} is decreased until a required convergence threshold to obtain a BR-DUE solution.

4.2.1.3 Temporal exploration and exploitation

The challenge in DTA mainly stems from the path extension in the temporal dimension. The previous CG algorithms for DTA assign flows to the generated paths across the whole-time horizon with a fixed time resolution. This strategy concerns the varied time resolutions for temporal exploration and exploitation.

Temporal exploration

Suppose that an acceptable path $\bar{p}$ is found by strategy (i) at iteration n. It may be the case that not all time intervals for $\bar{p}$ are potential for the traffic assignment, especially when the time intervals fall at the beginning or the end of the time horizon. The temporal exploration is adopted to find the potential time intervals and add the corresponding time-dependent paths to PTPS. Specifically, given path $p \in P_n^{rs}$, if there are time-dependent paths (p, k) for $\forall k \in K$ satisfying Eq. (4.3) and falling out of Φ_n^{rs}, add (p, k) to Φ_n^{rs} and assign the flows to them. Usually, the neighboring time intervals of k are likely to be potential. This process is conducted until no new time-dependent path satisfies Eq. (4.3).

Temporal exploitation

A higher temporal resolution of DTA means that the traffic flows are propagated more accurately. The side-effects of high temporal resolution are the increase in the size of time-dependent paths and the need of a long flow propagation process, and thus dramatically more computation time is required. It is well known that the traffic flows are assigned to a small proportion of continuous time regions rather the full time horizon in transport networks with bottlenecks. Based on this notion, the TBCG algorithm starts from a low temporal resolution to ensure converging to a satisfactory equilibrium result at a considerable speed and ends up with a high temporal resolution to meet the required criterion.

The temporal resolution at iteration n is denoted by Δ_n, and Δ is used as a lower bound of Δ_n. Whether to decrease Δ_n or not depends on the relationship between the acceptable path $\bar{p}$ and P_n^{rs}, which is similar to the two cases above. In Case (1), Δ_n is kept the same as the last iteration. When falling within Case (2), temporal exploitation is adopted before decreasing ε_n^{rs}. If $\Delta_n > \Delta$, temporal exploitation is trigged by the following formula

$$\Delta_{n+1} = \max(\lfloor \vartheta_2 \cdot \Delta_n \rfloor, \Delta) \tag{4.6}$$

where $\vartheta_2 \in (0,1)$ is a resolution parameter, $\lfloor \cdot \rfloor$ is an integer-floor operator. Besides transforming the link attributes (e.g., link capacity and free flow travel time) in relation to Δ_{n+1}, each time-dependent path (p,k) in Φ_n^{rs} is replaced by (p,k') for $\forall k'$ satisfying $k' \cdot \Delta_{n+1} \in [k, k+1) \cdot \Delta_n$ and the corresponding flow $f_p^{rs}(k)$ are divided into Δ_n/Δ_{n+1} parts equally and spread to each (p,k'). If $\Delta_n = \Delta$, the spatial exploitation is performed by decreasing ε_n^{rs} as shown in Eq. (4.5).

Regarding temporal exploration, it is a process of extending the time dimension of PTPS from several time intervals. Comparatively, strategy (*i*) can be regarded as spatial exploration, which is a process to add new acceptable paths to P_n^{rs} for temporal exploration. Traffic flows are assigned based on the updated PTPS and the unused paths are removed from P_n^{rs}. Although the path set P_n^{rs} may be contracted after one time of traffic assignment, the removed time-dependent paths have higher disutilities, which guarantees the occurrence of Case (2).

Remark 4.3 Strategy (*iii*) is performed from a low temporal resolution, which accelerates the original CG algorithm by decreasing the size of the path set. For example, when the resolution at iteration n is twice the required one, i.e., $\Delta_n = 2 \cdot \Delta$, half the time-dependent paths may be used to assign traffic flows. Among them, only the time-dependent paths satisfying Eq. (4.3) are added to PTPS according to the temporal exploration. The exploitation procedure leads to a decrease of Δ_n and ε_n^{rs}, which guarantees that the TBCG algorithm converges to a state of BR-DUE with the required temporal resolution and convergence tolerance.

4.2.1.4 Minimum disutility path search skipping

This strategy suggests that the TBCG algorithm performs the TBMDPS only at the time intervals that may generate acceptable paths. Whereas, the classical CG algorithm for DTA (Lu et al., 2009) finds the path with the minimum disutility at every departure time interval at every iteration. Note that the minimum disutility of paths with zero flow of rs at k, denoted as $c^{rs}(k, \mathbf{0})$, is the lower bound at k for rs. Whether or not to allocate traffic flows to interval k at iteration n depends on the relationship between $c^{rs}(k, \mathbf{0})$ and the minimum disutility of rs, $c_{\min}^{rs}(\boldsymbol{f_n})$. If $c^{rs}(k, \mathbf{0}) < c_{\min}^{rs}(\boldsymbol{f_n})$, interval k is a potential candidate and path search is performed. In contrast, it is impossible to assign traffic flows to the paths at k if $c^{rs}(k, \mathbf{0}) \geq c_{\min}^{rs}(\boldsymbol{f_n}) \cdot (1 + \varepsilon_n^{rs})$. In other words, interval k satisfying Eq. (4.7) means that the traffic flows are more likely to concentrate on the existing time-dependent paths. Hence, there is no need for path search at this interval at iteration n. The remaining intervals with $c^{rs}(k, \mathbf{0})$ falling between $c_{\min}^{rs}(\boldsymbol{f_n})$ and $c_{\min}^{rs}(\boldsymbol{f_n}) \cdot (1 + \varepsilon_n^{rs})$ may be assigned with traffic flows and path searches are conducted.

Table 4.1 Comparison of the CG algorithms for different UE models

	Reference	Path Search		Network Loading			Temporal resolution
		Search method	Search frequency per iteration	Loading method	Convergence threshold	Accuracy	
UE	Chen et al., 2011; Ryu et al., 2016.	minimum cost path search	once	static	fixed	ε	–
DUE	Zhou et al., 2008; Lu et al., 2013.	minimum cost path search	for each time interval	dynamic	fixed	Δ & ε	fixed
BR-DUE	*current chapter*	TBMDPS	for intervals dis-satisfying Eq. (4.7)	dynamic	self-adjusted	Δ & ε^{rs}	varied

$$c_{\min}^{rs}(\boldsymbol{f_n}) \cdot (1 + \varepsilon_n^{rs}) < c^{rs}(k, \mathbf{0}) \tag{4.7}$$

where $\mathbf{0}$ is a zero-flow vector.

Remark 4.4 Strategy (*iv*) accelerates the CG algorithm by decreasing the number of path searches. For the traditional CG algorithm, $|K|$ times of path searches are needed to find the potential paths. This value will decrease to $|K_n| - m_3$ when m_3 intervals satisfy Eq. (4.7), where K_n is the set of time intervals corresponding to Δ_n.

Table 4.1compares the CG algorithms for UE, DUE and BR-DUE models in terms of path search and network loading. The "cost" refers to generalized travel cost, which may be linked to one or multiple factors. As presented, the temporal resolution is listed after both path search and network loading as it is implicated in both processes. Compared with the CG algorithm for UE and DUE, the TBCG algorithm for BR-DUE has merits of self-adjustment without sacrificing accuracy at the final iteration. Regarding the spatial accuracy, the OD-related parameter ε^{rs} has the ability to reflect the heterogeneity of trips, while ε in this table is a convergence threshold for UE and DUE. When $\varepsilon^{rs} \cdot c_{\min}^{rs}(\boldsymbol{f_n})$ equals ε, TBCG algorithm has the same spatial accuracy as the CG algorithms for UE and DUE.

4.2.2 Tolerance-based column generation algorithm

The above four strategies extend the original CG algorithm from different aspects. Considering the run-time of the TBCG algorithm, time complexity analysis is described as follows. When the recursive formulations (Dean, 2004a) are used to search for the tolerance-based minimum disutility paths, the run-time complexity is $O(|N| \cdot |A| \cdot |K|)$ at one iteration. The path search skipping strategy and temporal resolution scheme are developed to decrease the value of $|K|$. The dynamic network loading phase consumes $O(\sum_{rs}|P^{rs}| \cdot |A'| \cdot |K| \cdot m_1)$ run-time in the worst case to load path flows according to Section 2.4. The TBMDPS strategy decreases $\sum_{rs}|P^{rs}|$, the fluctuating convergence

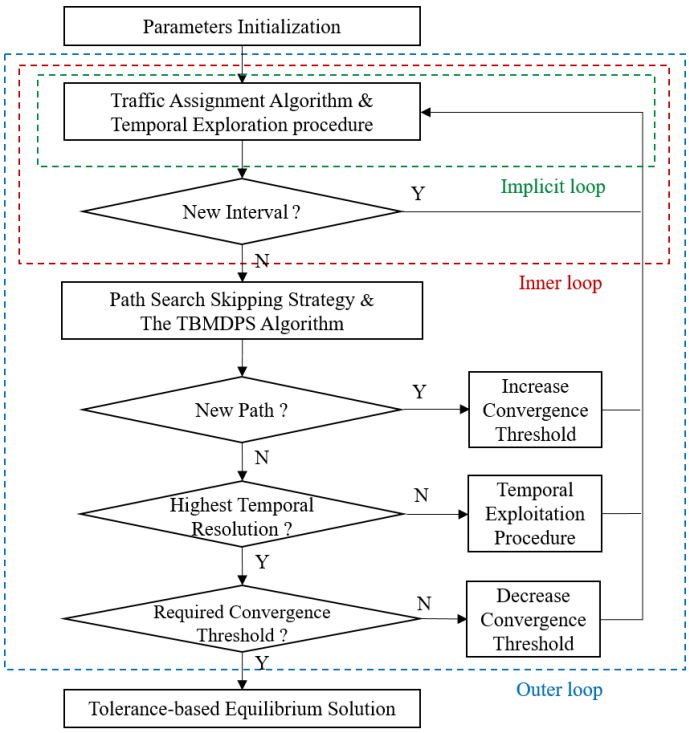

Figure 4.1 Flowchart of the TBCG algorithm.

threshold strategy decreases m_1, and the temporal resolution scheme decreases $|K|$. Conversely, the number of iterations may increase due to the changing temporal resolution. Thanks to the strategy of self-adjusted convergence thresholds, the TBCG algorithm can converge to an equilibrium state with fewer network loadings overall.

Accordingly, the TBCG algorithm has three loops as depicted in Figure 4.1. As shown within the blue box, the outer loop is for updating P_n^{rs}, enhancing Δ_n or decreasing ε_n^{rs}. When new paths p are generated at iteration n, which means that some flows will shift to these paths, a large ε_n^{rs} ensures fast convergence. When no new path is generated and the result at the current iteration has converged at a low temporal resolution, the temporal exploitation procedure is performed to enhance Δ_n. Whether or not to exit the outer loop also depends on ε_n^{rs}. If $\varepsilon_n^{rs} = \varepsilon^{rs}$, the algorithm has converged to a BR-DUE state with the required convergence tolerance at the highest temporal resolution; then, the outer loop is exited. Otherwise, traffic flows are assigned repeatedly by decreasing ε_n^{rs}. The inner loop denotes the temporal exploration procedure. Given a path set, all potential time intervals are added by alternately performing traffic assignment and temporal exploration. Besides, another loop is implicit in the traffic assignment algorithm to obtain a path flow pattern. It is noteworthy that the CG

algorithms generally converge in small numbers of outer iterations and do not enumerate all paths.

The proposed four strategies significantly revise the CG algorithm for speeding-up but do not modify the property of convergence. That is, if the convergence conditions of the original CG algorithm are satisfied, the TBCG algorithm can also converge to a BR-DUE state. This conclusion is presented as follows.

Theorem 4.1. The tolerance-based strategies in the TBCG algorithm maintain the convergence property of the CG algorithm.
Proof. See Appendix 4.A.

Incorporating the proportional swap system (Smith, 1984; Guo et al., 2017) for traffic assignment, the convergence of the TBCG algorithm is concluded as Corollary 4.1.

Corollary 4.1 The TBCG algorithm is convergent if the path disutility is a monotone function of path flows.
Proof. See Appendix 4.B.

Corollary 4.1 states the convergence of the TBCG algorithm under the monotonicity assumption. Besides the proportional swap system, other algorithms and convergence conditions can be embedded into the TBCG algorithm. For example, the convergence conditions of the self-adaptive projection method and proximal point method (Han et al., 2015) rely on pseudo-monotonicity and semi-strictly quasi-monotonicity respectively. However, the path disutility is not a monotone function with respect to the path flow in general (Huang and Lam, 2002). Compared with other algorithms for traffic assignment, the route-swapping algorithm, a form of the proportional swap system, forces the path flow sequence to converge to a feasible state even without the monotonicity assumption (Mounce and Carey, 2011). The iterative sequence can be viewed as an evolutionary process of flow pattern from one disequilibrium state to an equilibrium or local stable state. To measure the convergence of this algorithm, a relative gap function is defined as Eq. (4.8). The pseudo-code of the TBCG algorithm is presented in Algorithm 4.2.

$$Regap(k, \boldsymbol{f_n}) = \max\left\{\frac{c_p^{rs}(k, \boldsymbol{f_n}) - c_{\min}^{rs}(\boldsymbol{f_n})}{c_{\min}^{rs}(\boldsymbol{f_n})}\right\} \quad \forall\, p \in \{\, i \mid f_i^{rs}(k) > 0, rs \in RS \,\} \quad (4.8)$$

The proposed four strategies in the TBCG algorithm target spatial and temporal exploration and exploitation to generate the most relevant path sets and time ranges that are fed into the route-swapping algorithm. The intrinsic feature of the route-swapping

algorithm is shifting flows from time-dependent paths with high disutilities to low disutility paths. A BR-DUE state is achieved through iterative path generation and path-flow swapping processes provided that the flow adjustment parameters meet the convergence conditions (Nagurney and Zhang, 1997). The parameter setting and initial solution are two essential elements affecting the convergent flow patterns. According to Appendix 2.A, it is likely that different inputs result in non-unique BR-DUE solutions. To measure the distance between two different BR-DUE solutions $\boldsymbol{f}_1^*$ and $\boldsymbol{f}_2^*$, the Euclidean distance can be adopted as $E(\boldsymbol{f}_1^*, \boldsymbol{f}_2^*) = \|\boldsymbol{f}_1^* - \boldsymbol{f}_2^*\|_{\ell^2}$, where $\|\cdot\|_{\ell^2}$ is a ℓ^2-norm operator. To measure how good a BR-DUE solution is, the system cost, defined as the inner product of path flow and cost vectors, gives a yardstick. These two measures of distance have large implications for traffic prediction and control.

Algorithm 4.2 TBCG algorithm

Step 1: (Initialization)

Set $n = 1$, $\boldsymbol{f_1} = \boldsymbol{0}$ and initial Δ_1, ε_1^{rs}, ϵ^{rs}, $c^{rs}(k, \boldsymbol{0})$, P_1^{rs} and Φ_1^{rs}, $\forall rs \in RS, k \in K_n$.

Step 2: (Traffic assignment)

Step 2.1: Assign flows on Φ_n^{rs}.

Step 2.2: If $\exists(p,k)$ satisfies Eq. (4.3) and $(p,k) \notin \Phi_n^{rs}$, $\Phi_n^{rs} = (p,k) \cup \Phi_n^{rs}$ and return Step 2.1;

otherwise, go to Step 3.

Step 3: (Path search)

For $rs \in RS$:

Step 3.1: Find $\tilde{k}$ dissatisfying Eq. (4.7) and $\tilde{K} = \{\tilde{k}\}$.

For $\tilde{k} \in \tilde{K}$:

Step 3.2: Search for acceptable paths $\bar{p}$ by the TBMDPS.

End for

End for

Step 3.3: If $\forall \bar{p} \in P_n^{rs}$, continue; otherwise, update P_n^{rs}, Φ_n^{rs} and go to Step 3.6.

Step 3.4: If $\Delta_n = \Delta$, continue; otherwise, perform Eq. (4.6), update K_n, $\boldsymbol{f_n}$, Φ_n^{rs} and go to Step 3.6.

Step 3.5: If $\varepsilon_n^{rs} = \varepsilon^{rs}$, go to Step 4; otherwise, decrease ε_n^{rs} by Eq. (4.5) and go to Step 3.6.

Step 3.6: Set $n = n + 1$ and go to Step 2.

Step 4: (Termination) Stop the algorithm and obtain the BR-DUE solution.

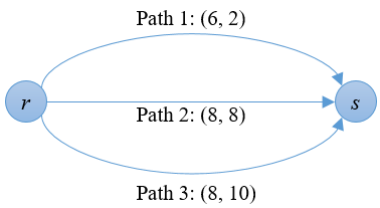

Figure 4.2 A two-node network of three parallel links.

Table 4.2 The path flows and disutilities at each iteration

Iter.	ε_n^{rs}	Item	Path	Time intervals				
				1	2	3	4	5
0	0.2	Disutility	1	1.20	1.20	1.20	1.80	2.40
1	0.2	Path flow	1	90.94	9.06	0	—	—
		Disutility	1	4.35	5.20	5.60	6.00	6.40
2	0.2	Path flow	1	42.38	0	0	—	—
			2	28.81	28.81	—	—	—
		Disutility	1	1.97	2.32	2.72	3.12	3.52
			2	1.66	1.92	2.32	2.80	3.40

Iter.	ε_n^{rs}	Item	Path	Time intervals									
				1	2	3	4	5	6	7	8	9	10
3	0.2	Path flow	1	23.21	17.31	0	0	0	0	—	—	—	—
			2	16.43	16.43	16.43	10.21	—	—	—	—	—	—
		Disutility	1	1.62	1.93	2.03	2.23	2.43	2.63	2.83	3.03	3.23	3.43
			2	1.64	1.68	1.73	1.94	2.14	2.34	2.54	2.80	3.10	3.40
4	0.1	Path flow	1	27.90	7.58	1.16	0	0	0	—	—	—	—
			2	21.12	21.12	21.12	0	—	—	—	—	—	—
		Disutility	1	1.72	1.83	1.83	2.03	2.23	2.43	2.63	2.83	3.03	3.23
			2	**1.67**	1.73	1.80	1.99	2.19	2.39	2.59	2.80	3.10	3.40

(—: not exist in the PTPS)

4.2.3 A case for illustrating tolerance-based strategies

These strategies are illustrated in a two-node network of three parallel links connecting one OD pair (Figure 4.2). The link free flow times and capacities are given near the links. The link travel time is calculated by Eq. (2.4), of which β_3 and β_4 are equal to 0.2 and 1 respectively. The targeted time interval range is from 1 min to 10 min. Other parameters are set as: $Q^{rs} = 100$, $\vartheta_1 = 0.5$, $\vartheta_2 = 0.5$, $\Delta = 1$ minute, $\eta_1 = 0.2$ \$/min, $\eta_2 = 0.1$ \$/min, $\eta_3 = 0.3$ \$/min, $k^{rs*} = 10$ min, $\kappa^{rs} = 2$ min, $\varepsilon^{rs} = \epsilon^{rs} = 0.1$, $\varepsilon_{\max}^{rs} = 0.2$. For initialization, $\Delta_1 = 2$ min, $\varepsilon_1^{rs} = 2$, $\Phi_1^{rs} = \{(1,1),(1,2),(1,3)\}$, $P_1^{rs} = \{1\}$ and $c^{rs}(k,\mathbf{0})$ $(k = 1,2,\cdots,5)$ are set as presented in Table 4.2. Besides the equilibrium results at each iteration after running the TBCG algorithm, the table exhibits the changes of the relative convergence threshold and temporal resolution.

At the first iteration, no time-dependent path satisfies Eq. (4.3) after reassigning path flows on Φ_1^{rs}, and the TBMDPSs are performed at all time intervals due to the large minimum disutility (4.35). As a result, path 2 is found and added to P_1^{rs}. To illustrate the process of each strategy more intuitively, the second iteration is presented using a timeline with time intervals shown above and path IDs on the left-side hand (Figure 4.3). The travel disutilities and flows at each interval are listed below the timeline. Moreover,

the current PTPS is displayed by the red segments; the new time-dependent paths satisfying Eq. (4.3) are displayed with yellow segments, and time intervals satisfying Eq. (4.7) are marked with rightward arrows. To explain strategy (iv), $c^{rs}(k, \mathbf{0})$ is repeated after each time interval in Figure 4.3(b).

At the second iteration, the time-dependent paths (2, 1) and (2, 2) have the minimum disutility (1.60) and fall out of Φ_2^{rs} as shown in Figure 4.3 (a). Consequently, both paths are added into Φ_2^{rs} during the temporal exploration. Then, the traffic assignment is implemented with the updated Φ_2^{rs} and the path disutilities are depicted in Figure 4.3 (b). Since the relative difference between the lower bound at interval 5 (2.40) and the minimum disutility (1.66) is larger than ε_2^{rs}, time interval 5 is skipped when performing the TBMDPS. Afterwards, the temporal exploitation is triggered by decreasing Δ_2 since no new path is generated. Figure 4.3 (c) presents the path disutilities, flows, and PTPS under the new temporal resolution.

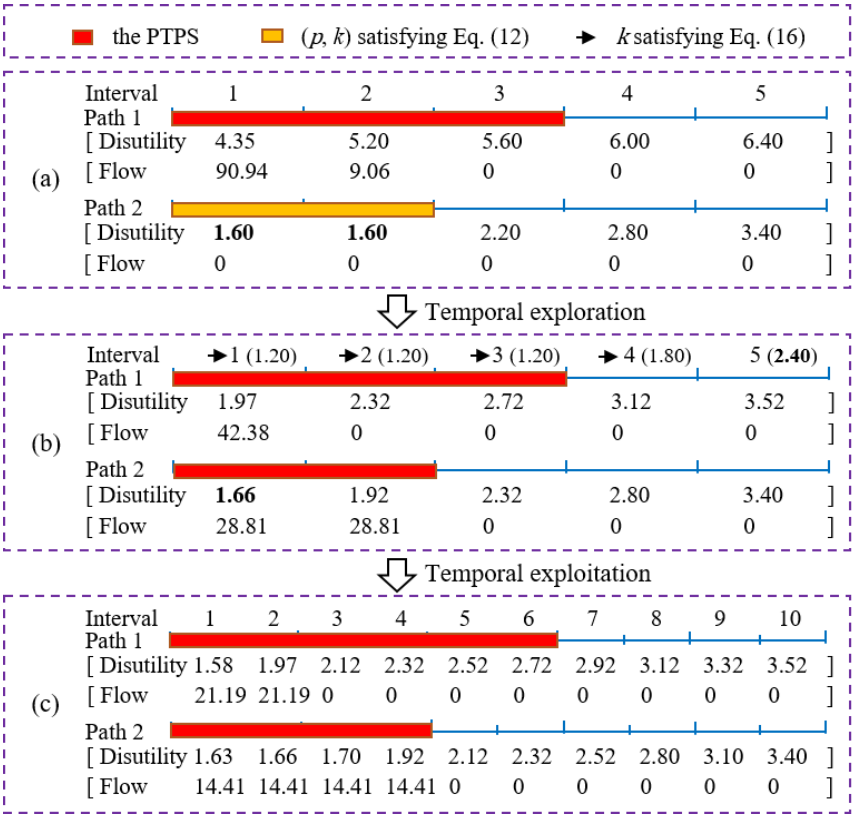

Figure 4.3 Three strategies at the second iteration.

The traffic assignment and path search are conducted alternately at the last two iterations, in which ε_3^{rs} is decreased at iteration 3 and the required equilibrium state is reached at the fourth iteration. It should be noted that path 3 has the same minimum disutility as path 2 (1.60 shown in Figure 4.3 (a)) since both paths have the same free flow time. As shown in Table 4.2, the minimum disutility at the last iteration is 1.67. Path 3 cannot be identified through the path search, which demonstrates the difference between the classic shortest path algorithm and the TBMDPS.

4.3 Numerical examples

This section presents numerical examples to assess the proposed TBCG algorithm for BR-DUE. Three aspects are concerned: the influence of the TBMDPS, the results of TBCG algorithm for DUE and BR-DUE, and the improvements due to the strategies. The solution algorithm is run on a personal computer with an Intel(R) Core(TM) i7-6700 3.40 GHz CPU and 8.00 GB RAM. The parameters are set as $\vartheta_1 = 0.5$ and $\vartheta_2 = 0.5$; $\Delta = 1$ minute; penalty coefficients $\eta_1 = 6.4$ \$/h , $\eta_2 = 3.9$ \$/h and $\eta_3 = 15.21$ \$/h; $k^{rs*} = 9$ am and $\kappa^{rs} = 0.1$ h; the time period is from 8 am to 12 pm; $\varepsilon^{rs} = \epsilon^{rs} = 0.1$ and $\varepsilon_1^{rs} = \varepsilon_{\max}^{rs} = 0.2$ unless otherwise explained. The link travel times are calculated by Eq. (2.4).

4.3.1 Example 1: six-node network

The six-node test network (Shao et al., 2013) is adopted for illustrating the effects of strategy (i) on path generation and the different solutions to the TBCG algorithm for DUE and BR-DUE. As shown in Figure 4.4, this network has two OD pairs, six nodes, seven links, and four paths.

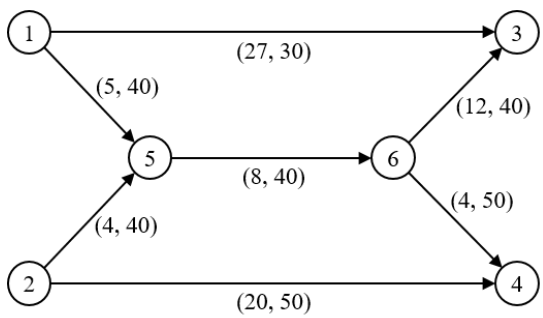

A path defined by a sequence of nodes

Path 1: 1-5-6-3

Path 2: 1-3

Path 3: 2-5-6-4

Path 4: 2-4

Figure 4.4 The test network.

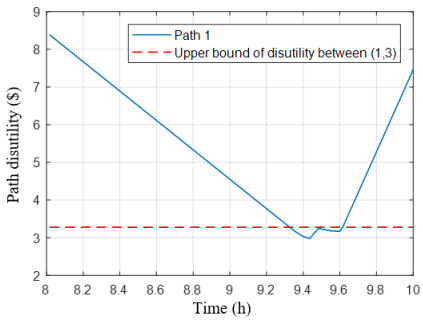

(a) Path disutility when $\epsilon^{rs} = 0.1$

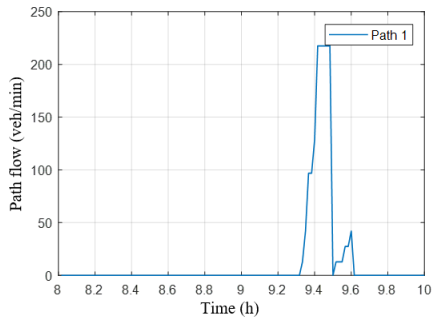

(b) Path flow when $\epsilon^{rs} = 0.1$

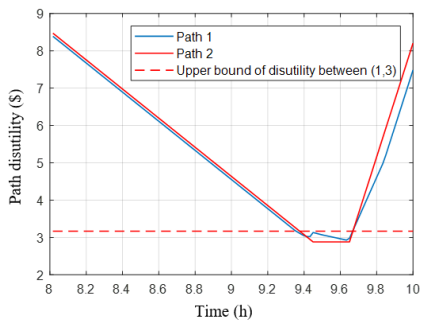

(c) Path disutility when $\epsilon^{rs} = 0$

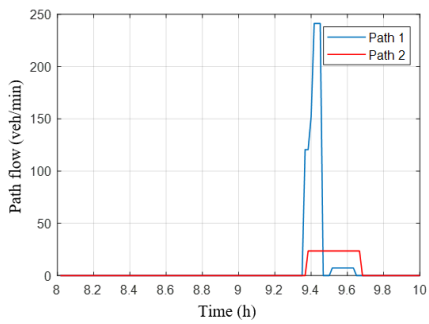

(d) Path flow when $\epsilon^{rs} = 0$

Figure 4.5 Equilibrium solution for BR-DUE

To illustrate the difference derived from the TBMDPS strategy, the demands for OD pairs (1, 3), (2, 4) are set as 1600 and 0 units respectively. Figure 4.5 indicates that the TBCG algorithm results in different equilibrium solutions compared with the traditional CG algorithm. As shown in Figure 4.5 (a) and (b), only path 1 is found and used for BR-DUE assignment. Recall that only the paths satisfying Eq. (4.2) are added to the path set. Path 2 does not satisfy this condition, although its disutility is smaller than path 1 in several intervals. This conclusion is deduced from Figure 4.5 (c) and (d), where two paths are generated and have non-zero path flows when ϵ^{rs} is equal to zero.

When the demand for OD pairs (1, 3) and (2, 4) increase to large values, such as $Q^{13} = 10^4$ and $Q^{24} = 8000$, traffic congestion occurs in this network. Some travelers depart early and shift paths to avoid late arrival penalty. Taking OD pair (1, 3) for example, in Figure 4.5 (b), travelers are assigned to the time period [9.3 am, 9.6 am] on path 1 when the OD demand is small, while this period shifts to [8.7 am, 9.3 am] on path 1 and path 2 as depicted in Figure 4.6 (d). Moreover, the equilibrium solution of the TBCG algorithm for BR-DUE model is different from that of the DUE. At the steady state of DUE, disutilities of used time-dependent paths are equal for the same OD pair

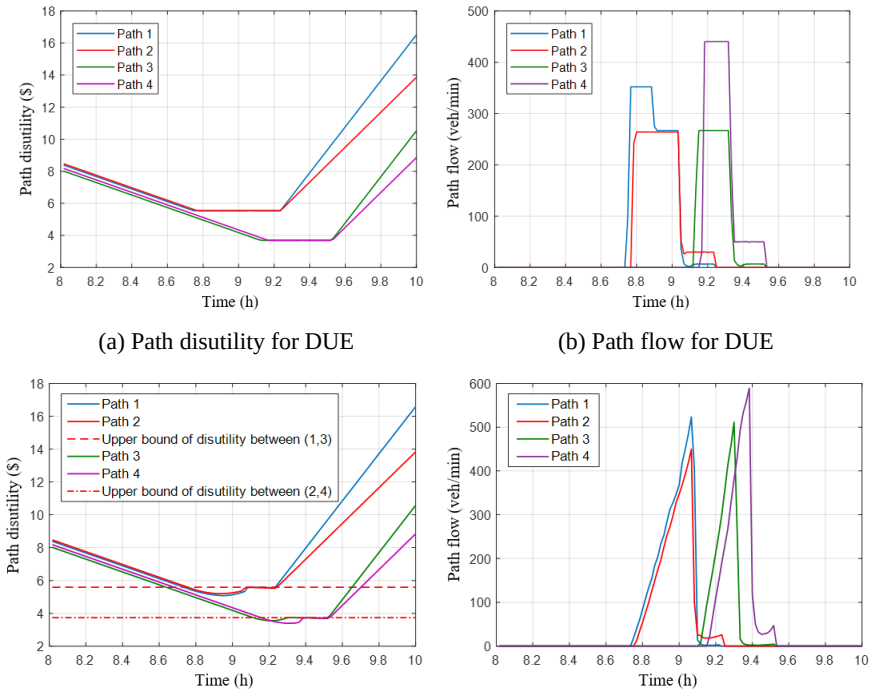

(a) Path disutility for DUE

(b) Path flow for DUE

(c) Path disutility for BR-DUE

(d) Path flow for BR-DUE

Figure 4.6 Equilibrium solutions for BR-DUE and DUE.

and the unused time-dependent paths have larger disutilities. These results are consistent with the DUE condition as depicted in Figure 4.6 (a) and (b). Regarding the BR-DUE, disutilities of the used time-dependent paths for the same OD pair are different and no larger than the critical values defined by Eq. (4.3), which are shown with the red dashed line in Figure 4.6 (c). Figure 4.6 indicates that the TBCG algorithm is capable of solving the BR-DUE problem.

4.3.2 Example 2: the Nguyen and Dupuis network

This example assesses the impact of the strategies (*ii*) - (*v*) on the improvement of the CG algorithm under different tolerances. For a fair comparison, the CG algorithms with and without these strategies both use the TBMDPS to generate paths. As depicted in Figure 4.7, this network (Long et al., 2013b; Li et al., 2018) has 13 nodes and four OD pairs including (1, 2), (1, 3), (4, 2), and (4, 3) with different traffic demand of 15360, 5120, 5120 and 8960 respectively. The link free flow times and capacities are marked near the corresponding links. The temporal resolution is initialized to $\Delta_1 = 2$ and $\vartheta_2 = 0.1$ in this example. For the route-swapping process, the step-size rule $\rho \cdot (1 +$

$\beta_5 m_4)/\lfloor 1 + m_5/2000 \rfloor$ is adopted, where $\rho = 0.1$ ensures a steady convergence, m_4 denotes the number of temporal exploitations, β_5 is a re-scaling factor, and m_5 is the number of path flow reassignments at each outer iteration.

The TBCG algorithm generates paths for traffic assignment driven by the tolerance-based travel behavior. The number of generated paths at BR-DUE is far less than that by path enumeration, which significantly decreases the size of time-dependent paths. Figure 4.8 presents a comparison of the number of paths derived from the TBCG algorithm and path enumeration. It shows the effectiveness even when traffic demand is large in this example.

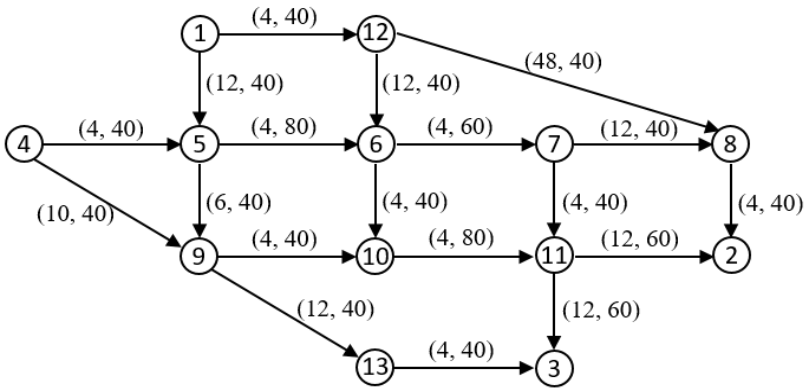

Figure 4.7 The Nguyen and Dupuis network.

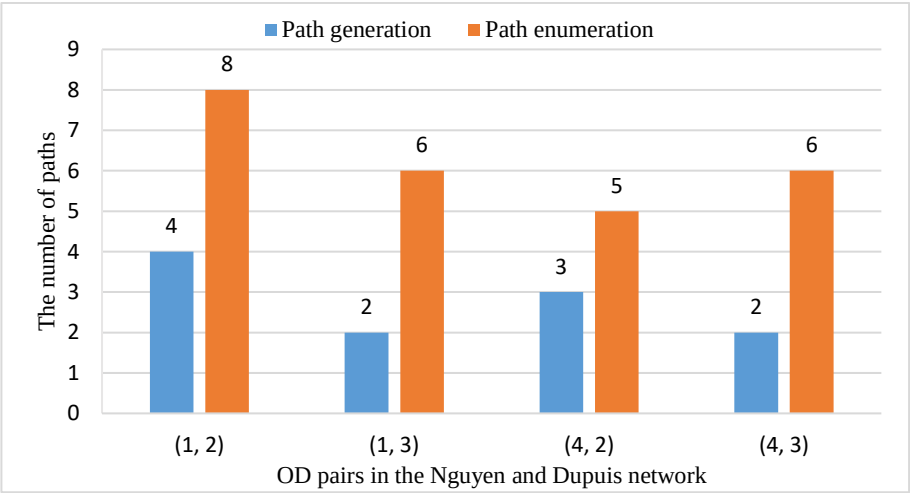

Figure 4.8 Comparison of the number of paths.

Table 4.3 Improvements of different strategies on CG algorithm

Strategies	Items	ε^{rs}					
		0.05	0.06	0.07	0.08	0.09	0.10
CG algorithm without strategy (*ii*)-(*iv*)	Number of path searches	722	722	722	722	722	722
	Number of network loadings	1855	1338	1217	1116	1103	931
	Computation time (s)	298.57	234.41	190.30	174.61	167.19	139.28
Strategy (*ii*)	Number of network loadings	1125	1000	866	907	737	687
	Computation time (s)	191.11	161.75	139.91	141.67	120.75	118.62
Strategy (*iii*)	Number of network loadings	2270	1847	1531	1082	986	854
	Computation time (s)	182.34	150.28	118.73	90.03	79.82	69.20
	Speedup factor	1.64	1.56	1.60	1.94	2.09	2.01
Strategy (*iv*)	Number of path searches	567	573	575	576	573	578
TBCG algorithm	Number of path searches	672	674	669	668	670	673
	Number of network loadings	861	707	687	686	651	608
	Computation time (s)	108.98	82.34	77.53	76.56	72.02	63.80
	Speedup factor	2.74	2.85	2.45	2.28	2.32	2.18

Table 4.4 Effects of the parameters of the TBCG algorithm

Parameters for comparison					CG algorithm	TBCG algorithm			
Δ_1	ϑ_2	Δ	$\varepsilon^{rs}_{\max}$	ϵ^{rs}	Computation time (s)	Number of network loadings	Number of path searches	Computation time (s)	Speedup factor
1	0.5	0.5	0.2	0.1		697	1336	162.60	2.95
2	0.5	0.5	0.2	0.1	479.85	614	1215	96.37	4.98
4	0.5	0.5	0.2	0.1		584	1137	48.69	9.85
4	**0.125**	0.5	0.2	0.1		656	851	96.80	4.96
4	**0.25**	0.5	0.2	0.1	479.85	638	1042	79.62	6.03
4	**0.5**	0.5	0.2	0.1		584	1137	47.46	10.11
4	0.5	**0.5**	0.2	0.1	479.85	584	1137	47.46	10.11
4	0.5	**1**	0.2	0.1	182.05	614	594	40.01	4.55
4	0.5	**2**	0.2	0.1	98.16	644	325	36.70	2.67
2	0.5	1	**0.15**	0.1		870	653	83.76	1.97
2	0.5	1	**0.2**	0.1		608	673	63.80	2.58
2	0.5	1	**0.25**	0.1	164.68	754	674	99.71	1.65
2	0.5	1	**0.3**	0.1		507	695	59.49	2.77
2	0.5	1	**0.35**	0.1		424	707	52.92	3.11
2	0.5	1	**0.4**	0.1		374	709	47.05	3.50
2	0.5	1	0.2	**0.05**		651	650	72.53	2.49
2	0.5	1	0.2	**0.1**		608	673	63.80	2.83
2	0.5	1	0.2	**0.15**	180.51	608	673	64.30	2.81
2	0.5	1	0.2	**0.2**		635	677	64.87	2.78
2	0.5	1	0.2	**0.25**		508	614	50.76	3.56
2	0.5	1	0.2	**0.3**		599	712	57.90	3.12

(Fixed parameter: $\vartheta_1 = 0.1, \varepsilon^{rs} = 0.1$. The parameter values in bold are the focus of attention.)

Table 4.3 shows the numbers of path searches, network loadings, and computation times of the CG algorithms with and without strategies (*ii*) - (*iv*) under a series of tolerances ε^{rs}. Compared with the CG algorithm without these strategies, strategy (*ii*) takes fewer network loadings and computation time to obtain the equilibrium results. More than 20 seconds are saved, although the differences in computation times decrease with the increase of ε^{rs}. Strategy (*iii*) increases the number of network loadings for some ε^{rs}. However, it gains more than 1.5 times speedup in computation time due to reduced time-dependent paths when $\Delta_n = 2$ minutes. Strategy (*iv*) skips around 150 tolerance-based path searches. Incorporating all strategies, the TBCG algorithm improves the CG algorithm in all aspects, leading to speedup factors larger than 2.

To demonstrate the effects of the spatial and temporal parameters of the four strategies, other parameters are fixed and the results are shown in Table 4.4. As shown in the first block, a larger Δ_1 leads to less dynamic network loadings and path searches, and hence a larger speedup factor. ϑ_2 impacts the occurrences of leaps from Δ_1 to Δ. Although more leaps are needed when ϑ_2 increases, the number of dynamic network loadings and computation time decrease. The reason is that decreasing Δ_n may generate new paths, which needs more path flow assignments to reach a new equilibrium state. Δ is related to the convergence precision. Decreasing Δ results in dramatic increases in the computation time of the CG algorithm, compared with the TBCG algorithm. $\varepsilon_{\max}^{rs}$ and ϵ^{rs} are related to the path flow assignment and path search process respectively. Larger $\varepsilon_{\max}^{rs}$ ensures the route-swapping algorithm to achieve the stop criterion with fewer iterations. However, this comes at the expense of current precision, as it may need extra iterations to generate new paths and perform path flow reassignments (e.g. $\varepsilon_{\max}^{rs} = 0.25$). When ϵ^{rs} taking a small value, more paths may satisfy Eq. (4.2) and be added to the path set for traffic assignment. As demonstrated, the TBCG algorithm obtains speedup factors significantly larger than 2 with most of the parameter setups.

4.3.3 Example 3: larger networks

The properties of path disutility function (Eq. (2.5)) make the projection-based algorithms used in, for example, Chen et al. (2001) and Long et al. (2013b), ineffective for DTA in large networks. This subsection uses larger networks, i.e., Sioux Falls network, Eastern Massachusetts (EMA) network, Anaheim network, and Chicago-Sketch network to illustrate the effectiveness of the TBCG algorithm in terms of computation time and the number of dynamic network loadings. The Sioux Falls network consists of 24 nodes and 76 links, the EMA network has 74 nodes and 258 links, the Anaheim network contains 416 nodes and 914 links, and the Chicago-Sketch network has 933 nodes and 2950 links. The network topology and OD demands are obtained from http://www.bgu.ac.il/~bargera/tntp/. Some data transformation is performed on the free-flow travel times and link capacities to fit the randomly selected OD pairs. Compared

with the settings of example 2, the same step-sizes are adopted in the route-swapping process except for ρ. The small demand result in a larger ρ (0.5) in this example to ensure an acceptable convergence. Other settings remain the same as example 2.

As an illustration of the convergence process, Figure 4.9 shows the convergence curves of the original CG algorithm and the TBCG algorithm in the Anaheim network with 1406 OD pairs. As depicted, the CG algorithm generates new paths only when the relative gap is less than 0.1, and it takes 38 path flow reassignments. For the TBCG algorithm, new path generation and temporal exploitation occur after 16 and 30 path flow reassignments respectively. Note that both processes are performed in a low temporal resolution. Moreover, the TBCG algorithm needs less path flow reassignments to converge to BR-DUE. A low temporal resolution guarantees faster convergence per iteration and a larger convergence threshold ensures fewer path flow reassignments, which lead to 2.14 speedup factor compared to the original CG algorithm.

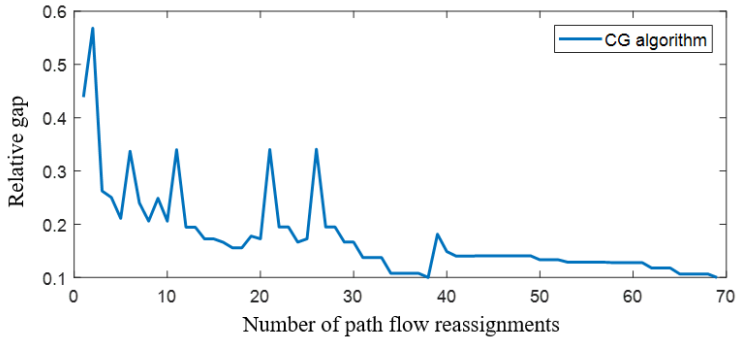

(a) Convergence of the CG algorithm

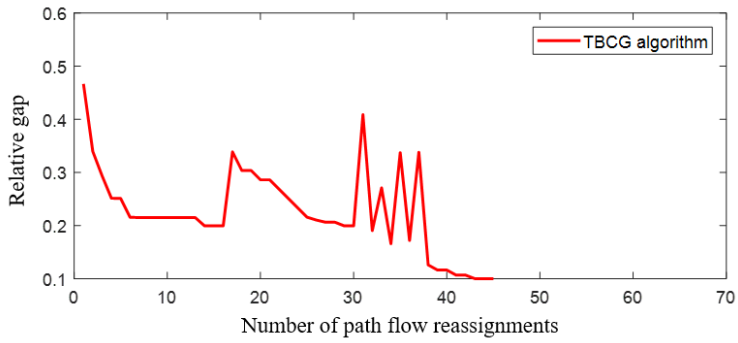

(b) Convergence of the TBCG algorithm

Figure 4.9 Convergence of two algorithms

Table 4.5 Performance of the TBCG algorithm

Network	Demand (*original demand)	OD pairs	Number of network loadings			Computation time (s)		
			CG algorithm	TBCG algorithm	Reductions (%)	CG algorithm	TBCG algorithm	Speedup factor
Sioux Falls	1	50	870	777	10.69	279.73	146.14	1.91
		100	1232	875	28.98	1165.24	476.72	2.44
	2	50	1294	827	36.09	520.4	262.76	1.98
		100	1620	1197	26.11	1565.71	730.63	2.14
EMA	10	100	219	193	11.87	712.55	359.05	1.98
		200	545	509	6.61	2160.49	1060.17	2.04
	20	100	309	231	25.24	546.01	272.86	2.00
		200	386	303	21.50	1799.14	823.95	2.18
Anaheim	1	1406	74	57	22.97	3116.79	1459.8	2.14
	10	200	149	78	47.65	807.25	304.84	2.65
		400	121	79	34.71	1247.66	612.33	2.04
	20	200	323	193	40.25	2334.37	980.02	2.38
		400	318	172	45.91	6236.97	2769.73	2.25
Chicago -Sketch	20	600	112	77	31.25	13940.34	7004.20	1.99
		1000	216	142	34.26	28363.46	13833.80	2.05
	50	200	112	72	35.71	3824.29	1810.8	2.11
		400	163	93	42.94	9432.38	4438.74	2.13
	100	100	162	96	40.74	2941.28	1203.57	2.44
		200	188	90	52.13	5990.14	1937.03	3.09

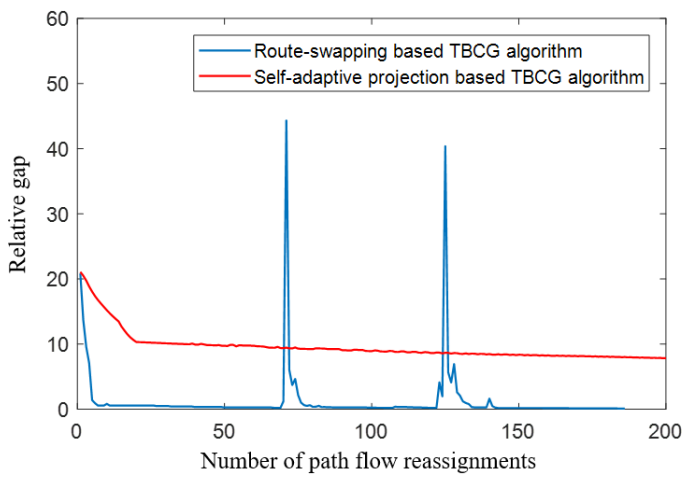

Figure 4.10 Comparison between two traffic assignment algorithms.

Table 4.5 provides the number of dynamic network loadings and the computation times required for both the original CG algorithm and the TBCG algorithm to achieve the BR-DUE. For different network configurations, the demands are enlarged from the original demands to produce congestion effects. It shows that the TBCG algorithm outperforms the original CG algorithm in terms of both indicators. The speedup factors of computation time are ranged from 1.91 to 3.09. In combination with example 2, it can be concluded that the speedup factors are significant and quite stable.

As an example to illustrate the flexibility of the TBCG algorithm, the self-adaptive projection method that is positioned in Han et al. (2015) with weak convergence condition and fast convergence is embedded into the TBCG scheme and compared with the route-swapping based TBCG algorithm. For a fair comparison, the same gap function shown in Eq. (4.8) is adopted in the EMA network with randomly selected 100 OD pairs. As depicted in Figure 4.10, the route-swapping based TBCG algorithm converges to a stable state with around 180 path flow reassignments crossing two major fluctuations, which manifest path generation and temporal exploitation. Regarding the self-adaptive projection based TBCG algorithm, the relative gap is still large after 200 path flow reassignments although it decreases steadily. The total computation times are 413.17s for the route-swapping based algorithm and 672.72s for the self-adaptive projection-based algorithm respectively. Thus, the route-swapping based TBCG algorithm performs better in this example.

4.4 Conclusions

This chapter proposed four tolerance-based strategies to extend the CG algorithm for solving the BR-DUE problem. By incorporating the characteristics of BR, the strategies combine the spatial-temporal exploration and exploitation of flow patterns for finding the BR-DUE solutions. It is notable that the four strategies maintain the convergence property of the CG algorithm. In particular, under the monotonicity assumption of the path disutility, the proposed TBCG algorithm is convergent. As illustrated in the numerical examples, the four strategies overall accelerate the original CG algorithm and reduce the numbers of path searches and dynamic network loadings. The TBCG algorithm is more efficient due to the smaller size of the path sets at most iterations.

Based on the TBCG algorithm, several extensions are worthy of investigation. First, the travel mode in this chapter is limited to private cars. Car-sharing services under the initiatives of sharing mobility can be embedded in the BR-DUE model and solved by the TBCG algorithm. Second, as travelers have different preferences, heterogeneity should be considered in the traffic assignment models as well. Lastly, as travel can be conceptualized as the derived demand from conducting activities at the destinations, the TBCG algorithm will be applied and further developed to address path generation and

personalized network formation in multi-state supernetwork models that are dedicated to activity-based travel demand analysis.

5

Analysis of FCFS Mechanisms in One-way CSS*

5.1 Introduction

Car-sharing services (CSS) receive increasing attention in the passenger mobility sector (Ferrero et al., 2018; Illgen and Höck, 2019). Without the necessity of car-ownership, CSS show potential solutions to tackle traffic congestion, reduce parking spaces, mitigate CO_2 emission, and save travel costs. According to Hampshire and Sinha (2011), more than four private cars (PCs) may be removed from the roads with the increase of one human-driven shared car (SC). Unlike the traditional car-renting services that have a full-day or multi-day time frame, CSS usually focus on short-term trips in urban environments. Based on the way of disposing of the SCs at the destinations, business-to-customer CSS typically have three categories: round-trip based (Ciari et al., 2013; Heilig et al., 2018), one-way station-based (Kaspi et al., 2014; Hu and Liu, 2016), and free-floating (Weikl and Bogenberger, 2015; Balac et al., 2017). Round-trip-based CSS require travelers to start and end the services at the same stations. As a more flexible service, one-way CSS (either station-based or free-floating) can be returned at any designated parking locations, which makes CSS attractive to travelers.

* This chapter is based on Wang, D., Liao, F., 2021. Analysis of first-come-first-served mechanisms in one-way car-sharing services. Transportation Research Part B: Methodological, 147, 22-41.

Responding to the growing interest in CSS, many studies have emerged to investigate the travel preferences and demand of CSS in general or specific categories. The pricing structure, access and egress time, personal attitudes, social influence, travel satisfaction, etc., are found to be key factors affecting travelers' decision to adopt CSS (Efthymiou et al., 2013; Balac et al., 2017; Becker et al., 2017; Rotaris et al., 2019; Zhou et al., 2020a, 2020b). Travel demand analyses are essential for the efficient deployment of CSS. Typically, the travel demand analyses rely on network-based equilibrium analyses and microsimulations to couple travel patterns and traffic flows. Network-based equilibriums (Atmani et al., 2014; Li et al., 2018) offer valuable comparison points of aggregate travel choices and flow patterns for CSS demand management. Alternatively, microsimulations have been applied to capture the microscopic behavior and demand patterns given CSS supplies. The paradigm of activity-based modeling has also been applied to investigate the detailed usage patterns of CSS when given service configurations (e.g., Heilig et al., 2018; Giorgione et al., 2019).

In parallel, a number of studies have been dedicated to managing supplies through deployment and operational strategies. For free-floating CSS, Weikl and Bogenberger (2013) introduced several relocation strategies and developed an integrated two-step model for optimal vehicle positioning and relocation. Nourinejad and Roorda (2014) proposed a dynamic optimization-simulation model for one-way car-sharing operations to capture the tradeoff between vehicle relocations and fleet size. Fan (2014) developed a multi-stage stochastic linear programming model to optimize the strategic allocation of SCs in space. For one-way CSS, Xu et al. (2018) suggested a mixed-integer nonlinear and nonconvex programming model to maximize the profit of car-sharing operators by determining the fleet size, trip pricing, vehicle relocations, and passenger assignment. Based on this work, Xu and Meng (2019) took dynamic vehicle relocation and nonlinear charging profile into consideration. To achieve better supply-demand alignment, Ströhle et al. (2019) explored the potentials of spatial and temporal customer flexibility under offline and online optimization. Illgen and Höck (2019) provided a comprehensive review of vehicle relocation problems in one-way CSS and concluded that a tradeoff among fleet size, relocation effort, and the service level is needed for efficient operations.

It should be noted that the above review concentrates on CSS facilitated by human-driven vehicles, given that such CSS have been deployed in many cities and will remain in the near future. Understanding the complex relations between the supply and demand of SCs is a critical step in the evaluation of CSS deployment and operational strategies. Similar to any public or third-party services, whether a traveler is served or not by CSS depends on the supply-demand dynamics at the service locations. However, most supply-oriented models (Weikl and Bogenberger, 2013; Fan, 2014; Boyaci et al., 2015; Chang et al., 2017; Xu et al., 2018; Ströhle et al., 2019; Xu and Meng, 2019) focused on the evaluation of the dynamic supplies subject to the constraints that the demands need to be satisfied, rather than the explicit supply-demand interactions.

Comparatively, less attention has been paid to the queueing mechanisms of CSS. Given that CSS only serve a niche market at this moment, the queueing phenomenon may not exist in some operational areas due to the low user acceptance and demand. However, the SC shortage may emerge at some CSS locations because of the unevenly distributed demand in space and time, especially during peak hours. In case the demand at a CSS location is not satisfied, the queue of CSS travelers may cumulate. To avoid waiting, some travelers may give up the car-sharing trip or move to other CSS locations. Hence, the demand of SCs is modified. The service mechanisms of treating the queues when supply insufficiency arises have significant impacts on the usage of SCs and the efficiency of CSS operations. Amongst, first-come-first-served (FCFS) (or broadly referred to as first-in-first-out (FIFO)) principle, restricting that travelers arriving first are served first, has been a widely used principle. Smartphone-based CSS applications facilitate the implementation of the FCFS principle in response to real-time service queries. For the same reason, it seems less problematic in disaggregate microsimulations with high time resolutions to address the queueing effects. However, it is notoriously difficult to analyze the supply-demand interactions and FCFS principle in aggregate network-based equilibrium studies in the discrete-time domain.

As an important component in CSS, the FCFS principle has only been weakly addressed in a few studies. Specifically, Clemente et al. (2013) characterized the one-way car-sharing process by six main phases, where the FCFS principle underlies the rental and use phases. However, the proposed discrete-event simulation approach did not provide detailed descriptions similar to other microsimulations. Levin et al. (2017) assumed that CSS travelers were served in an FCFS order if multiple travelers were waiting at the same location. However, the supply-demand dynamics under the FCFS principle were not explicitly formulated. The optimization model proposed by Chang et al. (2017) coped with the FCFS principle by several time-order constraints. A limitation is that the underlying queuing mechanism is not captured in the event of a supply shortage. Li et al. (2018) suggested an FCFS mechanism and modeled the CSS supply-demand interactions. However, the mechanism is based on a weak assumption that CSS travelers arriving at a location during the same interval would wait together until the demand is satisfied by incoming SCs. This assumption holds only when the unit of one time interval in the model system is extremely small.

This chapter aims to formulate and compare different FCFS mechanisms of one-way CSS, of which the first two were suggested in the literature and the latter two are suggested in this chapter. The FCFS mechanisms concern situations in which travelers wish to take SCs at a CSS location with a supply shortage. With the focus on short-term supply-demand interactions, only user-based relocations are considered in the one-way CSS. *No waiting* FCFS (NW-FCFS) is a naive mechanism supposing that travelers immediately leave the location by taking other transport modes if no SC is available (Chang et al., 2017). *Aggregate* FCFS (A-FCFS) mechanism adopts the assumption from

Li et al. (2018) that considers travelers arriving at a CSS location during the same interval as an aggregate unit. The aggregate unit is served immediately if the supply of SCs is sufficient. Otherwise, the travelers in this aggregate unit would wait and be served together until the stock is replenished. In that sense, SC stock and shortage may co-exist. Disaggregate FCFS (D-FCFS) mechanism relaxes the assumption of the second by allowing a part of travelers to use the SCs as long as the stock exists and other travelers to be served successively as the stock is continuously replenished. Consequently, SC stock and shortage exist exclusively at a CSS location. *VIP* (very important person) *membership* D-FCFS (VD-FCFS) mechanism further introduces the VIP services, in which the VIP travelers are allowed to jump the queue. For each mechanism, the supply-demand dynamics are formulated and the utilization rates at CSS locations are determined. To study the effects of different FCFS mechanisms and provide insightful comparisons, the mechanisms are embedded in a boundedly rational dynamic user equilibrium (BR-DUE) model in a bi-modal (PC and SC) transport network. Numerical examples demonstrate that different FCFS mechanisms tend to have different supply-demand dynamics and that the latter two mechanisms are more efficient in satisfying the SC demand. Under the VD-FCFS mechanism, ordinary travelers have to depart earlier for using SCs to escape from the competition with VIP travelers. There is a saturation point in the share of VIP travelers, beyond which VIP services would not benefit.

The remainder of the chapter is organized as follows. Section 5.2 presents the basic assumptions of the one-way CSS in a space-time bi-modal supernetwork. Section 5.3 formulates four variants of FCFS mechanisms and the supply-demand dynamics of SCs. Section 5.4 discusses BR-DUE conditions and properties. Moreover, a path expansion strategy is proposed for calculating the path disutilities associated with the suggested FCFS mechanisms. Numerical examples are given in Section 5.5 to illustrate the essential ideas of the proposed model. Finally, conclusions are provided in Section 5.6.

5.2 Basic assumptions and network representation

Given the focus of analyzing FCFS mechanisms at CSS locations, the car-sharing trips are studied in a bi-modal transport network. The network-based equilibrium model is chosen because it provides useful comparison points (holding other conditions unchanged) under different mechanisms. To convey the essential ideas, the following assumptions are made.

(1) The travelers make commuting trips in a bi-modal transport network during peak hours, for which the energy supply by fuel or electricity is not a concern. The bi-modal refers to PC and SC, which share the physical road network.

(2) All travelers' own PCs and have access to SCs depending on the availability. The origins and destinations are in the PC network. Transfer in terms of parking or picking-up is needed for switching the modes.

(3) Travelers demonstrate bounded rationality (BR) behavior and seek satisfactory choices of departure time, mode, and path in the bi-modal transport network. Travelers adapt the choices in a long-term process to achieve user equilibrium.
(4) Limited SCs are deployed in the study area under the same FCFS mechanism. A traveler needs to wait for an incoming SC when there is a supply shortage. Since the travelers do not know exactly when and how many SCs will come to the CSS location at the moment of arriving, the waiting time before the traveler accessing one SC is treated as an unknown.
(5) Parking a PC may involve parking fees at a certain location while parking an SC is free at all CSS locations. One SC serves one person per trip; thus, ride-sharing by multiple travelers is not considered.

Following the multi-state supernetwork (SNK) representation (Liao et al., 2010, 2013), a bi-modal supernetwork $SNK(N, A)$ is considered, where N and A denote the sets of locations and links respectively. According to the concept of vehicle state, a road network is copied into two networks, in which traversing a link represents the physical mobility by a specific mode. The sub-networks are interconnected by transition links, representing the transfer between the two modes at CSS locations. The bi-modal supernetwork endogenously embeds mode choice into path choice. Figure 5.1 gives an example of trip representation, in which G is the traditional road network. Travel links (PC link set A_{PC} in red and SC link set A_{SC} in green) and transition links (A_{TS} in blue) are two different types of links. r and s are nodes representing the origin and destination (OD) respectively; node b is a CSS location. As depicted in this figure, the path from r to s going through the blue links denotes a trip that the traveler picks up a PC at r and drives to b, then takes an SC to the destination s, and finally egresses the SC. For the sake of convenience, picking up PC at r and parking at b are not shown in Figure 5.1.

This trip can be extended in a 2-D space-time representation as depicted by Figure 5.2, in which shapes of circle, square, and diamond denote locations for origin (r), transfer node (b), and destination (s) respectively. To keep consistency, directed links in the same colors denote the same type of links, i.e., red for travel by PC, blue for transition links, and green for travel by SC. To exhibit transition states, locations r', b' and s' are copies of r, b and s respectively to denote the completion of switching modes. Dummy links in blue are created to denote picking up or parking PC or SC in Figure 5.2. The thick (highlighted) directed links together form one specific space-time trip that a traveler leaves home during time interval 1 and picks up a PC during t_1, arrives at transfer location b during t_2, then transfers until the end of time interval t_3, drives by SC to destination s during t_4, and egresses the SC during t_5. Other space-time trips can also be represented in Figure 5.2. For example, the thin directed links form two alternative space-time trips by PC and SC respectively.

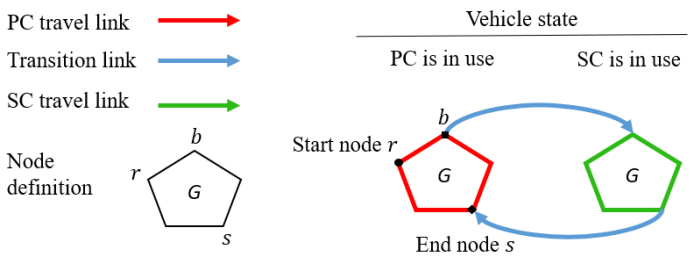

Figure 5.1 Bi-modal supernetwork representation.

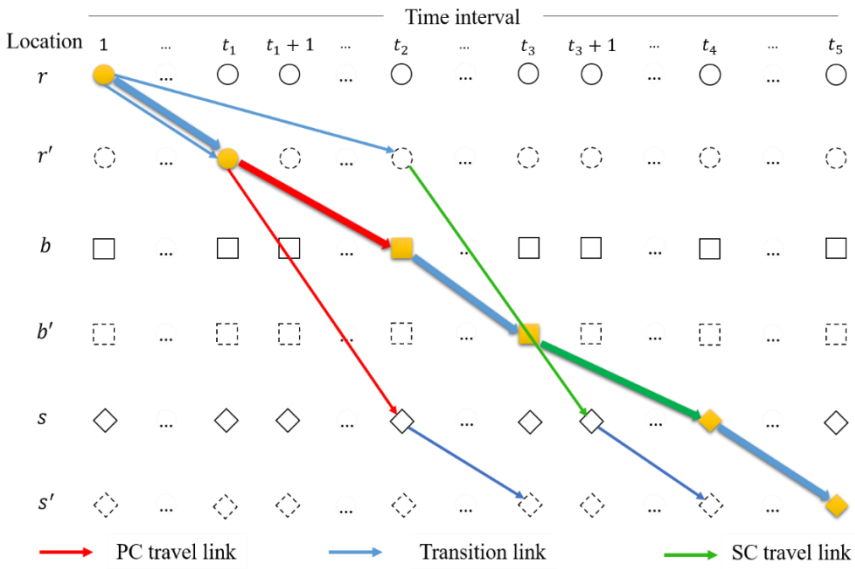

Figure 5.2 Example of 2-D space-time supernetwork.

5.3 FCFS mechanisms

FCFS is a service management principle that processes queuing requests chronologically. With the FCFS principle in CSS, travelers who come first are served first. In the context of discrete-time domain, this section discusses four typical variants of FCFS mechanisms, namely, NW-FCFS, A-FCFS, D-FCFS, and VD-FCFS. The latter two are proposed to relax the strong assumption from Li et al. (2018). Given CSS location a and time interval k, $S_a(k)$, $D_a(k)$, $h_a(k)$, and $g_a(k)$ are used to denote the supply, demand, stock, and shortage of SCs at a at the end of time interval k, respectively. Let $u_a(k)$ denote the arrival flow that completes SC trips at a during k, $v_a(k)$ the arrival

flow that requests to use SCs, $z_a(k,w)$ the flow arriving at a during k and served after waiting time w, and $\lambda_a(k,w)$ the proportion of travelers who arrive at a during k and are served after waiting w time intervals. For the convenience of analysis, $h_a(0)$ is set as the initial distribution of SC, $S_a(0) = h_a(0)$, and $D_a(0) = u_a(0) = v_a(0) = g_a(0) = 0$. For each FCFS mechanism, the supply-demand interactions are analyzed below to determine whether travelers' requests of SCs are served and how long the travelers need to wait (if served).

5.3.1 NW-FCFS mechanism

Chang et al. (2017) assumed that travelers are either served due to a sufficient SC supply or seek alternative modes immediately to avoid waiting. This assumption results in an imaginative phenomenon that the queue is dismissed right away and no waiting time is involved, referred to as NW-FCFS. Given a time interval $k \geq 1$, the supply is the sum of existing stock and newly added SC supply. Since unserved travelers do not opt to wait for incoming SCs, there is no shortage under this mechanism. Thus, the demand is equal to the incoming SC requests. While the shortage is forced to reset to zero, the stock is equal to the surplus supply. The supply-demand dynamics under the NW-FCFS mechanism are formulated as

$$S_a(k) = h_a(k-1) + u_a(k), \quad a \in N, k \in K \tag{5.1}$$

$$D_a(k) = v_a(k) \tag{5.2}$$

$$h_a(k) = \max\{0, S_a(k) - D_a(k)\} \tag{5.3}$$

$$g_a(k) = 0 \tag{5.4}$$

The zero waiting time results in Eq. (5.5).

$$z_a(k,w) = \begin{cases} \min\{D_a(k), S_a(k)\}, & w = 0 \\ 0, & \text{otherwise} \end{cases} \tag{5.5}$$

5.3.2 A-FCFS mechanism

The A-FCFS mechanism treats travelers arriving at a CSS location during the same interval as an aggregate unit that is served before other units who arrive during a later interval (Li et al., 2018). When there is a sufficient SC supply, travelers in the same aggregate unit are served immediately; otherwise, they would wait together for the replenishment of SCs.

Compared with the NW-FCFS mechanism, the A-FCFS mechanism has the same supply formulation but a different demand formulation due to possible queues at the CSS locations. As queueing is allowed, the demand exists until being satisfied. The demand is an accumulation of the incoming SC requests and the shortage at the end of the previous time interval. The SC stock is formulated in a neat form as the non-negative difference between the accumulation of SC arrivals and the served SC requests. The SC shortage equals the accumulation of unserved travelers. The supply-demand dynamics under the A-FCFS mechanism are formulated as

$$D_a(k) = g_a(k-1) + v_a(k) \tag{5.6}$$

$$h_a(k) = h_a(0) + \sum_{\tau=0}^{k} u_a(\tau) - \sum_{\tau=0}^{\hat{t}} v_a(\tau) \tag{5.7}$$

$$g_a(k) = \begin{cases} \sum_{\tau=\hat{t}+1}^{k} v_a(\tau), & S_a(k) < D_a(k) \\ 0, & \text{otherwise} \end{cases} \tag{5.8}$$

where $\hat{t}$ is the maximum time interval until the cumulative SC requests are served by the cumulative SCs at the end of interval k, formulated as $\hat{t} = \underset{t}{\operatorname{argmax}}\{\sum_{\tau=0}^{t} v_a(\tau) \leq h_a(0) + \sum_{\tau=0}^{k} u_a(\tau),\ t \leq k\}$. With the definition of $\hat{t}$, $\sum_{\tau=0}^{\hat{t}} v_a(\tau)$ in Eq. (5.7) denotes the SC requests served by k and $\sum_{\tau=\hat{t}+1}^{k} v_a(\tau)$ in Eq. (5.8) is the number of travelers that have not been served. Under the A-FCFS mechanism, the potential waiting time and the flow served during $k + w$ are expressed as Eqs. (5.9)-(5.10) respectively.

$$w_a(k) = \underset{t}{\operatorname{argmin}} \left\{ D_a(k) \leq h_a(k-1) + \sum_{\tau=k}^{t} u_a(\tau) \right\} - k \tag{5.9}$$

$$z_a(k, w) = \begin{cases} v_a(k), & w = w_a(k) \\ 0, & \text{otherwise} \end{cases} \tag{5.10}$$

5.3.3 D-FCFS mechanism

In reality, SC stock and shortage exist exclusively at a CSS location. When travelers arrive at a CSS location during the same time interval, a proportion of the travelers can use the SCs if there is an insufficient SC stock, while other travelers will be served by incoming SCs. Rather than considering travelers arriving during the same interval as an aggregate unit, the D-FCFS mechanism enables CSS to serve them during different time intervals, no later than the time point starting to serve travelers who arrive later.

The supply and demand formulations under the D-FCFS mechanism remain the same as Eqs. (5.1) and (5.6) respectively. However, the disaggregation of travelers results in different formulations of the SC stock and shortage as

$$h_a(k) = \max\{0, S_a(k) - D_a(k)\} \tag{5.11}$$

$$g_a(k) = \max\{0, D_a(k) - S_a(k)\} \tag{5.12}$$

where $h_a(k) \cdot g_a(k) = 0$ holds $\forall a, k$. With the D-FCFS mechanism, travelers arriving at a during k may be served at different time intervals. As a specific traveler cannot be identified from the flow, the potential waiting time cannot be formulated for a specific traveler. The first traveler is served when the demand at the end of interval $k-1$ is fully met and there is a surplus supply. The last traveler is served when the current demand is fully satisfied by the current or any future supply. Mathematically, the minimum and maximum potential waiting times are expressed respectively as

$$w_{a,\min}(k) = \underset{t}{\operatorname{argmin}}\left\{D_a(k-1) < S_a(k-1) + \sum_{\tau=k}^{t} u_a(\tau)\right\} - k \tag{5.13}$$

$$w_{a,\max}(k) = \underset{t}{\operatorname{argmin}}\left\{D_a(k) \le h_a(k-1) + \sum_{\tau=k}^{t} u_a(\tau)\right\} - k \tag{5.14}$$

For travelers arriving at a during $k+1$, the earliest time being served is expressed by

$$\begin{aligned} k + 1 + w_{a,\min}(k+1) &= \underset{t}{\operatorname{argmin}}\left\{D_a(k) < S_a(k) + \sum_{\tau=k+1}^{t} u_a(\tau)\right\} \\ &= \underset{t}{\operatorname{argmin}}\left\{D_a(k) < h_a(k-1) + \sum_{\tau=k}^{t} u_a(\tau)\right\} \\ &\ge k + w_{a,\max}(k) \end{aligned} \tag{5.15}$$

where $k + w_{a,\max}(k)$ is the maximum service time for travelers arriving at a during k. The second equation holds due to the definition of the SC supply in Eq. (5.1). The inequality in the third line means that travelers arriving later are not served earlier, which is consistent with the FCFS principle.

Under the D-FCFS mechanism, travelers arriving during the same interval are divided into several groups and served with different waiting times. The quantification of the number of CSS recipients in each group, $z_a(k, w)$, can be distinguished into two

circumstances. If $w_{a,\min}(k) = w_{a,\max}(k)$, all travelers arriving during k are served simultaneously and $z_a(k,w)$ is expressed by Eq. (5.10). Otherwise, $w_{a,\min}(k) < w_{a,\max}(k)$, $z_a(k,w)$ is calculated based on where w is located within $\left[w_{a,\min}(k), w_{a,\max}(k)\right]$. If $w = w_{a,\min}(k)$, the SC supply at a at the end of $k+w$ serves the travelers arriving at a earlier than the beginning of k first and then a group of travelers arriving at a during k. When w falls between $w_{a,\min}(k)$ and $w_{a,\max}(k)$, all arrival SCs during interval range $\left(k + w_{a,\min}(k), k + w_{a,\max}(k)\right)$ are used for serving those travelers arriving during k. If $w = w_{a,\max}(k)$, the remainder travelers are served. In sum, $z_a(k,w)$ is formulated as

$$z_a(k,w)=\begin{cases} h_a(k-1) + \sum_{\tau=k}^{k+w} u_a(\tau) - g_a(k-1), & w = w_{a,\min}(k) \\ u_a(k+w), & w \in \left(w_{a,\min}(k), w_{a,\max}(k)\right) \\ v_a(k) - \sum_{\tau=w_{a,\min}(k)}^{w_{a,\max}(k)-1} z_a(k,\tau), & w = w_{a,\max}(k) \\ 0, & \text{otherwise} \end{cases} \tag{5.16}$$

The above three FCFS mechanisms have different expressions of $z_a(k,w)$, but a common expression of the proportion of travelers arriving during k and being served at a after waiting for w intervals. The proportion is denoted by $\lambda_a(k,w)$ and formulated as

$$\lambda_a(k,w) = \frac{z_a(k,w)}{v_a(k)} \tag{5.17}$$

Node arriving flow $v_a(k)$ is reset to max $\{v_a(k), o\}$ in the algorithmic implementations to ensure the denominator larger than zero, where o is a very small positive number satisfying $o \to 0^+$.

5.3.4 VD-FCFS mechanism

The VD-FCFS mechanism adds privilege service to the D-FCFS mechanism. VD-FCFS mechanism allows VIP members who pay an extra VIP membership fee to jump the queue. Depending on the service industry, pricing policy, and equity considerations, various privilege services exist. This mechanism concerns two traveler classes (VIP and ordinary) and allows VIP travelers to be served ahead of ordinary travelers who are already waiting in the queue. Although VIP travelers may be served earlier than ordinary travelers, the FCFS principle is maintained when a queue of VIP travelers exists.

The demand and shortage of SCs have distinctions between the two classes of travelers. To keep consistency, the notations used above attached with superscripts "V" and "O" refer to the same entities for VIP and ordinary travelers respectively (wildcard $* \in \{\mathrm{V}, \mathrm{O}\}$); and notations without any superscripts denote the summation of both classes of travelers. Under the VD-FCFS mechanism, the total SC supply has the same formulation as Eq. (5.1). The demand, stock, and shortage of SCs are formulated as

$$D_a^*(k) = g_a^*(k-1) + v_a^*(k) \tag{5.18}$$

$$h_a(k) = \max\{0, S_a(k) - D_a^{\mathrm{V}}(k) - D_a^{\mathrm{O}}(k)\} \tag{5.19}$$

$$g_a^{\mathrm{V}}(k) = \max\{0, D_a^{\mathrm{V}}(k) - S_a(k)\} \tag{5.20}$$

$$g_a^{\mathrm{O}}(k) = \begin{cases} D_a^{\mathrm{O}}(k), & D_a^{\mathrm{V}}(k) \geq S_a(k) \\ D_a(k) - S_a(k), & D_a(k) \geq S_a(k) > D_a^{\mathrm{V}}(k) \\ 0, & \text{otherwise} \end{cases} \tag{5.21}$$

Eqs. (5.18)-(5.20) have similar expressions with the corresponding terms under the D-FCFS mechanism. Eq. (5.21) shows that the SC shortage of VIP travelers is satisfied before that of ordinary travelers.

The waiting times and the served flow of VIP travelers, which are not affected by ordinary travelers, are formulated as Eqs. (5.22)-(5.24) for completeness.

$$w_{a,\min}^{\mathrm{V}}(k) = \underset{t}{\operatorname{argmin}} \left\{ D_a^{\mathrm{V}}(k-1) < S_a(k-1) + \sum_{\tau=k}^{t} u_a(\tau) \right\} - k \tag{5.22}$$

$$w_{a,\max}^{\mathrm{V}}(k) = \underset{t}{\operatorname{argmin}} \left\{ D_a^{\mathrm{V}}(k) \leq h_a(k-1) + \sum_{\tau=k}^{t} u_a(\tau) \right\} - k \tag{5.23}$$

$$z_a^{\mathrm{V}}(k,w) = \begin{cases} h_a(k-1) + \sum_{\tau=k}^{k+w} u_a(\tau) - g_a^{\mathrm{V}}(k-1), & w = w_{a,\min}^{\mathrm{V}}(k) \\ u_a(k+w), & w \in \left(w_{a,\min}^{\mathrm{V}}(k), w_{a,\max}^{\mathrm{V}}(k)\right) \\ v_a^{\mathrm{V}}(k) - \sum_{\tau=w_{a,\min}^{\mathrm{V}}(k)}^{w_{a,\max}^{\mathrm{V}}(k)-1} z_a^{\mathrm{V}}(k,\tau), & w = w_{a,\max}^{\mathrm{V}}(k) \\ 0, & \text{otherwise} \end{cases} \tag{5.24}$$

Different from the above, ordinary travelers arriving at a during interval k begin to be served if two clusters of SC requests are served and a surplus supply exists. The first cluster is the demand of both classes of travelers at the end of interval $k-1$, $D_a(k-1)$, while the second is the inflow of cumulative VIP travelers from the beginning of k to the end of $k+w$, $\sum_{\tau=k}^{k+w} v_a^{\mathrm{V}}(\tau)$. Any VIP travelers arriving between the beginning of k and the end of $k+w$ jump the queue and delay the CSS for ordinary travelers. Similarly, the maximum potential waiting time depends on the inflow of cumulative VIP travelers from the beginning of k, the SC shortage of VIP travelers at the end of $k-1$, and the ordinary demand at the end of k. Hence, the bounded potential waiting times and served flow of ordinary travelers are

$$w_{a,\min}^{\mathrm{O}}(k)=\underset{t}{\operatorname{argmin}}\left\{D_a(k-1)+\sum_{\tau=k}^{t} v_a^{\mathrm{V}}(\tau) < S_a(k-1)+\sum_{\tau=k}^{t} u_a(\tau)\right\}-k \tag{5.25}$$

$$w_{a,\max}^{\mathrm{O}}(k)=\underset{t}{\operatorname{argmin}}\left\{D_a^{\mathrm{O}}(k)+g_a^{\mathrm{V}}(k-1)+\sum_{\tau=k}^{t} v_a^{\mathrm{V}}(\tau) \le h_a(k-1)+\sum_{\tau=k}^{t} u_a(\tau)\right\}-k \tag{5.26}$$

$$z_a^{\mathrm{O}}(k,w)=\begin{cases} h_a(k-1)+\sum_{\tau=k}^{k+w} u_a(\tau)-g_a^{\mathrm{O}}(k-1)-g_a^{\mathrm{V}}(k-1)-\sum_{\tau=k}^{k+w} v_a^{\mathrm{V}}(\tau), & w=w_{a,\min}^{\mathrm{O}}(k) \\ \max(u_a(k+w)-g_a^{\mathrm{V}}(k+w-1)-v_a^{\mathrm{V}}(k+w),0), & w\in\left(w_{a,\min}^{\mathrm{O}}(k),w_{a,\max}^{\mathrm{O}}(k)\right) \\ v_a^{\mathrm{O}}(k)-\sum_{\tau=w_{a,\min}^{\mathrm{O}}(k)}^{w_{a,\max}^{\mathrm{O}}(k)-1} z_a^{\mathrm{O}}(k,\tau), & w=w_{a,\max}^{\mathrm{O}}(k) \\ 0, & \text{otherwise} \end{cases} \tag{5.27}$$

For VIP travelers, the served flow formulated as Eq. (5.24) has a similar form with Eq. (5.16). The served flow of ordinary travelers, formulated as Eq. (5.27), is subject to the served flow of VIP travelers. Both classes of travelers have the same formulation of $\lambda_a^*(k,w)$ as

$$\lambda_a^*(k,w)=\frac{z_a^*(k,w)}{v_a^*(k)} \tag{5.28}$$

As seen above, under the four FCFS mechanisms, the supply-demand dynamics of SCs have different outcomes. Although the formulations are centered at user-based relocations, operator-based relocations of human-driven or autonomous SCs can also be incorporated into the supply-demand dynamics with modifications in $u_a(k)$ and $v_a(k)$. The following remarks are made regarding the relationships among the four FCFS mechanisms.

Remark 5.1 Given the same SC requests under the four FCFS mechanisms, the supply has the same formulation, but the demand is satisfied at different levels. The NW-FCFS mechanism avoids waiting time at the expense of possible demand loss. The co-existence of SC stock and shortage under the A-FCFS mechanism has a negative influence on the waiting time and utilization rate. Comparatively, SCs under the D-FCFS and VD-FCFS mechanisms can be used more efficiently. When the length of one time interval is sufficiently small, the A-FCFS mechanism approximates the D-FCFS mechanism. The VD-FCFS mechanism degenerates into the D-FCFS mechanism when there is only one traveler class.

Remark 5.2 The choices of SCs are reflections of the supply-demand dynamics and different at most cases across the FCFS mechanisms. However, when certain admissible conditions are met, the choices tend to be consistent. It is obvious that $S_a(k) \geq D_a(k)$ is an admissible condition among the NW-FCFS, A-FCFS, and D-FCFS mechanisms. When $S_a(k) < D_a(k)$, A-FCFS and D-FCFS mechanisms have the same supply-demand dynamics under the condition that there exists a t less than k satisfying $h_a(0) + \sum_{\tau=0}^{k} u_a(\tau) = \sum_{\tau=0}^{t} v_a(\tau)$. The condition indicates that the arriving SCs before the end of k can exactly serve the SC requests at an interval before k. Since the equation is hard to be fulfilled, D-FCFS outperforms A-FCFS in general. The supply-demand dynamics and admissible conditions under the four mechanisms are illustrated in Appendix 5.A.

5.4 Incorporation of FCFS mechanism in a BR-DUE model

This section first presents the link in a bi-modal supernetwork. Next, to address the different waiting times under the D-FCFS and VD-FCFS mechanisms, a path expansion strategy is proposed to express the path disutility.

5.4.1 Link disutility

As shown in Section 5.2, transition and travel links are two link types in the bi-modal supernetwork. Their link disutilities are discussed separately.

Transition links

Transition links connect the same nodes of different vehicle states to denote the process of parking/picking-up a PC or SC. The disutility of a transition link can be simply expressed as

$$c_l(k) = \eta_4 \cdot \psi_l(k) + \eta_5 \cdot \phi_l(k), \quad \forall\, k \in K, l \in A_{TS} \tag{5.29}$$

where $c_l(k)$ is the link disutility incurred by travelers that enter link l during k, $\psi_l(k)$ and $\phi_l(k)$ are the location- and time-dependent transition time and monetary cost respectively; η_4 and η_5 are the disutility coefficients of transition time and monetary cost respectively.

In addition to Eq. (5.29), the last transition link disutility $c_l(k)$ is added with an unpunctual term $\tilde{c}_l(k')$ to capture early and late arrivals.

$$\tilde{c}_l(k') = \begin{cases} \eta_2 \cdot [k^{rs*} - \kappa^{rs} - k'], & \text{if } k' < k^{rs*} - \kappa^{rs} \\ \eta_3 \cdot [k' - k^{rs*} - \kappa^{rs}], & \text{if } k' > k^{rs*} + \kappa^{rs} \\ 0, & \text{otherwise} \end{cases} \quad \forall\, l \in A_{TS}, rs \in RS \tag{5.30}$$

where k' is the arrival time at destination s. The unpunctual formulation (Eq. (5.30)) is consistent with Eq. (2.2).

Travel links

Travel links connect different nodes in the same sub-networks. Travel time and monetary expenses are considered in the link disutility. Particularly, for the start link of an SC trip, as shown in Section 5.3, travelers at a CSS location may experience waiting. For an ordinary traveler, the disutility of the start link of an SC trip is expressed as a weighted sum as

$$c_l(k) = \eta_6 \cdot w + \eta_7 \cdot g_l(k + w), \quad k \in K, l \in A_{SC} \tag{5.31}$$

where link l is the first link of an SC trip, w is the waiting time for travelers arriving at the entry node of l during k, η_6 denotes the disutility coefficient of waiting time, η_7 is the disutility coefficient of travel time by SC, the linear price of using SC is implicitly indicated by η_7, and $g_l(\cdot)$ is a travel time operator.

Let c_0 be the average VIP membership fee per trip. The disutility of the start link of an SC trip for a VIP traveler is expressed as

$$c_l^{\mathrm{V}}(k) = \eta_6 \cdot w + \eta_7 \cdot g_l(k + w) + \eta_8 \cdot c_0, \quad k \in K, l \in A_{SC} \tag{5.32}$$

where η_8 denotes the disutility coefficient of monetary cost for the VIP membership fee per trip.

For the subsequent SC links, no waiting time is needed. The disutility of these SC links has a similar formulation with the PC link disutility presented by Eq. (5.33), except for the disutility coefficient of link travel time by PC (η_1).

$$c_l(k) = \eta_1 \cdot g_l(k), \quad k \in K, l \in A_{PC} \tag{5.33}$$

Remark 5.3 Several traffic flow propagation models, for example, the point-queue system (Huang and Lam, 2002), the delay-function-based link model (Nie and Zhang, 2005), and the link transmission model (Yperman, 2007), can be employed to establish the travel time operator $\mathscr{g}_l(\cdot)$. The main factors affecting travel times are link flows and capacities. As the physical roads are shared by PCs and SCs, $\mathscr{g}_l(\cdot)$ is determined by the link flows of PCs and SCs.

5.4.2 Path disutility, path expansion, and BR-DUE model

By combining the disutilities of transition links, PC links, and SC links, the path disutility is calculated as the summation of the associate link disutilities as

$$c_p^{rs}(k, \boldsymbol{f}) = \sum_{l \in A} \sum_{\tau \in K} \delta_{plk}^{rs}(\tau) \cdot c_l(\tau), \quad \forall\, rs \in RS, p \in P^{rs}, k \in K \tag{5.34}$$

where $\delta_{plk}^{rs}(\tau)$ is a 0-1 indicator variable, $\delta_{plk}^{rs}(\tau) = 1$ if travelers of rs depart during k via path p and arrive at the entry node of link l during τ and $\delta_{plk}^{rs}(\tau) = 0$ otherwise.

Note that the link-path incidence variable $\delta_{plk}^{rs}(\tau)$ is often used in the literature to force that travelers departing during the same interval are bundled all the time on a path. Due to the aggregate property, the path disutility under the A-FCFS mechanism can be derived from Eq. (5.34). However, under the D-FCFS and VD-FCFS mechanisms, the travelers may wait for different times, as formulated in Section 5.3. In this situation, a path is extended into several time-expanded paths, which have the same source nodes but are split at the CSS location due to different waiting times. The travelers having the same waiting time for SCs are assigned to the same expanded path, and hence the disutility of each expanded path can still be obtained in the way of Eq. (5.34). Taking all expanded paths together, the weighted sum is applied to derive the path disutility as

$$c_p^{rs}(k, \boldsymbol{f}) = \sum_{p_j} \varpi_{p_j}(k) \cdot c_{p_j}^{rs}(k, \boldsymbol{f}), \quad \forall rs \in RS, p \in P^{rs}, k \in K \tag{5.35}$$

where p_j denotes an expanded path of path p, $c_{p_j}^{rs}(k, \boldsymbol{f})$ is the disutility of p_j, and $\varpi_{p_j}(k)$ is the proportion of travelers. The expanded paths enable the disaggregation of aggregate choice of SCs.

Figure 5.3 illustrates the path expansion of the highlighted space-time path in Figure 5.2 under the D-FCFS mechanism. After parking PCs at b, the travelers arrive at b' during t_3 and request SCs. Due to SC shortage, travelers may wait from $w_{b',\min}(t_3)$ to $w_{b',\max}(t_3)$ intervals to be served. Based on the different waiting times, the path is

transformed into several expanded paths. The number of expanded paths equals the number of different waiting time intervals. In this example, three time-expanded paths are generated. For the left-most expanded path, travelers arrive at b' and wait $w_{b',\min}(t_3)$ intervals. The proportion of travelers on this expanded path, $\varpi_{p_1}(k)$, equals $\lambda_{b'}(t_3, w_{b',\min}(t_3))$. Travelers on the middle and right-most expanded paths wait w and $w_{b',\max}(t_3)$ intervals, and the corresponding proportions are $\lambda_{b'}(t_3, w)$ and $\lambda_{b'}(t_3, w_{b',\max}(t_3))$, respectively. Traveler on these expanded paths finish their trips during t_7, t_8, and t_9, respectively.

Under the VD-FCFS mechanism, VIP and ordinary travelers have different SC link disutilities. Path expansion can also be used to calculate the path disutilities for VIP and ordinary travelers respectively.

Remark 5.4 Eq. (5.35) is a generalized form of path disutility after one-time path expansion. It can be extended to calculate path disutility including multiple SC trips in a trip chain. In that case, multiple path expansions are needed at different CSS locations. The travelers are divided and assigned to the expanded paths whenever path expansion is triggered at a CSS location. The proportion of travelers on each expanded path equals the product of $\lambda_a(\tau, w)$, $\forall a$. It is easy to show that the sum of the proportions of all expanded paths equals 1 based on Eqs. (5.17) and (5.28).

To model travel choices more realistically, the BR behavior is embedded in a DUE model. The BR-DUE condition is stated as: for each OD pair, the disutilities experienced by travelers fall within an acceptable range (Han et al., 2015). Formally, the condition can be expressed as Eq. (2.16). The corresponding variational inequality (VI) problem VI$(\boldsymbol{f}, \Omega)$ of this condition can be formulated as Eqs. (2.17)-(2.19).

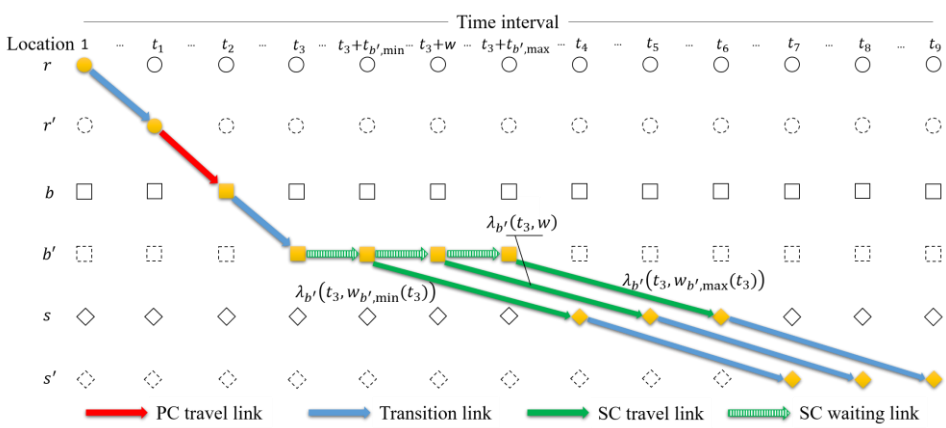

Figure 5.3 Illustration of path expansion.

The point queue method is adopted in the discrete-time domain for dynamic network loading and the route-swapping algorithm for flow reassignments (Huang and Lam, 2002). Eq. (2.18) indicates that the feasible set Ω is a compact closed convex set. The solutions to VI($\boldsymbol{f}, \Omega$) problem Eqs. (2.17)-(2.19) exist if $c_p^{rs}(k, \boldsymbol{f})$ is continuous with path flow $\boldsymbol{f}$. When $S_a(k) \geq D_a(k)$, $\forall a$, the continuity can be guaranteed according to Eqs. (5.29)-(5.35). Otherwise, the continuity may not be satisfied due to the non-separable SC supply-demand dynamics (the discontinuity is illustrated in Appendix 5.B). Coincidentally, the disutility tolerances due to the BR behavior soften the effects of discontinuity and contribute to the existence of BR-DUE solutions. According to Han et al. (2015), the solution to VI($\boldsymbol{f}, \Omega$) problem Eqs. (2.17)-(2.19) is not unique.

Remark 5.5 Remark 5.1 indicates that the D-FCFS and VD-FCFS mechanisms overall lead to more efficient usage of SCs than the A-FCFS mechanism. In the context of BR, the derived benefit at the BR-DUE state may be less obvious, especially when the length of one time interval is small. Due to the indifferent band of disutility in Eq. (2.16), travelers may not be sensitive to the disutility loss due to less waiting time. Consequently, the effects of disaggregating the SC requests during the same interval may be attenuated.

5.4.3 Path expansion strategy in a column generation algorithm

In the bi-modal supernetwork, a path choice encompasses the choice of departure time, mode, and path. As a result of the high choice dimensions, the number of possible time-dependent paths may be huge. To circumvent path enumeration, a column generation (CG) scheme is adapted to solve the BR-DUE problem. The recursive formulations of path disutilities (Dean, 2004; Liao, 2016) are applied in a space-time supernetwork for the path search. To speed up the intermediate iterations, the spatial-temporal exploitation and exploration strategies suggested in Chapter 4 are simplified. Furthermore, under the D-FCFS and VD-FCFS mechanisms, the path expansion strategy (Eq. (5.35)) is integrated into the CG scheme. The adaptive CG algorithm differs in three aspects compared with the one suggested by Chapter 4. First, the spatial exploration strategy of adjusting ε_n^{rs} up dynamically is discarded to reduce the number of intermediate network loadings. The refined adjustment of convergence thresholds can reduce the side-effects due to the discontinuity of path disutility. Second, the supply-demand dynamics of SCs need to vary with the temporal resolutions. Third, the path expansion strategy is embedded in network loadings to calculate the weighted path disutility.

The required temporal and spatial resolutions at the BR-DUE states are denoted by Δ and ε^{rs}, which are the minimum length of one time interval and the minimum relative convergence threshold of rs respectively. Within the current temporal resolution Δ_n, the following criterion is used to measure the convergence of the traffic assignment process.

$$Regap(k, \boldsymbol{f_n}) \leq \varepsilon_n^{rs}, \quad rs \in RS \tag{5.36}$$

where $Regap(k, \boldsymbol{f_n})$ is the relative gap to measure the convergence of the solution algorithm and calculated by Eq. (4.8).

The spatial-temporal exploitation strategies are used to adjust Δ_n and ε_n^{rs}. As shown in Table 5.1, when no new path is found at iteration n, the spatial exploitation is triggered by decreasing ε_n^{rs}. If ε_n^{rs} equals ε^{rs}, the temporal exploitation is performed by decreasing Δ_n. Without the exploration strategies, the spatial-temporal exploitation strategies alone can still ensure the proposed CG algorithm to converge to a solution with reduced computation times compared to the original CG.

Under the D-FCFS and VD-FCFS mechanisms, the path expansion strategy is used to record the expanded path inflows and outflows for calculating $\varpi_{p_j}(k)$ in Eq. (5.35). Denote the inflow of time-dependent path (p, k) by $f_p^{rs}(k)$ and the outflow of expanded path (p_j, k) by $f_{p_j}^{rs}(k)$ $(j = 1, 2, \ldots, h)$ through the dynamic network loading, where h is the number of expanded paths. $\varpi_{p_j}(k)$ is calculated as

$$\varpi_{p_j}(k) = \frac{f_{p_j}^{rs}(k)}{f_p^{rs}(k)} \tag{5.37}$$

The pseudo-codes of the adaptive CG algorithm with simplified strategies are shown by Algorithm 5.1 below. The algorithm starts with the parameter initialization and then equilibrates path flows in Step 2. Incorporating the path expansion strategy, $\varpi_{p_j}(k)$ is derived from the dynamic network loading process and $c_p^{rs}(k, \boldsymbol{f_n})$ is calculated according to Eqs. (5.34)-(5.35). Flow $\boldsymbol{f_n}$ is equilibrated on the current path set P_n^{rs} based on $c_p^{rs}(k, \boldsymbol{f_n})$ until Eq. (5.36) is satisfied. Step 3 adopts a tolerance-based minimum disutility path search to incorporate the travel behavior of BR. Step 4 lists three different stopping criteria. The first one detects whether a path already exists in the current path set and the latter two refer to the spatial-temporal exploitation processes. The algorithm is terminated when these criteria are satisfied simultaneously.

Table 5.1 The spatial-temporal exploitation strategies

Strategy	Condition	Operation
Spatial exploitation	no new path is found at iteration n	$\varepsilon_{n+1}^{rs} = \max(\vartheta_1 \cdot \varepsilon_n^{rs}, \varepsilon^{rs})$
Temporal exploitation	no new path is found & $\varepsilon_n^{rs} = \varepsilon^{rs}$	$\Delta_{n+1} = \max(\lfloor \vartheta_2 \cdot \Delta_n \rfloor, \Delta)$

Note: $\vartheta_1, \vartheta_2 \in (0, 1)$ are scaling parameters and $\lfloor \cdot \rfloor$ is an integer-floor operator.

Algorithm 5.1 Adaptive CG algorithm

Step 1: *Initialization*

Set iteration number $n = 1$, $\boldsymbol{f}_n = \mathbf{0}$ and initial Δ_n, ε_n^{rs} and P_n^{rs}, $\forall rs \in RS$.

Step 2: *Traffic assignment*

Calculate path disutility $c_p^{rs}(k, \boldsymbol{f_n})$ through path expansion strategy and equilibrate path flows $\boldsymbol{f_n}$

on P_n^{rs} by a route-swapping algorithm such that Eq. (5.36) is met.

Step 3: *Tolerance-based minimum disutility path search*

Search for acceptable paths $\bar{p}$ satisfying $c_{\min}^{rs}(\boldsymbol{f_n}) - c_{\bar{p}}^{rs}(k, \boldsymbol{f_n}) \geq \epsilon^{rs} \cdot c_{\min}^{rs}(\boldsymbol{f_n})$, where ϵ^{rs} denotes the relative indifference threshold of rs toward path-switching.

Step 4: *Stopping criteria*

Step 4.1: If $\forall \bar{p} \in P_n^{rs}$, continue; otherwise, update $P_n^{rs} = P_n^{rs} \cup \bar{p}$ and go to Step 4.4.

Step 4.2: If $\varepsilon_n^{rs} = \varepsilon^{rs}$, continue; otherwise, the spatial exploitation is triggered by decreasing ε_n^{rs}, update $\boldsymbol{f_n}$ and go to Step 4.4.

Step 4.3: If $\Delta_n = \Delta$, go to Step 5; otherwise, the temporal exploitation is triggered by decreasing Δ_n and go to Step 4.4.

Step 4.4: Set $n = n + 1$ and go to Step 2.

Step 5: *Termination*

Stop the algorithm and obtain the BR-DUE solution.

Remark 5.6 The essence of the path expansion strategy lies in flow separation and tracking during the dynamic network loadings. The time-expanded paths can be seamlessly integrated with the path generation process of the CG scheme. Given temporal resolution Δ_n at intermediate iteration n, the time complexities for path search and network loading are $O(|RS| \cdot |A| \cdot |K_n|)$ and $O(\sum_{rs} |P^{rs}| \cdot |A'| \cdot |K_n| \cdot m_1)$ respectively. When SC supplies are insufficient, the value of m_1 and the number of intermediate iterations may increase significantly, which prolongs the computation time.

5.5 Numerical examples

This section presents two numerical examples to illustrate the supply-demand dynamics and BR-DUE solutions under different FCFS mechanisms. The supply-demand dynamics and average waiting times are first compared in a six-node network. Next, the Sioux Falls network is used to run sensitivity tests and elaborate on the VD-FCFS mechanism. The solution algorithm is coded in MATLAB and run on a personal computer with an Intel(R) Core(TM) i5-7300U 2.60 GHz CPU and 8.00 GB RAM. The time horizon falls within [7:00 am, 10:00 am]. Based on the parameter setup by Chapter 4, Parameters are set as $\eta_1 = 6.4$, $\eta_2 = 3.9$, $\eta_3 = 15.21$, $\eta_4 = 3.0$, $\eta_5 = 1$, $\eta_6 = 3.5$, $\eta_7 = 8.2$, and $\eta_8 = 1$ in either one unit of disutility per hour (h) or dollar ($) (see Section 5.4), the preferred arrival time (PAT) to 9:00 am, $\kappa^{rs} = 0.1$ h in Eq. (5.30), the percentage of VIP members to 20%, the average VIP membership fee for one trip $c_0 =$

0.2 \$, $\varepsilon^{rs} = 0.1$, $\epsilon^{rs} = 0.01$, $\vartheta_1 = \vartheta_2 = 0.5$, $\Delta = 1$ min, $\varepsilon_1^{rs} = 0.2$ and $\Delta_1 = 2$ min in the adaptive CG algorithm.

5.5.1 Example 1: six-node network

Figure 5.4 is a six-node, seven-link network with two OD pairs, i.e., (1, 3) and (2, 6). Both OD pairs have 3000 travelers. The numbers given near each link are the corresponding link free-flow travel times and capacities respectively. The SC stocks at nodes 1, 4, and 6 are initialized to 600, 400, and 200, and the parking fees at nodes 3, 4, and 6 are set to 3 \$, 1 \$, and 2 \$, respectively. The four FCFS mechanisms are examined in the BR-DUE model and the results are presented below.

The average running time of the solution algorithm is 23.12 s under the four FCFS mechanisms. The maximum running time difference is less than 3 s between the NW-FCFS and VD-FCFS mechanisms. Each path is represented by a sequence of nodes in Table 5.2. As shown, paths 3 and 6 are bi-modal and involve transfer at nodes 6 and 4 respectively. Figure 5.5 depicts the equilibrium solutions of OD pair (1, 3) under different FCFS mechanisms. The thick and thin curves are used to denote the path flows and disutilities respectively. The SC travelers on path 2 (thick blue curves) depart earlier than PC travelers on path 1 (thick green curves), although the disutility coefficient of travel time by PC is smaller than that by SC. The reason is that the PC parking fee induces a part of travelers to switch to SC. Since the SC supply is less than the demand, travelers have to depart earlier (around 7:40 am by SC); otherwise, departing later may be associated with a large penalty due to the shortage of SCs. Without waiting, travelers on path 3 under the NW-FCFS (thick red curve in Figure 5.5 (a)) increase steeply at around 8:10 am. Figure 5.5 (b) and (c) show similar curves of flow patterns and disutilities under the A-FCFS and D-FCFS mechanisms due to a small value of Δ and the tolerance band in BR (see Remark 5.5). However, with VIP travelers under the VD-FCFS mechanism,

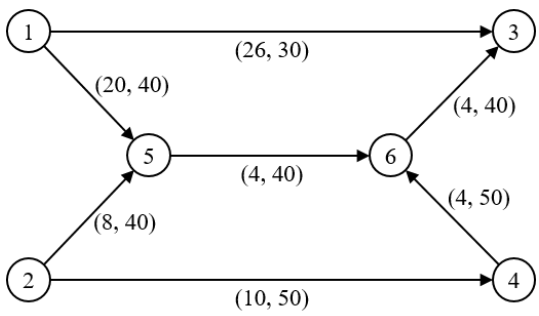

Figure 5.4 The six-node network.

Table 5.2 Path specification

OD	Path ID	Sequence of nodes
(1, 3)	Path 1	1 - **(PC)** - 3
	Path 2	1 - **(SC)** - 3
	Path 3	1 - **(PC)** - 5 - **(PC)** - 6 - **(SC)** - 3
(2, 6)	Path 4	2 - **(PC)** - 5 - **(PC)** - 6
	Path 5	2 - **(PC)** - 4 - **(PC)** - 6
	Path 6	2 - **(PC)** - 4 - **(SC)** - 6

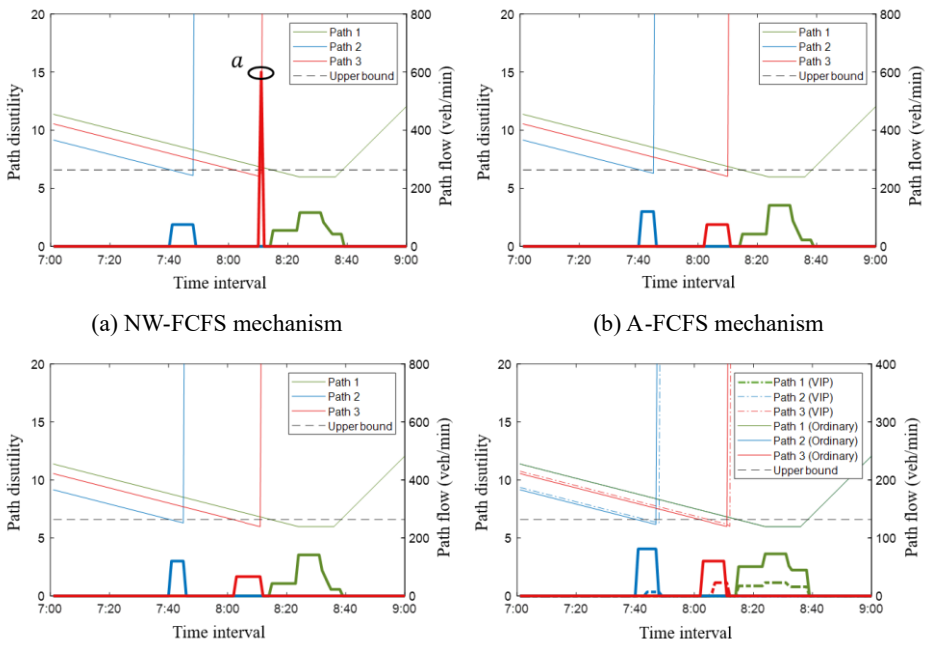

(a) NW-FCFS mechanism

(b) A-FCFS mechanism

(c) D-FCFS mechanism

(d) VD-FCFS mechanism

Figure 5.5 BR-DUE solutions of OD pair (1, 3) under different FCFS mechanisms.

different curves of path flows and disutilities are observed. As depicted by Figure 5.5 (d), both VIP and ordinary travelers have the same disutilities (the thin green curve coincides with the thin green dashed curve) and temporal flow distributions on path 1. For travelers using SCs, the temporal flow distribution of ordinary travelers is ahead of that of VIP travelers. The reason is that VIP travelers pay VIP membership fees to avoid early departure or long waiting. At the BR-DUE state, the disutilities of used time-dependent paths are no larger than the maximum acceptable disutilities (grey dashed lines). These results meet the BR-DUE user equilibrium condition in Eq. (2.16).

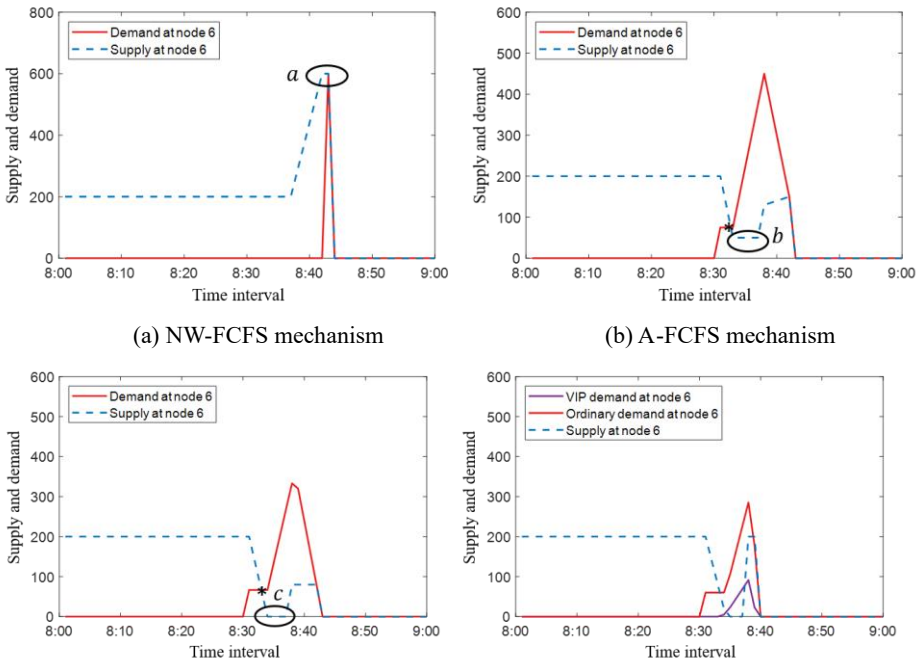

(a) NW-FCFS mechanism (b) A-FCFS mechanism

(c) D-FCFS mechanism (d) VD-FCFS mechanism

Figure 5.6 The dynamic supply and demand of SCs at node 6.

Node 6 is both the destination of OD pair (2, 6) and a transfer location for travelers of OD pair (1, 3). Thus, node 6 has more intense supply-demand interactions than other nodes. Figure 5.6 focuses on the evolutions of SC supply-demand dynamics of node 6 at the BR-DUE state. The demand (red solid curve) under the NW-FCFS mechanism increases to 600 at around 8:45 am (area *a* in Figure 5.6 (a)), and then the 600 travelers use SCs without waiting. These travelers departed from node 1 at around 8:00 am together. In Figure 5.6 (b) and (c), there are two intersections (marked with '*') of the demand and supply curves during [8:30 am, 8:40 am]. Since the demands are less than the supplies before the intersections, travelers can use the SCs directly. Subsequently, the demands start to accumulate. These travelers wait for the incoming SCs by travelers of OD pair (2, 6). However, the two demand curves have different inflection points. The value of the inflection point in Figure 5.6 (b) (area *b*) is around 50 and the value in area *c* is 0 in Figure 5.6 (c). The reason is that some travelers can use the inadequate supply under the D-FCFS mechanism, while all the travelers have to wait until the demand being satisfied under the A-FCFS mechanism. That is, SCs under the D-FCFS mechanism can be used more efficiently. Figure 5.6 (d) draws the supply-demand curves under the VD-FCFS mechanism. As depicted, the ordinary SC travelers depart earlier than the VIP travelers. The privilege service allows VIP travelers to depart late for using SCs.

Table 5.3 Average waiting time (min) of travelers at node 6

Formula	# SCs	NW-FCFS	A-FCFS	D-FCFS	VD-FCFS	
					VIP	ordinary
$\frac{\sum_{p_j}\sum_k w \cdot f_{p_j}(k)}{\sum_{p_j} f_{p_j}(k)}$	120	0	7.50	4.66	2.70	2.86
	600	0	4.50	3.92	2.00	2.67
	1200	0	3.63	2.67	1.67	2.35
	2400	0	3.00	2.41	0.54	1.70

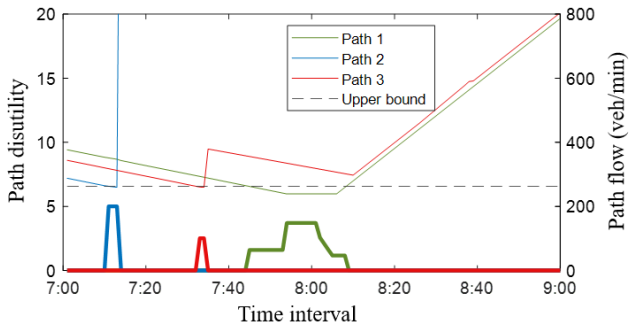

(a) 8:30 am and 9:00 am as the PATs for OD pairs (1, 3) and (2, 6) respectively

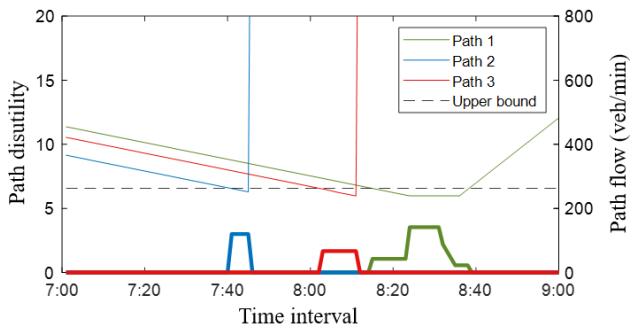

(b) 9:00 am and 8:30 am as the PATs for OD pairs (1, 3) and (2, 6) respectively

Figure 5.7 Effects of κ^{rs} on BR-DUE solutions of OD pair (1, 3).

To further illustrate the effects of the four mechanisms, the average waiting time of travelers at node 6 with different SC supplies is presented in Table 5.3. For the formula of average waiting time, the numerator is a sum of the waiting time of travelers and the denominator is a sum of flow. Suppose that the SC supplies are 0.1, 0.5, 1, and 2 times the initial stocks specified above, respectively. The NW-FCFS mechanism has no waiting time. Compared to the A-FCFS mechanism, as expected, the D-FCFS and VD-

FCFS mechanisms have less average waiting time. For example, D-FCFS results in 38% less waiting time as opposed to A-FCFS when the number of SCs is 120. VIP travelers wait even less time as a return of the VIP membership fee. It is interesting to note that under the VD-FCFS mechanism, ordinary travelers have less average waiting time than those under the D-FCFS mechanism. The reason is that ordinary travelers depart earlier to avoid the competition with VIP traveler. Expectedly, with the increase of SC supply, travelers have less average waiting time. For example, the waiting time of the VIP travelers under the VD-FCFS mechanism decreases from 2.70 min to 0.54 min. As seen, the average waiting times are relatively short (most are less than 5 min). As a matter of fact, in a bi-modal network, the travelers would switch to PC when the waiting time is long. In principle, the average waiting time and vacancy rate are negatively correlated. Sufficient SC supply comes along with less waiting time but probably a high vacancy rate. Whereas, insufficient SC supply leads to longer waiting times but fewer vacancies. As the SC supply is insufficient in general in Table 5.3, it is found the largest gap of SC vacancy rate across all FCFS mechanisms is less than 4%.

Figure 5.7 shows the BR-DUE solutions of OD pair (1, 3) with different PATs under the D-FCFS mechanism. Expectedly, travelers with earlier PAT depart from home earlier. For example, as depicted by flow patterns of path 2 (thick blue curves), the earliest departure time is about 7:10 am when κ^{13} equals 8:30 am, and this value increases to 7:40 am when κ^{13} equals 9:00 am. Different from the path disutility curves (thin red curves) in Figure 5.5 (c) and Figure 5.7 (b), interestingly, the path disutility curve has two valleys in Figure 5.7 (a). The first valley appears at around 7:35 am. At this point, 200 travelers on path 3 can use the SCs at node 6. If more travelers want to use SCs, they need to wait for the incoming SCs from OD pair (2, 6) at this CSS location. Travelers departing later have less waiting time and thus smaller path disutility. At around 8:10 am, the path disutility begins to increase due to the late arrival penalty. Moreover, larger values of κ^{13} lead to later departure times of travelers on path 3 (thick red curves in Figure 5.5 (c) and Figure 5.7 (b)) and hence later arrival times at transfer location 6. Consequently, the travelers can use the SCs relocated from node 4 by travelers of OD pair (2, 6) besides the initial stock. The illustration is consistent with the wider non-zero flow regions in Figure 5.5 (c) and Figure 5.7 (b).

5.5.2 Example 2: Sioux Falls network

The Sioux Falls network (24 nodes and 76 links) (Figure 5.8) is used to assess the effects of SC use price and VIP fee under the most comprehensive mechanism – VD-FCFS. Incorporating the land use map from http://www.siouxfalls.org/Planning, the network is divided into the city center and suburban area, where home zones (residential neighborhoods), work locations, and CSS locations (stations) are placed at the nodes. An OD pair is formed by a home zone and a randomly selected work location. Compared

with the traditional network, the bi-modal supernetwork has a larger scale due to the extension of vehicle states (Section 5.2). The demands of these OD pairs are randomly generated from 2000 to 3000. Data transformations are performed on the free-flow travel times and link capacities to fit the selected OD pairs (see Appendix 5.C). The SC stocks at work locations are set to zero. For other CSS locations, the numbers of SCs are initialized as 400 and 200 in the city center and suburban area respectively. PCs are allowed to park at CSS locations with different parking fees, which are set to 3 $ and 1 $ at nodes in the city center and suburban area respectively.

Figure 5.9 shows the convergence curve of the solution algorithm. There are two major peaks around 30 and 80 iterations respectively. The first peak occurs when new paths are generated and the second one appears when the spatial resolution is adjusted (referring to spatial exploitation). Afterwards, the relative gap (Eq. (4.8)) gradually decreases. The gap only changes when the flows shifted in the adjustment process are large enough to change the values of the maximum and minimum path disutilities. In this example, the solution algorithm needs 435 iterations and takes 570.30 s to satisfy the stopping criterion. For reference, the running time is only 93 s with 95 iterations if SC is not considered as a mode alternative. The slow equilibrium process is mainly caused by the dynamic SC supply-demand interactions at the intermediate iterations when SC supply is insufficient.

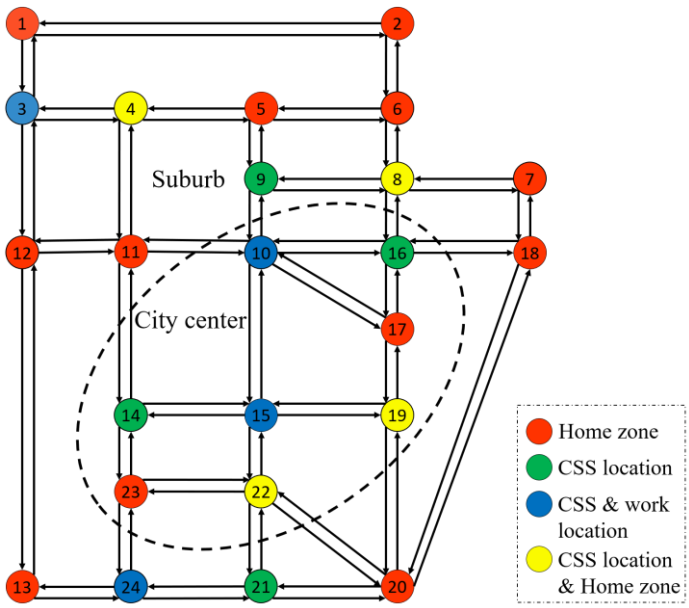

Figure 5.8 The transport network of Sioux Falls.

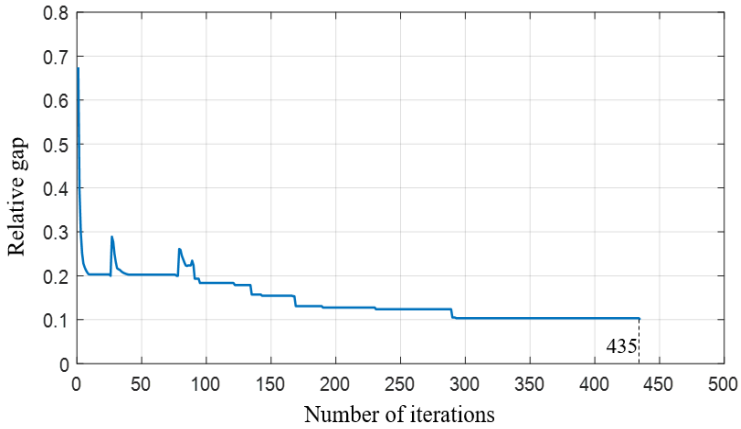

Figure 5.9 Convergence of the adaptive CG algorithm.

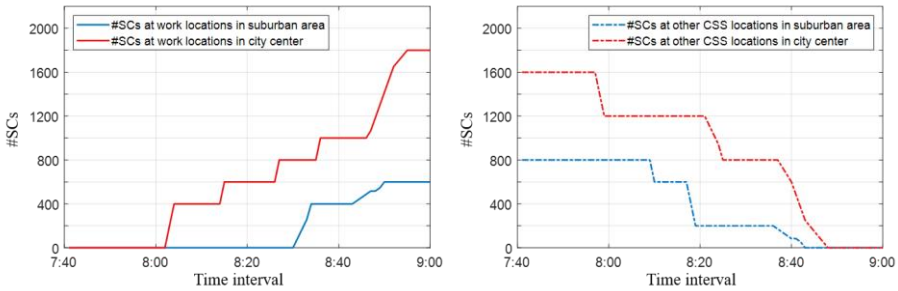

(a) #SCs at work locations when use price is 4 (b) #SCs at other CSS locations when use price is 4

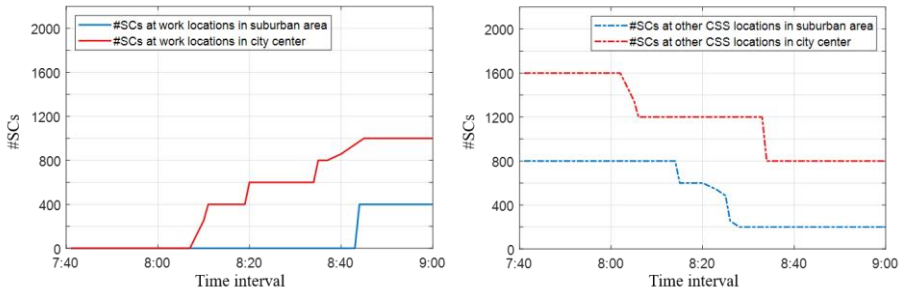

(c) #SCs at work locations when use price is 8.2 (d) #SCs at other CSS locations when use price is 8.2

Figure 5.10 Number of SCs in different areas.

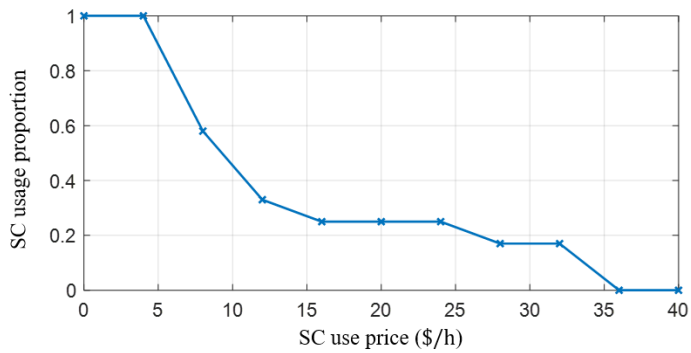

(a) Effect of SC use price

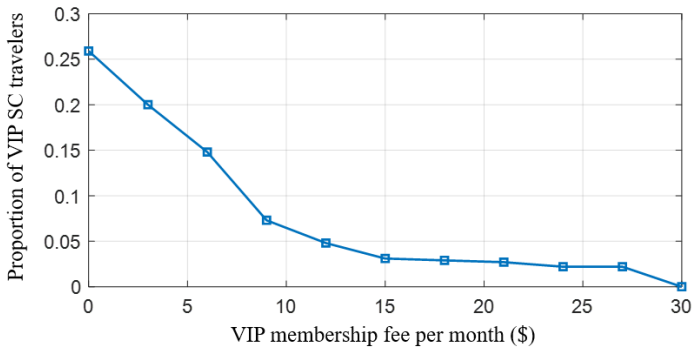

(b) Effect of the VIP membership fee

Figure 5.11 Effects of the parameters.

To show the effects of SC use price on the dynamic distribution of SCs, the evolutions of the number of SCs in different areas are depicted with two SC use prices. As shown in Figure 5.10, the red and blue solid curves denote the number of SCs at work locations in the city center and the suburban area respectively; the dashed curves represent the numbers at other CSS locations. Subgraphs (a, c) show the numbers of SCs at work locations, while subgraphs (b, d) show the numbers at other CSS locations.. Through the dynamic changes, it can be observed the effects of SC use price. Specifically, in Figure 5.10 (b), both dashed curves decrease to zero before 9:00 am when the price is 4 $/h, meaning that all SCs are chosen. When the price is increased to 8.2 $/h, Figure 5.10 (d) shows that 1400 SCs are used at CSS locations (excluding work locations) and the other 1000 SCs are not. On the one hand, it indicates that fewer travelers choose SC after the price is increased. On the other hand, although the SC use price is larger than that of PC, the PC parking fee still induces 3.87% of the trips by SC.

Figure 5.11 shows the influences of SC use price and VIP membership fee on the BR-DUE results respectively. With the increase of SC use price, the modal share of SC

decreases from 1 to 0. When the price is smaller than 4 $/h, all SCs are used; whereas, no one chooses SC when the price is higher than 36 $/h. If the price falls within [4 $/h, 12 $/h], CSS can still attract a large proportion of travelers to use SCs. When the price falls within [16 $/h, 32 $/h], the proportion is stable around 0.2. Figure 5.11 (b) shows the relation between the proportion of VIP SC travelers and the VIP membership fee per month. VIP membership fee per month is calculated by considering two trips per day and 30 days per month on average. Increased VIP membership fee per month results in a nonlinear decrease in the proportion of VIP SC travelers. It is unexpected to find that the proportion is 0.26 other than 1 when no VIP membership fee is needed. An explanation is that given the same SC supply, the benefits of VIP privilege are diminishing as the proportion of VIP travelers increases. When the VIP fee is larger than 30 $, no one will pay the high fee to acquire the privilege.

Based on the results of the two examples, it can be concluded that FCFS mechanisms have significant effects on the supply-demand dynamics and travel choices at BR-DUE states. Comparatively, the SC usages under the D-FCFS and VD-FCFS mechanisms are more efficient when the supply is insufficient. The reduction in SC trip costs and VIP membership fees can attract more people to shift from PC to SC and subscribe to VIP services. To use SCs in the presence of VIP travelers, ordinary travelers have to depart earlier. There is a saturation point in the share of VIP travelers, beyond which no travelers want to be VIP travelers even if the membership fee is extremely low.

5.6 Conclusions

CSS are expected to be prevalent due to the low cost, flexibility, and comfortability. This chapter formulated and analyzed the supply-demand dynamics of CSS under four FCFS mechanisms. Travelers under the NW-FCFS mechanism are assumed to either be served or seek an alternative mode immediately to avoid waiting. The A-FCFS mechanism supposes that travelers arriving at a CSS location during the same interval are served simultaneously. The D-FCFS mechanism treats travelers as disaggregate units and enables serving them during different time intervals. Based on the D-FCFS mechanism, the VD-FCFS mechanism allows VIP members to jump the queue. These FCFS mechanisms have been compared in a BR-DUE model given the same SC supplies. Numerical examples demonstrated that D-FCFS and VD-FCFS are more efficient in regulating the usages of SCs than NW-FCFS and A-FCFS.

This chapter adopts a modified CG algorithm for solving the BR-DUE problem in a bi-modal transport network. As another extension, the next chapter will improve the tolerance-based CG algorithm to solve the boundedly rational dynamic activity-travel assignment user equilibrium problem.

6

The Refined TBCG Algorithm for BR-DATA*

6.1 Introduction

Dynamic traffic assignment (DTA) is a core component for many transportation network analysis problems and has been widely applied due to the capacity of modeling complex traffic flow phenomena (Ukkusuri et al., 2012). Focusing on sequences or patterns of activity behavior, activity-based model (ABM) derives travel demand from activity participation and activity behavior patterns (Bhat and Koppelman, 1999) and is advantageous in that it can capture the short-term disaggregate behavior of travelers. As an endogenous integration of DTA and ABM, dynamic activity-travel assignment (DATA) (Liu et al., 2015) determines the demand-supply interactions at a high level of detail without losing the interdependency of activity-travel chains and draw much attention in recent years (Li et al., 2010; Liu et al., 2016, 2020; Fu and Lam, 2014, 2018; Li et al., 2016a, 2016b, 2018; Li and Liao, 2020).

However, no DATA model has hitherto exhibited applicability to networks of real sizes. Even in the three DATA models (Ramadurai and Ukkusuri, 2011; Ouyang et al., 2011; Fu and Lam, 2018) applying the original column generation (CG) scheme, the

* This chapter is based on Wang, D., Liao, F., Gao, Z., Rasouli, S., Huang, H.J., 2020. Tolerance-based column generation for boundedly rational dynamic activity-travel assignment in large-scale networks. Transportation Research Part E: Logistics and Transportation Review 141, 102034.

corresponding algorithms still fall short of tackling large scale networks. The major reasons are as follows. First, the number of potential activity-travel patterns (ATPs) encounters combinatorial explosion due to the high choice dimensions involved in conducting an ordinary activity program, such as choice of mode, path, location, timing, duration, and activity sequence. This fact renders the DATA models vulnerable to the curse of dimensionality. Second, the DATA models usually concentrate on a one-day time frame (which is essential to capture the trip chaining behavior) rather than a short period, which further enlarges the scale of the problem in the temporal dimension. Third, due to time window constraints at the activity locations and multiple activity-travel link attributes, the ATP disutilities are not consistent with the time first-in-first-out (FIFO) principle. It means that there is no efficient polynomial-time algorithm for searching the minimum disutility ATPs (MDAs). Lastly, the temporal resolution needs to be high to replicate the real-time network dynamics for supply management. For these reasons, the existing DATA problems were confined to small networks, such as a triangle network (e.g., Lam and Yin, 2001), a four-node diamond network (e.g., Fu and Lam, 2014; Liu et al., 2015), and the 13-node Nguyen-Dupuis network (e.g., Li et al., 2018).

In view of the above challenges, a few studies recognized the necessity of obviating ATP enumeration and extended the current small-sized networks to larger networks. Based on Algorithm B (Dial, 2006), Ramadurai and Ukkusuri (2011) made an extension, Algorithm B-Dynamic, in a DATA model. Although this algorithm does not need to store or enumerate ATPs, the notion of bushes (stored as nested maps in terms of data structure) is used as implicit expressions of ATPs. In Algorithm B-Dynamic, the number of bushes may explode and therefore, as stated by the authors, the algorithm in the proposed form was incapable of simulating large-scale networks. In addition, the augmented networks lack a valid representation of activity-travel behavior. Ouyang et al. (2011) developed an activity-time-space network expansion approach to solve the DATA problem. This approach reconstructs the activity-time-space network by extending nodes in the temporal dimension and connecting them with different types of links. Following this study, Fu and Lam (2018) considered travelers' joint activity-travel choices in DATA problems, which were transformed into static traffic assignment (STA) models and solved by the original CG algorithm. Chow and Djavadian (2015) examined the first/last mile problem of multimodal trips in constrained mixed logit models of activity schedule choice. Nevertheless, their study did not consider traffic flow characteristics. These approaches are pure applications of the original CG scheme to generate spatial ATPs without any treatments of the temporal dimension.

Despite four novel strategies proposed in Chapter 4, the tolerance-based CG (TBCG) has limitations to address DATA problems. First, the tolerance-based minimum disutility path search algorithm is not applicable in non-FIFO networks; second, the lower bounds of the self-adjusted convergence thresholds result in local optimal solutions; third, the fixed temporal exploration criterion restricts proper adjustments of

the feasible time regions; fourth, the combined temporal strategies are inefficient for addressing long-time frames of the DATA problems.

Therefore, this chapter aims to develop an improved CG algorithm in response to the modeling challenges in DATA. Based on the TBCG proposed in Chapter 4, the spatial-temporal exploration and exploitation strategies are refined to solve boundedly rational DATA (BR-DATA) problems. To that end, general forms of temporal and spatial strategies are suggested. Recursive formulations in varying space-time supernetworks are developed to generate time-dependent ATPs under space-time constraints. With these refinements, the solutions derived from the refined TBCG algorithm are proved to satisfy the BR-DATA user equilibrium conditions. It can be shown that the proposed algorithm can be applied to larger networks with less computation time compared with the original CG algorithm.

The remainder of this chapter is organized as follows. Section 6.2 introduces the multi-state supernetwork representation and the equilibrium condition of BR-DATA problems. Section 6.3 discusses the refined spatial-temporal strategies and gives a formal proof of the correctness of the TBCG algorithm. Section 6.4 illustrates the proposed algorithm in numerical examples. Finally, conclusions are provided in Section 6.5.

6.2 BR-DATA model

This section first presents the space-time supernetwork representation of ATPs and formulates the ATP disutilities. Next, the BR-DATA user equilibrium condition and the corresponding variational inequality (VI) problem are discussed. In what follows, the existence of solutions to the BR-DATA problem under several assumptions is analyzed.

6.2.1 Supernetwork representation

A car-only unimodal multi-state supernetwork (SNK) $SNK(N, A)$ composes of location set N and link set A. A_{PC} and A_{AT} are two sets of private car travel links and transaction links in SNK. It is noteworthy that every episode of activity participation is expressed in the form of a transaction link, which facilitates the congruent representation of multi-dimensional choice facets. Typically, home zones at the first and last activity states in SNK form an origin and destination (OD) pair, which is referred to as SNKOD. The path of an SNKOD defines an ATP, detailing the choice of path, activity location, and activity sequence. For convenience, *path* and *ATP* are interchangeably used hereafter. Incorporating a set of time intervals K, $SNK^T(N, A, K)$ is used to denote the space-time supernetwork, in which choice facets related to timing and duration are further represented.

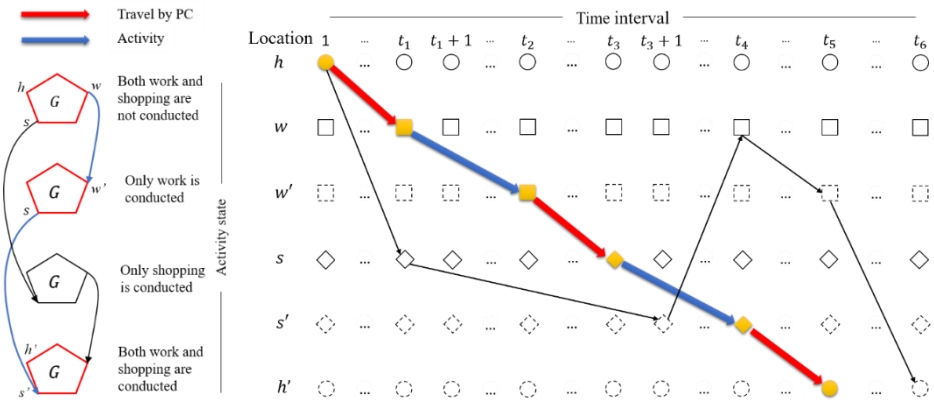

Figure 6.1 SNK representation (left) and space-time ATP representation (right).

As depicted on the left-hand side of Figure 6.1, the four-state supernetwork provides a spatial representation of ATPs, in which a pentagon represents the traditional transport network G, the vertices are locations of home (H), work (W) and shopping (S) denoted as h, w, and s respectively, and the directed links refer to activity participation. To exhibit activity state transitions, location w' and s' are copies of w and s respectively to denote the completion of activities. Location h' is a copy of h to denote the completion of the activity program. The path consisting of red and blue links from h to h' denotes the ATP that travelers leave h by car to work at w, then go shopping at s, and finally return to h'. This ATP can be extended to a 2-D space-time representation in the discrete-time domain on the right-hand side of Figure 6.1, in which shapes of circle, square, and diamond denote locations for home, work, and shopping respectively. Some shapes are filled in yellow if the corresponding locations are traversed as a part of the ATP. To keep consistency, links in both subfigures with the same colors correspond to the same type of links, i.e., red for travel links and blue for transaction links. The directed colored links together form one specific space-time ATP, in which travelers leave h during time interval 1 and arrive at w during time interval t_1, and go for shopping during t_2, then do shopping at s between t_3 and t_4, and finally return to h' during t_5. All other spatial-only and space-time ATPs can also be represented in Figure 6.1; for example, the black directed links form an alternative space-time ATP.

6.2.2 ATP disutility

Four types of disutilities, including travel disutility, activity disutility, parking disutility, and home-stay disutility, are considered and formulated as follows.

Travel disutility

Travel time is one of the main factors of travel disutility as other factors are highly correlated with travel time, such as monetary expense and cumulated crowding discomfort. For simplicity, travel link disutility is defined as

$$c_l^{i\mathrm{TD}}(\tau) = \lambda_1^i \cdot t_l(\tau), \quad \forall i \in I,\ l \in A_{PC}, \tau \tag{6.1}$$

where $c_l^{i\mathrm{TD}}(\tau)$ is the travel disutility incurred by class i arriving at link l during time interval τ, $t_l(\tau)$ is the travel time of link l during τ, and λ_1^i is the travel time disutility coefficient of i. $t_l(\tau)$ can be calculated by Eq. (2.4).

Activity disutility

The time window constraints at activity locations restrict travelers to perform activities within a specific time range. If travelers arrive at activity transaction link l too early, they need to wait until the activity location opening time t_l^{o}. If the arrival time falls within the time windows, travelers can carry out the activity directly but have to finish the activity no later than the closing time t_l^{e}. If the arrival time is later than t_l^{e}, the activity cannot be conducted at the location, i.e., waiting is irrelevant. Formally, the waiting time at l during time interval τ, $t_l^{\mathrm{W}}(\tau)$, is expressed by

$$t_l^{\mathrm{W}}(\tau) = \begin{cases} t_l^{\mathrm{o}} - \tau, & \text{if } \tau < t_l^{\mathrm{o}} \\ 0, & \text{otherwise} \end{cases} \tag{6.2}$$

In Eq. (6.2), $t_l^{\mathrm{W}}(\tau)$ is a nonnegative integer when t_l^{o} and τ are integers. For activities without time window constraints, $t_l^{\mathrm{W}}(\tau)$ =0, $\forall\tau$. To enhance behavioral realism, activity duration is considered as a choice facet. According to Liao (2016), the duration choice in the individual activity-travel scheduling problem is a positive integer and can be represented in a bipartite network. Let $t_l^{\mathrm{D}}(\tau)$ denote the duration for travelers who begin the activity on link l during τ, for all $i \in I$, $l \in A_{AT}$ and time τ, it should fall within the minimum and the maximum duration, i.e., $t_l^{\mathrm{D}}(\tau) \in [\sigma_{\min}^l, \sigma_{\max}^l]$. For travelers arriving at the activity locations too late, the activity duration $t_l^{\mathrm{D}}\left(\tau + t_l^{\mathrm{W}}(\tau)\right)$ may be less than $\sigma_{\min}^l$. In this case, the travelers receive a disutility penalty due to the late arrival. In sum, the activity disutility is formulated as

$$c_l^{i\mathrm{AD}}(\tau) = \lambda_2^i \cdot t_l^{\mathrm{W}}(\tau) + \lambda_3^i \cdot U_l\left(\tau + t_l^{\mathrm{W}}(\tau)\right) + \lambda_4^i \cdot \max\left\{\sigma_{\min}^l - t_l^{\mathrm{D}}\left(\tau + t_l^{\mathrm{W}}(\tau)\right), 0\right\} \tag{6.3}$$

where $c_l^{i\mathrm{AD}}(\tau)$ is the activity disutility incurred by i arriving at l during τ, λ_2^i is the disutility coefficient for waiting time, λ_3^i is a disutility coefficient for activity

participation, λ_4^i is the late arrival penalty coefficient. $U_l\left(\tau + t_l^{\mathrm{W}}(\tau)\right)$ is the activity participation disutility, which is defined as the gap between the ideal utility and the actual utility at l. Following Yasmin et al. (2017) and Li et al. (2018), a *log*-form disutility function is adopted and formulated as

$$U_l\left(\tau + t_l^{\mathrm{W}}(\tau)\right) = U_l^* - F_l^a\left(\tau + t_l^{\mathrm{W}}(\tau)\right) \cdot \frac{\ln\left(1 + \beta_6 \cdot t_l^{\mathrm{D}}\left(\tau + t_l^{\mathrm{W}}(\tau)\right)\right)}{\left(1 + \frac{q_l(\tau)}{e_l}\right)^{\beta_7}} \tag{6.4}$$

where U_l^* is the ideal utility, $F_l^a(\tau)$ is the coefficient for time-dependency at activity location a, $q_l(\tau)$ denotes the number of travelers exceeding location capacity e_l ($q_l(\tau) = 0$, otherwise), β_6 and β_7 are parameters.

The first term of Eq. (6.3) denotes the waiting disutility, and the last term is the late arrival penalty. Given the focus on the method of ATP generation in SNK^T, this chapter does not consider the effects of activity sequence on activity disutility (see Liao et al. (2011) for specifications).

Parking disutility

Parking at a location may involve parking costs. The duration of one episode of parking equals the difference between the time intervals of picking-up the car and parking. This duration is equivalent to the summation of waiting time and activity duration. Parking duration and disutility are formulated as

$$t_l^{\mathrm{PK}}(\tau) = t_l^{\mathrm{W}}(\tau) + t_l^{\mathrm{D}}\left(\tau + t_l^{\mathrm{W}}(\tau)\right) \tag{6.5}$$

$$c_l^{i\mathrm{PD}}(\tau) = \lambda_5^i \cdot t_l^{\mathrm{PK}}(\tau), \quad \forall i \in I, l \in A_{AT}, \tau \tag{6.6}$$

where $t_l^{\mathrm{PK}}(\tau)$ is the parking duration of travelers who arrive at transaction link l during τ, $c_l^{i\mathrm{PD}}(\tau)$ is the parking disutility incurred by i arriving at link l during τ, and λ_5^i is the disutility coefficient for parking duration.

Home-stay disutility

Home-stay duration choice can be modeled through an explicit or implicit representation. For the explicit representation, an episode of home-stay is regarded as an in-home activity, and the corresponding link is a transaction link. Alternatively, home-stay can be implicitly represented as waiting in the home zone, which incurs disutility but does not lead to a new activity state. Home-stay disutility is defined as

$$c_l^{i\mathrm{HD}}(\tau) = \lambda_6^i \cdot t_l(\tau), \quad \forall i \in I,\ l \in A_{AT},\ \tau \tag{6.7}$$

where $c_l^{i\mathrm{HD}}(\tau)$ is the home-stay disutility incurred by i arriving at link l during τ and λ_6^i denotes the disutility coefficient for home-stay duration $t_a(\tau)$.

ATP disutility

Let $c_l^i(\tau)$ denote the disutility incurred by i arriving at link l during time interval τ. The disutility of an ATP can be expressed as the summation of the disutilities of the associated activity-travel links, which can be derived from the above disutility specifications. A nested structure of link time expense captures time continuum along an ATP. For presentation convenience, link-path time incidence variables are adopted to formulate ATP disutility as

$$c_p^{ih}(k, \boldsymbol{f}) = \sum_{l \in A} \sum_{\tau \in K} \delta_{lk}^{ihp}(\tau) \cdot c_l^i(\tau), \quad \forall i \in I, h \in H, p \in P^{ih}, k \in K \tag{6.8}$$

where $\delta_{lk}^{ihp}(\tau)$ is a 0-1 indicator variable, $\delta_{lk}^{ihp}(\tau) = 1$ if a traveler of class i departs from h during k via ATP p and arrives at link l during τ and $\delta_{lk}^{ihp}(\tau) = 0$ otherwise.

6.2.3 BR-DATA user equilibrium condition

As an extension of the boundedly rational dynamic user equilibrium (BR-DUE) condition, the user equilibrium condition of BR-DATA is stated as for travelers in the same class and living in the same home zone, the experienced disutilities by travelers departing during the same time interval are no larger than the minimum value plus a threshold. Formally, the condition is expressed as

$$c_p^{ih}(k, \boldsymbol{f}^*) \in \left[c_{\min}^{ih}(\boldsymbol{f}^*),\ c_{\min}^{ih}(\boldsymbol{f}^*) \cdot (1 + \varepsilon^{ih})\right], \text{ if } f_p^{ih*}(k) > 0 \quad \forall p \in P^{ih}, k \in K, i, h \tag{6.9}$$

The corresponding finite-dimensional VI problem $\mathrm{VI}(\boldsymbol{f}, \Omega)$ is formulated as

$$\sum_{i \in I} \sum_{h \in H} \sum_{p \in P^{ih}} \sum_{k \in K} \tilde{c}_p^{ih}(k, \boldsymbol{f}^*) \cdot \left[f_p^{ih}(k) - f_p^{ih*}(k)\right] \geq 0, \quad \forall \boldsymbol{f} \in \Omega \tag{6.10}$$

$$\Omega = \left\{ \boldsymbol{f} \mid \boldsymbol{f} \geq 0, \sum_{p \in P^{ih}} \sum_{k \in K} f_p^{ih}(k) = Q^{ih}, \quad \forall\, h \in H, i \in I \right\} \tag{6.11}$$

where

$$\tilde{c}_p^{ih}(k, \boldsymbol{f}^*) = \max\left\{c_p^{ih}(k, \boldsymbol{f}^*),\ c_{\min}^{ih}(\boldsymbol{f}^*) \cdot (1 + \varepsilon^{ih})\right\} \tag{6.12}$$

The dynamic network loading relates to the traffic flow propagation inside a traffic network. With different dynamic network loading models, researchers have proved the continuity of path disutility in continuous-time and discrete-time formulations. For example, relying on a priori boundedness of path departure rates, Zhu and Marcotte (2000) and Bressan and Han (2013) showed the continuity using the link delay model and the LWR-Lax model respectively. Considering Vickrey's point queue model (Vickrey, 1969), Han et al. (2013) proved the strong continuity in the Hilbert space of interest. Similarly, Han et al. (2015) presented the continuity of a path delay operator base on several mild assumptions in the context of bounded rationality (BR). In the discrete-time domain, Lo and Szeto (2002) proved the continuity of path travel time for networks whose dynamics are described by the cell transmission model. Considering the discrete-time point queue model, Huang and Lam (2002) proved the continuity of path travel time with a nested formulation. Long et al. (2011) showed the continuity using a step function and linear interpolation to approximate cumulative flows.

Different from the general BR-DUE models, the BR-DATA models are developed in the SNKs, which express activity participation in the form of transaction links. In this chapter, the discrete-time point queue model is considered in the SNKs. The corresponding dynamic network loading is formulated as follows.

$$u_l(\tau) = \sum_{i \in I} \sum_{h \in H} \sum_{p \in P^{ih}} u_l^{ihp}(\tau), \quad \forall l \in A, \tau \in K, \tag{6.13}$$

$$u_l^{ihp}(\tau) = \zeta_l^{ihp} \cdot f_p^{ih}(\tau) + \zeta_{\ell l}^{ihp} \cdot v_\ell^{ihp}(\tau), \quad \forall l \in A_{PC}, \ell \in A, i, h, p, \tau \tag{6.14}$$

$$v_l(\tau) = \sum_{i \in I} \sum_{h \in H} \sum_{p \in P^{ih}} v_l^{ihp}(\tau), \quad \forall l \in A, \tau \in K, \tag{6.15}$$

$$v_l^{ihp}(\tau) = \pi_l(\tau) \cdot u_l^{ihp}(\tau - t_l^0) + \left(1 - \pi_l(\tau)\right) e_l \frac{u_l^{ihp}(j)}{u_l(j)}, \quad \forall l \in A_{PC}, i, h, p, \tau \tag{6.16}$$

$$r_l^{ihp}(\tau) = \zeta_{l\ell}^{ihp} \cdot v_\ell^{ihp}(\tau), \quad \forall l \in A_{AT}, \ell \in A, i, h, p, \tau \tag{6.17}$$

$$r_l^{ihp}(\tau) = u_l^{ihp}\left(\tau + t_l^{\mathrm{W}}(\tau)\right), \quad \forall l \in, i, h, p, \tau \tag{6.18}$$

$$u_l^{ihp}(\tau) = v_l^{ihp}\left(\tau + t_l^{\mathrm{D}}(\tau)\right), \quad \forall l \in A_{AT}, i, h, p, \tau \tag{6.19}$$

$$q_l(\tau) = \sum_{j_1 \le \tau} u_l(j_1) - \sum_{j_2 \le \tau} v_l(j_2) - e_l, \quad \forall a \in A_{AT}, \tau \in K \tag{6.20}$$

where $u_l^{ihp}(\tau)$, $v_l^{ihp}(\tau)$, and $r_l^{ihp}(\tau)$ are the inflow, outflow, and arrival flow of travelers of class i on link l during time interval τ via ATP p from home zone h; $\zeta_l^{ihp} = 1$ if link l is the first link of p and $\zeta_l^{ihp} = 0$ otherwise; $\varsigma_{\ell l}^{ihp} = 1$ if link ℓ is the predecessor link of l on p and $\varsigma_{\ell l}^{ihp} = 0$ otherwise; $v_l(\tau)$ is the outflow of link l during τ; $\pi_l(\tau) = 1$ if there is no vehicle in the queue on link l during τ and $\pi_l(\tau) = 0$ otherwise; j in Eq. (6.16) satisfies $j + t_l(j) = \tau$. Eq. (6.16) indicates that the link exit rate is either the entry rate during interval $\tau - t_l^0$ or a portion of the link capacity.

For transaction link l, as shown by Eqs. (6.17)-(6.20), $r_l^{ihp}(\tau)$ denotes the arrival flow of link l and equals the outflow of its predecessor link on p. The arrival flows start the activity after waiting time $t_l^{\mathrm{W}}(\tau)$, and then finish the activity after duration $t_l^{\mathrm{D}}(\tau)$. The queue on l, $q_l(\tau)$, is equal to the cumulative inflows minus the summation of cumulative outflows and the activity location capacity. With the above dynamic network loading procedure, the continuity of travel time and disutility can be directly derived based on Huang and Lam (2002). Activity duration and the incurred disutility (Eqs. (6.4) and (6.7)) are continuous with respect to the link inflow. Likewise, the continuity of the waiting and parking time (and disutility) can be easily derived from Eq. (6.2) and Eqs. (6.5)-(6.6) respectively. That is, all link disutilities are continuous with the link inflows. Therefore, the following remark is made.

Remark 6.1 The ATP disutility Eq. (6.8) is continuous with respect to ATP inflow in the SNKs.

The link inflow $u_l^{ihp}(\tau)$ without link capacity constraint is reduced to

$$u_l^{ihp}(\tau) = \delta_{lk}^{ihp}(\tau) \cdot f_p^{ih}(k) \tag{6.21}$$

Incorporating linear interpolation of link travel times, Liu et al. (2015) proved the continuity of ATP disutility if the time interval length is infinitely close to zero.

For the finite-dimensional BR-DUE problem VI($\boldsymbol{f}, \Omega$), Eqs. (2.17)-(2.19), Chapter 4 analyzed its existence based on the existence conditions of the continuous counterpart presented by Han et al. (2015). Here, $\boldsymbol{c}(\boldsymbol{f}) = \{c_p^{ih}(k, \boldsymbol{f})\}$ is used to denote the vector of ATP disutility $c_p^{ih}(k)$ and show the existence under a weaker condition in the framework of BR-DATA.

Proposition 6.1 If $\boldsymbol{c}(\boldsymbol{f})$ is continuous on Ω, there exists a solution to VI$(\boldsymbol{f}, \Omega)$ Eqs. (6.10)-(6.12), and the solution satisfies the BR-DATA user equilibrium condition (6.9).
Proof. The finite-dimensional linear and nonnegative constraints demonstrate that Ω is a compact closed convex set. With continuous $\boldsymbol{c}(\boldsymbol{f})$ on Ω, $\tilde{\boldsymbol{c}}(\boldsymbol{f})$ defined by Eq. (6.12) maintains continuity. Following Theorem 2 proposed by Browder (1968), there exists $\boldsymbol{f}^*$ in Ω satisfying VI$(\boldsymbol{f}, \Omega)$ Eqs. (6.10)-(6.12). In addition, it follows from Eq. (6.10) that for $\forall\ h, i$,

$$f_q^{ih}(\tau) > 0 \Longrightarrow \tilde{c}_q^{ih}(\tau, \boldsymbol{f}^*) = \min_p \min_k \tilde{c}_p^{ih}(k, \boldsymbol{f}^*) \tag{6.22}$$

where q is an ATP and τ denotes a time interval. Eq. (6.22) is a necessary but not sufficient condition of Eq. (6.10).

Recalling the definition of $\tilde{c}_q^{ih}(\tau, \boldsymbol{f}^*)$, for the discrete VI problem (6.10)-(6.12), it can be concluded that

$$\min_p \min_k \tilde{c}_p^{ih}(k, \boldsymbol{f}^*) = c_{\min}^{ih}(\boldsymbol{f}^*) \cdot (1 + \varepsilon^{ih}) \tag{6.23}$$

The minimum value is reached if and only if $c_q^{ih}(\tau, \boldsymbol{f}^*)$ falls within $\left[c_{\min}^{ih}(\boldsymbol{f}^*),\ c_{\min}^{ih}(\boldsymbol{f}^*) \cdot (1 + \varepsilon^{ih})\right]$. □

6.3 Column generation algorithms for BR-DATA

This section focuses on the theoretical analyses and developments of CG and TBCG algorithms. The four strategies in the TBCG algorithm are refined and classified into spatial-temporal exploration and exploitation for fitting the DATA context. Unless otherwise explained below, the term TBCG in the BR-DATA context refers to the one with refinements. To keep consistency, the notations used above attached with n refer to the same entities at iteration n. A time-dependent ATP is defined as a tuple of ATP and departure time (p, k). All (p, k) tuples form the global solution space $\Psi = \{(p, k) | p \in P, k \in K\}$ and $\Phi_n = \{(p, k) | p \in P_n, k \in K_p\}$ is the potential time-dependent ATP set at iteration n, where K_p is a p-related time interval set. Φ_n is created to store time-dependent ATPs as a potential solution for the BR-DATA user equilibrium.

6.3.1 CG algorithm

As mentioned above, the seminal CG algorithm has been applied widely for solving DTA problems. However, no formal proof has been given about the correctness in dynamic contexts. To fill the gap, the theoretical analyses are provided below.

Proposition 6.2 If $\boldsymbol{c}(\boldsymbol{f})$ is continuous on Ω, a solution derived from the CG algorithm satisfies the BR-DATA user equilibrium condition (6.9).

Proof. Initially, the ATP set P_0 is generated using the MDS search algorithm for $\forall h, i$,

$$P_0 = \bigcup_{i \in I, h \in H} P_0^{ih} \tag{6.24}$$

At iteration n, find a vector $\boldsymbol{f_n^*}$ satisfying the following VI($\boldsymbol{f_n}, \Omega_n$) sub-problem on ATP set P_n.

$$\sum_{i \in I} \sum_{h \in H} \sum_{p \in P_n^{ih}} \sum_{k \in K} \tilde{c}_p^{ih}(k, \boldsymbol{f_n^*}) \left[f_{pn}^{ih}(k) - f_{pn}^{ih*}(k) \right] \geq 0, \quad \forall \boldsymbol{f_n} \in \Omega_n \tag{6.25}$$

$$\Omega_n = \left\{ \boldsymbol{f_n} \middle| \, \boldsymbol{f_n} \geq 0, \sum_{p \in P_n^{ih}} \sum_{k \in K} f_{pn}^{ih}(k) = Q^{ih}, \quad \forall \, h \in H, i \in I \right\} \tag{6.26}$$

where $\tilde{c}_p^{ih}(k, \boldsymbol{f_n^*})$ is formulated as

$$\tilde{c}_p^{ih}(k, \boldsymbol{f_n^*}) = \max \left\{ c_p^{ih}(k, \boldsymbol{f_n^*}), \, c_{\min}^{ih}(\boldsymbol{f_n^*}) \cdot (1 + \varepsilon^{ih}) \right\} \tag{6.27}$$

If $\boldsymbol{c}(\boldsymbol{f})$ is continuous on Ω, according to Propositions 6.1, there exists a solution $\boldsymbol{f_n^*}$ to VI($\boldsymbol{f_n}, \Omega_n$) and the solution satisfies

$$c_p^{ih}(k, \boldsymbol{f_n^*}) \in \left[c_{\min}^{ih}(\boldsymbol{f_n^*}), \, c_{\min}^{ih}(\boldsymbol{f_n^*}) \cdot (1 + \varepsilon^{ih}) \right], \quad \text{if } f_{pn}^{ih*}(k) > 0 \quad \forall p \in P_n^{ih}, k \in K \tag{6.28}$$

Extending $\boldsymbol{f_n^*}$ to the global space Ψ gives

$$\boldsymbol{f}^* = \left\{ f_p^{ih}(k) \middle| f_p^{ih}(k) = \begin{cases} 0, & \text{if } p \in \bar{P}_n^{ih} \\ f_{pn}^{ih}(k), & \text{if } p \in P_n^{ih} \end{cases} \right\}, \quad \forall \, k \in K \tag{6.29}$$

where $\bar{P}_n^{ih} = P - P_n^{ih}$ is a set of unfound ATPs at h for i at iteration n. This extension ensures the feasibility of the solution to the original VI problem (6.10)-(6.12), which is consistent with constraint (6.11). Then, the algorithm searches the MDAs again. If no new ATP is found, it means

$$\min\{c_p^{ih}(k) | \, p \in \bar{P}_n^{ih}, \, k \in K\} \geq \, c_{\min}^{ih}(\boldsymbol{f_n^*}) \tag{6.30}$$

Eq. (6.28) is satisfied by substituting $\boldsymbol{f}_{\boldsymbol{n}}^{*}$ with $\boldsymbol{f}^{*}$ and thus $\boldsymbol{f}^{*}$ is a solution to VI problem (6.10)-(6.12). Otherwise, there exists at least one time-dependent ATP in $\{(\bar{p},k)|\bar{p}\in\bar{P}_n^{ih},\ k\in K\}$ and the corresponding minimum disutility satisfies

$$c_{\bar{p}}^{ih}(k,\boldsymbol{f}^{*})<c_{\min}^{ih}(\boldsymbol{f}_{\boldsymbol{n}}^{*}) \tag{6.31}$$

Due to the change of the minimum disutility, the disutilities of time-dependent ATPs with non-zero inflows may be outside of the range $\left[c_{\bar{p}}^{ih}(\boldsymbol{f}^{*}),\ c_{\bar{p}}^{ih}(\boldsymbol{f}^{*})\cdot(1+\varepsilon^{ih})\right]$. P_n^{ih} is extended by defining $P_{n+1}^{ih}=P_n^{ih}\cup\{\bar{p}\}$ and proceed to iteration $n+1$. Note that the number of ATPs in $\bar{P}_n^{ih}$ is finite. Maximally, $\sum_i\sum_h\left|\bar{P}_n^{ih}\right|$ iterations are needed to extend from P_n^{ih} to the global ATP set. The VI($\boldsymbol{f}_{\boldsymbol{n}},\Omega_n$) sub-problem (6.25)-(6.27) has the same formulation with VI problem (6.10)-(6.12) and thus the solution $\boldsymbol{f}_{\boldsymbol{n}}^{*}$ satisfies BR-DATA user equilibrium condition (6.9). □

Note that BR-DATA is a more general form and equivalent to DATA when the relative convergence threshold ε^{ih} equals zero. Based on Proposition 6.2, it can be concluded that the solution derived from the CG algorithm satisfies the DATA user equilibrium condition. Moreover, the existence of solutions to the VI sub-problem (6.25)-(6.27) is ensured under the assumption that ATP disutility is continuous. The BR-DUE and BR-DATA user equilibrium problems have similar VI formulations except for the specification of path disutility. The DUE problem can be transformed from the BR-DUE problem by setting the relative convergence threshold to zero. Thus, the following corollary is obtained.

Corollary 6.1 The solution derived from the CG algorithm satisfies the BR-DUE condition (or DUE condition if the threshold equals zero) if the path disutility is continuous.

In Chapter 4, the TBCG algorithm is proposed by integrating four strategies into the CG scheme: (1) using a tolerance-based criterion for minimum disutility path searches; (2) self-adjusting convergence thresholds to drive the intermediate steps fast; (3) adapting temporal resolutions to extend feasible time regions; and (4) skipping path searches by selecting potential time intervals. These strategies do not only maintain the convergence property of the CG algorithm but also improve the computation efficiency significantly. However, strategies 1 and 2 may influence the property of the solutions. Specifically, as strategy 2 uses ε^{irs} as the lower bound of the self-adjusted convergence threshold, the relative gap between the minimum and maximum path disutilities of the generated path set may reach ε^{irs}. According to strategy 1, paths with disutilities lower than the minimum disutility of the used paths may not be added to the final path set.

These unadded paths make the maximum relative gap larger than ε^{irs}, which contradicts the BR-DUE equilibrium condition (2.16). Moreover, some properties of DATA models may cause inapplicability and inefficiency of these strategies. For example, strategies 1 and 4 require modifications due to the non-FIFO property of ATP disutilities brought by space-time constraints in DATA models. The refinements of these strategies are discussed in the next subsection.

6.3.2 Refined TBCG algorithm

The TBCG algorithm improves the classical CG algorithm in both spatial and temporal dimensions and gains significant speedups. This subsection refines and analyses the strategies in the context of BR-DATA. Inspired by the meta-heuristic methods for combinatorial optimization (Reeves, 1993; Eiben and Schippers, 1998), the strategies are related to spatial-temporal exploration and exploitation.

6.3.2.1 Spatial-temporal exploration strategies

The spatial and temporal explorations aim to locate the potential distribution of the near-equilibrium flows. Based on the recursive formulations in space-time networks (Dean, 2004; Liao, 2019), an algorithm is developed for searching the boundedly rational minimum disutility ATPs (BR-MDA) with variable temporal resolutions. As for spatial exploration, the BR-MDA algorithm adds new acceptable ATPs to a generated ATP set. Regarding the temporal exploration, it explores the potential time region and adds the corresponding time-dependent ATPs to the potential time-dependent ATP set.

Spatial exploration strategy

In the CG algorithm, when a time-dependent ATP $(\bar{p}, k)$ is found with smaller disutility $c_{\bar{p}}^{ih}(k, \boldsymbol{f_n})$ than the minimum disutility $c_{\min}^{ih}(\boldsymbol{f_n})$ at iteration n, the current ATP set is extended by adding $\bar{p}$. This criterion is expressed by

$$c_{\min}^{ih}(\boldsymbol{f_n}) - c_{\bar{p}}^{ih}(k, \boldsymbol{f_n}) \geq 0 \tag{6.32}$$

In the BR context, even if there is a time-dependent ATP with the disutility satisfying Eq. (6.32), travelers may prefer their familiar paths and departure time intervals due to the inconspicuous difference between $c_{\min}^{ih}(\boldsymbol{f_n})$ and $c_{\bar{p}}^{ih}(k, \boldsymbol{f_n})$. As expressed by Eq. (6.8), an ATP in the BR-DATA model consists of more choice facets, for which BR tends to be more evident in choice-making. As a consequence, the following criterion is proposed for considering a tolerance band in adding any ATP to the current ATP set. Eq. (6.32) is replaced by

Algorithm 6.1 BR-MDA algorithm

The auxiliary notations are defined below to illustrate the BR-MDA algorithm.

a, b: start and end nodes of link l respectively

$\bar{C}_j^i(\tau)$: the minimum disutility of class i arriving at node j during time interval τ by departing from h at any time

$\bar{T}_b^i(\tau)$: the arrival time at node b of class i departing from node a during time interval τ

$t_l(\tau)$: the sum of waiting and duration time traversing link l when departing from a during τ

$F_j^i(\tau)$: two-tuple vector recording the preceding link and time interval

Input: $c_l^i(\tau)$ and $t_l(\tau)$, $\forall\, i \in I, l \in A, \tau \in K$

Initially, set $\bar{C}_j^i(\tau) = \infty$ and $\bar{C}_h^i(\tau) = 0$, $\forall i \in I, \tau \in K$, $\forall j \in N \backslash \{h\}$; $\tau = 1$.

```
for i ∈ I
    while τ ≤ |K|
        for l ∈ A
            T̄_b^i(τ) = τ + t_l(τ)
            if C̄_l^i(T̄_l^i(τ)) ≥ M or t_l^D(τ + t_l^W(τ)) < σ_min^l
                continue (skip the following steps in the for loop)
            else
                if C̄_b^i(T̄_b^i(τ)) > C̄_a^i(τ) + c_l^i(τ) and T̄_b^i(τ) ≤ |K|
                    C̄_b^i(T̄_b^i(τ)) = C̄_a^i(τ) + c_l^i(τ)
                    F_b^i(T̄_b^i(τ)) = ⟨l, τ⟩
        end
        τ = τ + 1
    end
    for all h′
        backtrack the optimal ATPs p̄ through F_j^i(τ)
        if the disutility on p̄ satisfies Eq. (6.33) and p̄ ∉ P^ih, add p̄ to P^ih
    end
end
```

$$c_{\min}^{ih}(\boldsymbol{f_n}) - c_{\bar{p}}^{ih}(k, \boldsymbol{f_n}) \geq \epsilon^{ih} \cdot c_{\min}^{ih}(\boldsymbol{f_n}) \tag{6.33}$$

where ϵ^{ih} ($\in [0, 1)$) is the relative indifference threshold of i at h toward ATP-switching. When ϵ^{ih} equals 0, this criterion degenerates to Eq. (6.32).

Travel link and transaction link are two types of links in SNK^T. For travel links, FIFO property is satisfied. Specifically, a traveler entering a travel link earlier will not exit the link later than those who enter the link during later time intervals. For transaction links, space-time constraints are involved. The space constraints ensure that locations of different activities of an activity program are included in an ATP, and the time constraints enforce the activities to be conducted within time windows at the locations. If a traveler

departs from home early and arrives at a shopping location before the shop opens, he/she has to wait and incurs disutility for waiting. The total disutility for shopping may be higher than that of departing from home later and arrives at the shop just after the shop opens. In that sense, the transaction link disobeys the FIFO property in terms of disutility. Once a link does not satisfy this FIFO property, the network or supernetwork is non-FIFO (Dean, 2004; Liao, 2016). SNK^T is a non-FIFO network after waiting disutility and time window constraints are incorporated. The tolerance-based path search algorithm suggested in Chapter 4 is not valid to find the optimal paths in non-FIFO supernetworks. Therefore, the BR-MDA algorithm is devised to search for the non-FIFO ATPs subject to space-time constraints, for which the pseudo-code is given above.

Temporal exploration strategy

The TBCG algorithm extends the time interval set of the generated ATPs via temporal exploration. Rather than assigning flows to all the time intervals, TBCG tentatively assigns flows to potential time regions. This strategy is based on the observation that ATP flows of specific classes of travelers are concentrated on narrow time regions. With these narrow potential time regions, the intermediate BR-DATA user equilibrium states are achieved fast. The discrete-time regions are composed of several blocks of continuous-time zones. The temporal exploration aims to approximately cover these time regions. Taking Figure 6.2 for example, subfigure (a) shows the resultant time-dependent ATPs. Subfigures (b), (c), and (d) represent time-dependent ATPs according to alternative algorithms. Traditional traffic assignment algorithms (e.g., Huang and Lam, 2002; Long et al., 2016) take all time intervals into account, shown in subfigure (b). According to the algorithm developed by Lu et al. (2009), if a new ATP p is found during time interval 3, only this time interval, as shown in subfigure (c), is added to the time-dependent ATP set. Other time-dependent ATPs will be added during the following ATP searches. Whereas, as reflected in subfigure (d), the temporal exploration strategy adds time intervals satisfying Eq. (6.34) to an ATP-related set K_p. The corresponding time-dependent ATPs $\{(p,k)|p,k \in K_p\}$ are added to Φ_n for BR-DATA.

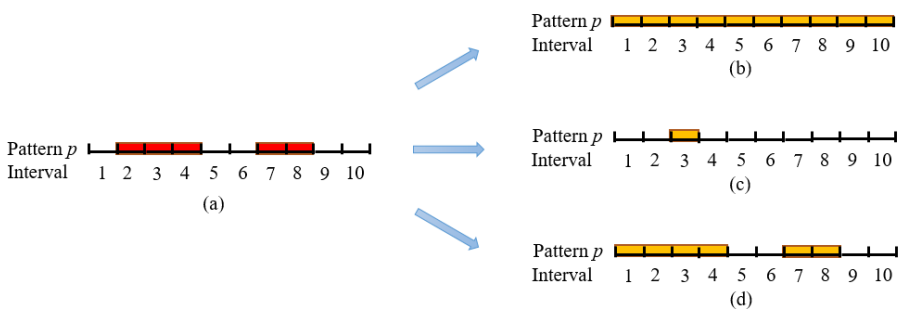

Figure 6.2 Different results of time-dependent ATPs.

$$c_p^{ih}(k, \boldsymbol{f_n}) - c_{\min}^{ih}(\boldsymbol{f_n}) \leq \vartheta_3 \cdot \varepsilon^{ih} \cdot c_{\min}^{ih}(\boldsymbol{f_n}) \tag{6.34}$$

where parameter ϑ_3 is equal to or larger than 1 to approximate the potential time interval sets of the BR-DATA solutions. If ϑ_3 is set too large, all (p, k) satisfy Eq. (6.34) and the resultant time-dependent ATPs become the case in subfigure (b). A smaller ϑ_3 leads to more times of updating Φ_n. $\vartheta_3 = 0$ results in the case in subfigure (c).

6.3.2.2 Spatial-temporal exploitation strategies

The exploitation strategies aim to discern the right moments to enforce the flow assignment with the required convergence precision. The TBCG algorithm starts with a large relative convergence threshold and a low temporal resolution to explore the solution space. The spatial exploitation reduces the number of intermediate iterations by adjusting the relative convergence threshold dynamically. The temporal exploitation intensifies the convergence process by increasing the temporal resolution. Eventually, both the relative convergence threshold and the temporal resolution would reach the required values.

Spatial exploitation strategy

A convergence gap is a measurement of how close the current solution is to the equilibrium solution. Some existing studies have used the gap of traffic flows or disutilities over successive iterations. For example, Han et al. (2015) employed the relative distance between the previous path flow vector and the current one as the termination condition. However, this may not be valid since the sufficient condition for the convergence cannot be guaranteed. For that matter, a relative gap function is defined as Eq. (6.35) to measure the convergence of the proposed algorithm.

$$Regap(k, \boldsymbol{f_n}) = \max\left\{\frac{c_p^{ih}(k, \boldsymbol{f_n}) - c_{\min}^{ih}(\boldsymbol{f_n})}{c_{\min}^{ih}(\boldsymbol{f_n})}\right\}, \quad \forall\, p \in P^{ih}, i \in I, h \in H, k \in K \tag{6.35}$$

The denominator $c_{\min}^{ih}(\boldsymbol{f_n})$ is always larger than 0. For $\forall\ h,\ i$, this measure is consistent with

$$c_p^{ih}(k, \boldsymbol{f_n}) - c_{\min}^{ih}(\boldsymbol{f_n}) \leq \varepsilon^{ih} \cdot c_{\min}^{ih}(\boldsymbol{f_n}) \tag{6.36}$$

The relative convergence threshold ε^{ih} is a parameter associated with traveler heterogeneity. Note that the convergence curves usually become flat when the solutions approach the equilibrium. The convergence criterion Eq. (6.36) may result in many iterations of flow transfers to reach the required convergence precision. Since the current

ATP set at iteration n is likely to be a subset of the solution set at an equilibrium state, the TBCG algorithm adopts a self-adjusted convergence threshold to perform rough assignments at intermediate iterations. This strategy is formulated as

$$c_p^{ih}(k, \boldsymbol{f_n}) - c_{\min}^{ih}(\boldsymbol{f_n}) \leq \varepsilon_n^{ih} \cdot c_{\min}^{ih}(\boldsymbol{f_n}) \tag{6.37}$$

where ε_n^{ih} is the relative convergence threshold at iteration n.

Suppose that a new ATP is found and added to the ATP set, meaning that some ATP flows are more likely to shift to this new ATP. The self-adjusted convergence strategy increases ε_n^{ih} (Eq. (6.38)) to ensure fast convergence.

$$\varepsilon_{n+1}^{ih} = \min\left(\frac{1}{\vartheta_1} \cdot \varepsilon_n^{ih},\ \varepsilon_{\max}^{ih}\right) \tag{6.38}$$

where $\vartheta_1 \in (0, 1)$ is a scaling parameter and $\varepsilon_{\max}^{ih}$ is the upper bound of convergence tolerance for travelers of class i at h. Iteration $n+1$ tends to have a larger relative convergence threshold, which reduces the computation time and provides an inclusive ATP set.

If no new ATP satisfying Eq. (6.33) is found at iteration n (i.e., the ATP set is saturated), the relative convergence threshold is decreased as Eq. (6.39) to intensify convergence.

$$\varepsilon_{n+1}^{ih} = \max\left(\vartheta_1 \cdot \varepsilon_n^{ih},\ \varepsilon_{\min}^{ih}\right) \tag{6.39}$$

where $\varepsilon_{\min}^{ih} = \varepsilon^{ih} - \epsilon^{ih} - \varepsilon^{ih}\epsilon^{ih}$ is the lower bound of convergence tolerance for travelers of class i at h. Different from the second strategy proposed in Chapter 4, $\varepsilon_{\min}^{ih}$ other than ε^{ih} is used as the lower bound of convergence tolerance in Eq. (6.39). It would prevent the violation of the global convergence condition. Note that $\varepsilon_{\min}^{ih}$ is related to ε^{ih} and ϵ^{ih}, and the value increases by decreasing ϵ^{ih}. If ϵ^{ih} is decreased to 0, meaning that travelers are assumed to choose the ATPs with smaller disutility in the BR-MDA algorithm, $\varepsilon_{\min}^{ih}$ is equal to ε^{ih}.

Temporal exploitation strategy

For the time dimension, a high temporal resolution is important for accuracy and fidelity. In this chapter, constant Δ is defined as the minimum length of a time interval, representing the required temporal resolution. A small Δ leads to high computation demand and slow convergence. The TBCG algorithm employs a variable temporal resolution Δ_n to balance the convergence speed and accuracy. If no new ATP satisfies Eq. (6.33) at iteration n and the relative convergence threshold ε_n^{ih} equals ε_{min}^{ih}, the

temporal exploitation strategy is performed as Eq. (6.40) to meet the required temporal resolution.

$$\Delta_{n+1} = \max(\lfloor \vartheta_2 \cdot \Delta_n \rfloor, \Delta) \tag{6.40}$$

where $\vartheta_2 \in (0, 1)$ is a resolution scaling parameter and $\lfloor \cdot \rfloor$ is an integer-floor operator.

All in all, for the spatial-temporal exploration strategies, the relative convergence thresholds and temporal resolutions are adaptively set to explore the potential time-dependent ATP set. For the spatial-temporal exploitation strategies, the values of Δ_n and ε_n^{ih} are dynamically modified until the required convergence precision is met. The exploration and exploitation are complementary and complete the convergence process of the TBCG algorithm together.

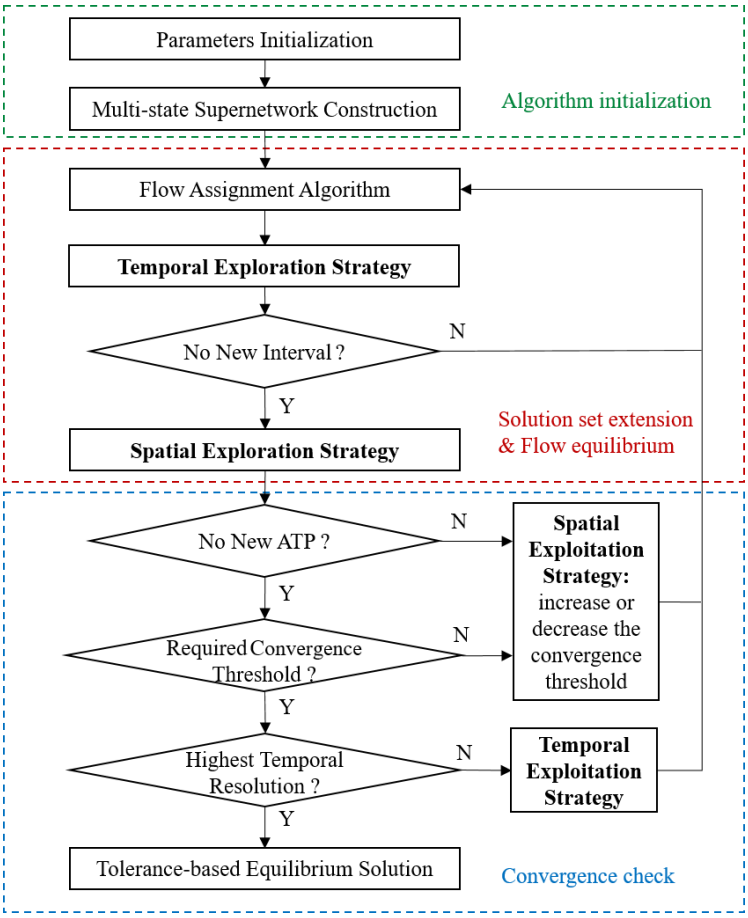

Figure 6.3 Flowchart of the refined TBCG algorithm.

Table 6.1 Comparison of three representative CG-related algorithms

Algo.	Ref.	Problems	Activity -based	*Spatial exploration*	*Temporal exploration*	*Spatial exploitation*	*Temporal exploitation*
				Disutility non-FIFO	ϑ_3	$\varepsilon_{\min}^{ih}$	Time horizon
CG	Friesz, 1985;	UE	No	No	–	–	–
TBCG	Chapter 4	BR-DUE	No	No	Fixed	ε^{ih} (loose)	Peak hours
Refined TBCG	*Current chapter*	BR-DATA	Yes	Yes	Flexible	$\varepsilon^{ih} - \epsilon^{ih} - \varepsilon^{ih}\epsilon^{ih}$ (tight)	One-day

(–: not applicable; Algo. is short for algorithm; Ref. is short for reference)

Different from the strategies used for solving BR-DUE in Chapter 4, the exploration strategies take into account time window constraints of activity chains in a long-time frame, and the exploitation strategies adjust the original lower bound of relative convergence thresholds. The refined TBCG algorithm regroups the modules so that the strategies are coupled better with each other. Accordingly, the flowchart of the TBCG algorithm is shown in Figure 6.3. Parameter initialization and SNK construction are within the module of algorithm initialization, which provides the necessary inputs. The second part, as shown within the red rectangle, consists of two procedures. Temporal and spatial exploration strategies extend potential time regions and ATPs respectively. The route-swapping algorithm is applied for equilibrating the flows. The mechanism has been proved by Nagurney and Zhang (1997) and Huang and Lam (2002) that the generated flow vector will converge to an equilibrate flow pattern even if the path cost functions are not monotonic. To measure the convergence of the TBCG algorithm, three different criteria are checked in turn. As shown within the blue rectangle, the violation of different criteria will induce different strategies. The solution to the BR-DATA problem is obtained when all these criteria are satisfied simultaneously.

Path search and network loading are two time-consuming components in traffic assignment models using CG techniques. Given temporal resolution Δ_n at intermediate iteration n, the run-time complexities to search ATPs and load ATP flows are $O(|I| \cdot |H| \cdot |A| \cdot |K_n|)$ and $O(\sum_{i,h}|P^{ih}| \cdot |A'| \cdot |K_n| \cdot m_1)$ respectively, where $|A'|$ is the maximum number of links in an ATP, m_1 is the number of dynamic network loadings, K_n the set of time intervals corresponding to Δ_n, and operator $|\cdot|$ gives the cardinality of a set. A large Δ_n leads to a significant decrease in the number of time intervals and time-dependent ATPs. Since ABMs focus on ATPs of a long-time frame, the ratio $|K|/|K_n|$ in DATA problems is much larger than that in DTA problems (usually focusing on peak hours). Thus, the temporal exploitation strategy is paramount in the BR-DATA context. Although the proposed algorithm does not reduce the run-time complexities in principle,

the proposed strategies lead to less computation time by decreasing $|K_n|$, $|P^{ih}|$ and m_1 during the intermediate iterations. Table 6.1 summarizes the comparison of the representative CG algorithms for addressing three different network equilibrium problems.

6.3.2.3 Properties of the TBCG algorithm

In view of the above, decreasing Δ_n leads to a more precise distribution of ATP flows and disutilities, while decreasing ε_n^{ih} forces the disutilities to fall within a predefined tolerance band. The following theoretical properties of the refined TBCG algorithm are derived.

Lemma 6.1: At iteration n, the solution $\boldsymbol{f}^*$ to BR-DATA problem (6.10)-(6.12) can be derived from $\boldsymbol{f}_{\boldsymbol{n}}^*$ if $\Delta_n = \Delta$, $\varepsilon_n^{ih} = \varepsilon_{\min}^{ih}$, no new time-dependent ATP satisfies Eq. (6.33), and $\boldsymbol{c}(\boldsymbol{f})$ is continuous.

Proof. Different from VI sub-problem (6.25)-(6.27), the TBCG algorithm uses K_p rather than K to form time-dependent ATPs set $\Phi_n^{ih} = \{(p,k)|p \in P_n^{ih}, k \in K_p\}$. Hence, the VI problem at iteration n is formulated as

$$\sum_{i\in I}\sum_{h\in H}\sum_{p\in P_n^{ih}}\sum_{k\in K_p}\tilde{c}_p^{ih}(k,\boldsymbol{f}_{\boldsymbol{n}}^*)\left[f_{pn}^{ih}(k)-f_{pn}^{ih*}(k)\right]\geq 0,\quad \forall \boldsymbol{f}_{\boldsymbol{n}}\in \Omega_n \tag{6.41}$$

$$\Omega_n=\left\{\boldsymbol{f}_{\boldsymbol{n}}|\ \boldsymbol{f}_{\boldsymbol{n}}\geq 0,\sum_{p\in P_n^{ih}}\sum_{k\in K_p}f_{pn}^{ih}(k)=Q^{ih},\quad \forall h\in H, i\in I\right\} \tag{6.42}$$

$$\tilde{c}_p^{ih}(k,\boldsymbol{f}_{\boldsymbol{n}}^*)=\max\left\{c_p^{ih}(k,\boldsymbol{f}_{\boldsymbol{n}}^*),\ c_{\min}^{ih}(\boldsymbol{f}_{\boldsymbol{n}}^*)\cdot(1+\varepsilon_n^{ih})\right\} \tag{6.43}$$

Under the condition that $\boldsymbol{c}(\boldsymbol{f})$ is continuous on Ω_n, there is a solution $\boldsymbol{f}_{\boldsymbol{n}}^*$ to this VI problem, and the solution satisfies the following equation according to Proposition 6.1.

$$c_p^{ih}(k,\boldsymbol{f}_{\boldsymbol{n}}^*)\in\left[c_{\min}^{ih}(\boldsymbol{f}_{\boldsymbol{n}}^*),\ c_{\min}^{ih}(\boldsymbol{f}_{\boldsymbol{n}}^*)\cdot(1+\varepsilon_n^{ih})\right],\quad \text{if } f_{pn}^{ih*}(k)>0\quad \forall p\in P_n^{ih}, k\in K_p, i, h \tag{6.44}$$

Let $\overline{\Phi}_n^{ih}=\{(p,k)|p\notin P_n^{ih}\cup k\notin K_p\}$. $\boldsymbol{f}_{\boldsymbol{n}}^*$ can be extended to the global region Ψ by defining

$$\boldsymbol{f}^* = \left\{ f_p^{ih*}(k) \middle| f_p^{ih*}(k) = \begin{cases} 0, & \text{if } (p,k) \in \bar{\Phi}_n^{ih} \\ f_{pn}^{ih*}(k), & \text{if } (p,k) \in \Phi_n^{ih} \end{cases} \right\} \tag{6.45}$$

Although no new time-dependent ATP satisfies Eq. (6.33), there may be one or more time-dependent ATPs in $\bar{\Phi}_n^{ih}$ with disutilities $c_p^{ih}(k, \boldsymbol{f}^*)$ less than $c_{\min}^{ih}(\boldsymbol{f}_{\boldsymbol{n}}^*)$. It is reasonable to assume that (p', k') has the minimum disutility $c_{p'}^{ih}(k', \boldsymbol{f}^*)$, that is $c_{\min}^{ih}(\boldsymbol{f}^*) = c_{p'}^{ih}(k', \boldsymbol{f}^*)$. Derived from this finding and Eq. (6.45), it can be obtained that for all $(p,k) \in \Psi$, if $f_p^{ih*}(k) > 0$,

$$\begin{aligned} \frac{c_p^{ih}(k, \boldsymbol{f}^*) - c_{\min}^{ih}(\boldsymbol{f}^*)}{c_{\min}^{ih}(\boldsymbol{f}^*)} &= \frac{c_p^{ih}(k, \boldsymbol{f}^*) - c_{p'}^{ih}(k', \boldsymbol{f}^*)}{c_{p'}^{ih}(k', \boldsymbol{f}^*)} \\ &\leq \frac{c_p^{ih}(k, \boldsymbol{f}^*) - (1-\epsilon^{ih}) \cdot c_{\min}^{ih}(\boldsymbol{f}_{\boldsymbol{n}}^*)}{(1-\epsilon^{ih}) \cdot c_{\min}^{ih}(\boldsymbol{f}_{\boldsymbol{n}}^*)} \\ &\leq \frac{c_{\min}^{ih}(\boldsymbol{f}_{\boldsymbol{n}}^*) \cdot (1+\varepsilon_n^{ih}) - (1-\epsilon^{ih}) \cdot c_{\min}^{ih}(\boldsymbol{f}_{\boldsymbol{n}}^*)}{(1-\epsilon^{ih}) \cdot c_{\min}^{ih}(\boldsymbol{f}_{\boldsymbol{n}}^*)} \\ &= \frac{\varepsilon_{\min}^{ih} + \epsilon^{ih}}{1-\epsilon^{ih}} = \varepsilon^{ih} \end{aligned} \tag{6.46}$$

The first inequality is derived since $(1-\epsilon^{ih}) \cdot c_{\min}^{ih}(\boldsymbol{f}_{\boldsymbol{n}}^*)$ is a lower bound of $c_{p'}^{ih}(k', \boldsymbol{f}^*)$ according to Eq. (6.33), and the second inequality holds due to Eq. (6.44). Note that the denominator is always larger than 0 since $\epsilon^{ih} \in [0, 1)$. This conclusion is consistent with the BR-DATA condition (6.9). Thus, $\boldsymbol{f}^*$ is a solution to BR-DATA problem (6.10)-(6.12). □

Lemma 6.2: The first three conditions posited in Lemma 6.1 can be reached within finite iterations.

Proof. This lemma can be proved by showing that the number of iterations of spatial-temporal exploration and exploitation is finite in the TBCG algorithm. Specifically, for the spatial exploration, only when the time-dependent ATP $(p,k) \in \{(p,k) | p \notin P_n^{ih}, k \in K_n\}$ with disutility satisfying Eq. (6.33), p is added to the current ATP set P_n^{ih} and processed in the next iteration. The number of ATPs in P leads to the result that no more than $|P|$ iterations of ATP extensions are needed from $\emptyset$ to P. It should be noted that the actual number of used ATPs is significantly less than $|P|$. Regarding the temporal exploration, it adds time interval k to K_p only if time interval k satisfies Eq. (6.34). Then, the VI problem is solved with the new K_p. At iteration n, the maximum number of K_p extensions is $|K_n|$ since $K_p \sqsubseteq K_n$. Taken together, the new ATP and time interval extension are completed within finite steps. On the other hand, Eq. (6.40) is performed $\lceil \ln(\Delta/\Delta_0)/\ln \vartheta_2 \rceil$ times at most to increase the time resolution to Δ, and Eq. (6.39) is

performed at most $\left\lceil \ln\left(\varepsilon_{min}^{ih}/\varepsilon_{max}^{ih}\right)/\ln\vartheta_1 \right\rceil$ times to reach ε_{min}^{ih}. These are consistent with the conditions noted in Lemma 6.1.□

According to Lemmas 6.1 and 6.2, the following proposition is obtained.

Proposition 6.3 If $\boldsymbol{c}(\boldsymbol{f})$ is continuous, the solution derived from the TBCG algorithm satisfies the BR-DATA user equilibrium condition under the required convergence precision.

Proof. According to Lemma 6.2, the required convergence precision can be reached within finite iterations of spatial and temporal exploitation. As shown by Eq. (6.45), the extension of $\boldsymbol{f}_{\boldsymbol{n}}^{*}$ to the global region Ψ ensures that all used time-dependent ATPs in Ψ by class i departing from h has disutilities within $\left[c_{\min}^{ih}(\boldsymbol{f}^{*}),\ c_{\min}^{ih}(\boldsymbol{f}^{*})\cdot(1+\varepsilon^{ih})\right]$. □

The continuity of $\boldsymbol{c}(\boldsymbol{f})$ ensures that there is at least one solution to BR-DATA problem (6.10)-(6.12). However, the monotonicity of the ATP disutilities, $c_p^{ih}(k,\boldsymbol{f})$, cannot be guaranteed based on Eq. (6.8); hence, the uniqueness of solutions may not hold. The refined strategies make major revisions to the original CG algorithm. Comparatively, the TBCG algorithm searches the solutions to the BR-DATA problems in reduced space but produces uncompromised solutions. In the numerical example section, it will be shown that the TBCG algorithm produces approximately the same BR-DATA solutions as the original CG algorithm with significantly reduced computation time.

6.4 Numerical examples

In this section, numerical examples are carried out to assess the TBCG algorithm for BR-DATA problems. The solution algorithm is coded in MATLAB and runs on a personal computer with an Intel(R) Core(TM) i5-7300U 2.60 GHz CPU and 8.00 GB RAM. The time horizon is taken from 7:00 am to 8:00 pm on an average day. To illustrate traveler heterogeneity, three different traveler classes are considered according to their incomes. The ratio among low, medium, and high-income travelers is 1:3:1. Travelers are assumed to conduct activities from a pool of activities, including work (W), shopping (S), and leisure (L), constituting seven different daily activity programs. The percentages of travelers on different activity programs are W 20%, S 20%, L 20%, W+S 8%, W+L 8%, S+L 8%, and W+S+L 16%. After performing link attribute transformations in the studied transport networks, travelers with work activity are assumed to work at locations where can be reached within 1 hour of free-flow travel time. The attraction of a work location is inversely proportional to the distance between the home zone and the workplace. The parameters are set as $\Delta=$ 1 minute and $\varepsilon^{ih}=0.1$ in the CG and TBCG algorithms. F_a^l is

defined as $-0.001(t-7.5)(t-8)(t-17)(t-18)+1$ for work, $-0.001(t-7.5)(t-8)(t-18)(t-19)+1$ for shopping, and $-0.001(t-7.5)(t-8.5)(t-17)(t-19)+1$ for leisure. Other common parameters are listed in Table 6.2. The newly- developed BR-MDA is used in both algorithms. One main difference is that the CG algorithm uses Eq. (6.32) as the ATP-adding criterion, while the TBCG uses Eq. (6.33). In addition, $\vartheta_1 = 0.1$, $\vartheta_2 = 0.3$, $\vartheta_3 = 1$, $\Delta_1 = 2$ minutes, $\epsilon^{ih} = 0.1$, and $\varepsilon_0^{ih} = \varepsilon_{\max}^{ih} = 0.2$ are defined only for the TBCG algorithm (some parameters are modified for sensitivity analyses below).

Table 6.2 Parameter settings

Activity	t_l^o (h)	t_l^e (h)	U_l^*	$\sigma_{\min}^l$(h)	$\sigma_{\max}^l$(h)	e_l
W	8	17	10	6	8	100
S	8	19	3	0.17	1	100
L	8	19	5	0.33	1.5	100
Class	λ_1^i	λ_2^i	λ_3^i	λ_4^i	λ_5^i	λ_6^i
1	0.30	0.33	1	100	1	-0.083
2	0.36	0.40	1.3	100	0.8	-0.075
3	0.39	0.43	1.3	100	0.8	-0.067

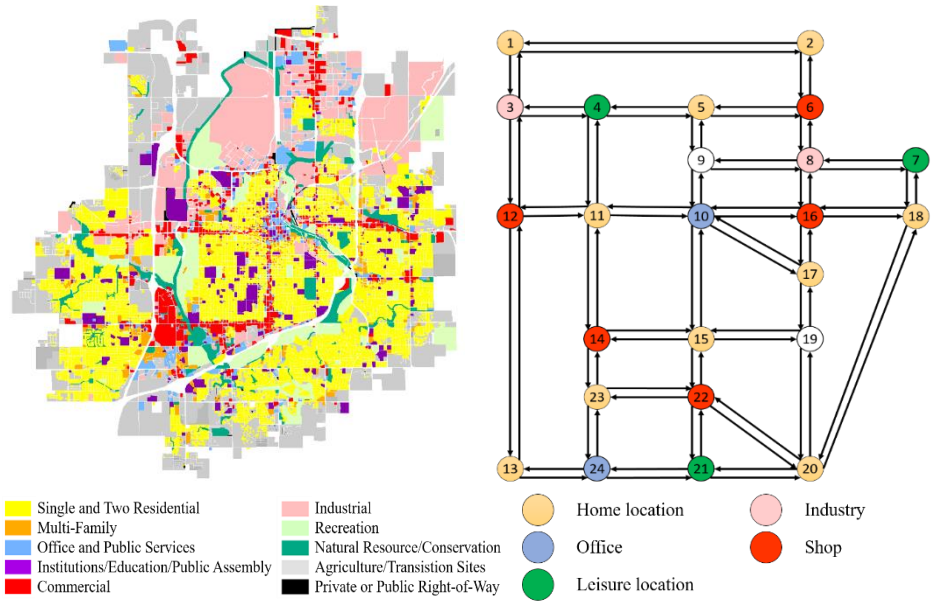

(a) Land use map (b) Transport network

Figure 6.4 Land use and transport network of Sioux Falls.

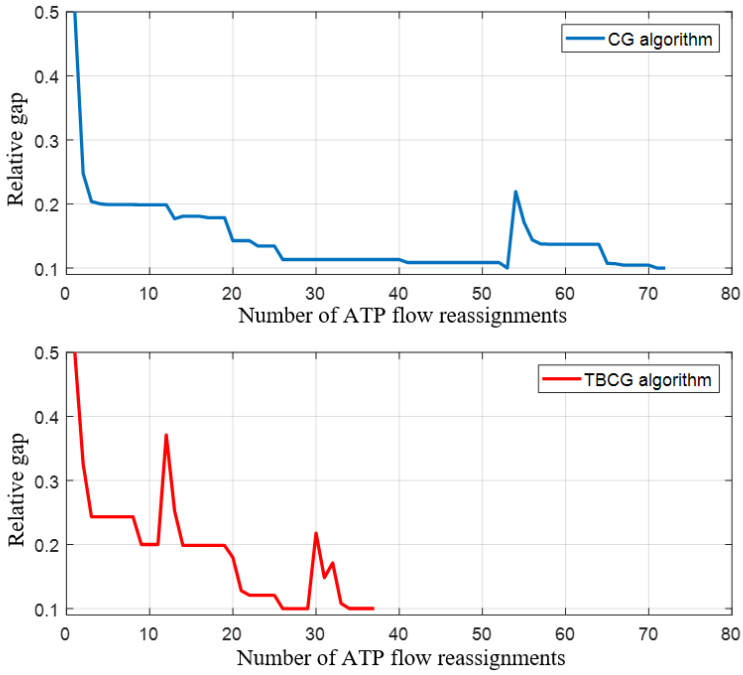

Figure 6.5 Convergence curves of the CG and TBCG algorithms.

6.4.1 Sioux Falls network

The application of the TBCG algorithm is first elaborated in the Sioux Falls network consisting of 24 nodes and 76 links. To illustrate the activity participation of travelers, 10 home zones (residential neighborhoods), 4 workplaces (including offices and industries), 5 shops, and 3 leisure locations are defined. The demands of these 10 home zones are randomly generated from 1 to 6 times of 1000. The layout of these locations given in Figure 6.4 (b) corresponds to the land use map shown in Figure 6.4 (a) from http://www.siouxfalls.org/Planning.

Figure 6.5 shows the convergence curves of CG and TBCG algorithms. Both algorithms go through oscillations. These fluctuations in the course of convergence are a common issue of many flow assignment algorithms (e.g., Huang and Lam, 2002; Long et al., 2013; Han et al., 2015). For the flat parts, the relative gaps remain unchanged when the flows shifted in the assignment process are not large enough to change the values of the maximum and minimum disutilities. For the peaks, the relative gaps change considerably when new time-dependent ATPs are generated. The first peak of the TBCG algorithm appears when the relative gap reaches $\varepsilon_{\max}^{ih}$ (0.2). At that point, the BR-MDA algorithm is run to find new ATPs, and the new generated ATP provides a new start for the following iterations. The total computation times are 214.79 s for TBCG algorithm

and 512.06 s for CG algorithm (note that the computation times should be substantially reduced when using a compiling programming language). The horizontal axes in the subfigures denote the number of ATP flow reassignments, which is consistent with the number of dynamic network loadings. In this example, the TBCG and CG algorithms need 37 and 72 ATP flow reassignments respectively to satisfy the stopping criterion.

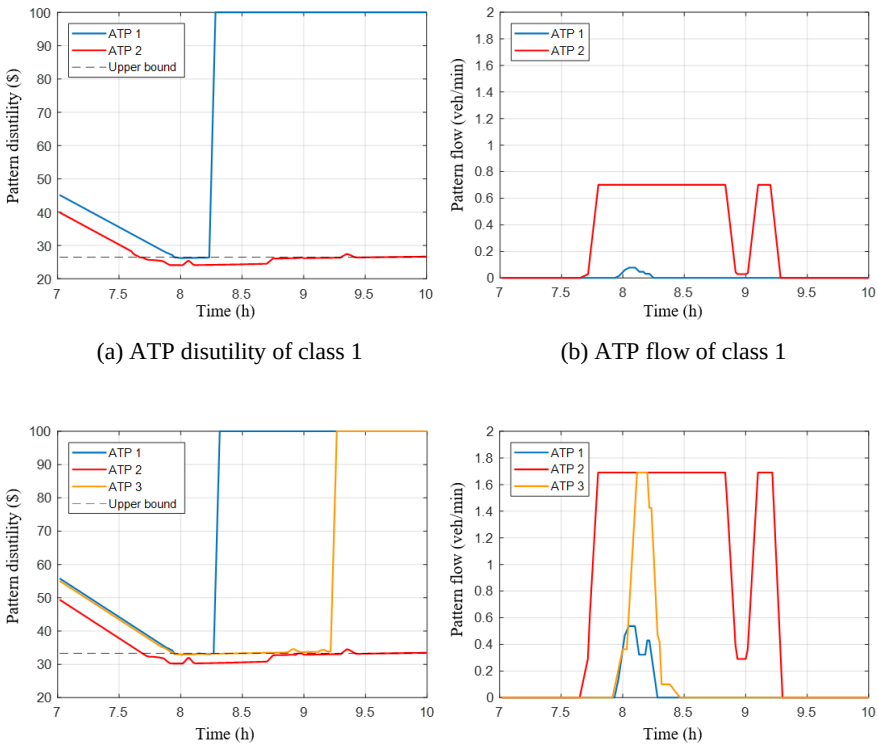

(a) ATP disutility of class 1

(b) ATP flow of class 1

(c) ATP disutility of class 2

(d) ATP flow of class 2

Figure 6.6 Equilibrium solutions of class 1 and class 2.

Table 6.3 ATP specification

Class	ATP ID	Sequence of nodes
1	ATP 1	15 - **22 (shopping)** - **21 (leisure)** - **24 (work)** - 21 - 22 - 15
	ATP 2	15 - 22 - 21 - **24 (work)** - **21 (leisure)** - **22 (shopping)** - 15
2	ATP 1	15 - **22 (shopping)** - **21 (leisure)** - **24 (work)** - 21 - 22 - 15
	ATP 2	15 - 22 - 21 - **24 (work)** - **21 (leisure)** - **22 (shopping)** - 15
	ATP 3	15 - 22 - **21 (leisure)** - **24 (work)** - 23 - **22 (shopping)** - 15

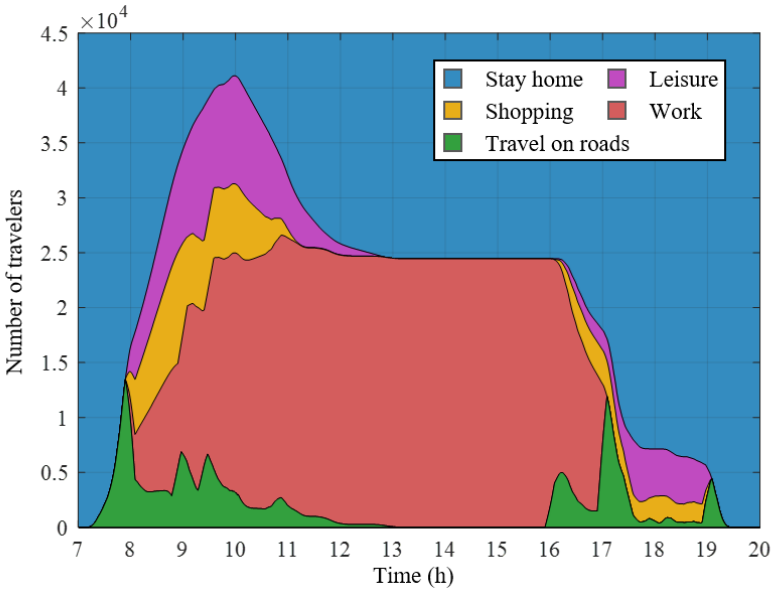

Figure 6.7 The number of travelers at different states.

Travelers belonging to classes 1 and 2 of the same home zone are chosen to illustrate the effects of traveler heterogeneity on BR-DATA user equilibrium states. As shown in Figure 6.6, ATPs 1 and 2 are generated for class 1 (the upper two subfigures), while travelers in class 2 have three ATPs (the lower two subfigures). Each ATP is represented by a sequence of nodes in Table 6.3. At the steady state, the disutilities of used time-dependent ATPs are no larger than the upper bound defined by Eq. (6.37). These results meet the BR-DATA user equilibrium condition. The disutility of ATP 1, shown by the blue curve, has a steep increase at around 8:15 am. Travelers who depart later than this time cannot finish three activities subject to space-time constraints and consequently receive a large penalty. It is interesting to find that the flow curves of ATP 2 in Figure 6.6 (b) and (d) have major fluctuations at around 9:00 am as the corresponding ATP disutilities have larger values. The reason is that a large part of travelers departing at around 8:00 am choose to go shopping first, which leads to a mild traffic peak at around 9:00 am. Hence, travelers departing later may either alter departure times or switch to other ATPs to avoid congestion. Similarly, travelers who conduct leisure activities in the morning would be involved in dense traffic at around 9:30 am. This explanation is verified by Figure 6.7. Moreover, ATPs 1, 2, and 3 have different activity sequences. Based on Eqs. (6.3) and (6.4), the activity disutility decreases with increased duration, which is partly due to the log-shape activity disutility function.

Throughout a day, travelers may go through five different states, i.e., staying at home, traveling on roads, working, shopping, and doing leisure. The travelers at these

states are marked with blue, green, red, orange, and purple colors respectively, as depicted in Figure 6.7. The time use of travelers on roads shows that the plausible morning and evening peaks appear during [7:30 am, 9:30 am] and [4:30 pm, 5:30 pm] respectively. During the morning peak hours, three peaks occur, consistent with the ATP disutilities in Figure 6.6. Travelers prefer shopping during the time range [8:00 am, 12:00 pm] in the morning and [4:00 pm, 7:00 pm] in the afternoon. The departure time range is pre-set as [7:00 am, 10:00 am] to examine the departure time choice across peak and non-peak hours. The pre-set time range causes travelers who only have shopping in the activity program to conduct shopping in the morning. Therefore, the yellow area in the morning is larger than that in the afternoon. Travelers doing leisure have a similar distribution. This may be because both activities have similar opening hours and duration choice constraints. In addition, travelers going shopping and/or doing leisure after work are involved in a mild traffic peak at around 7:00 pm.

To test the effects of parameter settings on the convergence of the TBCG algorithm, Table 6.4 shows the effects of three parameters, ϑ_1, $\varepsilon_{\max}^{ih}$ and ϵ^{ih} by fixing other parameters. As seen, the run-time, the number of BR-MDA algorithm queries (expressed as PS - pattern search in Table 6.4), and the number of dynamic network loadings (NL) fluctuate with the parameters. Overall, the speedup factors of TBCG over CG fall within the range [2, 3] whilst producing approximately the same BR-DATA solutions. In this example, it is found that 94.22% of the common ATPs are generated by both algorithms.

Table 6.4 Effects of the parameters of the TBCG algorithm

Comparison parameters			CG algorithm			TBCG algorithm			Speedup factor
ϑ_1	$\varepsilon_{\max}^{ih}$	ϵ^{ih}	# PS	# NL	Run-time (s)	# PS	# NL	Run-time (s)	
0.5	0.2	0.1	4	80	512.06	9	49	214.79	2.38
0.6	0.2	0.1				10	50	221.15	2.32
0.75	0.2	0.1				11	39	203.02	2.52
0.8	0.2	0.1				12	42	211.67	2.42
0.1	**0.4**	0.1	4	76	619.43	9	34	267.84	2.31
0.1	**0.3**	0.1				9	34	236.18	2.62
0.1	**0.2**	0.1				10	44	266.14	2.33
0.1	**0.15**	0.1				10	53	278.47	2.22
0.1	0.2	**0.8**	4	62	699.06	9	51	248.05	2.82
0.1	0.2	**0.4**				10	57	321.83	2.17
0.1	0.2	**0.2**				10	56	294.40	2.37
0.1	0.2	**0.1**				10	56	297.59	2.35

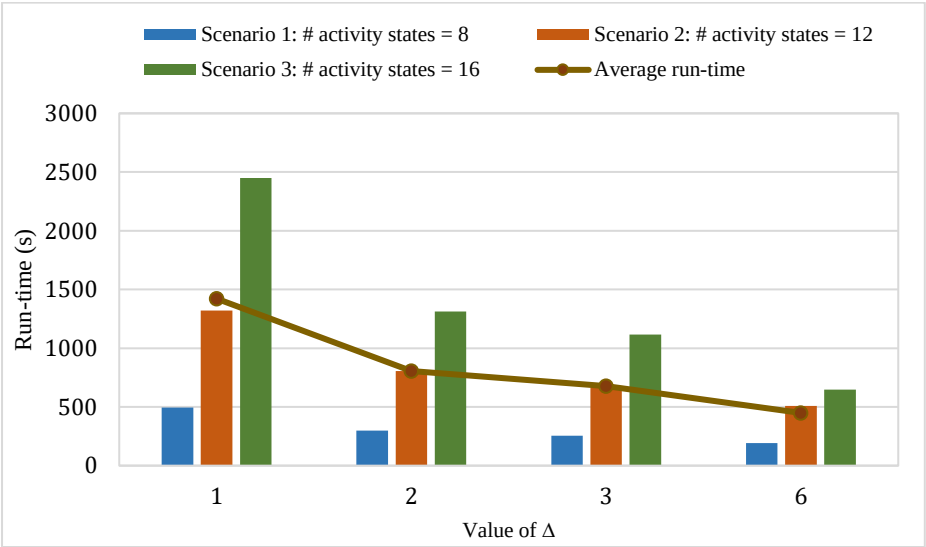

Figure 6.8 Run-time under different scenarios.

6.4.2 Space-time scalability

Various activity states and time resolutions in the Sioux Falls network and another four larger transport networks are chosen to illustrate the space-time scalability. As shown in Figure 6.8, the number of activities is increased in an activity program and three scenarios of the BR-DATA problem are considered based on the number of activity states in the Sioux Falls network, while other setups remain unchanged. Figure 6.8 also shows the influence of the time interval Δ. Note that a larger value of Δ means a smaller temporal resolution in the discrete-time domain. Scenario 1 has 3 activities and 8 activity states. Scenarios 2 and 3 consider 4 activities, in which nodes 9 and 19 in Figure 6.4 (b) are used as the locations of a new activity. Scenario 2 has 12 activity states under the sequencing that the new activity can only be done after work. Scenario 3 removes this sequencing, and the number of activity states increases to 16. Although a traveler may perform more than 4 activities a day, it is likely that the majority of activity states will not exceed 16 due to the implicit sequences between these activities. As depicted, the increase in Δ leads to a decrease in the average run-time. Compared with scenario 1, more activity states of scenarios 2 and 3 lead to a larger scale of SNK, and hence more run-time. This example specifically shows the applicability of the TBCG algorithm to BR-DATA problem variants in a one-day frame.

The four larger transport networks include the Eastern Massachusetts (EMA) network (74 nodes, 258 links, and 74 zones), the Berlin Friedrichshain (BF) network (224 nodes, 523 links, and 23 zones), the Anaheim network (416 nodes, 914 links, and

38 zones), and the Chicago-sketch network (933 nodes, 2950 links, and 387 zones). The network topologies are obtained from http://www.bgu.ac.il/~ bargera/tntp/. The free-flow travel times and link capacities are transformed to fit activity-based travel demand analysis. 15%, 20%, 30% of zones are randomly selected in the EMA network, about 50%, 75%, 100% of zones in the BF and Anaheim networks, and about 8%, 13%, and 26% zones in the Chicago-sketch network as home zones. In addition, the zones for offices, industrial areas, and shops, etc. are distributed proportionally in the networks. According to the run-time complexities given in Section 4.2, the TBCG algorithm affords various spatial distributions of home zones. Specifically, given i, a limited number of paths are usually generated for h, implying $O(\sum_h |P^{ih}|) = O(|H|)$. A larger number of origins means a larger $|H|$, which also results in a larger $\sum_h |P^{ih}|$. From the viewpoint of complexity theory, the number of home zones only has linear effects in terms of computation time on path searches and network loadings.

Table 6.5 provides five indicators of the TBCG algorithm, i.e., the numbers of network loadings and ATP searches, run-time per network loading and ATP search, and the total computation time. As shown, the average values of these five terms increase with the increase of the network scale and the number of home zones. Compared with the number of network loadings and ATP searches, the increases in the other three indicators are more obvious.

These four representative networks have been thus far the largest general networks in the field of DATA modeling. Combining the results under different scenarios in the Sioux Falls network, it is concluded that the TBCG algorithm shows solid space-time scalability and has large gains in computation time without losing solution quality.

Table 6.5 Application of the TBCG algorithm in larger networks

Network	# Home zones	Network loading		ATP search		Computation time (s)
		NO.	Time per NL (s)	NO.	Time per PS (s)	
EMA	11	44	2.03	7	5.64	129.05
	14	31	2.60	9	7.59	149.35
	22	31	3.25	7	7.42	153.00
BF	12	75	5.65	9	32.68	719.15
	18	83	8.22	9	48.53	1123.27
	23	80	8.85	9	69.63	1337.05
Anaheim	20	83	9.55	10	52.12	1315.63
	30	78	14.52	9	92.51	1967.98
	38	82	14.91	9	112.31	2237.13
Chicago-Sketch	30	97	10.80	10	205.01	3100.43
	50	110	24.80	11	333.31	6401.57
	100	147	31.85	11	828.64	14025.70

6.5 Conclusions

DATA in SNKs is an innovative extension of DTA in traditional transport networks. Given the flexibility in network extensions, a DATA model is capable of carrying similar levels of behavioral realism that are required in activity-based travel demand analyses, such as various decision-making mechanisms and high-order choice facets. Due to the vulnerability to combinatorial explosion, most theoretical developments in this research field had been focusing on the model capability of capturing new mobility patterns rather than applicability in large networks. With the spatial-temporal exploration and exploitation strategies, the TBCG algorithm was refined for solving the BR-DATA problems in large car-only SNKs. A formal proof was provided that the proposed TBCG algorithm solves the BR-DATA and its variant problems, which is the first presented in the literature within the dynamic context. The numerical examples demonstrated that the TBCG algorithm substantially speeds up the original CG algorithm without compromising the solutions.

7

Conclusions and Future Research

7.1 Conclusions

Traffic network equilibrium models and algorithms are important in transportation planning and operational management and have attracted much research interest in the areas of transportation research, operations research, and computer science. The consideration of multi-modal and heterogeneity of travelers enriches and complicates the traffic equilibrium problems. Higher time accuracy and larger network scale further enlarge the complexity of the problems from both the temporal and spatial dimensions. Incorporating several travel behavior mechanisms and mobility services, this thesis contributes to the modeling and algorithms of traffic network equilibrium problems.

To capture the influence of risk attitudes on path choice, a generalized mean-variance metric (GMV)-based user equilibrium (GMVUE) model is proposed. Travelers have different risk attitudes towards travel time uncertainty, for example, due to different travel purposes. The GMV metric is formulated as a generalization of expected travel time, variance, and expected early or late arrival penalties. It can capture the influence of travelers' on-time arrival probability and schedule delays on travelers' path choice simultaneously. Due to the non-additivity of GMV, GMV-based dominance definitions and conditions are established and result in a new reliable shortest path searching algorithm. Then, an effective column generation (CG) algorithm integrates the path searching algorithm with the method of successive average (MSA) and is applied to solving the GMVUE problem for real networks.

Four tolerance-based strategies are proposed for extending the CG algorithm to the boundedly rational dynamic user equilibrium (BR-DUE) model in the dynamic context. Due to factors such as travel habits, inertia, and cognition limitations, travelers have the behavior of bounded rationality (BR) in path choice. For solving the BR-DUE problem, four strategies, including tolerance-based minimum disutility path search strategy, self-adjusted convergence threshold strategy, varied temporal resolution strategy, and path search skipping strategy, are proposed and embedded in an efficient tolerance-based CG (TBCG) algorithm to accelerate the original CG algorithm. Theoretically, these strategies can accelerate the original algorithm in terms of time complexity and maintain the convergence property of the CG algorithm. As illustrated in the numerical examples, the four strategies overall accelerate the original CG algorithm and reduce the numbers of path searches and dynamic network loadings.

The supply-demand dynamics under different first-come-first-served (FCFS) mechanisms are suggested and embedded in a BR-DUE problem. Car-sharing services (CSS) are drawing growing interest in recent years. Rather than travel preferences and supply management, the supply-demand dynamics of one-way CSS are formulated and analyzed under four FCFS mechanisms. Compared with the existing no waiting FCFS (NW-FCFS) mechanism and aggregate FCFS (A-FCFS) mechanism, the disaggregate FCFS (D-FCFS) mechanism and VIP membership FCFS (VD-FCFS) mechanism are suggested to improve the utilization of shared cars by treating travelers as disaggregate units. Furthermore, a path expansion strategy congruently bridges the aggregate-disaggregate analyses and is incorporated in an adaptive CG algorithm to solve the BR-DUE problem. As demonstrated by numerical examples, that D-FCFS and VD-FCFS mechanisms are more efficient in regulating the usages of shared cars.

To cope with the evolution from the aggregate trip-based models to disaggregate ABMs, several strategies of the TBCG algorithm are refined for solving boundedly rational dynamic activity-travel assignment (BR-DATA) problems in multi-state supernetworks without activity-travel pattern (ATP) enumeration. The refined spatial-temporal exploration can allocate activity-travel flows only to potential ATPs in the intermediate assignment process and the spatial-temporal exploitation results in fewer iterations by intensifying ATP generation and network loading. In the dynamic context, the formal proof is presented to show that the refined TBCG algorithm solves the BR-DATA and its variant problems. The numerical examples demonstrate that the refined TBCG algorithm outperforms the original CG algorithm in terms of computation time for solving BR-DATA problems.

7.2 Future research

Based on the proposed traffic network equilibrium models and algorithms, several extensions are worthy of investigation in future studies.

First, the GMV metric is proposed under the assumption that path travel times follow normal distributions in the static context. However, this assumption is unlikely or even logically impossible to hold in reality. Many other travel time distributions, such as lognormal or truncated normal distributions, should be investigated for considering the asymmetry of the distributions. Moreover, the GMV metric can be embedded into the BR-DUE or BR-DATA models to capture the dynamics and BR behavior.

Second, travel demands in this thesis are assumed to be constants. Uncertain travel demand should be investigated, and thus demand and supply fluctuations should be captured simultaneously.

Third, temporal resolution variations have been mainly considered in the TBCG algorithm for exploitation. Temporal resolution variations should also be considered in the temporal exploration process.

Fourth, the relocation of SCs in this thesis is user-based. Operator-based relocations of human-driven or autonomous shared cars should also be incorporated in the equilibrium model. Similar extensions include vehicle reservations and pricing strategies from the supply side.

Fifth, other transport modes (e.g., bus, bike, and walking) should be considered in BR-DATA models to capture the multi-modal choice behavior and model the interactions between travel choices and activity chains.

Lastly, some other travel demand analysis problems, such as population synthesis, network design, and policy evaluations, need to be consistently integrated with the TBCG algorithm to increase its relevance for addressing societal challenges. These issues will be addressed in future work.

References

Arentze, T., Timmermans, H., 2004. Multistate supernetwork approach to modelling multi-activity, multimodal trip chains. International Journal of Geographical Information Science 18(7), 631–651.

Atmani, D., Lebacque, J.P., Bhouri, N., Haj-Salem, H., 2014. Dynamic assignment with user information in multimodal networks. Transportation Research Procedia 3, 895–904.

Auld, J., Hope, M., Ley, H., Sokolov, V., Xu, B., Zhang, K., 2016. POLARIS: Agent-based modeling framework development and implementation for integrated travel demand and network and operations simulations. Transportation Research Part C: Emerging Technologies 64, 101–116.

Balac, M., Ciari, F., Axhausen, K.W., 2017. Modeling the impact of parking price policy on free-floating carsharing: Case study for Zurich, Switzerland. Transportation Research Part C: Emerging Technologies 77, 207–225.

Ban, X., Liu, H.X., Ferris, M.C., Ran, B., 2008. A link-node complementarity model and solution algorithm for dynamic user equilibria with exact flow propagations. Transportation Research Part B: Methodological 42(9), 823–842.

Bates, J., Polak, J., Jones, P., Cook, A., 2001. The valuation of reliability for personal travel. Transportation Research Part E: Logistics and Transportation Review 37(2), 191–229.

Becker, H., Loder, A., Schmid, B., Axhausen, K.W., 2017. Modeling car-sharing membership as a mobility tool: A multivariate Probit approach with latent variables. Travel Behaviour and Society 8, 26–36.

Bekhor, S., Ben-Akiva, M.E., Ramming, M.S., 2002. Adaptation of logit kernel to route choice situation. Transportation Research Record (1805), 78–85.

Bekhor, S., Toledo, T., 2005. Investigating path-based solution algorithms to the stochastic user equilibrium problem. Transportation Research Part B: Methodological 39(3), 279–295.

Bell, M.G.H., 1995. Stochastic user equilibrium assignment in networks with queues. Transportation Research Part B 29(2), 125–137.

Bell, M.G.H., Shield, C.M., Busch, F., Kruse, G., 1997. A stochastic user equilibrium path flow estimator. Transportation Research Part C: Emerging Technologies 5(3–

4), 197–210.
Bellman, R., 1958. On a routing problem. Quarterly of Applied Mathematics 16(1), 87–90.
Ben-Akiva, M., Koutsopoulos, H.N., Antoniou, C., Balakrishna, R., 2010. Traffic simulation with dynamit, in: Fundamentals of Traffic Simulation. Springer, pp. 363–398.
Bhat, C.R., Guo, J.Y., Srinivasan, S., Sivakumar, A., 2004. Comprehensive econometric microsimulator for daily activity-travel patterns. Transportation Research Record 1894, 57–66.
Bhat, C.R., Koppelman, F.S., 1999. Activity-based modeling of travel demand, in: Handbook of Transportation Science. Springer, pp. 35–61.
Bhat, C.R., Lawton, T.K., 2000. Passenger travel demand forecasting. Transportation Research Board of the National Academies.
Bhat, C.R., Pendyala, R.M., 2005. Modeling intra-household interactions and group decision-making. Transportation 32(5), 443–448.
Bowman, J.L., Ben-Akiva, M.E., 2001. Activity-based disaggregate travel demand model system with activity schedules. Transportation Research Part A: Policy and Practice 35(1), 1–28.
Boyaci, B., Zografos, K.G., Geroliminis, N., 2015. An optimization framework for the development of efficient one-way car-sharing systems. European Journal of Operational Research 240(3), 718–733.
Boyce, D.E., Zhang, Y.-F., Lupa, M.R., 1994. Introducing" feedback" into four-step travel forecasting procedure versus equilibrium solution of combined model. Transportation Research Record 1443, 65.
Bressan, A., Han, K., 2013. Existence of optima and equilibria for traffic flow on networks. Networks and Heterogeneous Media 8(3), 627–648.
Browder, F.E., 1968. The fixed point theory of multi-valued mappings in topological vector spaces. Mathematische Annalen 177(4), 283–301.
Carey, M., Ge, Y.E., 2012. Comparison of methods for path flow reassignment for dynamic user equilibrium. Networks and Spatial Economics 12(3), 337–376.
Carey, M., Watling, D., 2012. Dynamic traffic assignment approximating the kinematic wave model: System optimum, marginal costs, externalities and tolls. Transportation Research Part B: Methodological 46(5), 634–648.
Chang, J., Yu, M., Shen, S., Xu, M., 2017. Location design and relocation of a mixed car-sharing fleet with a CO2 emission constraint. Service Science 9(3), 205–218.
Chapin, F.S., 1974. Human activity patterns in the city: Things people do in time and in space. Wiley-Interscience.
Chen, A., Chootinan, P., Recker, W., 2009. Norm approximation method for handling traffic count inconsistencies in path flow estimator. Transportation Research Part B: Methodological 43(8–9), 852–872.
Chen, A., Lo, H.K., Yang, H., 2001. A self-adaptive projection and contraction algorithm for the traffic assignment problem with path-specific costs. European Journal of Operational Research 135(1), 27–41.
Chen, A., Ryu, S., Chootinan, P., 2010. L∞-norm path flow estimator for handling traffic count inconsistencies: formulation and solution algorithm. Journal of Transportation Engineering 136(6), 565–575.
Chen, A., Zhou, Z., 2010. The alpha-reliable mean-excess traffic equilibrium model with stochastic travel times. Transportation Research Part B: Methodological 44(4),

493–513.
Chen, B.Y., Lam, W.H.K., Sumalee, A., Li, Q., Shao, H., Fang, Z., 2013. Finding reliable shortest paths in road networks under uncertainty. Networks and Spatial Economics 13(2), 123–148.
Chen, B.Y., Lam, W.H.K., Sumalee, A., Shao, H., 2011. An efficient solution algorithm for solving multi-class reliability-based traffic assignment problem. Mathematical and Computer Modelling 54(5), 1428–1439.
Chen, X., Liu, Z., Zhang, K., Wang, Z., 2020. A parallel computing approach to solve traffic assignment using path-based gradient projection algorithm. Transportation Research Part C 120(October 2019), 102809.
Chen, Y.J., Li, Z.C., Lam, W.H.K., 2018. Cordon toll pricing in a multi-modal linear monocentric city with stochastic auto travel time. Transportmetrica A: Transport Science 14(1–2), 22–49.
Chorus, C.G., 2012. Regret theory-based route choices and traffic equilibria. Transportmetrica 8(4), 291–305.
Chow, J.Y.J., Djavadian, S., 2015. Activity-based market equilibrium for capacitated multimodal transport systems. Transportation Research Procedia 7, 2–23.
Chow, J.Y.J., Nurumbetova, A.E., 2015. A multi-day activity-based inventory routing model with space–time–needs constraints. Transportmetrica A: Transport Science 11(3), 243–269.
Ciari, F., Schuessler, N., Axhausen, K.W., 2013. Estimation of carsharing demand using an activity-based microsimulation approach: model discussion and some results. International Journal of Sustainable Transportation 7(1), 70–84.
Clemente, M., Fanti, M.P., Iacobellis, G., Ukovich, W., 2013. A discrete-event simulation approach for the management of a car sharing service. 2013 IEEE International Conference on Systems, Man, and Cybernetics 403–408.
Çolak, S., Lima, A., González, M.C., 2016. Understanding congested travel in urban areas. Nature Communications 7.
Cormen, T.H., Leiserson, C.E., Rivest, R.L., Stein, C., 2009. Introduction to algorithms. MIT press.
Daganzo, C.F., 1995. The cell transmission model, part II: network traffic. Transportation Research Part B: Methodological 29(2), 79–93.
Daganzo, C.F., Sheffi, Y., 1977. On stochastic models of traffic assignment. Transportation Science 11(3), 289–303.
Daskin, M.S., 1985. Urban transportation networks: Equilibrium analysis with mathematical programming methods.
de Dios Ortúzar, J., Willumsen, L.G., 2011. Modelling transport. John wiley & sons.
de Jong, G.C., Bliemer, M.C.J., 2015. On including travel time reliability of road traffic in appraisal. Transportation Research Part A: Policy and Practice 73, 80–95.
Dean, B.C., 2004a. Shortest paths in FIFO time-dependent networks: Theory and algorithms. Rapport technique, Massachusetts Institute of Technology 1–13.
Dean, B.C., 2004b. Algorithms for minimum-cost paths in time-dependent networks with waiting policies. Networks 44(1), 41–46.
Di Lorenzo, D., Galligari, A., Sciandrone, M., 2014. A convergent and efficient decomposition method for the traffic assignment problem. Computational Optimization and Applications 60(1), 151–170.
Di, X., Liu, H.X., 2016. Boundedly rational route choice behavior: A review of models and methodologies. Transportation Research Part B: Methodological 85, 142–179.

Di, X., Liu, H.X., Pang, J., Je, X., 2013. Boundedly rational user equilibria (BRUE): mathematical formulation and solution sets. Transportation Research Part B: Methodological 57, 300–313.

Dial, R.B., 2006. A path-based user-equilibrium traffic assignment algorithm that obviates path storage and enumeration. Transportation Research Part B: Methodological 40(10), 917–936.

Dijkstra, E.W., 1959. A note on two problems in connexion with graphs. Numerische mathematik 1(1), 269–271.

Efthymiou, D., Antoniou, C., Waddell, P., 2013. Factors affecting the adoption of vehicle sharing systems by young drivers. Transport Policy 29, 64–73.

Eiben, A.E., Schippers, C.A., 1998. On evolutionary exploration and exploitation. Fundamenta Informaticae 35(1–4), 35–50.

Fan, D., 2014. Optimizing strategic allocation of vehicles for one-way car-sharing systems under demand uncertainty. Journal of the Transportation Research Forum 53(3), 7–20.

Ferrero, F., Perboli, G., Rosano, M., Vesco, A., 2018. Car-sharing services: An annotated review. Sustainable Cities and Society 37, 501–518.

Fisk, C., 1980. Some developments in equilibrium traffic assignment. Transportation Research Part B: Methodological 14(3), 243–255.

Florian, M., Constantin, I., Florian, D., 2009. A new look at projected gradient method for equilibrium assignment. Transportation Research Record: Journal of the Transportation Research Board 2090(1), 10–16.

Fosgerau, Mogens and Karlstrom, A., 2010. The value of reliability. Transportation Research Part B: Methodological 44(1), 38–49.

Fosgerau, M., Karlström, A., 2010. The value of reliability. Transportation Research Part B: Methodological 44(1), 38–49.

Frank, H., 1969. Shortest paths in probabilistic graphs. Operations Research 17(4), 583–599.

Fredman, M.L., Tarjan, R.E., 1987. Fibonacci heaps and their uses in improved network optimization algorithms. Journal of the ACM (JACM) 34(3), 596–615.

Friesz, T.L., 1985. Transportation network equilibrium, design and aggregation: Key developments and research opportunities. Transportation Research Part A: General 19(5–6), 413–427.

Friesz, T.L., Han, K., 2019. The mathematical foundations of dynamic user equilibrium. Transportation Research Part B 126, 309–328.

Fu, X., Lam, W.H.K., 2018. Modelling joint activity-travel pattern scheduling problem in multi-modal transit networks. Transportation 45(1), 23–49.

Fu, X., Lam, W.H.K., 2014. A network equilibrium approach for modelling activity-travel pattern scheduling problems in multi-modal transit networks with uncertainty. Transportation 41(1), 37–55.

Galligari, A., Sciandrone, M., 2017. A convergent and fast path equilibration algorithm for the traffic assignment problem. Optimization Methods and Software 6788, 1–18.

Gentile, G., 2018. New formulations of the stochastic user equilibrium with logit route choice as an extension of the deterministic model. Transportation Science Publication 52, 1531–1547.

Giorgione, G., Ciari, F., Viti, F., 2019. Availability-based dynamic pricing on a round-trip carsharing service: an explorative analysis using agent-based simulation.

Procedia Computer Science 151(2018), 248–255.
Guo, R., Yang, H., Huang, H., Li, X., 2017. Day-to-day departure time choice under bounded rationality in the bottleneck model. Transportation Research Part B-Methodological 23, 551–570.
Guo, X., Liu, H.X., 2011. Bounded rationality and irreversible network change. Transportation Research Part B: Methodological 45(10), 1606–1618.
Gupta, S., 2010. Stochastic user equilibrium. Infrastructure and transportation planning 1, 1.
Hall, R.W., 1986. The fastest path through a network with random time-dependent travel times. Transportation Science 20(3), 182–188.
Hampshire, R.C., Sinha, S., 2011. A simulation study of Peer-to-Peer carsharing. 2011 IEEE Forum on Integrated and Sustainable Transportation Systems, FISTS 2011 159–163.
Han, K., Eve, G., Friesz, T., 2019. Computing dynamic user equilibria on large-scale networks with software implementation. Networks and Spatial Economics 19, 869–902.
Han, K., Friesz, T.L., Yao, T., 2013. Existence of simultaneous route and departure choice dynamic user equilibrium. Transportation Research Part B: Methodological 53, 17–30.
Han, K., Szeto, W.Y., Friesz, T.L., 2015. Formulation, existence, and computation of boundedly rational dynamic user equilibrium with fixed or endogenous user tolerance. Transportation Research Part B: Methodological 79, 16–49.
Han, L., Ukkusuri, S., Doan, K., 2011. Complementarity formulations for the cell transmission model based dynamic user equilibrium with departure time choice, elastic demand and user heterogeneity. Transportation Research Part B: Methodological 45(10), 1749–1767.
Han, Q., Timmermans, H., 2006. Interactive learning in transportation networks with uncertainty, bounded rationality, and strategic choice behavior: Quantal response model. Transportation research record 1964, 27–34.
Han, S., 2000. Dynamic traffic assignment techniques for general road networks. University of London, London, England.
Heilig, M., Mallig, N., Schröder, O., Kagerbauer, M., Vortisch, P., 2018. Implementation of free-floating and station-based carsharing in an agent-based travel demand model. Travel Behaviour and Society 12, 151–158.
Himpe, W., Corthout, R., Tamp??re, M.J.C., 2016. An efficient iterative link transmission model. Transportation Research Part B: Methodological 92, 170–190.
Ho, C., Mulley, C., 2015. Intra-household interactions in transport research: a review. Transport Reviews 35(1), 33–55.
Hu, L., Liu, Y., 2016. Joint design of parking capacities and fleet size for one-way station-based carsharing systems with road congestion constraints. Transportation Research Part B: Methodological 93, 268–299.
Huang, H.J., Lam, W.H.K., 2002. Modeling and solving the dynamic user equilibrium route and departure time choice problem in network with queues. Transportation Research Part B: Methodological 36(3), 253–273.
Illgen, S., Höck, M., 2019. Literature review of the vehicle relocation problem in one-way car sharing networks. Transportation Research Part B 120, 193–204.
Jackson, W.B., Jucker, J. V, 1982. An empirical study of travel time variability and travel choice behavior. Transportation Science 16(4), 460–475.

Jang, W., Ran, B., Choi, K., 2005. A discrete time dynamic flow model and a formulation and solution method for dynamic route choice. Transportation Research Part B: Methodological 39(7), 593–620.

Javani, B., Babazadeh, A., 2020. Path-based dynamic user equilibrium model with applications to strategic transportation planning. Networks and Spatial Economics 20, 329–366.

Jones, P., 1977. New approaches to understanding travel behaviour: the human activity approach. University of Oxford, Transport Studies Unit.

Jones, P.M., Dix, M.C., Clarke, M.I., Heggie, I.G., 1983. Understanding travel behavior.

Kaspi, M., Raviv, T., Tzur, M., 2014. Parking reservation policies in one-way vehicle sharing systems. Transportation Research Part B: Methodological 62, 35–50.

Lam, W.H.K., Huang, H.J., 2002. A combined activity/travel choice model for congested road networks with queues. Transportation 29(1), 5–29.

Lam, W.H.K., Shao, H., Sumalee, A., 2008. Modeling impacts of adverse weather conditions on a road network with uncertainties in demand and supply. Transportation Research Part B: Methodological 42(10), 890–910.

Lam, W.H.K., Yin, Y., 2001. An activity-based time-dependent traffic assignment model. Transportation Research Part B: Methodological 35(6), 549–574.

Larsson, T., Patriksson, M., 1992. Simplicial decomposition with disaggregated representation for the traffic assignment problem. Transportation Science 26(1), 4–17.

Larsson, T., Patriksson, M., Rydergren, C., 2004. A column generation procedure for the side constrained traffic equilibrium problem. Transportation Research Part B: Methodological 38(1), 17–38.

Leventhal, T., Nemhauser, G., Trotter Jr, L., 1973. A column generation algorithm for optimal traffic assignment. Transportation Science 7(2), 168–176.

Levin, M.W., Kockelman, K.M., Boyles, S.D., Li, T., 2017. A general framework for modeling shared autonomous vehicles with dynamic network-loading and dynamic ride-sharing application. Computers, Environment and Urban Systems 64, 373–383.

Levin, M.W., Pool, M., Owens, T., Juri, N.R., Travis Waller, S., 2015. Improving the convergence of simulation-based dynamic traffic assignment methodologies. Networks and Spatial Economics 15(3), 655–676.

Li, M., Huang, H.J., 2017. A regret theory-based route choice model. Transportmetrica A: Transport Science 13(3), 250–272.

Li, Q., Liao, F., 2020. Incorporating vehicle self-relocations and traveler activity chains in a bi-level model of optimal deployment of shared autonomous vehicles. Transportation Research Part B: Methodological 140, 151–175.

Li, Q., Liao, F., Timmermans, H., Huang, H.J., Zhou, J., 2018. Incorporating free-floating car-sharing into an activity-based dynamic user equilibrium model: A demand-side model. Transportation Research Part B: Methodological 107, 102–123.

Li, Q., Liao, F., Timmermans, H.J.P., Zhou, J., 2016a. A reference-dependent user equilibrium model for activity-travel scheduling. Transportation 43(6), 1061–1077.

Li, Q., Liao, F., Timmermans, H.J.P., Zhou, J., 2016b. A user equilibrium model for combined activity–travel choice under prospect theoretical mechanisms of decision-making under uncertainty. Transportmetrica A: Transport Science 12(7),

629–649.
Li, Z., Hensher, D.A., 2013. Behavioural implications of preferences, risk attitudes and beliefs in modelling risky travel choice with travel time variability. Transportation 40(3), 505–523.
Li, Z., Hensher, D.A., Rose, J.M., 2010. Willingness to pay for travel time reliability in passenger transport: A review and some new empirical evidence. Transportation Research Part E: Logistics and Transportation Review 46(3), 384–403.
Li, Z.C., Lam, W.H.K., Sumalee, A., 2008a. Modeling impact of transit operator fleet size under various market regimes with uncertainty in network. Transportation Research Record: Journal of the Transportation Research Board 2063(1), 18–27.
Li, Z.C., Lam, W.H.K., Wong, S.C., 2011. On the allocation of new lines in a competitive transit network with uncertain demand and scale economies. Journal of Advanced Transportation 45(2011), 233–251.
Li, Z.C., Lam, W.H.K., Wong, S.C., Huang, H.J., Zhu, D.L., 2008b. Reliability evaluation for stochastic and time-dependent networks with multiple parking facilities. Networks and Spatial Economics 8(4), 355–381.
Li, Z.C., Lam, W.H.K., Wong, S.C., Sumalee, A., 2010. An activity-based approach for scheduling multimodal transit services. Transportation 37(5), 751–774.
Liao, F., 2017. Joint travel problem in space–time multi-state supernetworks. Transportation 46(4), 1319–1343.
Liao, F., 2016. Modeling duration choice in space-time multi-state supernetworks for individual activity-travel scheduling. Transportation Research Part C: Emerging Technologies 69, 16–35.
Liao, F., 2013. Synchronizing networks: the modeling of supernetworks for activity-travel behavior. Eindhoven University of Technology.
Liao, F., Arentze, T., Molin, E., Bothe, W., Timmermans, H., 2017. Effects of land-use transport scenarios on travel patterns: a multi-state supernetwork application. Transportation 44(1), 1–25.
Liao, F., Arentze, T., Timmermans, H., 2013. Incorporating space-time constraints and activity-travel time profiles in a multi-state supernetwork approach to individual activity-travel scheduling. Transportation Research Part B: Methodological 55, 41–58.
Liao, F., Arentze, T., Timmermans, H., 2011. Constructing personalized transportation networks in multi-state supernetworks: a heuristic approach. International Journal of Geographical Information Science 25(11), 1885–1903.
Liao, F., Arentze, T., Timmermans, H., 2010. Supernetwork approach for multimodal and multiactivity travel planning. Transportation Research Record: Journal of the Transportation Research Board 2175(1), 38–46.
Liao, F., Rasouli, S., Timmermans, H., 2014. Incorporating activity-travel time uncertainty and stochastic space–time prisms in multistate supernetworks for activity-travel scheduling. International Journal of Geographical Information Science 28(5), 928–945.
Lighthill, M.J., Whitham, G.B., 1955. On kinematic waves I. Flood movement in long rivers. Proceedings of the Royal Society of London. Series A. Mathematical and Physical Sciences 229(1178), 281–316.
Lin, D., Eluru, N., Waller, S., Bhat, C., 2008. Integration of activity-based modeling and dynamic traffic assignment. Transportation Research Record: Journal of the Transportation Research Board 2076, 52–61.

Liu, P., Liao, F., Huang, H.J., Timmermans, H., 2016. Dynamic activity-travel assignment in multi-state supernetworks under transport and location capacity constraints. Transportmetrica A: Transport Science 12(7), 572–590.

Liu, P., Liao, F., Huang, H.J., Timmermans, H., 2015. Dynamic activity-travel assignment in multi-state supernetworks. Transportation Research Part B: Methodological 81, 656–671.

Liu, P., Liao, F., Tian, Q., Huang, H.J., Timmermans, H., 2020. Day-to-day needs-based activity-travel dynamics and equilibria in multi-state supernetworks. Transportation Research Part B: Methodological 132, 208–227.

Lo, H.K., Chen, A., 2000. Traffic equilibrium problem with route-specific costs: formulation and algorithms. Transportation Research Part B: Methodological 34, 493–513.

Lo, H.K., Luo, X.W., Siu, B.W.Y., 2006. Degradable transport network: Travel time budget of travelers with heterogeneous risk aversion. Transportation Research Part B: Methodological 40(9), 792–806.

Lo, H.K., Szeto, W.Y., 2002. A cell-based variational inequality formulation of the dynamic user optimal assignment problem. Transportation Research Part B: Methodological 36(5), 421–443.

Long, J., Gao, Z., Szeto, W.Y., 2011. Discretised link travel time models based on cumulative flows: Formulations and properties. Transportation Research Part B: Methodological 45(1), 232–254.

Long, J., Huang, H.J., Gao, Z., 2013a. Discretised route travel time models based on cumulative flows. Journal of Advanced Transportation 47(1), 105–125.

Long, J., Huang, H.J., Gao, Z., Szeto, W.Y., 2013b. An intersection-movement-based dynamic user optimal route choice problem. Operations Research 61(5), 1134–1147.

Long, J., Szeto, W.Y., Gao, Z., Huang, H.J., Shi, Q., 2016. The nonlinear equation system approach to solving dynamic user optimal simultaneous route and departure time choice problems. Transportation Research Part B: Methodological 83, 179–206.

Lu, C.C., Liu, J., Qu, Y., Peeta, S., Rouphail, N.M., Zhou, X., 2016. Eco-system optimal time-dependent flow assignment in a congested network. Transportation Research Part B: Methodological 94, 217–239.

Lu, C.C., Mahmassani, H.S., Zhou, X., 2009. Equivalent gap function-based reformulation and solution algorithm for the dynamic user equilibrium problem. Transportation Research Part B: Methodological 43(3), 345–364.

Lu, C.C., Zhou, X., Zhang, K., 2013. Dynamic origin-destination demand flow estimation under congested traffic conditions. Transportation Research Part C: Emerging Technologies 34, 16–37.

Mahmassani, H.S., Chang, G.-L., 1987. On boundedly rational user equilibrium in transportation systems. Transportation science 21(2), 89–99.

Mahut, M., Florian, M., 2010. Traffic simulation with dynameq, in: Fundamentals of Traffic Simulation. Springer, pp. 323–361.

McFadden, D., 1978. Modeling the choice of residential location. Transportation Research Record (673).

McNally, M.G., 2007. The four-step model. Emerald Group Publishing Limited.

Mcnally, M.G., Rindt, C., Org, E., 2000. The activity-based approach. Handbook of transport modelling 1, 35–52.

Miller-Hooks, E., Mahmassani, H., 2003. Path comparisons for a priori and time-adaptive decisions in stochastic, time-varying networks. European Journal of Operational Research 146(1), 67–82.

Mounce, R., 2007. Existence of equilibrium in a continuous dynamic queueing model for traffic networks, in: 4th IMA International Conference on Mathematics in TransportInstitute of Mathematics and Its Applications.

Mounce, R., Carey, M., 2015. On the convergence of the method of successive averages for calculating equilibrium in traffic networks. Transportation Science 49(3), 535–542.

Mounce, R., Carey, M., 2011. Route swapping in dynamic traffic networks. Transportation Research Part B: Methodological 45(1), 102–111.

Nagurney, A., Zhang, D., 1997. Projected dynamical systems in the formulation, stability analysis, and computation of fixed-demand traffic network equilibria. Transportation Science 31(2), 147–158.

Najmi, A., Rashidi, T.H., Vaughan, J., Miller, E.J., 2019. Calibration of large-scale transport planning models: a structured approach, Transportation. Springer US.

Nie, X., Zhang, H.M., 2005. Delay-function-based link models: Their properties and computational issues. Transportation Research Part B: Methodological 39(8), 729–751.

Nie, Y. (Marco), Wu, X., 2009. Shortest path problem considering on-time arrival probability. Transportation Research Part B: Methodological 43(6), 597–613.

Nikolova, E., Stier-Moses, N.E., 2014. A mean-risk model for the traffic assignment problem with stochastic travel times. Operations Research 62(2), 366–382.

Noland, R.B., Small, K.A., 1995. Travel-time uncertainty, departure time choice, and the cost of the morning commute. Institute of Transportation Studies, University of California, Irvine.

Nourinejad, M., Roorda, M.J., 2014. A dynamic carsharing decision support system. Transportation Research Part E: Logistics and Transportation Review 66, 36–50.

Ouyang, L., Lam, W.H.K., Li, Z.C., Huang, D., 2011. Network user equilibrium model for scheduling daily activity travel patterns in congested networks. Transportation Research Record: Journal of the Transportation Research Board 2254, 131–139.

Panicucci, B., Pappalardo, M., Passacantando, M., 2007. A path-based double projection method for solving the asymmetric traffic network equilibrium problem. Optimization Letters 1(2), 171–185.

Patriksson, M., 2015. The traffic assignment problem: models and methods. Courier Dover Publications.

Paul, D., Kjær, T., Giacomo, C., Anker, O., 2018. Stochastic user equilibrium with a bounded choice model. Transportation Research Part B 114, 254–280.

Prato, C.G., 2009. Route choice modeling: past, present and future research directions. Journal of choice modelling 2(1), 65–100.

Qureshi, A.G., Taniguchi, E., Yamada, T., 2009. An exact solution approach for vehicle routing and scheduling problems with soft time windows. Transportation Research Part E: Logistics and Transportation Review 45(6), 960–977.

Ramadurai, G., Ukkusuri, S., 2011. B-dynamic: an efficient algorithm for dynamic user equilibrium assignment in activity-travel networks. Computer-Aided Civil and Infrastructure Engineering 26(4), 254–269.

Ramadurai, G., Ukkusuri, S., 2010. Dynamic user equilibrium model for combined activity-travel choices using activity-travel supernetwork representation. Networks

and Spatial Economics 10(2), 273–292.
Rasmussen, T.K., Watling, D.P., Prato, C.G., Nielsen, O.A., 2015. Stochastic user equilibrium with equilibrated choice sets: Part II - Solving the restricted SUE for the logit family. Transportation Research Part B: Methodological 77, 146–165.
Rasouli, S., Timmermans, H., 2014. Activity-based models of travel demand: Promises, progress and prospects. International Journal of Urban Sciences 18(1), 31–60.
Reeves, C.R., 1993. Improving the efficiency of tabu search for machine sequencing problems. Journal of the operational research society 44(4), 375–382.
Rotaris, L., Danielis, R., Maltese, I., 2019. Carsharing use by college students: The case of Milan and Rome. Transportation Research Part A: Policy and Practice 120, 239–251.
Rubio-Ardanaz, J.M., Wu, J.H., Florian, M., 2003. Two improved numerical algorithms for the continuous dynamic network loading problem. Transportation Research Part B: Methodological 37(2), 171–190.
Ryu, S., Chen, A., Choi, K., 2016. Solving the stochastic multi-class traffic assignment problem with asymmetric interactions, route overlapping, and vehicle restrictions. Journal of Advanced Transportation 50(2), 512–525.
Ryu, S., Chen, A., Choi, K., 2014. A modified gradient projection algorithm for solving the elastic demand traffic assignment problem. Computers & Operations Research 47, 61–71.
Seshadri, R., Srinivasan, K.K., 2017. Robust traffic assignment model: Formulation, solution algorithms and empirical application. Journal of Intelligent Transportation Systems 2450, 1–1.
Shao, H., Lam, W.H.K., Sumalee, A., Chen, A., 2013. Journey time estimator for assessment of road network performance under demand uncertainty. Transportation Research Part C: Emerging Technologies 35, 244–262.
Shao, H., Lam, W.H.K., Tam, M.L., 2006. A reliability-based stochastic traffic assignment model for network with multiple user classes under uncertainty in demand. Networks and Spatial Economics 6(3), 173–204.
Sheffi, Y., 1985. Urban transportation networks, Prentice-Hall, Englewood Cliffs, NJ.
Simon, H.A., 1957. Models of man: social and rational. Mathematical Essays on Rational Human Behavior in a Social Setting.
Simon, H.A., 1955. A behavioural model of rational choice. The Quarterly Journal of Economics 69(1), 99–118.
Sivak, M., 2002. How common sense fails us on the road: Contribution of bounded rationality to the annual worldwide toll of one million traffic fatalities. Transportation Research Part F: Traffic Psychology and Behaviour 5(4), 259–269.
Small, K.A., 1982. The scheduling of consumer activities: work trips. The American Economic Review 72(3), 467–479.
Smilowitz, K.R., Atamtürk, A., Daganzo, C.F., 2003. Deferred item and vehicle routing within integrated networks. Transportation Research Part E: Logistics and Transportation Review 39(4), 305–323.
Smith, M.J., 1984. The stability of a dynamic model of traffic assignment-an application of a method of lyapunov. Transportation Science 18(3), 245.
Smith, M.J., Wisten, M.B., 1995. A continuous day-to-day traffic assignment model and the existence of a continuous dynamic user equilibrium. Annals of Operations Research 60, 59–79.
Srinivasan, K.K., Prakash, A.A., Seshadri, R., 2014. Finding most reliable paths on

networks with correlated and shifted log-normal travel times. Transportation Research Part B: Methodological 66, 110–128.

Ströhle, P., Flath, C.M., Gärttner, J., 2019. Leveraging customer flexibility for car-sharing fleet optimization. Transportation Science 53(1), 42–61.

Sun, C., Cheng, L., Ma, J., 2018. Travel time reliability with boundedly rational travelers. Transportmetrica A: Transport Science 14(3), 210–229.

Sun, Z., Arentze, T., Timmermans, H.J.P., 2005. Modeling the impact of travel information on activity-travel rescheduling decisions under conditions of travel time uncertainty. Transportation Research Record (1926), 79–87.

Sweet, M.N., Chen, M., 2011. Does regional travel time unreliability influence mode choice? Transportation 38(4), 625–642.

Szeto, W., Lo, H.K., 2006. Dynamic traffic assignment: properties and extensions. Transportmetrica 2(1), 31–52.

Szeto, W.Y., Jiang, Y., Sumalee, A., 2011. A cell-based model for multi-class doubly stochastic dynamic traffic assignment. Computer-Aided Civil and Infrastructure Engineering 26(8), 595–611.

Szeto, W.Y., Lo, H.K., 2004. A cell-based simultaneous route and departure time choice model with elastic demand. Transportation Research Part B: Methodological 38(7), 593–612.

Tan, Z., Yang, H., Guo, R., 2014. Pareto efficiency of reliability-based traffic equilibria and risk-taking behavior of travelers. Transportation Research Part B: Methodological 66, 16–31.

Tilahun, N.Y., Levinson, D.M., 2010. A moment of time: Reliability in route choice using stated preference. Journal of Intelligent Transportation Systems: Technology, Planning, and Operations 14(3), 179–187.

Tong, C.O., Wong, S.C., 2000. A predictive dynamic traffic assignment model in congested capacity-constrained road networks. Transportation Research Part B: Methodological 34(8), 625–644.

U.S. Traffic assignment manual, 1964. U.S. Department of Commerce, Washington, D.C.

Ukkusuri, S. V., Han, L., Doan, K., 2012. Dynamic user equilibrium with a path based cell transmission model for general traffic networks. Transportation Research Part B: Methodological 46(10), 1657–1684.

Vickrey, W.S., 1969. Congestion theory and transport investment. The American Economic Review 59(2), 251–260.

Wang, J.Y.T., Ehrgott, M., Chen, A., 2014. A bi-objective user equilibrium model of travel time reliability in a road network. Transportation Research Part B: Methodological 66, 4–15.

Wardrop, J.G., 1952. Some theoretical aspects of road traffic research. Proceedings of the Institute of Civil Engineers 1, 325–378.

Watling, D., 2006. User equilibrium traffic network assignment with stochastic travel times and late arrival penalty. European Journal of Operational Research 175(3), 1539–1556.

Weikl, S., Bogenberger, K., 2015. A practice-ready relocation model for free-floating carsharing systems with electric vehicles - Mesoscopic approach and field trial results. Transportation Research Part C: Emerging Technologies 57, 206–223.

Weikl, S., Bogenberger, K., 2013. Relocation strategies and algorithms for free-floating car sharing systems. IEEE Intelligent Transportation Systems Magazine 5(4), 100–

111.
Wen, C.H., Koppelman, F.S., 2001. The generalized nested logit model. Transportation Research Part B: Methodological 35(7), 627–641.
Woodard, D., Nogin, G., Koch, P., Racz, D., Goldszmidt, M., Horvitz, E., 2017. Predicting travel time reliability using mobile phone GPS data. Transportation Research Part C: Emerging Technologies 75, 30–44.
Wu, J., Sun, H., Wang, D.Z.W., Zhong, M., Han, L., Gao, Z., 2013. Bounded-rationality based day-to-day evolution model for travel behavior analysis of urban railway network. Transportation Research Part C: Emerging Technologies 31, 73–82.
Xiong, C., Zhou, X., Zhang, L., 2018. AgBM-DTALite: An integrated modelling system of agent-based travel behaviour and transportation network dynamics. Travel Behaviour and Society 12, 141–150.
Xu, M., Meng, Q., 2019. Fleet sizing for one-way electric carsharing services considering dynamic vehicle relocation and nonlinear charging profile. Transportation Research Part B: Methodological 128, 23–49.
Xu, M., Meng, Q., Liu, Z., 2018. Electric vehicle fleet size and trip pricing for one-way carsharing services considering vehicle relocation and personnel assignment. Transportation Research Part B: Methodological 111, 60–82.
Yang, D., 2018. Integrating activity-based travel demand and dynamic traffic assignment model: a behaivioral user equilibrium approach. University of Maryland, College Park, Maryland, U.S.
Yang, H., Bell, M.G.H., 1998. Models and algorithms for road network design: A review and some new developments. Transport Reviews 18(3), 257–278.
Yasmin, F., Morency, C., Roorda, M.J., 2017. Macro-, meso-, and micro-level validation of an activity-based travel demand model. Transportmetrica A: Transport Science 13(3), 222–249.
Yin, Y., Lam, W.H.K., Ieda, H., 2004. New technology and the modeling of risk-taking behavior in congested road networks. Transportation Research Part C: Emerging Technologies 12(3–4), 171–192.
Yperman, I., 2007. The Link Transmission Model for dynamic network loading, Ph.D. dissertation, Katholieke Universiteit Leuven, Leuven, Belgium.
Zhan, F.B., Noon, C.E., 1998. Shortest path algorithms: An evaluation using real road networks. Transportation Science 32(1), 65–73.
Zhang, K., 2009. Dynamic stochastic user equilibrium: Models and algorithms for multidimensional network choices. Northwestern University.
Zhang, K., Mahmassani, H.S., Lu, C.C., 2013. Dynamic pricing, heterogeneous users and perception error: Probit-based bi-criterion dynamic stochastic user equilibrium assignment. Transportation Research Part C: Emerging Technologies 27, 189–204.
Zhang, L., 2006. Search, information, learning, and knowledge in travel decision-making. Citeseer.
Zhou, F., Zheng, Z., Whitehead, J., Perrons, R.K., Washington, S., Page, L., 2020a. Examining the impact of car-sharing on private vehicle ownership. Transportation Research Part A: Policy and Practice 138, 322–341.
Zhou, F., Zheng, Z., Whitehead, J., Washington, S., Perrons, R.K., Page, L., 2020b. Preference heterogeneity in mode choice for car-sharing and shared automated vehicles. Transportation Research Part A: Policy and Practice 132, 633–650.
Zhou, X., Mahmassani, H.S., Zhang, K., 2008. Dynamic micro-assignment modeling approach for integrated multimodal urban corridor management. Transportation

Research Part C: Emerging Technologies 16(2), 167–186.
Zhou, X., Taylor, J., 2014. DTAlite: A queue-based mesoscopic traffic simulator for fast model evaluation and calibration. Cogent Engineering 1(1), 1–19.
Zhou, Z., Chen, A., Bekhor, S., 2012. C-logit stochastic user equilibrium model: formulations and solution algorithm. Transportmetrica 8(1), 17–41.
Zhu, D., Marcotte, P., 2000. On the existence of solutions to the dynamic user equilibrium problem. Transportation Science 34(4), 402–414.

Appendix

Appendix 1.A Notations

$SNK(N, A)$	multi-state supernetwork composed of node set N and link set A
$SNK^T(N, A, K)$	space-time supernetwork composed of N, A, and time interval set K
$G(N, A)$	the traffic network composed of N and A
$A_{TS}, A_{PC}, A_{SC}, A_{AT}$	link sets of transition, PC, SC, and transaction
l	link of SNK, $l \in A$
a, b, c	three nodes of SNK, $a, b, c \in N$
RS	set of OD pairs
rs	an OD pair, $rs \in RS$
Δ	minimum length of a time interval
K	set of time intervals corresponding to Δ
K_p	set of time intervals of p
k, τ, t, w	time intervals, $k, \tau, t, w \in K$
k^{rs*}	preferred arrival time of rs
P^{rs}	set of paths of rs
$\bar{P}^{rs}$	complement set of P^{rs}
$p, \bar{p}, q$	three paths
p_j	an expanded path of p
Q^{rs}	the demand of rs
$\vartheta_j, j = 1,2,3$	scale parameters, $\vartheta_1, \vartheta_2 \in (0, 1)$ $\vartheta_3 \geq 1$,
ϵ^{rs}	relative indifference threshold of travelers of rs toward path switch
ε	convergence threshold

$\varepsilon_{\max}^{rs}$, $\varepsilon_{\min}^{rs}$	maximum and minimum relative convergence thresholds of rs
Ψ	time-dependent path set, $\Psi = \{(p,k)\|p \in P, k \in K\}$
Φ	time-dependent path set, $\Phi = \{(p,k)\| \in P, k \in K_p\}$
Φ^{rs}	potential time-dependent path set of rs, $\Phi^{rs} = \{(p,k)\|p \in P^{rs}, k \in K_p\}$
$f_p^{rs}(k)$	flow that enters path p of rs during k
$\boldsymbol{f}$	vector of $f_p^{rs}(k)$
$u_l(k)$	inflow of link l during k
$v_l(k)$	outflow of link l during k
e_l	the capacity of link l
t_l^0	free flow travel time of link l
$t_l(k,\boldsymbol{f})$	travel time of link l for travelers entering at interval k
$t_p^{rs}(k,\boldsymbol{f})$	travel time incurred by $f_p^{rs}(k)$
$c_l(k)$	disutility incurred by travelers arriving at the entry node of link l during k
$c_p^{rs}(k,\boldsymbol{f})$	disutility incurred by $f_p^{rs}(k)$
$c_{\min}^{rs}(\boldsymbol{f})$	minimum disutility of rs
$c^{rs}(k,\mathbf{0})$	minimum disutility of paths with zero flow of rs at k
$\boldsymbol{c}(\boldsymbol{f})$	vector of $c_p^{rs}(k,\boldsymbol{f})$
$t_l^{\mathrm{W}}(\tau)$	waiting time of link l during τ
$t_l^{\mathrm{D}}(\tau)$	duration (or travel time) of link l during τ
$w_a(k)$	potential waiting time at node a during time k
$w_{a,\min}(k)$	minimum potential value of $w_a(k)$
$w_{a,\max}(k)$	maximum potential value of $w_a(k)$
$u_a(k)$	arrival flow for ending the SC trip at a during k
$v_a(k)$	arrival flow for starting the SC trip at a during k
$S_a(k)$, $D_a(k)$	supply and demand of SC at node a at the end of k
$h_a(k)$, $g_a(k)$	stock and shortage of SC at a the end of k
$z_a(k,w)$	travel flow arriving at a during k and served after waiting time w
$\lambda_a(k,w)$	proportion of served travelers arriving at a during k and waiting for w
$\varpi_{p_j}(k)$	proportion of travelers on expanded path p_j
$\delta_{plk}^{rs}(\tau)$	0-1 variable, $\delta_{plk}^{rs}(\tau)$=1 if travelers of rs depart during k via p and arrive at the entry node of l during τ
n	iteration index, n is attached to entities at iteration n
$\|SET\|$	the number of elements in an arbitrary set SET

Appendix 1.B Abbreviations

ABM	activity-based model	ATP	activity-travel pattern
BPR	Bureau of Public Road	BR	bounded rationality
BR-DUE	boundedly rational DUE	BR-MDA	boundedly rational MDA
BR-DATA	boundedly rational DATA	CG	column generation
CDF	cumulative distribution function	CTM	cell transmission model
CSS	car-sharing services	DTA	dynamic traffic assignment
DATA	dynamic activity-travel assignment	DUE	dynamic UE
DSUE	dynamic SUE	FCFS	first-come-first-served
FIFO	first-in-first-out	GMV	generalized mean-variance
LTM	link transmission model	MDA	minimum disutility ATP
METT	mean-excess travel time	MLTT	mean-less travel time
MSA	method of successive average	MTT	mean travel time
M-GMV	mean-GMV	M-V	mean-variance
OD	origin and destination	PTPS	potential time-dependent path set
PAT	preferred arrival time	RUE	reliability-based UE
SD	standard deviation	SNK	multi-state supernetwork
STA	static traffic assignment	SUE	stochastic UE
TBCG	tolerance-based CG	TTB	travel time budget
TTR	travel time reliability	UE	user equilibrium
VI	variational inequality	VIP	very important person

Appendix 2.A Existence and non-uniqueness of the solutions.

Existence: According to Theorem 5.6 proposed by Han et al. (2015), the sufficiency for the existence of BR-DUE includes two conditions, which are both satisfied in this chapter.

First, $\tilde{c}_p^{rs}(k, \boldsymbol{f})$ is continuous with path flows.

This condition has been shown to be true for the VI problems in the continuous time domain, of which the dynamic network loading can be performed based on the Vickrey model (Han et al., 2013) and LWR-Lax model (Bressan and Han, 2013), etc. Regarding the finite-dimensional VI problem, the continuity of $\tilde{c}_p^{rs}(k, \boldsymbol{f})$ depends on the continuity of $c_p^{rs}(k, \boldsymbol{f})$, which has also been shown by Long et al. (2013a) through linear interpolation of link travel times.

Second, for each $rs \in RS$, let path travel disutility $c_p^{rs}(k, \boldsymbol{f})$ be decomposed into two additive components, i.e. $c_{rs}^1(\cdot)$ and $c_{rs}^2(\cdot)$; moreover, the former one is monotonically increasing and the latter is Lipschitz continuous with constant L_{rs}.

This condition holds for the path disutility formulated in Eq. (2.5) with $\eta_3 > \eta_1 > \eta_2 > 0$ by supposing $c_{rs}^2(k) = -\eta_1 k$ and

$$\begin{aligned} c_{rs}^1\left(k + t_p^{rs}(k, \boldsymbol{f})\right) &= \eta_1\left(k + t_p^{rs}(k, \boldsymbol{f})\right) \\ &+ \begin{cases} \eta_2\left[k^{rs*} - \kappa^{rs} - k - t_p^{rs}(k, \boldsymbol{f})\right] & \text{if } k + t_p^{rs}(k, \boldsymbol{f}) < k^{rs*} - \kappa^{rs} \\ \eta_3\left[k + t_p^{rs}(k, \boldsymbol{f}) - k^{rs*} - \kappa^{rs}\right] & \text{if } k + t_p^{rs}(k, \boldsymbol{f}) > k^{rs*} + \kappa^{rs} \\ 0 & \text{otherwise} \end{cases} \end{aligned} \tag{2.A.1}$$

Non-uniqueness: As proved by Szeto and Lo (2006) and Han et al. (2015), the solutions to the BR-DUE problem are non-unique. Specifically, when the threshold of the acceptable relative difference ε^{rs} approaches infinity, it is obvious that any path flow vector in Ω satisfies Eq. (2.16). On the contrary, the BR-DUE problem is degenerated to the general DUE when ε^{rs} equals zero. The uniqueness of DUE solutions requires the path disutilities to be strictly monotone with path flow, which do not hold in general (Huang and Lam, 2002; Mounce and Carey, 2015).

Based on the above analyses, the existence and non-uniqueness of the solutions to the discrete time $\mathrm{VI}(\boldsymbol{f}, \Omega)$ problem are confirmed.

Appendix 3.A Proof of Remark 3.1.

Proof. While the correctness of Remark 3.1 (i-ii) is obvious, Remark 3.1 (iii) and (iv) need some manipulations to prove. Recalling the definition of GMV, it is obtained that

$$c_p^{rs} = \mu_p + \frac{1}{1-\alpha} E\left(T_p - \xi_p(\alpha)\right)^+ + \gamma(\alpha)\sigma_p \tag{3.A.1}$$

Based on the definition of TTB in Eq. (3.7), Eq. (3.A.1) is rewritten as

$$c_p^{rs} = \xi_p(\alpha) + \frac{1}{1-\alpha} E\left(T_p - \xi_p(\alpha)\right)^+ \tag{3.A.2}$$

The second term of the right-hand side of Eq. (3.A.2) can be derived as follows

$$\begin{aligned}\frac{1}{1-\alpha}E\big(T_p-\xi_p(\alpha)\big)^+ &= \frac{1}{1-\alpha}\int_{\xi_p(\alpha)}^{b_p}\big(T_p-\xi_p(\alpha)\big)*y\big(T_p\big)dT_p \\ &= \int_{\xi_p(\alpha)}^{b_p}\big(T_p-\xi_p(\alpha)\big)*\frac{y\big(T_p\big)}{Pr\ (T_p\geq\xi_p(\alpha))}dT_p \\ &= E\big(T_p-\xi_p(\alpha)|T_p\geq\xi_p(\alpha)\big)\end{aligned} \tag{3.A.3}$$

where $y(T_p)$ denotes the probability density function of the T_p. Substituting Eq. (3.A.3) into Eq. (3.A.2), it is obtained that

$$c_p^{rs}=\xi_p(\alpha)+E\big(T_p-\xi_p(\alpha)|T_p\geq\xi_p(\alpha)\big)=E\big(T_p|T_p\geq\xi_p(\alpha)\big) \tag{3.A.4}$$

Eq. (3.A.4) is consistent with the definition of METT proposed by Chen and Zhou (2010). The proof of Remark 3.1 (iv) is similar and thus omitted here. □

Appendix 3.B Proof of Proposition 3.1.

Proof of continuity. Path travel time T_p is a random variable, so is the late schedule delay $(T_p-\xi_p(\alpha))^+$ denoted by $\tilde{T}_p$ given by

$$\tilde{T}_p=(T_p-\xi_p(\alpha))^+=\begin{cases}0, & T_p<\xi_p(\alpha)\\ T_p-\xi_p(\alpha), & T_p\geq\xi_p(\alpha)\end{cases} \tag{3.B.1}$$

As T_p follows a normal distribution, the CDF of $\tilde{T}_p$ is given by

$$P\big(\tilde{T}_p\leq x\big)=\begin{cases}0, & x<0\\ Y\big(x+\xi_p\big), & x\geq 0\end{cases} \tag{3.B.2}$$

where $\xi_p(\alpha)$ is abbreviated as ξ_p for convenience. The expectation of $\tilde{T}_p$ is calculated by

$$E(\tilde{T}_p)=0*P\big(\tilde{T}_p=0\big)+\int_{\xi_p}^{+\infty}\big(T_p-\xi_p\big)*y\big(T_p\big)dT_p=\int_{\xi_p}^{+\infty}\big(T_p-\xi_p\big)*y\big(T_p\big)dT_p \tag{3.B.3}$$

where $y(T_p)$ denotes the probability density function of T_p. Similarly, the expectation of early schedule delay is expressed below

$$E(T_p-\xi_p(\alpha))^-=\int_{-\infty}^{\xi_p}\big(\xi_p-T_p\big)*y\big(T_p\big)dT_p \tag{3.B.4}$$

According to Eq. (3.12),

$$
\begin{aligned}
&c_p^{rs} \\
&= \omega_1\mu_p + \omega_2(\alpha)\int_{-\infty}^{\xi_p}(\xi_p\text{-}T_p)\cdot y(T_p)dT_p + \omega_3(\alpha)\int_{\xi_p}^{+\infty}(T_p\text{-}\xi_p)\cdot y(T_p)dT_p \\
&+ \omega_1\gamma(\alpha)\sigma_p \\
&= \omega_1\xi_p + \omega_2(\alpha)\alpha\xi_p - \omega_2(\alpha)\int_{-\infty}^{\xi_p}T_p\cdot y(T_p)dT_p \\
&+ \omega_3(\alpha)\int_{\xi_p}^{+\infty}T_p\cdot y(T_p)dT_p - \omega_3(\alpha)(1\text{-}\alpha)\xi_p
\end{aligned}
\tag{3.B.5}
$$

The second line of Eq. (3.B.5) starts with the definition of TTB as shown in Eq. (3.7). Through integral manipulations, the fourth term on the right-hand side of Eq. (3.B.5) is rewritten as

$$
\omega_3(\alpha)\int_{\xi_p}^{+\infty}T_p * y(T_p)dT_p = \omega_3(\alpha)\mu_p(1-\alpha) + \frac{\omega_3(\alpha)\sigma_p}{\sqrt{2\pi}}e^{-\left(\frac{\xi_p-\mu_p}{\sqrt{2}\sigma_p}\right)^2} \tag{3.B.6}
$$

Similarly, the third term on the right-hand side of Eq. (3.B.5) is represented as

$$
-\omega_2(\alpha)\int_{-\infty}^{\xi_p}T_p * y(T_p)dT_p = -\omega_2(\alpha)\mu_p\alpha + \frac{\omega_2(\alpha)\sigma_p}{\sqrt{2\pi}}e^{-\left(\frac{\xi_p-\mu_p}{\sqrt{2}\sigma_p}\right)^2} \tag{3.B.7}
$$

By combining Eqs. (3.B.5)-(3.B.7), c_p^{rs} is reduced to

$$
\begin{aligned}
c_p^{rs} = \omega_1\xi_p + \omega_2(\alpha)\alpha(\xi_p-\mu_p) + \omega_3(\alpha)(1-\alpha)(\mu_p \\
-\xi_p) + \frac{(\omega_2(\alpha)+\omega_3(\alpha))\sigma_p}{\sqrt{2\pi}}e^{-\left(\frac{\xi_p-\mu_p}{\sqrt{2}\sigma_p}\right)^2}
\end{aligned}
\tag{3.B.8}
$$

Substituting Eq. (3.7) into Eq. (3.B.8), it is obtained that

$$
\begin{aligned}
c_p^{rs} = \omega_1[\mu_p + \gamma(\alpha)\sigma_p] + \omega_2(\alpha)\alpha\gamma(\alpha)\sigma_p - \omega_3(\alpha)(1-\alpha)\gamma(\alpha)\sigma_p \\
+ \frac{(\omega_2(\alpha)+\omega_3(\alpha))\sigma_p}{\sqrt{2\pi}}e^{-\left(\frac{\gamma(\alpha)}{\sqrt{2}}\right)^2}
\end{aligned}
\tag{3.B.9}
$$

Recalling the definition of $\gamma(\alpha)$ shown in Eq. (3.9), $\gamma(\alpha)$ is continuous with α; thus, the GMV c_p^{rs} calculated by Eq. (3.B.9) is also continuous with α. □

Proof of monotonicity. Based on the relation between $\gamma(\alpha)$ and α shown in Eq. (3.9), α is represented as

$$\alpha = X\big(\gamma(\alpha)\big) = \int_{-\infty}^{\gamma(\alpha)} \frac{1}{\sqrt{2\pi}} e^{\left(-\frac{x^2}{2}\right)} dx \tag{3.B.10}$$

For TTB, the first order of derivatives of u_p^{rs} with respect to $\gamma(\alpha)$ are

$$(u_p^{rs})' = \sigma_p \tag{3.B.11}$$

Recalling Remark 3.1 (iii) and (iv) in Section 3.1, coefficients $\omega_2(\alpha)$ and $\omega_3(\alpha)$ of GMV are α-related. The mathematical form of the first order derivative of METT and MLTT with respect to $\gamma(\alpha)$ can be derived from the following equations respectively.

$$\big(u_p^{rs}\big)' = \frac{\sigma_p \cdot X'(\gamma(\alpha))}{\sqrt{2\pi}[1 - X(\gamma(\alpha))]^2} \int_{\gamma(\alpha)}^{+\infty} (x - \gamma(\alpha)) e^{-\frac{x^2}{2}} dx \tag{3.B.12}$$

$$\big(u_p^{rs}\big)' = \frac{\sigma_p \cdot [\gamma(\alpha) \cdot X\big(\gamma(\alpha)\big) + X'\big(\gamma(\alpha)\big)]}{\sqrt{2\pi} \cdot X^2(\gamma(\alpha))} e^{-\frac{\gamma(\alpha)^2}{2}} \tag{3.B.13}$$

It is obvious that the values of Eqs. (3.B.11)-(3.B.13) are positive. Therefore, TTB, METT, and MLTT are monotonically increasing with $\gamma(\alpha)$. As $\gamma(\alpha)$ is monotonically increasing with α, it is concluded that TTB, METT, and MLTT are monotonically increasing with α.□

Appendix 3.C Proof of Proposition 3.2 and Proposition 3.3.

Proof of Proposition 3.2. Let $p_1^{rj} = p_1^{ri} \oplus p^{ij}$ and $p_2^{rj} = p_2^{ri} \oplus p^{ij}$ be two paths from node r to j with the same sub-path p^{ij}, the deviation between c_1^{rj} and c_2^{rj} is

$$\mathcal{f}^{ri}(p^{ij}) = c_1^{rj} - c_2^{rj} = \omega_1\big(\mu_1^{ri} - \mu_2^{ri}\big) + z\left(\sqrt{\big(\sigma_1^{ri}\big)^2 + (\sigma^{ij})^2} - \sqrt{\big(\sigma_2^{ri}\big)^2 + (\sigma^{ij})^2}\right) \tag{3.C.1}$$

The derivative of the above equation with respect to $(\sigma^{ij})^2$ can be formulated as follows

$$(\mathbf{f}^{ri})'(p^{ij}) = \frac{d\mathbf{f}^{ri}(p^{ij})}{d(\sigma^{ij})^2} = \frac{z}{2} * \frac{\sqrt{\left(\sigma_2^{ri}\right)^2 + (\sigma^{ij})^2} - \sqrt{\left(\sigma_1^{ri}\right)^2 + (\sigma^{ij})^2}}{\sqrt{\left(\left(\sigma_1^{ri}\right)^2 + (\sigma^{ij})^2\right)\left(\left(\sigma_2^{ri}\right)^2 + (\sigma^{ij})^2\right)}} \tag{3.C.2}$$

When $\sigma_1^{ri} < z\sigma_2^{ri}$, $(\mathbf{f}^{ri})'(p^{ij}) > 0$. Note that $(\sigma^{ij})^2 \in (0, +\infty)$, thus $\mathbf{f}^{ri}(p^{ij}) < \mu_1^{ri} - \mu_2^{ri} \leq 0$. The last inequality is followed by $\mu_1^{ri} \leq \mu_2^{ri}$. This completes the proof of case (a) according to Definition 3.1, and case (b) can be concluded similarly. □

Proof of Proposition 3.3. When $z\sigma_1^{ri} < z\sigma_2^{ri}$ and $\mu_1^{ri} \leq \mu_2^{ri}$, $(\mathbf{f}^{ri})'^{(p^{ij})} > 0$ is obtained according to Eq. (3.C.2). Thus, $\mathbf{f}^{ri}(p^{ij}) < \omega_1\left(\mu_1^{ri} - \mu_2^{ri}\right) \leq 0$. When $z\sigma_1^{ri} > z\sigma_2^{ri}$ and $c_1^{ri} < c_2^{ri}$, it can be obtained that $\mathbf{f}^{ri'}(p^{ij}) > 0$. Thus, $\mathbf{f}^{ri}(p^{ij}) \leq c_1^{ri} - c_2^{ri} < 0$. When $z\sigma_1^{ri} = z\sigma_2^{ri}$ and $c_1^{ri} < c_2^{ri}$, $\mathbf{f}^{ri'}(p^{ij}) = 0$. Thus, $\mathbf{f}^{ri}(p^{ij}) = c_1^{ri} - c_2^{ri} < 0$. Therefore $p_1^{ri} \succ p_2^{ri}$ if p_1^{ri} and p_2^{ri} satisfy $\mu_1^{ri} \leq \mu_2^{ri}$ and $c_1^{ri} < c_2^{ri}$. □

Appendix 3.D Proof of Proposition 3.6.

Proof. Given α and u_l, the value of TTB $\xi_p(\alpha)$ is a constant, which can be calculated by Eqs. (3.1)-(3.5), (3.7). According to Eq. (3.B.8), the GMV can be simplified as

$$\begin{aligned} c_p^{rs} = {} & \omega_1\xi_p + \omega_2(\alpha)\alpha(\xi_p - \mu_p) + \omega_3(\alpha)(1-\alpha)(\mu_p - \xi_p) \\ & + \frac{(\omega_2(\alpha)+\omega_3(\alpha))\sigma_p}{\sqrt{2\pi}} e^{-\left(\frac{\xi_p - \mu_p}{\sqrt{2}\sigma_p}\right)^2} \end{aligned} \tag{3.D.1}$$

For any path p, the continuity of c_p^{rs} is conditional on the continuity of ξ_p, μ_p, and σ_p because the weight coefficients and on-time arrival probability are constants. Referring to Eqs. (3.2)-(3.3), it is obvious that μ_l and σ_l are continuous with link traffic flows u_l. Hence, μ_p and σ_p are continuous (Eqs. (3.4)-(3.5)). In addition, as shown in Eq. (3.7), TTB is continuous since it is a weighted sum of μ_p and σ_p.

Let o be the smallest possible positive real number, and the link traffic flows are set as $u_l = \max\{o, u_l\}$ for calculating GMV. This modification ensures $u_l > 0$, and therefore a positive σ_p, as shown in Eqs. (3.3) and (3.5). Moreover, σ_p hardly changes if o is sufficiently small. With this pretreatment, the denominator in Eq. (3.D.1) is larger than zero.

Therefore, GMV is continuous with the link traffic flows. □

Appendix 4.A Proof of Theorem 4.1.

Proof. Instead of using Eq. (4.1) as the criterion to add new paths, strategy (*i*) adopts Eq. (4.2) to model travelers' BR behavior for path choice. When ϵ^{rs} equals zero, this strategy is degenerated to the general minimum disutility path search method. Let $P_n^{rs\prime}$ denote the path set, of which the members satisfy Eq. (4.1) but violate Eq. (4.2). Based on strategy (*i*), these paths do not belong to P_n^{rs} despite having lower path disutilities. The minimum disutility of paths in $P_n^{rs\prime}$, denoted by $c_{\min}^{rs\prime}(\boldsymbol{f_n})$, has a lower bound as follows

$$c_{\min}^{rs\prime}(\boldsymbol{f_n}) > (1-\epsilon^{rs}) \cdot c_{\min}^{rs}(\boldsymbol{f_n}) \tag{4.A.1}$$

where $c_{\min}^{rs}(\boldsymbol{f_n})$ is the minimum disutility of paths in P_n^{rs}.

The relative gap of the path disutility in path set $P_n^{rs\prime} \cup P_n^{rs}$ can be expressed as

$$\begin{aligned}\frac{c_p^{rs}(k,\boldsymbol{f_n}) - c_{\min}^{rs\prime}(\boldsymbol{f_n})}{c_{\min}^{rs\prime}(\boldsymbol{f_n})} &< \frac{c_p^{rs}(k,\boldsymbol{f_n}) - (1-\epsilon^{rs}) \cdot c_{\min}^{rs}(\boldsymbol{f_n})}{(1-\epsilon^{rs}) \cdot c_{\min}^{rs}(\boldsymbol{f_n})} \\ &= \frac{c_p^{rs}(k,\boldsymbol{f_n}) - c_{\min}^{rs}(\boldsymbol{f_n})}{c_{\min}^{rs}(\boldsymbol{f_n})} + \frac{\epsilon^{rs} \cdot c_p^{rs}(k,\boldsymbol{f_n})}{(1-\epsilon^{rs}) \cdot c_{\min}^{rs}(\boldsymbol{f_n})} \\ &\le \varepsilon_n^{rs} + \frac{\epsilon^{rs} \cdot (1+\varepsilon_n^{rs})}{1-\epsilon^{rs}} \quad \forall p \in P_n^{rs\prime} \cup P_n^{rs}, k \in K_n\end{aligned} \tag{4.A.2}$$

The last inequality is derived from Eq. (4.3). $P_n^{rs\prime} \cup P_n^{rs}$ is the newly generated path set if the minimum disutility path search method is used instead of the TBMDPS and inequality (4.A.2) gives the corresponding relative convergence threshold. That is, strategy (*i*) is equivalent to the minimum path search method combined with a ϵ^{rs}-related relative convergence threshold. Thus, strategy (*i*) does not really relax the condition of convergence.

Regarding strategy (*ii*) and (*iii*), ε_n^{rs}, Δ_n and K_n at the intermediate iterations are constants and have no influence on the convergence of the original CG algorithm. At the last iteration, ε_n^{rs} and Δ_n are equal to the required values to obtain the BR-DUE solution. Analogous to the spatial path extension, temporal exploration is the extension in the temporal dimension that only occurs at the intermediate iterations. For time intervals satisfying Eq. (4.7), the free flow path disutility are larger than the upper bound of the tolerance disutility. Strategy (*iv*) skips these unnecessary path searches and thus has no effect on path generation. In sum, none of the strategies modifies the convergence conditions of the original CG algorithm. □

Appendix 4.B Proof of Corollary 4.1.

Proof. The proof is based on the conclusions in the studies of Leventhal et al. (1973) and Smith (1984), who have analyzed the convergence of the CG algorithm and the proportional swap system respectively.

First, under the monotonicity assumption of the path disutility, the dynamical proportional swap system of $\mathrm{VI}(\boldsymbol{f_n}, \Omega_n)$ is convergent to an equilibrium, where $\mathrm{VI}(\boldsymbol{f_n}, \Omega_n)$ is the sub-problem of the $\mathrm{VI}(\boldsymbol{f}, \Omega)$ Eqs. (2.17)-(2.19) at iteration n and written as

$$\sum_{rs \in RS} \sum_{p \in P_n^{rs}} \sum_{k \in K_n} \tilde{c}_p^{rs}(k, \boldsymbol{f_n^*}) \left[f_p^{rs}(k) - f_p^{rs*}(k) \right] \geq 0 \ \ \forall \boldsymbol{f_n} \in \Omega_n \tag{4.B.1}$$

$$\Omega_n = \left\{ \boldsymbol{f_n} \middle| \, \boldsymbol{f_n} \geq 0, \sum_{p \in P_n^{rs}} \sum_{k \in K_n} \Delta_n \cdot f_p^{rs}(k) = Q^{rs}, \quad \forall \, rs \in RS \right\} \tag{4.B.2}$$

where P_n^{rs}, K_n and Δ_n are fixed.

The proportional swap system proposed by Guo et al. (2017) for the bottleneck problem towards BR-DUE can be extended to solve $\mathrm{VI}(\boldsymbol{f_n}, \Omega_n)$ by the following formulas

$$f_{pn}^{rs(\tau+1)}(k) = F_p^{rs}(\boldsymbol{f}_n^\tau) = f_{pn}^{rs(\tau)}(k) + \beta_5 \Gamma_{pn}^{rs}(k, \boldsymbol{f}_n^\tau) \tag{4.B.3}$$

$$\begin{aligned} \Gamma_{pn}^{rs}(k, \boldsymbol{f}_n^\tau) = \sum_{p' \in P_n^{rs}} \sum_{k' \in K_n} \Big(& f_{p'n}^{rs(\tau)}(k') \left[\tilde{c}_{p'n}^{rs(\tau)}(k', \boldsymbol{f_n^\tau}) - \tilde{c}_{pn}^{rs(\tau)}(k, \boldsymbol{f_n^\tau}) \right]_+ \\ & - f_{pn}^{rs(\tau)}(k) \left[\tilde{c}_{pn}^{rs(\tau)}(k, \boldsymbol{f_n^\tau}) - \tilde{c}_{p'n}^{rs(\tau)}(k', \boldsymbol{f_n^\tau}) \right]_+ \Big) \end{aligned} \tag{4.B.4}$$

where a mapping $[\cdot]_+ = \max\{\cdot, \ 0\}$ is used.

The continuity of $\tilde{c}_p^{rs}(k, \boldsymbol{f})$ makes $F_p^{rs}(\boldsymbol{f}_n^\tau)$ continuous on Ω_n. Moreover, Ω_n is nonempty, compact and convex. According to Guo et al. (2017), the proportional swap system has at least one stationary point, which is a BR-DUE state. The equivalence between a stationary point and a BR-DUE state can be derived directly from the equivalence theorems of Smith (1984) and Guo et al. (2017). Under the monotonicity assumption of the path disutility, Mounce (2007) and Mounce and Carey (2011) proved that the dynamical proportional swap system is convergent to an equilibrium.

Second, the CG algorithm can find the optimal solution to the $\mathrm{VI}(\boldsymbol{f}, \Omega)$ problem through path extensions. Ignorance of the time dimension, the difference between the

sub-problem Eqs. (4.B.1)-(4.B.2) and the original VI($\boldsymbol{f}, \Omega$) problem Eqs. (2.17)-(2.19) lies in the path set. The number of paths of the original problem may be very large especially for large networks, but only a few paths have positive flows. The CG algorithm proposed by Leventhal et al. (1973) is able to find paths with positive flows as stated in Section 2.4. When no new path is found at iteration n, the rest any path $p \in P^{rs} \backslash P_n^{rs}$ has larger disutility and flows only concentrate on those identified paths. Therefore, the solution to the sub-problem Eqs. (4.B.1)-(4.B.2) is an equilibrium state of the BR-DUE problem.

According to Theorem 4.1, the above complete the proof of Corollary 4.1. □

Appendix 5.A Illustration of the supply-demand dynamics and admissible conditions under the four mechanisms

As shown in Table A.**1**, the network has one OD pair connected by one SC link. The length of one time interval Δ is set as 20 minutes and assume that 200 travelers arrive at node 1 during each interval. In the VD-FCFS context, the 200 travelers are divided into half VIP travelers and half ordinary travelers. The arrival SCs are distinguished into three cases during the time horizon [7:00 am, 9:00 am].

Case 1 is used to demonstrate the supply-demand dynamics under the four FCFS mechanisms. As shown in Figure A.1, four different mechanisms result in different supply-demand patterns. Under the NW-FCFS mechanism, the red curve is high than the blue curve during the first three intervals. For each interval, 100 travelers use SCs without waiting and the rest demand of SCs is lost, which is denoted by the vertical gap between the two curves. During [8:00 am, 9:00 am], all demands can use SCs due to sufficient supply. Without considering the queues of SC requests at node 1, the NW-FCFS mechanism leads to 300 demand losses. Under the A-FCFS mechanism, the SC stocks during [7:00 am, 7:20 am), [7:40 am, 8:00 am), and [8:20 am, 8:40 am) equal 100, which is smaller than the number of arrival travelers during each interval (200). Since the A-FCFS mechanism postulates that travelers who arrive at a CSS location during any interval are served simultaneously, the supply of SCs accumulates once the stocks of the previous intervals are not consumed. This result is verified by the steep increase of supply at 8:00 am in Figure A.1 (b). In contrast, under the D-FCFS mechanism, the arrival SCs are used immediately by a part of the demand. The supply during each interval in Figure A.1 (c) equals the number of newly arrived SCs. The demand accumulates due to the smaller supplies before 8:00 am and then decrease during the last two intervals. Under the VD-FCFS mechanism, the curves of VIP and ordinary demands show different patterns despite the same arrival rate. The privilege of VIP travelers can be demonstrated by the fact that the purple curve is always below the red one in Figure A.1 (d).

Table A.1 An illustrative example

Case	Item						
		Arrival travelers Arrival SCs					
-	Time	[7:00, 7:20)	[7:20, 7:40)	[7:40, 8:00)	[8:00, 8:20)	[8:20, 8:40)	[7:40, 9:00]
-	Arrival travelers	200	200	200	200	200	200
1	Arrival SCs	100	100	100	300	300	300
2		300	300	300	300	300	300
3		0	0	400	0	200	600

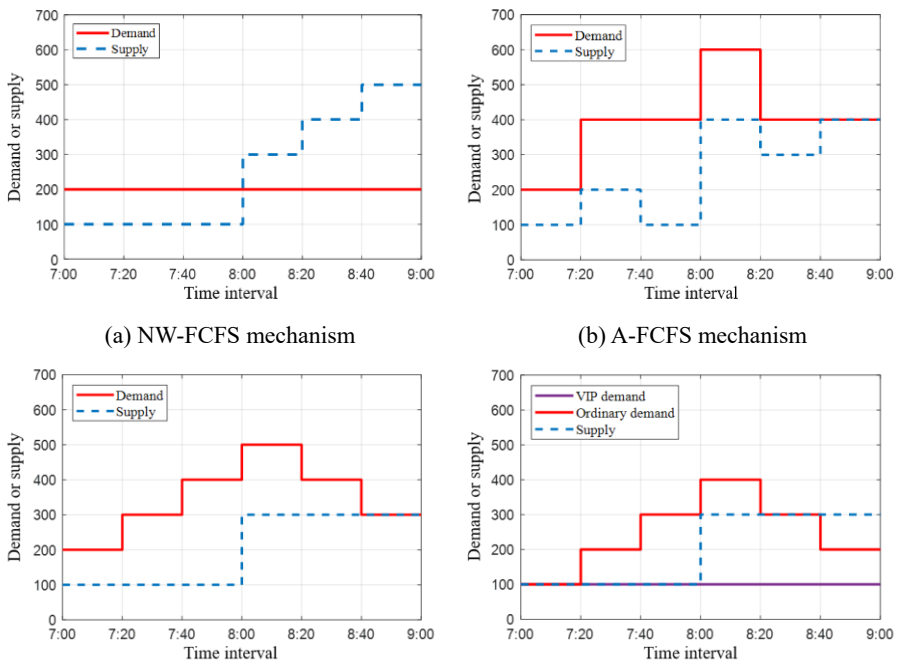

(a) NW-FCFS mechanism (b) A-FCFS mechanism

(c) D-FCFS mechanism (d) VD-FCFS mechanism

Figure A.1. Evolutions of demand and supply under four FCFS mechanisms.

The SC supply in case 2 is greater than SC demand during each interval. The supply-demand dynamics under the NW-FCFS, A-FCFS, and D-FCFS can be calculated by Eqs. (5.1), (5.2), and (5.6). As shown in Table A.2, three mechanisms have the same demand-supply dynamics, consistent with the admissible condition stated in Remark 5.2. The relation between $v_a(k)$ and $u_a(k)$ in case 3 satisfies the admissible condition between A-FCFS and D-FCFS mechanisms. As shown, the A-FCFS and D-FCFS mechanisms have the same supply-demand dynamics.

Table A.2 The supply-demand dynamics under different mechanisms

Case	Mechanism	Item	Time interval (am)					
			[7:00, 7:20)	[7:20, 7:40)	[7:40, 8:00)	[8:00, 8:20)	[8:20, 8:40)	[7:40, 9:00]
2	NW-FCFS & A-FCFS & D-FCFS	Demand	200	200	200	200	200	200
		Supply	300	400	500	600	700	800
3	NW-FCFS	Demand	0	0	200	200	200	200
		Supply	0	0	400	200	200	600
	A-FCFS & D-FCFS	Demand	200	400	600	400	600	600
		Supply	0	0	400	0	200	600

Appendix 5.B Discontinuity of the path disutility

Figure A.2 is a two-node network with one OD pair rs and one mode – SC. Three intervals ($k = 1, 2, 3$) can be chosen by homogeneous travelers. The initial SC stock is 5 at r and 0 at s. The free-flow travel time is 8 and the disutilities by SC is 3. The preferred arrival time at s is 10 and the unit disutility of early and late arrival time is 2. Travel congestion and transition disutility are not considered in this example. The path (link) disutility can be easily calculated as $2 \cdot |k - 2| + 3$.

As shown in Table A.3, case 1 shows the initial disutility and flow. If the demand of rs is 5, as presented in case 2, time interval 2 has the minimum disutility and is chosen by 5 travelers. Adding the number of travelers $\Delta f \to 0$ on this path during interval 2 results in different disutilities under different FCFS mechanisms. The flow distribution and disutility under the A-FCFS and D-FCFS mechanisms are shown by cases 3 and 4 respectively. According to the A-FCFS mechanism, these travelers will wait until the stock at r is larger than or equal to $5 + \Delta f$, meaning that they cannot finish the trip within the time horizon. Therefore, the disutilities of intervals 2 and 3 are a large number M.

Under the D-FCFS mechanism, the path disutility during interval 2 can be calculated by the weighted sum according to Eq. (5.35), i.e., $\tilde{c} = 5/(5 + \Delta f) \times 3 + \Delta f/(5 + \Delta f) \times M$. The continuity of disutility is kept during this interval. However, the disutility of interval 3 increases to M, which leads to Eq. (5.B.1), meaning that the continuity of path disutility is not satisfied due to the dynamic supply-demand of SCs.

$$\lim_{\Delta f \to 0} \Delta c \neq 0 \tag{5.B.1}$$

where c is the vector of $c_p^{rs}(k, f)$ and Δc denotes the change of c.

Figure A.2. Two-node network.

Table A.3 The path flows and disutilities

Case	Demand	Item	Time interval		
			1	2	3
1	0	Disutility	5	3	5
		Flow	0	0	0
2	5	Disutility	5	3	5
		Flow	0	5	0
3	$5+\Delta f$	Disutility	5	M	M
		Flow	0	$\mathbf{5+\Delta f}$	0
4	$5+\Delta f$	Disutility	5	$\tilde{c}$	M
		Flow	0	$\mathbf{5+\Delta f}$	0

Appendix 5.C Sioux Falls network

The Sioux Falls network (Figure 5.8) has 24 nodes and 76 links. Incorporating the land use map from http://www.siouxfalls.org/Planning, the network is divided into the city center and suburban area, where home zones, work locations, and CSS locations (stations) are placed at the nodes. Nodes in red are home zones, which denotes residential neighborhoods in reality. Three different types of CSS locations are defined in Figure 5.8. Nodes in green are only for CSS locations, where travelers can access/egress SCs or park vehicles. Besides the function of CSS locations, nodes in yellow and blue are also home zones and work locations respectively.

5.C1 Setting of nodes and links

Table A.4 shows the characteristics of directed links, including the information of entrance and exit nodes, link capacity, and free-flow travel time. Note that PC and SC share the same physical roads.

Table A.4 Basic settings of links

Link ID	Start node	End node	Capacity (veh/min)	Travel time (min)
1	17	19	48	4
2	19	17	48	4
3	6	8	49	4
4	8	6	49	4
5	23	24	51	4
6	24	23	51	4
7	16	17	52	4
8	17	16	52	4
9	21	22	52	4
10	22	21	52	4
11	4	5	178	4
12	5	4	178	4
13	7	18	234	4
14	18	7	234	4
15	21	24	49	6
16	24	21	49	6
17	7	8	78	6
18	8	7	78	6
19	15	22	96	6
20	22	15	96	6
21	9	10	139	6
22	10	9	139	6
23	15	19	146	6
24	19	15	146	6
25	16	18	197	6
26	18	16	197	6
27	12	13	259	6
28	13	12	259	6
29	10	16	49	8
30	16	10	49	8
31	11	14	49	8
32	14	11	49	8
33	14	23	49	8
34	23	14	49	8
35	5	6	49	8
36	6	5	49	8
37	22	23	50	8
38	23	22	50	8
39	19	20	50	8
40	20	19	50	8
41	13	24	51	8

42	24	13	51	8
43	3	4	171	8
44	4	3	171	8
45	1	3	234	8
46	3	1	234	8
47	3	12	234	8
48	12	3	234	8
49	18	20	234	8
50	20	18	234	8
51	2	6	50	10
52	6	2	50	10
53	8	16	50	10
54	16	8	50	10
55	20	22	51	10
56	22	20	51	10
57	14	15	51	10
58	15	14	51	10
59	5	9	100	10
60	9	5	100	10
61	10	11	100	10
62	11	10	100	10
63	4	11	49	12
64	11	4	49	12
65	11	12	49	12
66	12	11	49	12
67	20	21	51	12
68	21	20	51	12
69	10	15	135	12
70	15	10	135	12
71	1	2	259	12
72	2	1	259	12
73	10	17	50	16
74	17	10	50	16
75	8	9	51	20
76	9	8	51	20

Table A.5 displays the attributes of nodes, including whether they are home zones, work locations, and CSS locations or not (0: no; 1: yes), whether they are city center or not (0: no; 1: yes), the initial supply of SCs, and parking fees.

Table A.5 Basic settings of nodes

Node ID	Home zone	Work location	CSS location	Number of SCs	City center or not	Parking fee ($)
1	1	0	0	0	0	1

2	1	0	0	0	0	1
3	0	1	1	0	0	1
4	1	0	1	200	0	1
5	1	0	0	0	0	1
6	1	0	0	0	0	1
7	1	0	0	0	0	1
8	1	0	1	200	0	1
9	0	0	1	200	0	1
10	0	1	1	0	1	3
11	1	0	0	0	0	1
12	1	0	0	0	0	1
13	1	0	0	0	0	1
14	0	0	1	400	1	3
15	0	1	1	0	1	3
16	0	0	1	400	1	3
17	1	0	0	0	1	3
18	1	0	0	0	0	1
19	1	0	1	400	1	3
20	1	0	0	0	0	1
21	0	0	1	200	0	1
22	1	0	1	400	1	3
23	1	0	0	0	1	3
24	0	1	1	0	0	1

Table A.6 Settings of travel demand

OD pair ID	Origin	Destination	Demand
1	1	10	2300
2	2	3	2000
3	4	10	2000
4	5	3	2100
5	6	3	2000
6	7	3	2100
7	8	24	2100
8	11	15	2000
9	12	24	2500
10	13	24	2700
11	17	15	2200
12	18	15	2300
13	19	15	2300
14	20	10	2700
15	22	24	2300
16	23	15	2600

5.C2 Setting of travel demand

Table A.6 shows the settings of travel demand. An OD pair is formed by a home zone and a randomly selected work location. The demands of these OD pairs are randomly generated from 2000 to 3000.

5.C3 Setting of other parameters

The time horizon falls within [7:00 am, 10:00 am] and the preferred arrival time is 9:00 am. The percentage of VIP members and ordinary travelers are 20% and 80% respectively. Table A.7 shows the settings of other parameters, where η_1-η_4 and ρ_1-ρ_4 are in either one unit of disutility per hour or dollar.

Table A.7 Settings of other parameters

η_1	η_2	η_3	η_4	η_5	η_6	η_7	η_8	c_0 (\$)	κ^{rs} (h)	Δ (min)	ε^{rs}	ϵ^{rs}
6.4	3.9	15.21	3.0	1.0	3.5	8.2	1	0.2	0.1	1	0.1	0.01

Author index

Subject index

M

N

P

R

S

T

U

V

Curriculum Vitae

Dong Wang was born on the 17th February 1989 in Shandong, China. He obtained his bachelor degree in 2012 at Shandong University of Science and Technology. He continued his master study in computing mathematics at the same university. In 2015, he started his PhD at Beijing Jiaotong University. His major is systems science. From September 2017, he became a joint PhD student of Beijing Jiaotong University and Eindhoven University of Technology under the support of the China Scholarship Council. His research interests include dynamic traffic assignment, reliable shortest path search, car-sharing services, and activity-travel pattern scheduling.

List of publications

Journal papers

Wang, D., Liao, F., Gao, Z., Timmermans, H., 2019. Tolerance-based strategies for extending the column generation algorithm to the bounded rational dynamic user equilibrium problem. Transportation Research Part B: Methodological 119, 102–121.

Wang, D., Liao, F., Gao, Z., Rasouli, S., Huang, H.J., 2020. Tolerance-based column generation for boundedly rational dynamic activity-travel assignment in large-scale networks. Transportation Research Part E: Logistics and Transportation Review 141, 102034.

Wang, D., Liao, F., Gao, Z., Timmermans, H., 2020. A generalized mean-variance metric of route choice model under travel time uncertainty. Transportmetrica A: Transport Science, 1-25.

Wang, D., Liao, F., 2021. Analysis of first-come-first-served mechanisms in one-way car-sharing services. Transportation Research Part B: Methodological, 147, 22-41.

Conference and workshop papers

Wang, D., Liao, F., Gao, Z., Timmermans, H., 2018. A scheduling utility budget–based user equilibrium model under travel time uncertainty. Transportation Research Board 97th Annual Meeting, No. 18-02390.

Wang, D., Liao, F., Gao, Z., Timmermans, H., 2019. A tolerance-based path generation algorithm for the boundedly rational dynamic user equilibrium model. Transportation Research Board 98th Annual Meeting, No. 19-04357.

Wang, D., Liao, F., Gao, Z., Rasouli, S., Huang, H.J., 2020. Tolerance-based column generation algorithm to the bounded rational dynamic activity-travel assignment problem. Transportation Research Board 99th Annual Meeting.

Wang, D., Liao, F., Gao, Z., 2018. Improved column generation algorithm for dynamic activity-travel assignment model inclusive of mobility services. International Post-Conference (HKSTS) Workshop on “Advances in Supernetwork Modeling and Mobility Pattern Analysis”. 12.

Bouwstenen is een publicatiereeks
van de Faculteit Bouwkunde,
Technische Universiteit Eindhoven.
Zij presenteert resultaten van
onderzoek en andere activiteiten op
het vakgebied der Bouwkunde,
uitgevoerd in het kader van deze
Faculteit.

Bouwstenen en andere proefschriften van de
TU/e zijn online beschikbaar via:
https://research.tue.nl/

Reeds verschenen in de serie
Bouwstenen

nr 1
Elan: A Computer Model for Building Energy Design: Theory and Validation
Martin H. de Wit
H.H. Driessen
R.M.M. van der Velden

nr 2
Kwaliteit, Keuzevrijheid en Kosten: Evaluatie van Experiment Klarendal, Arnhem
J. Smeets
C. le Nobel
M. Broos
J. Frenken
A. v.d. Sanden

nr 3
Crooswijk: Van 'Bijzonder' naar 'Gewoon'
Vincent Smit
Kees Noort

nr 4
Staal in de Woningbouw
Edwin J.F. Delsing

nr 5
Mathematical Theory of Stressed Skin Action in Profiled Sheeting with Various Edge Conditions
Andre W.A.M.J. van den Bogaard

nr 6
Hoe Berekenbaar en Betrouwbaar is de Coëfficiënt k in x-ksigma en x-ks?
K.B. Lub
A.J. Bosch

nr 7
Het Typologisch Gereedschap: Een Verkennende Studie Omtrent Typologie en Omtrent de Aanpak van Typologisch Onderzoek
J.H. Luiten

nr 8
Informatievoorziening en Beheerprocessen
A. Nauta
Jos Smeets (red.)
Helga Fassbinder (projectleider)
Adrie Proveniers
J. v.d. Moosdijk

nr 9
Strukturering en Verwerking van Tijdgegevens voor de Uitvoering van Bouwwerken
ir. W.F. Schaefer
P.A. Erkelens

nr 10
Stedebouw en de Vorming van een Speciale Wetenschap
K. Doevendans

nr 11
Informatica en Ondersteuning van Ruimtelijke Besluitvorming
G.G. van der Meulen

nr 12
Staal in de Woningbouw, Korrosie-Bescherming van de Begane Grondvloer
Edwin J.F. Delsing

nr 13
Een Thermisch Model voor de Berekening van Staalplaatbetonvloeren onder Brandomstandigheden
A.F. Hamerlinck

nr 14
De Wijkgedachte in Nederland: Gemeenschapsstreven in een Stedebouwkundige Context
K. Doevendans
R. Stolzenburg

nr 15
Diaphragm Effect of Trapezoidally Profiled Steel Sheets: Experimental Research into the Influence of Force Application
Andre W.A.M.J. van den Bogaard

nr 16
Versterken met Spuit-Ferrocement: Het Mechanische Gedrag van met Spuit-Ferrocement Versterkte Gewapend Betonbalken
K.B. Lubir
M.C.G. van Wanroy

nr 17
De Tractaten van Jean Nicolas Louis Durand
G. van Zeyl

nr 18
Wonen onder een Plat Dak: Drie Opstellen over Enkele Vooronderstellingen van de Stedebouw
K. Doevendans

nr 19
Supporting Decision Making Processes: A Graphical and Interactive Analysis of Multivariate Data
W. Adams

nr 20
Self-Help Building Productivity: A Method for Improving House Building by Low-Income Groups Applied to Kenya 1990-2000
P. A. Erkelens

nr 21
De Verdeling van Woningen: Een Kwestie van Onderhandelen
Vincent Smit

nr 22
Flexibiliteit en Kosten in het Ontwerpproces: Een Besluitvormingondersteunend Model
M. Prins

nr 23
Spontane Nederzettingen Begeleid: Voorwaarden en Criteria in Sri Lanka
Po Hin Thung

nr 24
Fundamentals of the Design of Bamboo Structures
Oscar Arce-Villalobos

nr 25
Concepten van de Bouwkunde
M.F.Th. Bax (red.)
H.M.G.J. Trum (red.)

nr 26
Meaning of the Site
Xiaodong Li

nr 27
Het Woonmilieu op Begrip Gebracht: Een Speurtocht naar de Betekenis van het Begrip 'Woonmilieu'
Jaap Ketelaar

nr 28
Urban Environment in Developing Countries
editors: Peter A. Erkelens
George G. van der Meulen (red.)

nr 29
Stategische Plannen voor de Stad: Onderzoek en Planning in Drie Steden
prof.dr. H. Fassbinder (red.)
H. Rikhof (red.)

nr 30
Stedebouwkunde en Stadsbestuur
Piet Beekman

nr 31
De Architectuur van Djenné: Een Onderzoek naar de Historische Stad
P.C.M. Maas

nr 32
Conjoint Experiments and Retail Planning
Harmen Oppewal

nr 33
Strukturformen Indonesischer Bautechnik: Entwicklung Methodischer Grundlagen für eine 'Konstruktive Pattern Language' in Indonesien
Heinz Frick arch. SIA

nr 34
Styles of Architectural Designing: Empirical Research on Working Styles and Personality Dispositions
Anton P.M. van Bakel

nr 35
Conjoint Choice Models for Urban Tourism Planning and Marketing
Benedict Dellaert

nr 36
Stedelijke Planvorming als Co-Produktie
Helga Fassbinder (red.)

nr 37
Design Research in the Netherlands
editors: R.M. Oxman
M.F.Th. Bax
H.H. Achten

nr 38
Communication in the Building Industry
Bauke de Vries

nr 39
Optimaal Dimensioneren van Gelaste Plaatliggers
J.B.W. Stark
F. van Pelt
L.F.M. van Gorp
B.W.E.M. van Hove

nr 40
Huisvesting en Overwinning van Armoede
P.H. Thung
P. Beekman (red.)

nr 41
Urban Habitat: The Environment of Tomorrow
George G. van der Meulen
Peter A. Erkelens

nr 42
A Typology of Joints
John C.M. Olie

nr 43
Modeling Constraints-Based Choices for Leisure Mobility Planning
Marcus P. Stemerding

nr 44
Activity-Based Travel Demand Modeling
Dick Ettema

nr 45
Wind-Induced Pressure Fluctuations on Building Facades
Chris Geurts

nr 46
Generic Representations
Henri Achten

nr 47
Johann Santini Aichel: Architectuur en Ambiguiteit
Dirk De Meyer

nr 48
Concrete Behaviour in Multiaxial Compression
Erik van Geel

nr 49
Modelling Site Selection
Frank Witlox

nr 50
Ecolemma Model
Ferdinand Beetstra

nr 51
Conjoint Approaches to Developing Activity-Based Models
Donggen Wang

nr 52
On the Effectiveness of Ventilation
Ad Roos

nr 53
Conjoint Modeling Approaches for Residential Group preferences
Eric Molin

nr 54
Modelling Architectural Design Information by Features
Jos van Leeuwen

nr 55
A Spatial Decision Support System for the Planning of Retail and Service Facilities
Theo Arentze

nr 56
Integrated Lighting System Assistant
Ellie de Groot

nr 57
Ontwerpend Leren, Leren Ontwerpen
J.T. Boekholt

nr 58
Temporal Aspects of Theme Park Choice Behavior
Astrid Kemperman

nr 59
Ontwerp van een Geïndustrialiseerde Funderingswijze
Faas Moonen

nr 60
Merlin: A Decision Support System for Outdoor Leisure Planning
Manon van Middelkoop

nr 61
The Aura of Modernity
Jos Bosman

nr 62
Urban Form and Activity-Travel Patterns
Daniëlle Snellen

nr 63
Design Research in the Netherlands 2000
Henri Achten

nr 64
Computer Aided Dimensional Control in Building Construction
Rui Wu

nr 65
Beyond Sustainable Building
editors: Peter A. Erkelens
Sander de Jonge
August A.M. van Vliet
co-editor: Ruth J.G. Verhagen

nr 66
Das Globalrecyclingfähige Haus
Hans Löfflad

nr 67
Cool Schools for Hot Suburbs
René J. Dierkx

nr 68
A Bamboo Building Design Decision Support Tool
Fitri Mardjono

nr 69
Driving Rain on Building Envelopes
Fabien van Mook

nr 70
Heating Monumental Churches
Henk Schellen

nr 71
Van Woningverhuurder naar Aanbieder van Woongenot
Patrick Dogge

nr 72
Moisture Transfer Properties of Coated Gypsum
Emile Goossens

nr 73
Plybamboo Wall-Panels for Housing
Guillermo E. González-Beltrán

nr 74
The Future Site-Proceedings
Ger Maas
Frans van Gassel

nr 75
Radon transport in Autoclaved Aerated Concrete
Michel van der Pal

nr 76
The Reliability and Validity of Interactive Virtual Reality Computer Experiments
Amy Tan

nr 77
Measuring Housing Preferences Using Virtual Reality and Belief Networks
Maciej A. Orzechowski

nr 78
Computational Representations of Words and Associations in Architectural Design
Nicole Segers

nr 79
Measuring and Predicting Adaptation in Multidimensional Activity-Travel Patterns
Chang-Hyeon Joh

nr 80
Strategic Briefing
Fayez Al Hassan

nr 81
Well Being in Hospitals
Simona Di Cicco

nr 82
Solares Bauen: Implementierungs- und Umsetzungs-Aspekte in der Hochschulausbildung in Österreich
Gerhard Schuster

nr 83
Supporting Strategic Design of Workplace Environments with Case-Based Reasoning
Shauna Mallory-Hill

nr 84
ACCEL: A Tool for Supporting Concept Generation in the Early Design Phase
Maxim Ivashkov

nr 85
Brick-Mortar Interaction in Masonry under Compression
Ad Vermeltfoort

nr 86
Zelfredzaam Wonen
Guus van Vliet

nr 87
Een Ensemble met Grootstedelijke Allure
Jos Bosman
Hans Schippers

nr 88
On the Computation of Well-Structured Graphic Representations in Architectural Design
Henri Achten

nr 89
De Evolutie van een West-Afrikaanse Vernaculaire Architectuur
Wolf Schijns

nr 90
ROMBO Tactiek
Christoph Maria Ravesloot

nr 91
External Coupling between Building Energy Simulation and Computational Fluid Dynamics
Ery Djunaedy

nr 92
Design Research in the Netherlands 2005
editors: Henri Achten
Kees Dorst
Pieter Jan Stappers
Bauke de Vries

nr 93
Ein Modell zur Baulichen Transformation
Jalil H. Saber Zaimian

nr 94
Human Lighting Demands: Healthy Lighting in an Office Environment
Myriam Aries

nr 95
A Spatial Decision Support System for the Provision and Monitoring of Urban Greenspace
Claudia Pelizaro

nr 96
Leren Creëren
Adri Proveniers

nr 97
Simlandscape
Rob de Waard

nr 98
Design Team Communication
Ad den Otter

nr 99
Humaan-Ecologisch Georiënteerde Woningbouw
Juri Czabanowski

nr 100
Hambase
Martin de Wit

nr 101
Sound Transmission through Pipe Systems and into Building Structures
Susanne Bron-van der Jagt

nr 102
Het Bouwkundig Contrapunt
Jan Francis Boelen

nr 103
A Framework for a Multi-Agent Planning Support System
Dick Saarloos

nr 104
Bracing Steel Frames with Calcium Silicate Element Walls
Bright Mweene Ng'andu

nr 105
Naar een Nieuwe Houtskeletbouw
F.N.G. De Medts

nr 106 and 107
Niet gepubliceerd

nr 108
Geborgenheid
T.E.L. van Pinxteren

nr 109
Modelling Strategic Behaviour in Anticipation of Congestion
Qi Han

nr 110
Reflecties op het Woondomein
Fred Sanders

nr 111
On Assessment of Wind Comfort by Sand Erosion
Gábor Dezsö

nr 112
Bench Heating in Monumental Churches
Dionne Limpens-Neilen

nr 113
RE. Architecture
Ana Pereira Roders

nr 114
Toward Applicable Green Architecture
Usama El Fiky

nr 115
Knowledge Representation under Inherent Uncertainty in a Multi-Agent System for Land Use Planning
Liying Ma

nr 116
Integrated Heat Air and Moisture Modeling and Simulation
Jos van Schijndel

nr 117
Concrete Behaviour in Multiaxial Compression
J.P.W. Bongers

nr 118
The Image of the Urban Landscape
Ana Moya Pellitero

nr 119
The Self-Organizing City in Vietnam
Stephanie Geertman

nr 120
A Multi-Agent Planning Support System for Assessing Externalities of Urban Form Scenarios
Rachel Katoshevski-Cavari

nr 121
Den Schulbau Neu Denken, Fühlen und Wollen
Urs Christian Maurer-Dietrich

nr 122
Peter Eisenman Theories and Practices
Bernhard Kormoss

nr 123
User Simulation of Space Utilisation
Vincent Tabak

nr 125
In Search of a Complex System Model
Oswald Devisch

nr 126
Lighting at Work: Environmental Study of Direct Effects of Lighting Level and Spectrum on Psycho-Physiological Variables
Grazyna Górnicka

nr 127
Flanking Sound Transmission through Lightweight Framed Double Leaf Walls
Stefan Schoenwald

nr 128
Bounded Rationality and Spatio-Temporal Pedestrian Shopping Behavior
Wei Zhu

nr 129
Travel Information: Impact on Activity Travel Pattern
Zhongwei Sun

nr 130
Co-Simulation for Performance Prediction of Innovative Integrated Mechanical Energy Systems in Buildings
Marija Trčka

nr 131
Niet gepubliceerd

nr 132
Architectural Cue Model in Evacuation Simulation for Underground Space Design
Chengyu Sun

nr 133
Uncertainty and Sensitivity Analysis in Building Performance Simulation for Decision Support and Design Optimization
Christina Hopfe

nr 134
Facilitating Distributed Collaboration in the AEC/FM Sector Using Semantic Web Technologies
Jacob Beetz

nr 135
Circumferentially Adhesive Bonded Glass Panes for Bracing Steel Frame in Façades
Edwin Huveners

nr 136
Influence of Temperature on Concrete Beams Strengthened in Flexure with CFRP
Ernst-Lucas Klamer

nr 137
Sturen op Klantwaarde
Jos Smeets

nr 139
Lateral Behavior of Steel Frames with Discretely Connected Precast Concrete Infill Panels
Paul Teewen

nr 140
Integral Design Method in the Context of Sustainable Building Design
Perica Savanović

nr 141
Household Activity-Travel Behavior: Implementation of Within-Household Interactions
Renni Anggraini

nr 142
Design Research in the Netherlands 2010
Henri Achten

nr 143
Modelling Life Trajectories and Transport Mode Choice Using Bayesian Belief Networks
Marloes Verhoeven

nr 144
Assessing Construction Project Performance in Ghana
William Gyadu-Asiedu

nr 145
Empowering Seniors through Domotic Homes
Masi Mohammadi

nr 146
An Integral Design Concept for Ecological Self-Compacting Concrete
Martin Hunger

nr 147
Governing Multi-Actor Decision Processes in Dutch Industrial Area Redevelopment
Erik Blokhuis

nr 148
A Multifunctional Design Approach for Sustainable Concrete
Götz Hüsken

nr 149
Quality Monitoring in Infrastructural Design-Build Projects
Ruben Favié

nr 150
Assessment Matrix for Conservation of Valuable Timber Structures
Michael Abels

nr 151
Co-simulation of Building Energy Simulation and Computational Fluid Dynamics for Whole-Building Heat, Air and Moisture Engineering
Mohammad Mirsadeghi

nr 152
External Coupling of Building Energy Simulation and Building Element Heat, Air and Moisture Simulation
Daniel Cóstola

nr 153
Adaptive Decision Making In Multi-Stakeholder Retail Planning
Ingrid Janssen

nr 154
Landscape Generator
Kymo Slager

nr 155
Constraint Specification in Architecture
Remco Niemeijer

nr 156
A Need-Based Approach to Dynamic Activity Generation
Linda Nijland

nr 157
Modeling Office Firm Dynamics in an Agent-Based Micro Simulation Framework
Gustavo Garcia Manzato

nr 158
Lightweight Floor System for Vibration Comfort
Sander Zegers

nr 159
Aanpasbaarheid van de Draagstructuur
Roel Gijsbers

nr 160
'Village in the City' in Guangzhou, China
Yanliu Lin

nr 161
Climate Risk Assessment in Museums
Marco Martens

nr 162
Social Activity-Travel Patterns
Pauline van den Berg

nr 163
Sound Concentration Caused by Curved Surfaces
Martijn Vercammen

nr 164
Design of Environmentally Friendly Calcium Sulfate-Based Building Materials: Towards an Improved Indoor Air Quality
Qingliang Yu

nr 165
Beyond Uniform Thermal Comfort on the Effects of Non-Uniformity and Individual Physiology
Lisje Schellen

nr 166
Sustainable Residential Districts
Gaby Abdalla

nr 167
Towards a Performance Assessment Methodology using Computational Simulation for Air Distribution System Designs in Operating Rooms
Mônica do Amaral Melhado

nr 168
Strategic Decision Modeling in Brownfield Redevelopment
Brano Glumac

nr 169
Pamela: A Parking Analysis Model for Predicting Effects in Local Areas
Peter van der Waerden

nr 170
A Vision Driven Wayfinding Simulation-System Based on the Architectural Features Perceived in the Office Environment
Qunli Chen

nr 171
Measuring Mental Representations Underlying Activity-Travel Choices
Oliver Horeni

nr 172
Modelling the Effects of Social Networks on Activity and Travel Behaviour
Nicole Ronald

nr 173
Uncertainty Propagation and Sensitivity Analysis Techniques in Building Performance Simulation to Support Conceptual Building and System Design
Christian Struck

nr 174
Numerical Modeling of Micro-Scale Wind-Induced Pollutant Dispersion in the Built Environment
Pierre Gousseau

nr 175
Modeling Recreation Choices over the Family Lifecycle
Anna Beatriz Grigolon

nr 176
Experimental and Numerical Analysis of Mixing Ventilation at Laminar, Transitional and Turbulent Slot Reynolds Numbers
Twan van Hooff

nr 177
Collaborative Design Support: Workshops to Stimulate Interaction and Knowledge Exchange Between Practitioners
Emile M.C.J. Quanjel

nr 178
Future-Proof Platforms for Aging-in-Place
Michiel Brink

nr 179
Motivate: A Context-Aware Mobile Application for Physical Activity Promotion
Yuzhong Lin

nr 180
Experience the City: Analysis of Space-Time Behaviour and Spatial Learning
Anastasia Moiseeva

nr 181
Unbonded Post-Tensioned Shear Walls of Calcium Silicate Element Masonry
Lex van der Meer

nr 182
Construction and Demolition Waste Recycling into Innovative Building Materials for Sustainable Construction in Tanzania
Mwita M. Sabai

nr 183
Durability of Concrete with Emphasis on Chloride Migration
Przemysław Spiesz

nr 184
Computational Modeling of Urban Wind Flow and Natural Ventilation Potential of Buildings
Rubina Ramponi

nr 185
A Distributed Dynamic Simulation Mechanism for Buildings Automation and Control Systems
Azzedine Yahiaoui

nr 186
Modeling Cognitive Learning of Urban Networks in Daily Activity-Travel Behavior
Şehnaz Cenani Durmazoğlu

nr 187
Functionality and Adaptability of Design Solutions for Public Apartment Buildings in Ghana
Stephen Agyefi-Mensah

nr 188
A Construction Waste Generation Model for Developing Countries
Lilliana Abarca-Guerrero

nr 189
Synchronizing Networks: The Modeling of Supernetworks for Activity-Travel Behavior
Feixiong Liao

nr 190
Time and Money Allocation Decisions in Out-of-Home Leisure Activity Choices
Gamze Zeynep Dane

nr 191
How to Measure Added Value of CRE and Building Design
Rianne Appel-Meulenbroek

nr 192
Secondary Materials in Cement-Based Products: Treatment, Modeling and Environmental Interaction
Miruna Florea

nr 193
Concepts for the Robustness Improvement of Self-Compacting Concrete: Effects of Admixtures and Mixture Components on the Rheology and Early Hydration at Varying Temperatures
Wolfram Schmidt

nr 194
Modelling and Simulation of Virtual Natural Lighting Solutions in Buildings
Rizki A. Mangkuto

nr 195
Nano-Silica Production at Low Temperatures from the Dissolution of Olivine - Synthesis, Tailoring and Modelling
Alberto Lazaro Garcia

nr 196
Building Energy Simulation Based Assessment of Industrial Halls for Design Support
Bruno Lee

nr 197
Computational Performance Prediction of the Potential of Hybrid Adaptable Thermal Storage Concepts for Lightweight Low-Energy Houses
Pieter-Jan Hoes

nr 198
Application of Nano-Silica in Concrete
George Quercia Bianchi

nr 199
Dynamics of Social Networks and Activity Travel Behaviour
Fariya Sharmeen

nr 200
Building Structural Design Generation and Optimisation including Spatial Modification
Juan Manuel Davila Delgado

nr 201
Hydration and Thermal Decomposition of Cement/Calcium-Sulphate Based Materials
Ariën de Korte

nr 202
Republiek van Beelden:
De Politieke Werkingen van het Ontwerp in Regionale Planvorming
Bart de Zwart

nr 203
Effects of Energy Price Increases on Individual Activity-Travel Repertoires and Energy Consumption
Dujuan Yang

nr 204
Geometry and Ventilation:
Evaluation of the Leeward Sawtooth Roof Potential in the Natural Ventilation of Buildings
Jorge Isaac Perén Montero

nr 205
Computational Modelling of Evaporative Cooling as a Climate Change Adaptation Measure at the Spatial Scale of Buildings and Streets
Hamid Montazeri

nr 206
Local Buckling of Aluminium Beams in Fire Conditions
Ronald van der Meulen

nr 207
Historic Urban Landscapes:
Framing the Integration of Urban and Heritage Planning in Multilevel Governance
Loes Veldpaus

nr 208
Sustainable Transformation of the Cities: Urban Design Pragmatics to Achieve a Sustainable City
Ernesto Antonio Zumelzu Scheel

nr 209
Development of Sustainable Protective Ultra-High Performance Fibre Reinforced Concrete (UHPFRC):
Design, Assessment and Modeling
Rui Yu

nr 210
Uncertainty in Modeling Activity-Travel Demand in Complex Uban Systems
Soora Rasouli

nr 211
Simulation-based Performance Assessment of Climate Adaptive Greenhouse Shells
Chul-sung Lee

nr 212
Green Cities:
Modelling the Spatial Transformation of the Urban Environment using Renewable Energy Technologies
Saleh Mohammadi

nr 213
A Bounded Rationality Model of Short and Long-Term Dynamics of Activity-Travel Behavior
Ifigeneia Psarra

nr 214
Effects of Pricing Strategies on Dynamic Repertoires of Activity-Travel Behaviour
Elaheh Khademi

nr 215
Handstorm Principles for Creative and Collaborative Working
Frans van Gassel

nr 216
Light Conditions in Nursing Homes: Visual Comfort and Visual Functioning of Residents
Marianne M. Sinoo

nr 217
Woonsporen: De Sociale en Ruimtelijke Biografie van een Stedelijk Bouwblok in de Amsterdamse Transvaalbuurt
Hüseyin Hüsnü Yegenoglu

nr 218
Studies on User Control in Ambient Intelligent Systems
Berent Willem Meerbeek

nr 219
Daily Livings in a Smart Home: Users' Living Preference Modeling of Smart Homes
Erfaneh Allameh

nr 220
Smart Home Design: Spatial Preference Modeling of Smart Homes
Mohammadali Heidari Jozam

nr 221
Wonen: Discoursen, Praktijken, Perspectieven
Jos Smeets

nr 222
Personal Control over Indoor Climate in Offices: Impact on Comfort, Health and Productivity
Atze Christiaan Boerstra

nr 223
Personalized Route Finding in Multimodal Transportation Networks
Jianwe Zhang

nr 224
The Design of an Adaptive Healing Room for Stroke Patients
Elke Daemen

nr 225
Experimental and Numerical Analysis of Climate Change Induced Risks to Historic Buildings and Collections
Zara Huijbregts

nr 226
Wind Flow Modeling in Urban Areas Through Experimental and Numerical Techniques
Alessio Ricci

nr 227
Clever Climate Control for Culture: Energy Efficient Indoor Climate Control Strategies for Museums Respecting Collection Preservation and Thermal Comfort of Visitors
Rick Kramer

nr 228
Fatigue Life Estimation of Metal Structures Based on Damage Modeling
Sarmediran Silitonga

nr 229
A multi-agents and occupancy based strategy for energy management and process control on the room-level
Timilehin Moses Labeodan

nr 230
Environmental assessment of Building Integrated Photovoltaics: Numerical and Experimental Carrying Capacity Based Approach
Michiel Ritzen

nr 231
Performance of Admixture and Secondary Minerals in Alkali Activated Concrete: Sustaining a Concrete Future
Arno Keulen

nr 232
World Heritage Cities and Sustainable Urban Development: Bridging Global and Local Levels in Monitoring the Sustainable Urban Development of World Heritage Cities
Paloma C. Guzman Molina

nr 233
Stage Acoustics and Sound Exposure in Performance and Rehearsal Spaces for Orchestras: Methods for Physical Measurements
Remy Wenmaekers

nr 234
Municipal Solid Waste Incineration (MSWI) Bottom Ash: From Waste to Value Characterization, Treatments and Application
Pei Tang

nr 235
Large Eddy Simulations Applied to Wind Loading and Pollutant Dispersion
Mattia Ricci

nr 236
Alkali Activated Slag-Fly Ash Binders: Design, Modeling and Application
Xu Gao

nr 237
Sodium Carbonate Activated Slag: Reaction Analysis, Microstructural Modification & Engineering Application
Bo Yuan

nr 238
Shopping Behavior in Malls
Widiyani

nr 239
Smart Grid-Building Energy Interactions: Demand Side Power Flexibility in Office Buildings
Kennedy Otieno Aduda

nr 240
Modeling Taxis Dynamic Behavior in Uncertain Urban Environments
Zheng Zhong

nr 241
Gap-Theoretical Analyses of Residential Satisfaction and Intention to Move
Wen Jiang

nr 242
Travel Satisfaction and Subjective Well-Being: A Behavioral Modeling Perspective
Yanan Gao

nr 243
Building Energy Modelling to Support the Commissioning of Holistic Data Centre Operation
Vojtech Zavrel

nr 244
Regret-Based Travel Behavior Modeling: An Extended Framework
Sunghoon Jang

nr 245
Towards Robust Low-Energy Houses: A Computational Approach for Performance Robustness Assessment using Scenario Analysis
Rajesh Reddy Kotireddy

nr 246
Development of sustainable and functionalized inorganic binder-biofiber composites
Guillaume Doudart de la Grée

nr 247
A Multiscale Analysis of the Urban Heat Island Effect: From City Averaged Temperatures to the Energy Demand of Individual Buildings
Yasin Toparlar

nr 248
Design Method for Adaptive Daylight Systems for buildings covered by large (span) roofs
Florian Heinzelmann

nr 249
Hardening, high-temperature resistance and acid resistance of one-part geopolymers
Patrick Sturm

nr 250
Effects of the built environment on dynamic repertoires of activity-travel behaviour
Aida Pontes de Aquino

nr 251
Modeling for auralization of urban environments: Incorporation of directivity in sound propagation and analysis of a framework for auralizing a car pass-by
Fotis Georgiou

nr 252
Wind Loads on Heliostats and Photovoltaic Trackers
Andreas Pfahl

nr 253
Approaches for computational performance optimization of innovative adaptive façade concepts
Roel Loonen

nr 254
Multi-scale FEM-DEM Model for Granular Materials: Micro-scale boundary conditions, Statics, and Dynamics
Jiadun Liu

nr 255
Bending Moment - Shear Force Interaction of Rolled I-Shaped Steel Sections
Rianne Willie Adriana Dekker

nr 256
Paralympic tandem cycling and hand-cycling: Computational and wind tunnel analysis of aerodynamic performance
Paul Fionn Mannion

nr 257
Experimental characterization and numerical modelling of 3D printed concrete: Controlling structural behaviour in the fresh and hardened state
Robert Johannes Maria Wolfs

nr 258
Requirement checking in the building industry: Enabling modularized and extensible requirement checking systems based on semantic web technologies
Chi Zhang

nr 259
A Sustainable Industrial Site Redevelopment Planning Support System
Tong Wang

nr 260
Efficient storage and retrieval of detailed building models: Multi-disciplinary and long-term use of geometric and semantic construction information
Thomas Ferdinand Krijnen

nr 261
The users' value of business center concepts for knowledge sharing and networking behavior within and between organizations
Minou Weijs-Perrée

nr 262
Characterization and improvement of aerodynamic performance of vertical axis wind turbines using computational fluid dynamics (CFD)
Abdolrahim Rezaeiha

nr 263
In-situ characterization of the acoustic impedance of vegetated roofs
Chang Liu

nr 264
Occupancy-based lighting control: Developing an energy saving strategy that ensures office workers' comfort
Christel de Bakker

nr 265
Stakeholders-Oriented Spatial Decision Support System
Cahyono Susetyo

nr 266
Climate-induced damage in oak museum objects
Rianne Aleida Luimes

nr 267
Towards individual thermal comfort: Model predictive personalized control of heating systems
Katarina Katic

nr 268
Modelling and Measuring Quality of Urban Life: Housing, Neighborhood, Transport and Job
Lida Aminian

nr 269
Optimization of an aquifer thermal energy storage system through integrated modelling of aquifer, HVAC systems and building
Basar Bozkaya

nr 270
Numerical modeling for urban sound propagation: developments in wave-based and energy-based methods
Raúl Pagán Muñoz

nr 271
Lighting in multi-user office environments: improving employee wellbeing through personal control
Sanae van der Vleuten-Chraibi

nr 272
A strategy for fit-for-purpose occupant behavior modelling in building energy and comfort performance simulation
Isabella I. Gaetani dell'Aquila d'Aragona

nr 273
Een architectuurhistorische waardestelling van naoorlogse woonwijken in Nederland: Het voorbeeld van de Westelijke Tuinsteden in Amsterdam
Eleonore Henriette Marie Mens

nr 274
Job-Housing Co-Dependent Mobility Decisions in Life Trajectories
Jia Guo

nr 275
A user-oriented focus to create healthcare facilities: decision making on strategic values
Emilia Rosalia Catharina Maria Huisman

nr 276
Dynamics of plane impinging jets at moderate Reynolds numbers – with applications to air curtains
Adelya Khayrullina

nr 277
Valorization of Municipal Solid Waste Incineration Bottom Ash - Chemical Nature, Leachability and Treatments of Hazardous Elements
Qadeer Alam

nr 278
Treatments and valorization of MSWI bottom ash - application in cement-based materials
Veronica Caprai

nr 279
Personal lighting conditions of office workers - input for intelligent systems to optimize subjective alertness
Juliëtte van Duijnhoven

nr 280
Social influence effects in tourism travel: air trip itinerary and destination choices
Xiaofeng Pan

nr 281
Advancing Post-War Housing: Integrating Heritage Impact, Environmental Impact, Hygrothermal Risk and Costs in Renovation Design Decisions
Lisanne Claartje Havinga

nr 282
Impact resistant ultra-high performance fibre reinforced concrete: materials, components and properties
Peipeng Li

nr 283
Demand-driven Science Parks: The Perceived Benefits and Trade-offs of Tenant Firms with regard to Science Park Attributes
Wei Keat Benny Ng

nr 284
Raise the lantern; how light can help to maintain a healthy and safe hospital environment focusing on nurses
Maria Petronella Johanna Aarts

nr 285
Modelling Learning and Dynamic Route and Parking Choice Behaviour under Uncertainty
Elaine Cristina Schneider de Carvalho

nr 286
Identifying indoor local microclimates for safekeeping of cultural heritage
Karin Kompatscher

nr 287
Probabilistic modeling of fatigue resistance for welded and riveted bridge details. Resistance models and estimation of uncertainty.
Davide Leonetti

nr 288
Performance of Layered UHPFRC under Static and Dynamic Loads: Effects of steel fibers, coarse aggregates and layered structures
Yangyueye Cao

nr 289
Photocatalytic abatement of the nitrogen oxide pollution: synthesis, application and long-term evaluation of titania-silica composites
Yuri Hendrix

nr 290
Assessing knowledge adoption in post-disaster reconstruction: Understanding the impact of hazard-resistant construction knowledge on reconstruction processes of self-recovering communities in Nepal and the Philippines
Eefje Hendriks

nr 291
Locating electric vehicle charging stations: A multi-agent based dynamic simulation
Seheon Kim

nr 292
De invloed van Lean Management op de beheersing van het bouwproces
Wim van den Bouwhuijsen

nr 293
Neighborhood Environment and Physical Activity of Older Adults
Zhengying Liu

nr 294
Practical and continuous luminance distribution measurements for lighting quality
Thijs Willem Kruisselbrink

nr 295
Auditory Distraction in Open-Plan Study Environments in Higher Education
Pieternella Elizabeth Braat-Eggen

nr 296
Exploring the effect of the sound environment on nurses' task performance: an applied approach focusing on prospective memory
Jikke Reinten

nr 297
Design and performance of water resistant cementitious materials– Mechanisms, evaluation and applications
Zhengyao Qu

nr 298
Design Optimization of Seasonal Thermal Energy Storage Integrated District Heating and Cooling System: A Modeling and Simulation Approach
Luyi Xu

nr 299
Land use and transport: Integrated approaches for planning and management
Zhongqi Wang

nr 300
Multi-disciplinary optimization of building spatial designs: co-evolutionary design process simulations, evolutionary algorithms, hybrid approaches
Sjonnie Boonstra

nr 301
Modeling the spatial and temporal relation between urban land use, temperature, and energy demand
Hung-Chu Chen

nr 302
Seismic retrofitting of masonry walls with flexible deep mounted CFRP strips
Ömer Serhat Türkmen

nr 303
Coupled Aerostructural Shape and Topology Optimization of Horizontal-Axis Wind Turbine Rotor Blades
Zhijun Wang

nr 304
Valorization of Recycled Waste Glass and Converter Steel Slag as Ingredients for Building Materials: Hydration and Carbonation Studies
Gang Liu

nr 305
Low-Carbon City Development based on Land Use Planning
Gengzhe Wang

nr 306
Sustainable energy transition scenario analysis for buildings and neighborhoods - Data driven optimization
Shalika Saubhagya Wickramarachchi Walker

nr 307
In-between living and manufactured: an exploratory study on biobuilding components for building design
Berrak Kirbas Akyurek

nr 308
Development of alternative cementitious binders and functionalized materials: design, performance and durability
Anna Monika Kaja

nr 309
Development a morphological approach for interactive kinetic façade design: Improving multiple occupants' visual comfort
Seyed Morteza Hosseini

nr 310
PV in urban context: modeling and simulation strategies for analyzing the performance of shaded PV systems
Ádám Bognár

nr 311
Life Trajectory, Household Car Ownership Dynamics and Home Renewable Energy Equipment Adoption
Gaofeng Gu

nr 312
Impact of Street-Scale Built Environment on Walking/Cycling around Metro Stations
Yanan Liu